RESEARCH ON BEHAVIOR OF GROUNDWATER AND ITS APPLICATION TO FOUNDATION ENGINEERING(Dissertation_全文)

AUTHOR(S):

Nishigaki, Makoto

RESEARCH ON BEHAVIOR OF GROUNDWATER AND ITS APPLICATION TO FOUNDATION ENGINEERING

BY

MAKOTO NISHIGAKI

RESEARCH ON BEHAVIOR OF GROUNDWATER AND ITS APPLICATION TO FOUNDATION ENGINEERING

September 1979

BY

MAKOTO NISHIGAKI

TABLE OF CONTENTS

SUMMARY

The purposes of this thesis are primarily to research on behavior of groundwater flow in saturated and unsaturated zone, to present the fundamentals of the theory of groundwater flow, and to develop the most effective methods for solving groundwater flow problems related to civil engineering practice. The mathematical model provides a finite element solution to two- or three-dimensional problems involving transient flow in the saturated and unsaturated domains of nonhomogeneous, anisotropic porous media. In order to determine relationships between volumetric moisture content (θ) and hydraulic conductivity (K), and between pressure head (ψ) and volumetric moisture content (θ) in a laboratory, an apparatus was constructed and test procedures were developed to measure pressure head and volumetric moisture content by using pressure transducers and low-energy gamma ray attenuation. The validity and the accuracy of the two- or three-dimensional finite element approach have been investigated with comparing the numerical results with the laboratory experimental data. The relationships, K-θ and ψ-θ , which were obtained by the new apparatus were used as input data for numerical analyses. Good agreements between computed and measured pressure head profiles have been obtained. To estimate hydraulic properties of aquifers, new methods of analyzing drawdown test data were developed and illustrated with some examples. Namely, analyses of drawdown test data for partially penetrating well in a confined or an unconfined aquifer have been shown to determine anisotropic hydraulic conductivities and storage coefficients, and analyses of drawdown test data which are obtained in the much groundwater supplied aquifer were developed with a conception of "Island Model". To demonstrate the flexibility of the finite element approach and its capability in treating complex situations which are often encountered in the field, the groundwater flow through sand bank at flood water levels and the flow through aquifer due to an excavation were analyzed.

ACKNOWLEDGMENT

The author wishes to express his gratitude to Professor Koichi Akai of Kyoto University for his stimulating discussions, sustained guidance and support throughout the course of this research. He is also most grateful to Associate Professor Yuzo Ohnishi for many stimulating discussions on finite element analyses, for valuable suggestions during the course of the research work and for his final critique of the manuscript.

Through many hours of thoughtprovoking discussions on the fundamentals of flow through porous media, Professor Iichiro Kono of Okayama University has significantly contributed to the present work and given support for laboratory tests. The author is indebted to him for these and for his final critical evaluation of the manuscript.

His sincere thanks are due to Associate Professor Toshihisa Adachi of the Disaster Prevension Research Institute of Kyoto University for constructive suggestions and due to Associate Professor Takao Uno of Gifu University for many helpful suggestions on the flow through unsaturated porous media.

Thanks are also extended to Mr. Mituo Teramoto who has offered convenience to the author using computer and to Miss Kazumi Okabe who typed the manuscript.

Finally, the author expresses his utmost appreciations for the help of many members in the Foundation Engineering Laboratory in Kyoto University and members in Department of Civil Engineering in Okayama University.

CHAPTER 1

INTRODUCTION

1.1 Introduction

Water is an essential commodity to mankind, and the largest available source of fresh water lies underground. While throughout recorded history there is evidence that mankind has feared and respected the destructive power of water. In the form of tides and floods, it is one of the most powerful forces of nature. Hidden in rock crevices and soil pores, it exerts unbelievable forces that tear down mountainsides and destroy engineering works. Dam designers and builders, highway people, railroad engineers, and many others have long known of the great importance of controlling water in pores and cracks in earth and rock formations. When groundwater and seepage are uncontrolled, they can cause serious economic losses and take many human lives.

In brief, most failures caused by groundwater and seepage can be classified in one of two categories.

(1) Those that take place when soil parcticles migrate to an escape exit and cause piping or erosional failures.

(2) Those that are caused by uncontrolled seepage patterns that lead to saturation, internal flooding, excessive uplift, or excessive seepage forces.

Category 1 includes failures of dams, levees, reservoirs, and the like, caused by the migration of soil particles induced by a variety of defects. Category 2 includes failures of dams, drydocks, and retaining walls caused by excessive saturation, seepage forces, and uplift pressures. In this category are listed the deterioration and failure of pavements from internal flooding, the uplifting of canal linings after drawdown, failures of fills and foundations caused by seepage forces, and uplift pressures in trapped water, landslides, and

similar cases.

The specific problems which are to be dealt with can be divided into three parts:

(1) Estimation of the quantity of seepage

(2) Definition of the flow domain

(3) Stability analysis

In general, these problem is to determine the velocity and the pressure of the water in the interior of a soil mass with given boundaries, under certain imposed conditions along these boundaries. Mathematically speaking, the problem is in the class of boundary-value problems. During the last few decades great progress has been made in the mathematical analysis and the simulation techniques of these problems.

In the first preceding works, the Laplace equation was commonly used as the governing equation of steady state flow in porous media. Namely there is no change in conditions with respect to time, and regarding water as an incompressible flow makes the density of water a constant. In dealing with the steady state seepage of water through, for example, earth dams and embankments, civil engineers have traditionally relied on the graphical method of flow nets, theory of complex variables, and conformal mapping.

However, as a great many kinds of civil engineering works are perfomed with expedition by using many kinds of construction machineries, it becomes necessary to obtain useful solutions to seepage conditions during the non-steady period. For many years, the hydrologist has been accustomed to analyzing the flow behavior with approach of analytical mathematics. Engineers and hydrogeologists who have attempted to use analytical methods are well aware that these approach is very useful in some cases, but unfortunately, there are far too many situations where the real geologic system under investigation does not match the simplified version adopted by early researchers. In other words,

if one attempts to analyze almost any given hydrogeologic problem in the field, he soon finds that the natural variation in the hydraulic properties of the flow regime presents many problems if he limits his approach to analytic mathematics.

With the advent of the digital computer, however, various numerical methods have been perfected in recent years that have made it possible to solve rather complex problems in the flow of groundwater. Such methods have enabled engineers and hydrogeologists to develop a much better understanding of the way in which complex geological conditions control water movement. The methods have been concerned with both regional groundwater flow problems and the question of the local distribution of seepage around wells and structures such as dams and canals.

In all of the preceding work, the effect of flow in the unsaturated zone on the position of the free surface has been consistently neglected. While there are many steady state situations where one can safely make this assumption, the case of transient, free surface movement is an entirely different matter. There are probably a number of situations where drainage or imbibition is rapid enough that one does not commit a serious error in using the nonsteady numerical methods, but it is becoming clear that the role of the unsaturated zone in contributing to groundwater seepage needs more attention than it has received and with considering the effect of unsaturated zone in analysis it will be possible to solve the problems, which are almost impossible to be solved by the conventional method, such as behaviors of flow through an earth dam when water level raised at the upstream side, flow through an embankment when the water level of a river changed and ground water level fractuation due to water injection to a well or infiltration of rain.

Therefore the purpose of this thesis is primarily to research on behavior of groundwater flow in the saturated-unsaturated zone and its application to

fundation engineering. Namely in this thesis following four steps of investigation will be taken systematically:

(1) Evaluations and discussions of the governing equation of flow in the saturated-unsaturated porous media

(2) Development of numerical methods to analyses the behavior of groundwater flow in both zones using two-and three-dimensional finite element method

(3) Improvement of some methods to determine hydraulic properties of both zones in the laboratory and the field

(4) Application of developed methods to real geologic systems

1.2 Review of Previous Studies

The study of physics of flow through porous media has become basic to many scientific and engineering fields, quite apart from the interest it holds for purely scientific reasons. Such diversified field as soil mechanics, groundwater hydrology, petroleum engineering, water purification, industrial filtration, ceramic engineering, powder metallurgy, and the study of gas masks all rely heavily upon it as fundamental to their individual problems. All these branches of science and engineering have contributed a vast amount of literatures on the subject.

When the previous studies on the flow through porous media are reviewed, it is convenient to classify them into the following groups;

(1) Studies on fundamentals of groundwater flow

(2) Studies on methods for determining hydraulic properties in the field

(3) Studies on methods for determining hydraulic properties in the laboratory

(4) Studies on methods for estimating groundwater behaviors.

The objects of the studies in (1) are to investigate the governing equation of flow through porous media. Although the fundamentals of groundwater flow were established more than a century ago, it is only within recent years

that the subject has met with scientific treatment. Information on flow through porous media is scattered in a multitude of journals and books. Among the books that deal generally with this topic, one that must be mentioned is a comprehensive text book published by Muskat[1], which in spite of its age, still contains many useful informations. More specialized aspects of the physics of flow through porous media are contained in books for specific applications. Thus, on groundwater hydrology one must mention a classic books by Todd[2], Harr[3], and Polubarinova-Kochina[4]. On soil physics, there are books by Childs[5], Scheidegger[6], and Hillel[7]. De Wiest[8] edited a compilation of recent development on the subject. Bear[9] presented, in an ordered manner, the theory of dynamics of fluids in porous media, as applicable to many disciplines of science and engineering.

The objects of the studies in (2) are primarily to develop methods of determining the hydraulic characteristics of aquifers or water bearing layers with a drawdown test. The previous studies in dealing with a drawdown test are summarized in section 1.2.1.

The studies in (3) are to develop experimental methods of determining the hydraulic properties of unsaturated soils. This subject has been mainly studied in agricultural engineering. Recently, it is recognized that in the movement of the groundwater the water content and permeability of the unsaturated region usually play very important roles as well as the hydraulic properties of saturated soils, so that many researches have been done on this subject. Some of these previous works will be reviewed in section 4.1.

The objects of the studies in (4) are to develop rational techniques of the seepage analyses and to predict the distribution of pressure head and the velocity in soils taking into account the geological formation and the hydraulic boundary. In dealing with steady state seepage traditionally the graphical method of flow nets has been relied by civil engineers[10]. For unsteady state seepage the earliest investigators attempted to solve unsteady governing equation

by finding analytical solutions, using such techniques as separation of variables, Laplace transformation, Green's functions and conformal mapping. A distinct advantage of such analytical methods is that the solutions are derived in algebraic forms and it is easy to study the behavior of the systems in terms of convenient dimensionless variables. However, the process of finding an analytical solution becomes cumbersome and difficult except in the case of simple initial and boundary conditions and material composition of the flow region

In many practical problems, however, the degree of heterogeneity and anisotropy that the engineer encounters in the field may be such that these traditional methods are extremely difficult to apply unless certain simplifying assumptions are made. Such difficulties have led to the development of numerical methods. The previous studies on the numerical approach will be presented in section 1.2.2.

1.2.1 Previous studies on drawdown test

The following is a summary of theoretical and experimental work that has been done in the area of flow to wells. Several major areas outside the scope of the present study have been excluded from this compilation. These include multi-phase flow, anisotropic and heterogeneous porous media, compressible fluid flow, stratified and multiple-aquifer situations, multiple-well problems, and leaky-aquifer boundaries. With the above exclusions, the field of flow toward wells in porous media breaks down into the following classifications.

(1) Steady-state, confined flow in an aquifer of finite thickness; totally penetrating well (Fig.1.1)

For the purposes of this discussion, confined flow means that the aquifer is bounded of above and below by horizontal, impermeable surface. An aquifer considered is finite in lateral extent. Confined flow toward a totally penetrating well is purely radial flow and is often modeled by flow between two

concentric circles of constant piezometric head. The governing differential equation is

$$\frac{1}{r}\frac{\partial}{\partial r}\left(r\frac{\partial h}{\partial r}\right) = 0 \qquad (1.1)$$

where $h=\psi+x_3$. Muskat[11] and Polubarinova-Kochina[12] have derived the solution, which can be found in any basic text on ground water flow. The outer circle is the "radius of influence" of the well. This concept is not well difined, since the piezometric head varies logarithmically with the radius. However, Muskat[11] observed that any reasonable assumption for the "radius of influence" gives sufficiently precise values for the discharge flow rate.

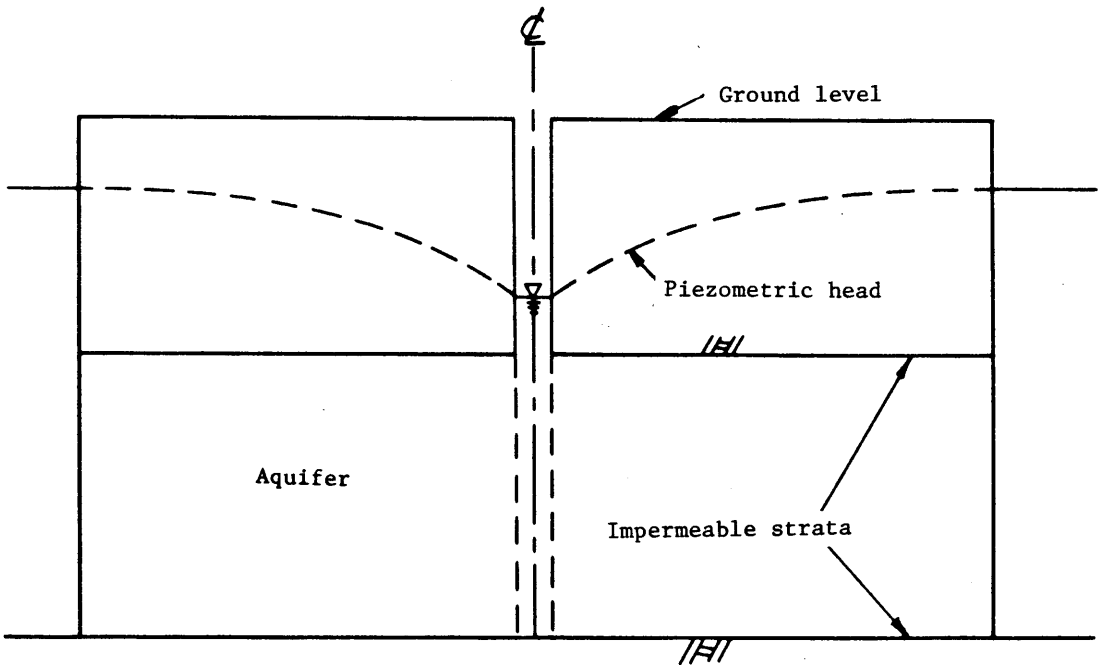

Fig.1.1 Totally penetrating well

(2) Steady-state, confined flow in an aquifer of finite thickness; partially penetrating well (Fig.1.2)

Now there is an additional velocity component in the vertical direction. Thus, the differential equation is

$$\frac{1}{r}\frac{\partial}{\partial r}\left(r\frac{\partial h}{\partial r}\right) + \frac{\partial^2 h}{\partial z^2} = 0 \qquad (1.2)$$

Muskat[11] distributed sinks along the well axis and adjusted their intensity to approximate the boundary condition of constant potential along the well bore. A theoretical solution for the case of a finite well radius was proposed by Kirkham[13]. Kirkham used numerical techniques to evaluate coefficients of a Fourier-Bessel series.

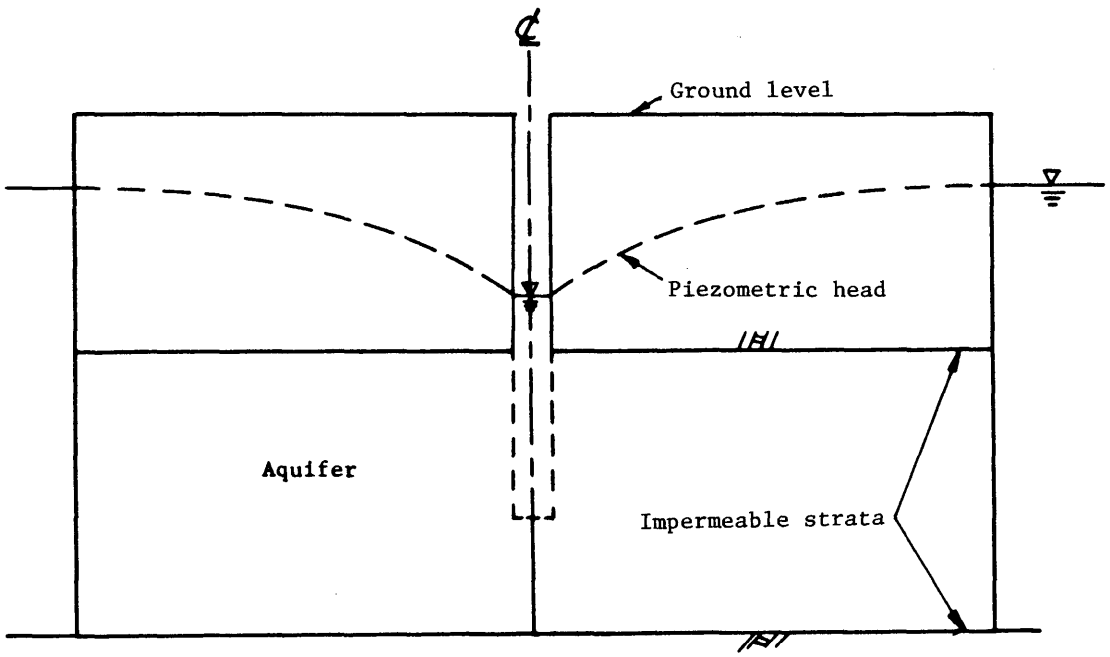

Fig.1.2 Partially penetrating well

(3) Steady-state, unconfined flow in an aquifer of finite thickness; totally penetrating well (Fig.1.3)

Unconfined flow means that part of the boundary of the flow domain is a free surface whose location is initially unknown. This makes the mathematical solution much more difficult to obtain. The most common way to handle the free surface theoretically has been to use the Dupuit-Forchheimer theory. This theory is based on the assumptions, as presented by Dupuit, that 1) for small inclinations of the free surface, the stream lines are essentially horizontal; and 2) velocities are proportional to the slope of the free surface and independent of depth. Actually, one does not need the assumption of depth-independent velocities to formulate the theory. Flow that obeys Darcy's law and that has negligible vertical velocity (implied by assumption 1) enables the equations of flow to be averaged in the vertical direction yielding the Dupuit equation

$$\frac{1}{r}\frac{\partial}{\partial r}\left(r\frac{\partial h^2}{\partial r}\right) = 0 \qquad (1.3)$$

As mentioned previously, surfaces of seepage are neglected in this theory. Flow rates are exact, but the free-surface profiles are in error, especially where curvatures of the free surface are large; e.g., in the neighbourhood of a well bore. The mathematical difficulties of free-surface flow motivated many researchers to turn to experimental and numerical methods. Finite difference techniques were used by Boulton[14] to obtain flow rates and free-surface profiles which included the surface of seepage. Boulton also worked with a sandbed model for experimental verification.[15] Kirkham gave an analytical solution based upon a fictitious flow region above the free surface and employing an interation procedure. An alternate approach, using force analysis and trialngles of filtration requiring no iteration, was developed by Kashef.[16]

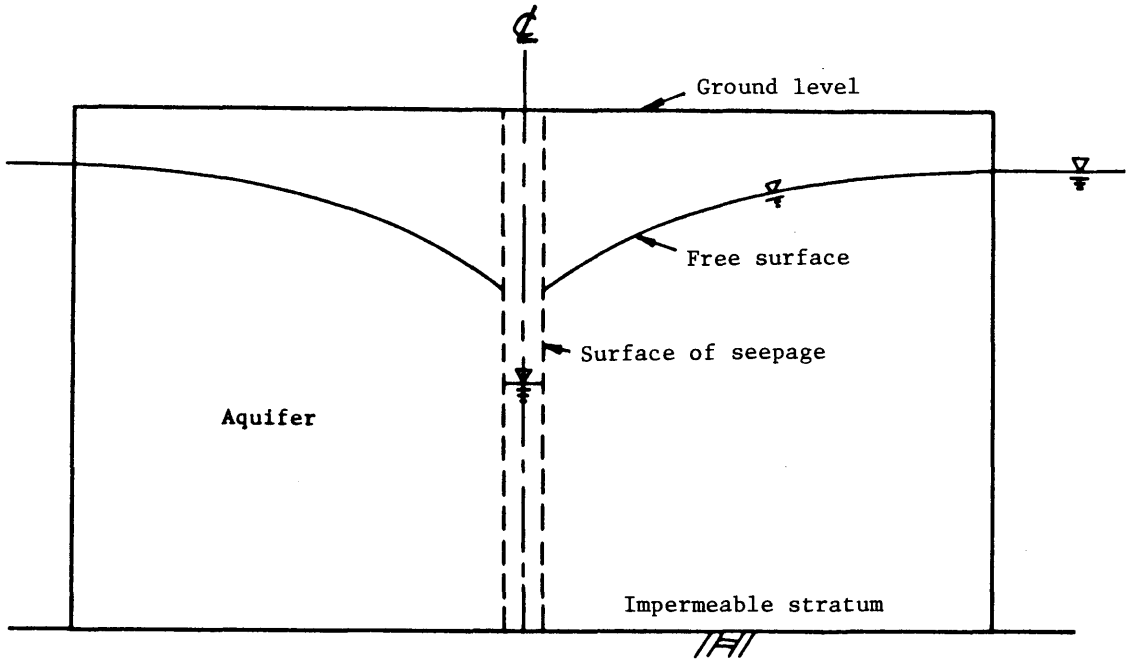

Fig.1.3 Totally penetrating well

(4) Steady-state, unconfined flow in an aquifer of finite thickness; partially penetrating well (Fig.1.4)

Dupuit theory cannot be applied to this case because the vertical velocity near the bottom of the well is not negligible. The finite difference techniques, similar one by Boulton[17] was also employed by Boreli[18] for the flow to a partially penetrating well. Taylor and Brown[19] obtained numerical solutions from a finite element analysis. Dagan used matched asymptotic expansions to derive an analytical solution. The well was modeled by a line sink of uniform strength, and the surface of seepage was neglected. An inner expansion, valid for distances far from a well bore, was obtained by the method of matched asymptotic expansions. The zeroth order term of the outer solution is the Dupuit solution for a totally penetrating well. This technique gives an approximate analytical solution to the problem plus insight into the validity of the Dupuit solution

and Muskat's[10] confined flow solution for a partially penetrating well.

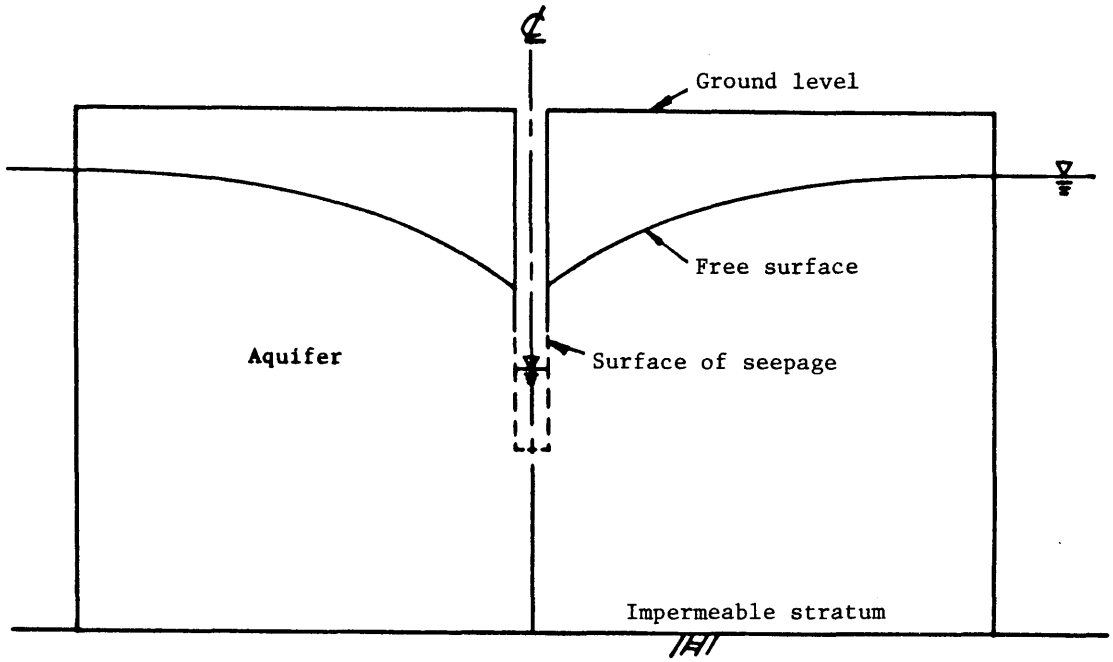

Fig.1.4 Partially penetrating well

(5) Steady-state, partally penetrating well in an infinitely thick aquifer with an impermeable roof (Fig.1.5)

An approximate solution was first presented by Harr.[20] The well was represented by a line-sink of constant intensity per unit length, and the well wall became an ellipsoid of constant potential. Polubarinova-Kochina[12] gave the same solution and showed that it was valid for free-surface flow with the linearized, free-surface boundary condition. She mentioned that improved accuracy can be obtained by varying the strength of the sink distribution alog the well axis. Mathemetically, the linearized, free-surface boundary condition says that the free-surface for unconfined flow is at the same elevation as the piezometric head for confined flow.

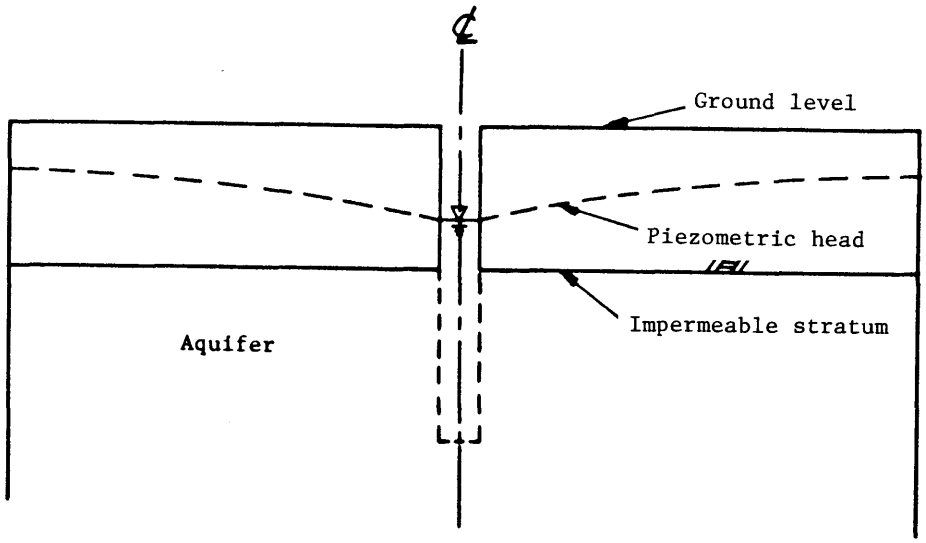

Fig.1.5 Confined flow in an infinitely thick aquifer

(6) Unsteady, confined flow in an aquifer of finite thickness; totally penetrating well (Fig.1.6)

The introduction of time complicates the mathematical solution considerably. Here one is concerned with time-dependent, radial flow. The aquifer considered is infinite in lateral extent. The differential equation, which includes water and aquifer compressibility effects, was lucidly derived by Nomitsu[21] in the form as follow

$$\frac{1}{r}\frac{\partial}{\partial r}\left(r\frac{\partial h}{\partial r}\right) = \frac{S}{T}\frac{\partial h}{\partial t} \qquad (1.4)$$

where h is the piezometric head, S is the storage coefficient [$S=\gamma b(\alpha+n\beta)$], and T is the transmissivity of the aquifer. Note that the vertical coordinate

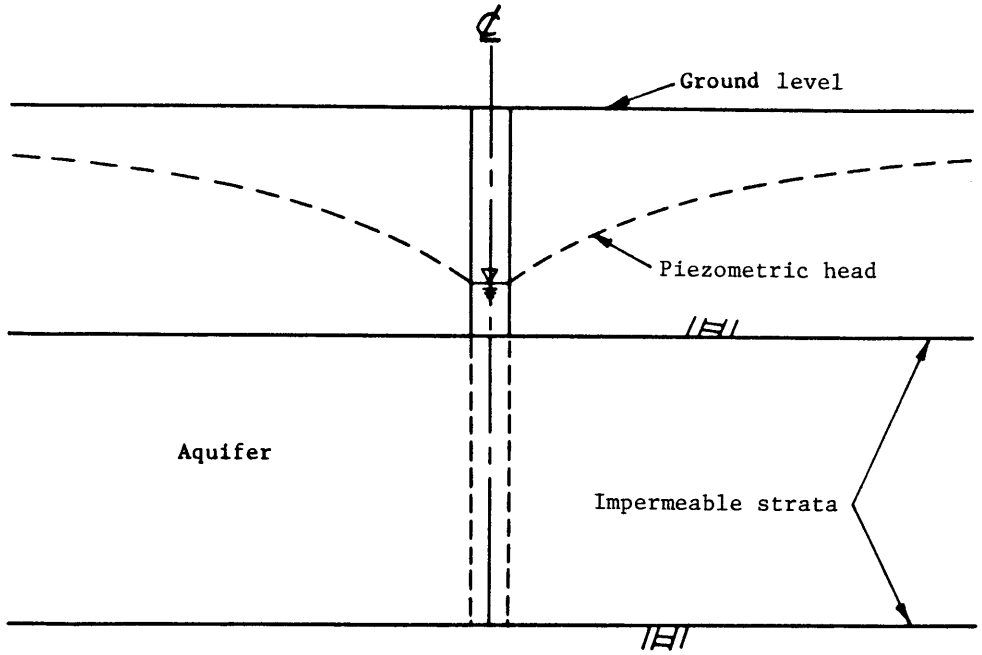

Fig.1.6 Totally penetrating well

dependence has been integrated out of the equation.

Theis, known as the father of unsteady well solutions, gave the first, widely popularized, unsteady solution. His"well function" solution to the above equation has been extensively tabulated. The differential equation strictly describes a confined, artesian aquifer, but Theis' solution has also been used as an approximate solution for free-surface flow with a linearized, free-surface boundary condition.

Jacob and Lohman[22] solved the case of the time-varying discharge under conditions of constant head and compared their results with field tests. Hantush[23] dealt with wells in sands of non-uniform thickness. Boulton[24] introduced elastic and delayed-yield effects to the Theis model by adding a time-dependent integral term to the differential equation. Discharge flow rates that were certain spe-

cified functions of time were treated by Abu-Zied[25] and Scott and Hantush[26]. Periodic pumping rates were investigated by Lennox and Berg[27]. Kriz, et al.[28] derived the Theis solution by reducing the partial differential equation to an ordinary differential equation through a similarity transform of dimensionless variables. They developed an improved procedure for determination of the storage coefficient and transmissivity using graphical "type curves".

(7) Unsteady, unconfined flow in an aquifer of finite thickness; totally penetrating well (Fig.1.7)

The basis for many analyses in this area is the Boussinesq equation utilizing the Dupuit assumptions:

$$\frac{1}{r}\frac{\partial}{\partial r}\left(rh\frac{\partial h}{\partial r}\right) = \frac{S_y}{k}\frac{\partial h}{\partial t} \qquad (1.5)$$

where h is the piezometric head. This non-linear partial differential equation must still be linearized in order to obtain an analytical solution. As mentioned previously, the Theis' solution has been applied as an approximation to the case of unconfined flow. Thus, the free-surface drawdown near the well is quite inaccurate because no account is taken of the vertical velocity. This vertical velocity is significant near the well bore.

The potential theory formulation was solved by Boulton[29] using a linearized, free-surface, boundary condition which was valid for relatively small drawdowns. He modeled the well with a line-sink of constant discharge per unit length. The surface of seepage was neglected, but a correction was applied to the solution to compensate for this assumption. The solution for the free-surface drawdown as a function of time was obtained for constant discharge conditions by using a Fourier-Bessel analysis. The Theis' solution was shown to be valid for flow in

an unconfined well provided the duration of pumping was sufficiently long. Through numerical integration, correction curves were obtained for times near the start of pumping.

Glover and Bittenger[30] improved the Theis' solution by employing an iteration procedure to take into account the reduction in saturated thickness of the aquifer as the free surface falls. A linearized Boussinesq equation was derived by Hantush[31] for wells in sloping sands under conditions of constant discharge. McNeary, et al.[32] solved the case of constant-head operation with variable storativity and transmissivity by numerical integration of the parabolic Boussinesq equation.

Boulton[33] extended his earlier solution in the case of constant-head production for a well of finite radius by Fourier-Bessel analysis and contour integration. For this type of pumping operation, the surface of seepage can be retained in the mathematical formulation. The solution for the well discharge as a function of time is nearly constant at first, but then approaches the Jacob and Lohman[22] result for an artesian aquifer at long times after pump startup. An analog model using an RC network was built by Stallman.[34]

Numerical integration of the non-linear Boussinesq equation was performed by Kriz, et al.[35] for constant discharge flow rates and large drawdowns. The partial differential equation was transformed into and ordinary differential equation by a dimensional similarity transformation. An approach using the hydraulic theory of free-surface flow was taken by Mahdaviani,[36] who numerically integrated the characteristic equations obtained from the energy and continuity equations for the system. Hydrostatic equilibrium was assumed, which made this approach similar to the Boussinesq theory. Fox and Ali[37] duplicated this work. Esmali and Scott[38] extended the results of Kriz, et al.[35] to constant-head operation.

Boulton's analytical solution[33] was verfied by Herbert[39] with a resistance

network analog. This solution is particularly useful for short times after the start of constant-head well drawdown test. Taylor and Luthin[40] have treated a finite-radius well with a surface of seepage and partially saturated flow above the free-surface using a finite-difference method. Boulton[41] analyzed some drawdown tests for totally penetrating wells in an unconfined aquifer. He took into account the slow yield of water from above the free surface as it falls, and concluded that drawdown versus distance curves were less sensitive to delayed yield effects than drawdown versus time curves.

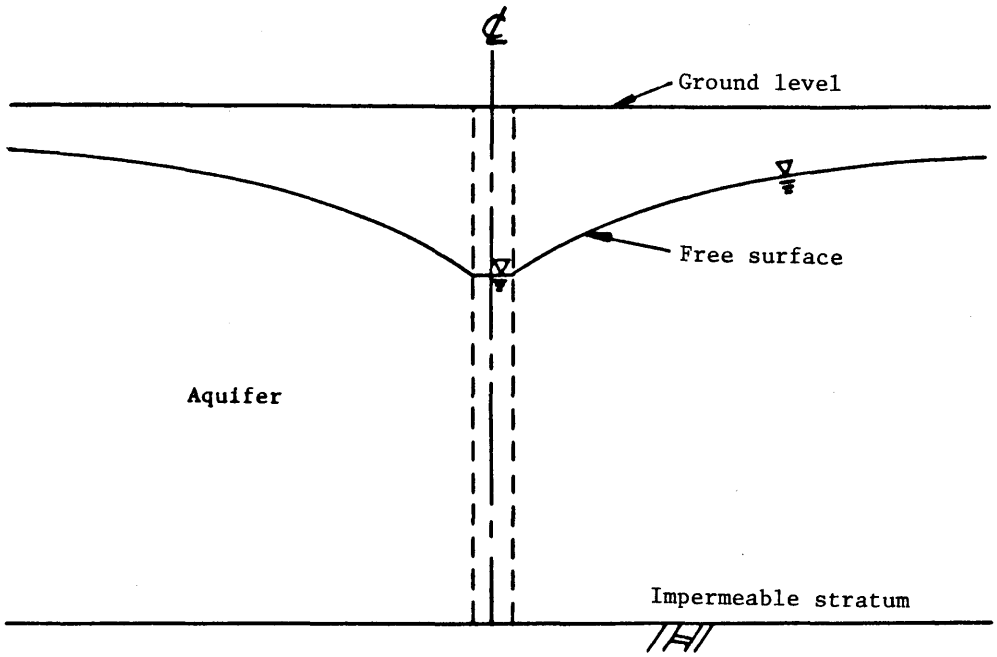

Fig.1.7 Totally penetrating well

1.2.2 Previous studies on numerical approach

The explosive development of the numerical approach in recent times has been mainly due to the rapid evolution of high speed digital computers in the last twenty-five years. Thanks to the numerical approach, in several fields of

science and technology, complex problems have now come within the reach of critical analysis. Finnemore and Perry[42] have adapted a relaxation technique in analyzing steady seepage through an earth dam. Another finite difference approach to the steady state seepage problem has been described by Jeppson.[43),44] In recent years an increasing number of attempts have been made to simulate nonsteady flow with a free surface by means of finite difference model by Desai, Szabo and McCraig.[45] [46]

Finite difference models have certain restrictions as to the kind of geological situations that can be handled. The finite element method, on the other hand, has been found to be easily adapted to problems of seepage through complex systems where a free surface exists. The finite element method, which was first devised as a procedure for structural analysis, has come to be recognized as an effective analysis tool for a wide range of physical problems. Among these are problems in the field of flow analysis, a subject of which is herein interpreted to encompass not only the flow of fluids but also heat flow.

The application of the finite element method to flow analysis problems was developed by Zienkiewicz in relatively recent years,[47),48] but, nevertheless, a significant literature on the topic has already emerged. Taylor and Brown[49] and Finn[50] were the first to apply this method to steady state,free surface problems. Finn's approach has been extended by Volker to include nonlinear flow.[51] Neuman was able to develop an iterative method of converging to a solution that eliminates the ambiguity effect reported by Taylor and Brown.[49] [52] Neuman has developed a finite element method for analyzing nonsteady flow with a free surface that is an extension of the technique used in solving steady state problems [Neuman and Witherspoon, 1970]. The method is based on the original form of the nonlinear governing equations and therefore enables one to investigate nonsteady free surface problems for a wide variety of conditions. Large vertical gradients are easily handled in systems with complex boundaries and arbitrary degrees

of anistropy and heterogeneity. When dealing with radial flow to a well operating at a prescribed rate, one must take into account both storage in the well and the actual distribution of velocities along the well bore. The method can also handle the effects of elastic storage, an important consideration in analyzing multiple aquifer systems. In addition, water can be added to or taken away from the free surface at prescribed rates to simulate infiltration and evaportranspiration. To obtain variations with time, the method uses an implicit, time centered scheme that is accurate and unconditionally stable. As a result only a small number of time steps are required to reach the final steady state.

In all of the preceding work, the unsaturated region above the free surface is not considered in the calculation. It stands to reason that in order to model a flow region where both saturated and unsaturated regimes coexist, one should combine the physical features governing the nature of each of these important phenomena. In recent years, there have been a growing number of attempts to consider flow in the saturated and unsaturated zones simultaneously. Finite difference schemes for simulating both of these zones have been employed by Rubin[54], Taylor and Lutin[55], Verma and Brutsaert[56], and Freeze[57),58]. Freeze has been able to simulate transient subsurface flow in a three-dimensional. With this three-dimensional model[58], Freeze has been able to simulate natural flow systems in hypothetical basins and develop an insight into the mechanisms involved in the development of perched water tables and in the areal variation of water table fluctuations. These problems are almost impossible to be solved by the preceding work. The finite element method was first applied to problems involving saturated-unsaturated flow in porous media by Neuman[59], but not many researches have been done yet.

1.3 Scope of This Study

The present work is essentially an attempt to develop the finite element method for analyzing transient, multi-dimensional fluid flow in saturated-unsaturated, heterogeneous porous media. This new method makes it possible to identify those field situations where flow in the unsaturated region is an important factor that cannot be neglected and in the multiple-aquifer with free surface. Unfortunately, consideration of the unsaturated zone involves added mathematical complexity and requires data on unsaturated soil properties. Then, the purposes of this thesis are to break the ice in treating both zones simultaneously.

Chapter 2 discusses the physics of the saturated-unsaturated groundwater motion. The governing equation of saturated-unsaturated flow is derived from the law of mass conservation and from the Darcy's law and Richard's equation of motion and is compared with the Klute's diffusion equation which has been widely used in the analysis of unsaturated flow. Typical boundary conditions are enumerated.

In Chapter 3, the governing equation of flow through saturated-unsaturated zones is formulated into the finite element discretizations which are evolved into the study of either two-dimensional models or three-dimensional models with radial symmetry. These models take into account the effects of hysteresis in the volumetric moisture content-pressure head relationships in unsaturated zone. In conjunction with the finite element discretization weighted residual procedures, particularly the Galerkin method is used.

Chapter 4 deals with the experimental study of hydraulic properties of unsaturated soil. In treating unsaturated zone, a great deal more data are required than are required for the saturated zone, but these properties of soils must be known to apply the finite element approach to actual flow problems. The main purposes of this chapter are to propose a rational basis of getting experimental relationships between pressure head(ψ) and hydraulic

conductivity(K) and between pressure head(ψ) and volumetric moisture content(θ) with "the instantaneous profile method" by using the source of low-energy gamma ray attenuation and pressure transducer, and to utilize these experimental data in Chapter 5 to check the numerical solutions.

In Chapter 5, in order to check the validity of the finite element approach developed in Chapter 3, laboratory experimental study on infiltration and drainage in two-and three-dimensional sand model box is carried out respectively. The numerical model is then used to solve these typical problems and the results are compared with experimental results for consistency. The relationships of the pressure head - moisture content and the hydraulic conductivity - moisture content which are obtained in Chapter 4 are used as input data.

In Chapter 6, new methods of analyzing drawdown tests are described and illustrated with some examples to determine hydraulic properties that are required to simulate a practical flow problem in the field. Firstly, some methods of analyzing drawdown tests with partially penetrating well is developed to determine anisotropic hydraulic conductivities which are taken into account quite easily in the finite element method. Methods of handling the effect of partial penetration are described in section 6.2, where the results of such methods are successful, one can not only determine the anisotropic permeabilities and storage coefficient but also obtain some idea of the thickness of the aquifer being tested. Secondarily, the analytical solutions of unsteady flow due to drawdown test are derived in the conception of "Island Model" that the shape of groundwater level is fixed by the circular water supply which is equilibrium with the pumping rate. By using these solutions, new methods of analyzing drawdown tests which are performed in a confined aquifer and an unconfined aquifer are given respectively and the effect of influence region is evaluated.

In Chapter 7, having looked into the reasonableness and validity of this finite element model in Chapter 5, the possible application of this model is

finally described. Before progressing into the various levels of applications the input data and boundary conditions are discussed and evaluated. The applications of models to field situation are the flows through sand bank at flood water levels and the flow through aquifer due to excavation.

Finally, in Chapter 8, the summary of this thesis is presented and the various suggestions for future studies are given.

References

1) Muskat,M.: The flow of homogeneous fluids through porous media, 1st ed. McGraw Hill, 1937.

2) Todd,D.K.: Groundwater hydrology, Wiley,New York, 1959.

3) Harr,M.E.: Groundwater and seepage, McGraw-Hill, New York, 1962.

4) Polubarinova-Kochina,P.Ya: Theory of groundwater movement, Princeton University Press, 1962.

5) Childs,E.C.: An introduction to the physical basis of soil water phenomena, Wiley, New York, 1969.

6) Scheidegger,A.E.: Teh physics of flow through porous media, Third edition, University of Toronto Press, 1974.

7) Hillel,D.: Soil and Water, physical principles and process, Academic Press, New York, 1971.

8) Dewiest,R.J.M.: Flow through porous media, Academic Press, New York, 1969.

9) Bear,J.: Dynamics of fluids in porous media, American elsevier, New York, 1972.

10) Cedergren,H.R.: Seepage, drainage, and flow nets, John Wiley, New York, 1967.

11) Muskat,M.: The Flow of homogeneous fluids through porous media; McGrau Hill, N.Y., 1937, pp.15-276.

12) Polubarinova-Kochina,P.Ya.: Theory of ground water movement, (Trans. by R.J.M.SeWiest), Princeton Univ. Press, Princeton, N.J., 1962, pp.360-362.

13) Kirkham,D.: Exact theory of flow into a partially-penetrating well, Jour. Geophys. Res., 64, 9, 1959, pp.1317-1327.

14) Boulton,N.S.: The flow pattern near a gravity well in a uniform waterbearing medium, Jour. Inst. Civil Eng., 36, 1951, pp.534-550.

15) Kirkham,D.: Exact theory for the shape of the free water surface about a well in a semi-confined aquifer, Jour. Geophys. Res., 69, 12, 1964, pp.2537-2549.

16) Kashef,A.I.: Exact free surface of gravity wells, Proc. Amer. Soc. Civil Eng., 91, HY4, 1965, pp.167-184.

17) Boreli,M.: Free-surface flow toward partially penetrating wells, Trans. Am. Geophys. Union, 36, 4, 1955, pp.664-672.

18) Taylor,R.L. & C.B.Brown: Darcy flow solutions with a free surface, Proc. Amer. Soc. Civil Eng., 93, HY2, 1967, pp.25-33.

19) Dagan,G.: A derivation of dupuit solution of steady flow toward wells by matched asymptotic expansions, Water Resources Res., 4, 2, 1968, pp.403-412.

20) Harr,M.E.: Groundwater and seepage, McGraw HIll, N.Y. 1962, pp.259-262.

21) Momotsu,T. & K.Yamashita: An advance in the theory of wells, II, Chikyūbutsuri (Geophsics) 7, 1, pp.21-40, (1943)

22) Jacob,C.E. & S.W.Lohman, Non-steady flow to a well of constant drawdown in an extensive aquifer, Trans. Amer. Geophys.Union, 33, 4, 1952, pp.559-569.

23) Hantush,M.S.: Flow of ground water in sands of non-uniform thickness-3, flow to well, Jour. Geophys. Res., 67, 4, 1962C, pp.1527-1534.

24) Boulton,N.A.: Analysis of data from non-equilibrium pumping tests allowing for delayed yield from storage, Proc. Inst. Civil Eng., 26, pt.3, 1963. pp.469-482.

25) Abu-Zied,M. & V.H.Scott: Non-steady flow for wells with decreasing discharge, Proc. Amer. Soc. Civil Eng., 89, HY3, 1963, pp.119-132.

26) Hantush,M.S.: Drawdown around wells of variable discharge, Jour. Geophys. Res., 69, 20, (1964B). pp.4221-4235.

27) Lennox,D.H. & A.V.Berg: Drawdowns due to cyclic pumping, Proc. Amer. Soc. Civil Eng., 93, HY6, 1967, pp.35-51.

28) Kriz,G.J., V.H.Scott & R.H.Burgy: Graphical determination of confined aquifer parameters, Proc. Amer. Soc. Civil Eng., 92, HY5, 1966A, pp.39-48.

29) Boulton,N.S.: The drawdown of the water table under non-steady conditions near a pumped well in an unconfined formation, Proc. Inst. Civil Eng., 3.

pt.3, 1954, pp.564-579.

30) Glover,R.E. & M.W.Bittinger: Drawdown due to pumping from an unconfined aquifer, Proc. Amer. Soc. Civil Eng., 86, IR3, 1960, pp.63-70.

31) Hantush,M.S.: Hydraulics of gravity wells in sloping sands, Proc. Amer. Soc. Civil Eng., 88, HY4, 1962, pp.1-15.

32) McNeary,S.S. I.Remson & S.C.Chen: Hydraulics of wells in unconfined aquifers, Proc. Amer. Soc. Civil Eng., 88. HY6, 1962, pp.115-123.

33) Boulton,N.S.: The discharge to a well in an extensive, unconfined aquifer with constant pumping level, J.Hydrology, 3, 2, 1965, pp.124-130.

34) Stallman,R.W.: Effects of water table conditions of water level changes near pumping wells, Water Resources Res., 1, 2, 1965, pp.295-311.

35) Kriz,G.J. V.H.Scott & R.H.Burgy: Analysis of paramination of an unconfined aquifer, Proc. Amer. Soc. Civil Eng., 92, HY5, 1966, pp.49-56.

36) Mahdaviani,M.A.: Steady and unsteady flow towards gravity wells, Proc. Amer. Soc. Civil Eng., 93, HY6, 1967, pp.135-146.

37) Fox,J.A. & I.Ali: Unsteady, unconfined flow to gravity wells, Proc. Inst. Civil Eng., 40, 1968, pp.451-469.

38) Esmali,H. & V.H.Scott: Unconfined aquifer characteristics and well flow, Proc. Amer. Soc. Civil Eng., 94, IR1, 1968, pp.115-136.

39) Herbert,R.: Time variant ground water flow by resistance network analogues, Jour, Hydrology, 6, 3, 1968, pp.237-264.

40) Taylor,G.S. & J.N.Luthin: Computer methods for transient analysis of water table aquifers, Water Resources Res., 5, 1, 1969, pp.144-152.

41) Boulton,N.S.: Analysis of data from pumping tests in unconfined aquifers, J.Hydrology, 10, 4, 1970, pp.369-378.

42) Finnemore,E.J. & B.Perry: Seepage through an earth dam computed by the relaxation technique, Water Reso. Res., Vol.4(5), 1968, pp.1059-1064.

43) Jeppson,R.W.: Seepage from ditches solution by finite differences, Proc. ASCE, 94(HY1), 1968, pp.259-267.

44) Jeppson,R.W.: Seepage through dams in the complex potential plane, Proc. ASCE, 94(IR1), 1968, pp.23-30.

45) Desai,E.S. & Sherman,W.C.: Unconfined transient seepage in sloping banks, Proc. ASCE, (SM2), 1971, pp.357-373.

46) Szabo,B.A. & McCraig,I.W.: A mathematical model for transient free surface flow in non-homogeneous or anisotropic porous media, Water Reso. Bull. Vol.4(3), 1968, pp.5-23.

47) Zienkiewicz,O.C. & Cheung,Y.K.: Finite elements in the solution of field problems, The Engineer, 1965, pp.501-510.

48) Zienkiewicz,O.C. & Cheung,Y.K.: Solution of anisotropic seepage problems by finite elements, Proc. ASCE, Vol.92, (EM1), 1966, pp.111-120.

49) Taylor,R.L. & Brown,C.B.: Darcy flow solutions and a free surfaces, Proc. ASCE, Vol.93, (HY2), 1967, pp.25-33.

50) Finn,W.D.: Finite element analysis of seepage through dams, Proc. ASCE, Vol.93, (SM6), 1967, pp.41-48.

51) Volker.R.E.: Nonlinear flow in porous media by finite elements, Proc. ASCE, Vol.95, (HY6), 1969, pp.2093-2101.

52) Neuman,S.P. & Witherspoon,P.A.: Finite element method of analyzing steady seepage with a free surface, Water Reso. Res., Vol.6, No.3, 1970, pp.889-897.

53) Neuman,S.P. & Witherspoon,P.A.: Analysis of nonsteady flow with a free surface using the finite element method, Water Reso. Res.,Vol.7, 1971, pp.611-623.

54) Rubin,J.: Theoretical analysis of two-dimensional transient flow of water in unsaturated and partly unsaturated soils, Soil Sci. Soc. Amer. Proc., 32, 1968, pp.607-615.

55) Taylor,G.S. & Luthin,J.N.: Computer methods for transient analysis of water-table aquifers, Water Reso. Res., Vol.5, No.1, 1969, pp.144-152.

56) Verma,R.D. & W.Brutsaert: Unconfined aquifer seepage by capillary flow theory, Proc. ASCE, Vol.96(HY6), 1970, pp.1331-1344.

57) Freeze,R.A.: The mechanism of natural ground-water recharge and discharge, 1, one-dimensional, vertical, unsteady, unsaturated flow above a recharging or discharging ground-water flow system, Water Reso. Res., Vol.5, No.1, 1969, pp.153-171.

58) Freeze,R.A.: Three-dimensional, transient, saturated-unsaturated flow in a groundwater basin, Water Reso. Res., Vol.7, No.2, 1971, pp.347-365.

59) Neuman,S.P.: Saturated-unsaturated seepage by finite elements, Proc., ASCE, Vol.99, No.12, (HY12), 1973, pp.2233-2250.

CHAPTER 2

PHYSICS OF SATURATED-UNSATURATED GROUNDWATER MOTION

2.1 Introduction

In solving a specific physical problem, such as the flow of a liquid through a specified porous medium domain, it is necessary to develop the fundamental equations describing the transport of fluid in a porous medium.

In this chapter, firstly, Darcy's law is discussed as the equation of motion. The experiment of Darcy will not be uniquely defined, therefore, there is considerable ambiguity in postulating a differential equation which would be equivalent to the results of the experiments. In fact, the differential equation which is now commonly called " Darcy's law " is not an equivalent expression for Darcy's finding, although these do follow from it. However, they would equally well follow from other types of differential equations.

This is especially true if generalizations of Darcy's law to anisotropic compressible and unsaturated porous media are attempted. Some discussion will be devoted to this subject later in this chapter.

It is to be expected that Darcy's law will have limitations. Indeed, such limitations occur generally as high and low flow rates, as well as in relation to various other effects. The range of validity of Darcy's law and its limitations will also be discussed in this chapter.

Secondly, Richard's equation is discussed as the law of continuity or conservation of mass. Coupled the equation of motion with the law of continuity, the governing equations for saturated-unsaturated flow will be derived and compared with the Klute's diffusion equation which was widely used in the analysis of unsaturated flow.

When a problem is described simultaneously by a number of dependent varia-

bles, the same number of equations is needed for a complete solution. Being a general description of an actual phenomena, it is obvious that the partial differential equation itself does not contain any information concerning the specific values of quantities characterizing a specific case of a phenomenon. Therefore, any partial differential equation has an infinite number of possible solutions, each of which corresponds to a particular case of the phenomenon. To obtain from this multitude of possible solutions corresponding to a certain specific problem of interest, it is necessary to provide supplementary to a certain specific problem of interest, it is necessary to provide supplementary information that is not contained in the partial differential equation. Finally section 2.5 will include a discussion of the initial and boundary conditions of flow of fluids through porous media.

2.2 Equation of Motion

In 1865, Henri Darcy published in an appendix to his book " Les Fontaines Publiques de la Ville de Dijon " the results of his experiments on the flow of water through granular material. Using a cylindrical sample, the direction of flow being along the cylinder, he found the discharge per unit area of cross-section to be proportional to the gradient of piezometric head in the direction of flow, i.e.

$$\frac{Q}{A} = K\frac{\Delta h}{\Delta \ell} \tag{2.1}$$

Here, Q is the discharge through the sample, A is the gross area of the sample's cross-section, Δh is the head lost in a length $\Delta \ell$ and K is constant for a given sample. This expression, and various rearrangements of it, have been named

Darcy's law and it is the basic relationship in quantitative study of the flow of fluids through porous media.

Darcy's law originally was limited to one-dimensional flow in a steady state for a homogeneous incompressible fluid. When Darcy's law is extended to a formal generalization of the equation of motion, some problems arise as follows:

(1) to three-dimensional flow

(2) to the flow in an isotropic medium

(3) to the flow in an anisotropic medium

(4) to unsteady state flow

Several researchers have derived Darcy's law from the general Navier-Stokes equations for viscous flow to extend Darcy's law to above problems. Under unsteady state conditions the Navier-Stokes equation for low Reynolds numbers (neglecting the higher order inertial term) becomes

$$\rho\frac{\partial v_i}{\partial t} + \rho\frac{\partial \Phi}{\partial x_i} = \mu\nabla^2 v_i \tag{2.2}$$

Here Φ is a force potential defined as

$$\Phi = -x_i g_i + \frac{p}{\rho} \tag{2.3}$$

$g_i=(0,0,-g)$ is the acceleration due to gravity, p, μ and ρ are respectively the pressure, viscosity and density of the fluid. The mass average velocity[1] v_i^* is introduced into Eq.(2.2).

$$\rho\frac{\partial v_i^*}{\partial t} + \rho\frac{\partial \Phi}{\partial x_i} = \mu\nabla^2 v_i^* \tag{2.4}$$

In above equation $\mu\nabla^2 v_i^*$ represents the density of the force due to the fluid's viscosity, which resists the motion. It is a viscous force per unit volume of fluid. These resistance forces depend upon the friction of fluid particles with

soil particles. The forces of internal friction —— fluid particles with fluid particles —— are negligibly small in comparison with the forces of external friction. The resistance forces offered by a single sphere for the special case of slow viscous flow of a Newtonian fluid is given by Stokes'[2),3)] law. This law can be expressed in a generalized form as

$$f_p = \lambda \mu d v_i^* \tag{2.5}$$

in which f_p is the resistance or drag of a single particle, μ represents the dynamic viscosity of the fluid, d is the particle diameter; for irregular-shape nonuniform particles, d would be the characteristic length of the average-size particle and would have to be determined by some appropriate technique. v_i^* denotes the local average velocity of flow around the particle (i.e., the seepage velocity), and λ represents a coefficient that takes into account the effects of neighboring particles. The coefficient λ will depend upon the local streamline configuration around the particle and, hence, must be some function of the geometry of the pore system. More specifically λ will depend upon the porosity, the shape of the particles, and the distribution of the sizes of the particles.

The total resistance F_R offered by all of the particles in the element will thus be

$$F_R = N f_p \tag{2.6}$$

in which N represents the number of particles in the element. F_R is rewritten in the another form

$$F_R = (\mu/B) v_i^* \tag{2.7}$$

Considering that the coefficient B retains the same value for the unsteady movement as for the steady. Eq.(2.4) with the help of Eq.(2.7) becomes

$$\rho \frac{\partial v_i^*}{\partial t} + \rho \frac{\partial \Phi}{\partial x_i} = -(\mu/B) v_i^* \tag{2.8}$$

and this equation can be shown in the next form

$$v_i^* = -\left(\frac{B}{\mu}\right)\rho\frac{\partial\Phi}{\partial x_i} - \left(\frac{B}{\mu}\right)\rho\frac{\partial v_i^*}{\partial t} \qquad (2.9)$$

Averaging over the cross-section we obtain [4)]

$$v_i^* = -\frac{K_{ij}}{n\bar{\mu}}\bar{\rho}\frac{\partial\Phi^*}{\partial x_i} - \left(\frac{\bar{B}}{\bar{\nu}}\right)\frac{\partial v_i^*}{\partial t} \qquad (2.10)$$

where $\bar{\nu}$ is the average kinematic viscosity ($\simeq\bar{\mu}/\bar{\rho}$). Thus, the equation of motion derived in the form of Eq.(2.10) is valid for an inhomogeneous fluid in laminar flow through an anisotropic porous medium. The coefficient K_{ij} —— the medium's permeability —— will be discussed in detail in other chapter. Eq.(2.10) is the generalized form of Darcy's law for nonsteady state flow and the form of the extension of Darcy's law to three-dimensional flow in anisotropic media.

Another derivations of Darcy's law from Navier-Stokes eq. are presented by Whitaker [4),5),6)] (1966, 1967, 1969) and by Slattery [7),8),9)] (1967, 1969, 1972). They used the Slattery-Whitaker averaging theorem which discovered simultaneously and independently by Slattery [7)] (1967) and by Whitaker [5)] (1967). This theorem enables one to express the volume averages of space derivatives in terms of the space derivatives of volume averages, thereby making it possible to proceed with the integration of differential equations from one scale of measurement to another in a mathematically reigorous fashion.

The second term on the right-hand side of the motion equation Eq.(2.10) expresses the average acceleration. Since in practice Darcy's law is always expressed in the form neglecting the last term in Eq.(2.10), it is important to know under what conditions can one justify neglecting this term. For flows in which the local inertial forces can be neglected with respect to the viscous (resistance) forces, Polubarinova-Kochina [10)] (1962) has indeed shown that the

acceleration term in the equation of motion tends very rapidly (e.g., within a fraction of a second) to zero after the onset of flow. Hence, one is justified in deleting this term from the equation.

The same interesting way of looking at this problem has been suggested by Whitaker. To use the author's own words (Whitaker[6],1969,pp.25) " If a tube filled with fluid is subjected to a sudden change is the pressure drop, essentially steady flow occurs for times greater than to where to $\approx d^2/4\nu$. Here d is the tube diameter and ν is the kinematic viscosity. For the purpose of estimating microscopic transient times in porous media, a practical lower bound on ν is $10^{-2}cm^2/sec$, and an upper bound on d might be on the order of $10^{-1}cm$. This gives a microscopic transient time on the order of 1 sec, and if the transient time for the macroscopic process is much larger (say on the order of minutes), we should be treat the flow as quasi-stead ..." When the fluid is incompressible and the porous medium is rigid, all the transient effects are caused entirely by temporal change in the external boundary conditions. In practice the characteristic time of such changes is usually at least on the order of minutes, indicating that the time derivative in Eq.(2.10) can probably be neglected in many situations.

Then for a homogeneous incompressible fluid, $\bar{\rho}$=const, $\bar{\mu}$=const and the motion Eq.(2.10) may be written in terms of the piezometric head $\bar{h}=z+\bar{p}/\bar{\gamma}$.

$$v_i^* = - (K_{ij}\bar{\gamma}/\bar{\mu}) \frac{\partial \bar{h}}{\partial x_j} \qquad (2.11)$$

This equation is Darcy's experimental law.

Although upper evaluations do not contribute to the formulation of a new law, these confirm the early belief that Darcy's law is of the nature of statistical result giving the empirical equivalent of Navier-Stokes equations.

It is important to define a range of validity of Darcy's law, because Darcy's

law is not universally valid for all conditions of liquid flow in porous media. In derivation of Darcy's law from Navier-Stokes equation, it is assumed that the flow is laminar (i.e., non turbulent slippage of parallel layers of the fluid one atop another, and inertial forces are negligible compared to viscos forces). Laminar flow prevails in silts and finer materials for any commonly occurring hydraulic gradients found in nature. In coarse sands and gravels, however, hydraulic gradients much in excess of unity may result in nonlaminar flow conditions, and Darcy's law may not always be applicable. In flow through conduits, the Reynolds number (R_e), a dimensionless number expressing the ratio of inertial to viscous forces, is used as a criterion to distinguish between laminar flow and turbulent flow. By analogy, a Reynolds number is defined also for flow through porous media:

$$R_e = v^*d/\nu \tag{2.12}$$

where v^* is the mean flow velocity, d the effective pore diameter, and ν is the kinematic viscosity of the fluid.

The limit can be found by plotting the dimensionless fanning friction factor f, used in hydraulics, against R_e. The factor f is defined by

$$f = \frac{d\Delta p}{2\rho L v^{*2}} \tag{2.13}$$

where Δp is the pressure difference over a length of porous media, L measured along the line of flow and other quantities are as defined above. Data from several investigations are plotted in Fig.2.1. Departures from a linear relationship appear when R_e reaches the range between about 1 and 10, thus indicating an upper limit for the validity of Darcy's law.[12)]

If we take $\nu=0.018 cm^2/sec$ (for water), then

$$v^*d < 0.018 \sim 0.18 \tag{2.14}$$

where v* is expressed in cm/sec , d - in cm next, we take d=0.1 cm, then

$$v^* < 0.18 \sim 1.8 \text{ (cm/sec)} \tag{2.15}$$

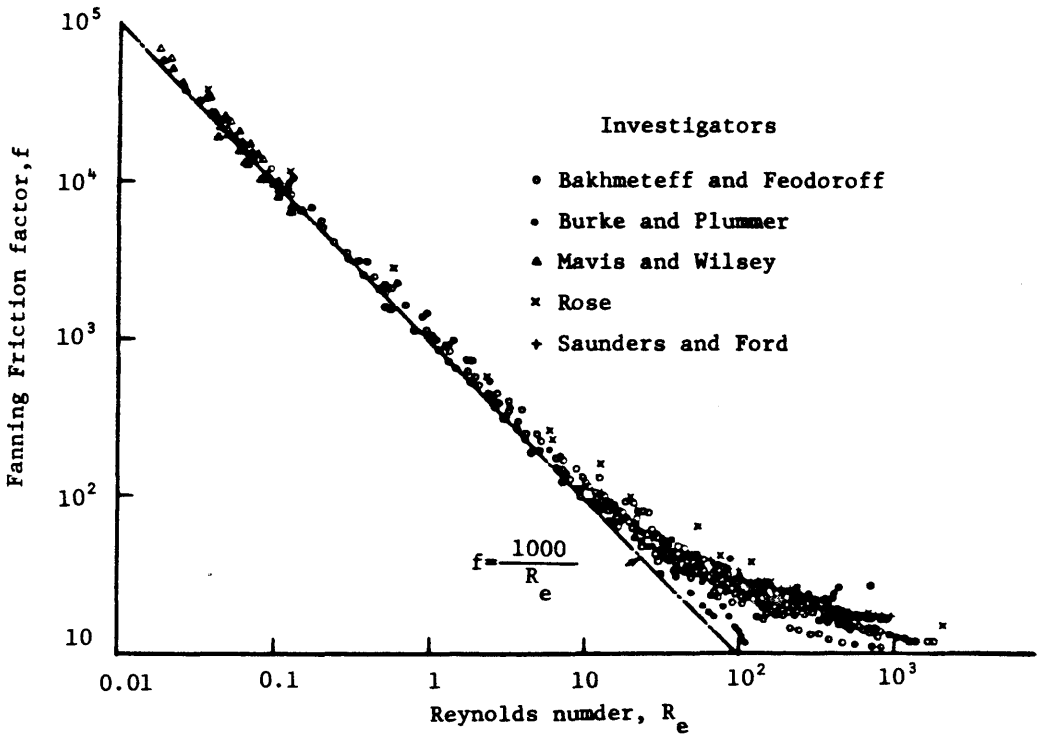

Fig.2.1 Relation of fanning friction factor to Reynolds number for flow through granular porous media [12]

this means used Darcy's law, then,

$$v^* = K\frac{\partial h}{\partial x} < 0.18 \sim 1.8 \ (\mathrm{cm/sec}) \tag{2.16}$$

when we take $K=1.0\times10^{-2}$cm/sec

$$\frac{\partial h}{\partial x} < 18 \sim 180 \tag{2.17}$$

this values are very large hydraulic gradient, and Darcy's law can be employed in the vast majority of cases concerning the flow of water in soil.

On the contrary, for very low velocities, some investigators (Swartzendruber[13](1962), Miller and Low[14](1963)) have claimed that, in clayey soils, low hydraulic gradients may cause no flow or only low flow rates that are less than proportional to the gradient, while others have disputed some of these findings (Olsen[15](1965)). A possible reason for this anomaly is that the water in close proximity to the particles and subject to their adsorptive force field may be more rigid than ordinary water, and exhibit the properties of a "Bingham liquid" (having a yield value) rather than a "Newtonian liquid." The adsorbed, or bound, water may have a quasicrystalline structure similar to that of ice, or even a totally different structure. Some soils may exhibit an apparent "threshold gradient," below which the flux is either zero (the water remaining apparently immobile), or at least lower than predicted by the Darcy relation, and only at gradients exceeding the threshold value does the flux become proportional to the gradient Fig.2.2.

Finally there seem to be a very important hydrological problem that may require the application of the Darcy's law to the flow in unsaturated soils. For the above problem, an experiment for the direct verification of Darcy's law in unsaturated materials has been carried out (Childs and Collis-George,1950[16]). They devised a method whereby the moisture content and suction down a long column

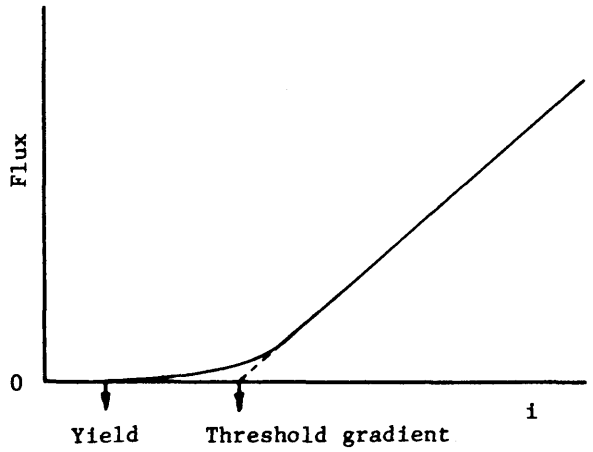

Fig.2.2 Possible deviations from Darcy's law at low gradients

of porous conductor were uniform, the potential gradient being due solely to the gravitational component. Various magnitudes of potential gradient were imposed by suspending the column at various angles of inclination to the vertical. From the results it could be safely inferred that the rate of flow for a given degree of saturation was proportional to the potential gradient, as in the case of saturated materials. Thus if may be possible to assume that the Darcy's law is applicable to unsaturated flow in anisotropic media in the form:

$$v_i = -K_{ij}(\psi)\frac{\partial h}{\partial x_j} \tag{2.18}$$

where v_i is the (volumetric) flux (volume of water per unit area unit time), $\partial h/\partial x_i$ is the hydraulic head gradient, which may include both suction and gravitational components and K_{ij} is a function of the pressure head (ψ) or a function of the volumetric water content (θ), and not a constant, as in saturated flow. Eq.(2.18) is sometimes called the Richard's equation, because Richards[17] has shown firstly that the modified Darcy's law applies to unsaturated soils. Miller and Miller[18][19] (1956) point out an important difference that since the moisture characteristic is subject to hysteresis, the pressure head (or suction)(ψ) is not uniquely related to the volumetric moisture content (θ), for it depends also upon

the history of wetting and drying by which that volumetric moisture content is reached.

However, the relation of hydraulic conductivity (sometimes called capillary conductivity) to volumetric moisture content $K_{ij}(\theta)$ is affected by hysteresis to a much lesser degree than is the $K_{ij}(\psi)$ function, at least in the media thus for examined (Topp and Miller[20], 1966). Thus, Darcy's law for unsaturated soil can also be written as

$$v_i = -K_{ij}(\theta)\frac{\partial h}{\partial x_j} \tag{2.19}$$

which, however, still leaves one with the problem of dealing with the hysteresis between ψ and θ. A more complete review of this problem will be brought at a later chapter of this research.

2.3 Equation of Continuity

In trasient groundwater motion, the distribution of potential within the flow region undergoes continual change with time. The nature of the time-dependence of conservation of mass, subject to the constraints of the equations of motion and of state. The conservation law as applied to fluid or heat transfer is also known as the equation of continuity.

Consider a finite subregion of the flow region as depicted in Fig.2.3. Under transient conditions of flow, water enters and leaves the flow region at different rates at different parts of the enclosing surface (control surface). The amount and identity of matter in the control volume may change with time, but the shape and position of this volume remain fixed. The special case, when the inflow exactly equals the outflow so that there is neither a mass excess

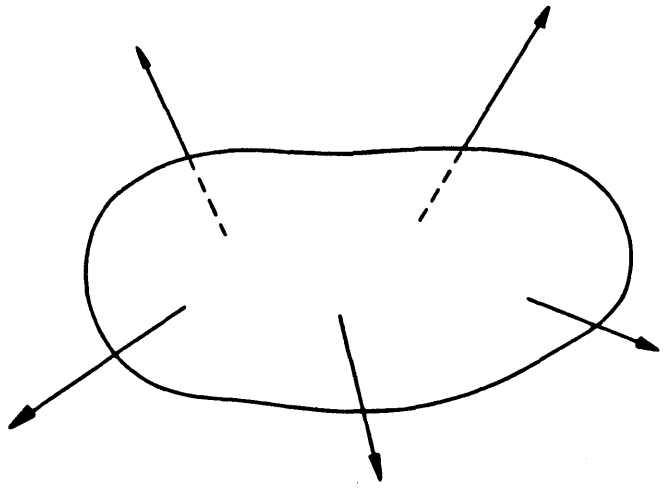

Fig.2.3 Fluxes crossing boundary surface of an arbitrary subregion of the flow region

nor a mass deficiency, is the phenomenon of steady state flow. Since mass can neither be created nor destroyed, the mass condition has to be adsorbed into or released from the particular small part of the flow region under consideration. The equation of continuity, then, is a statement, equating the summation of the rates at which mass enters or leaves the control volume of the flow region and the rate at which mass is absorbed by the subregion. According to Sokolnikoff and Redheffer[21] (1966), the law of conservation of mass can be stated as

$$\int_S \vec{V}\cdot\vec{n}\, d\delta = \int_V \text{div}\, \vec{V}\, dV \qquad (2.20)$$

where $\vec{V}$ is the velocity of the fluid

$\vec{n}$ is the unit normal

S is the control surface

and $d\delta$ is the differential surface area. Physically, the right hand side of

Eq. (2.20) amounts to dividing a finite region S into a large number of small voume elements and summing up the rate of fluid increase in each elemnt in order to obtain the overall fluid mass increase in V. The left hand side of Eq(2.20) simply states that the fluid excess arising out of trasient flow of fluid across control surface (left hand side of Eq. (2.20)) is accommodated by an equivalent increase in the fluid content within the element (right hand side of Eq.(2.20)). This is but a restatment of the conservation equation. Note also that the left hand side of Eq.(2.20) is the cause and the right hand side is the effect.

In soil physics literature, Richards (1931)[17] was probably the earliest to express the equation of continuity for transient soil water movement in the form of a parabolic, partial differential equation. Familiarly known as the Richard's equation, it can be written in cartesian coordinates as,

$$-\text{div}\rho\vec{V} = -\vec{\nabla}\cdot\rho\vec{V} = \frac{\partial}{\partial t}(\rho\theta) \qquad (2.21)$$

where ρ is the density of water, $\vec{V}$ is specific flux or Darcy velocity vector and θ is the volumetric moisture content, defined as the volume of water per unit volume of soil. In Eq. (2.21) the density of water ρ is assumed to be independent of space and time, Eq. (2.21) reduced to,

$$-\text{div}\vec{V} = -\vec{\nabla}\cdot\vec{V} = \frac{\partial\theta}{\partial t} \qquad (2.22)$$

which is also an expression of the conservation of mass.

2.4 Governing Equation of Flow in Porous Media

In practical problems of fluid flow in porous media, the most easily measured physical parameter is the fluid potential. Also, in itself, the variation in fluid potential is a phenomenon of considerable interest in studying flow through porous media. Hence, in the practical use of Eq. (2.22), it is convenient to make fluid potential the dependent variable. Thus, substituting Eq.(2.19) into Eq.(2.22), assuming that x_3 is a constant during the time interval

$$\text{div } K(\theta) \vec{\nabla} h = \frac{\partial}{\partial t}(\theta) \tag{2.23}$$

Eq. (2.23) is the governing equation for flow through porous media.

Rewriting Eq.(2.23) in the cartesian coordinate and in the tensor notation, one has

$$\frac{\partial \theta}{\partial t} = \frac{\partial}{\partial x_i} \left[D(\theta) \frac{\partial \theta}{\partial x_j} + K_{i3}(\theta) \right] \tag{2.24}$$

$$(i,j = 1,2,3)$$

which is the so-called diffusion equation derived by Klute,[22] and

$$D(\theta) = K_{ij}(\theta) \frac{\partial \psi}{\partial \theta} \tag{2.25}$$

where $D(\theta)$ is the soil-moisture diffusivity in soil physics literature. It may be appreciated that $\partial\psi/\partial\theta$ is a measure of the storage properties of the geological material and is the first derivative of the pressure head, ψ, to the increment of the volumetric moisture content, θ. The functional relationship between ψ and θ (so-called water retention curve) is shown in Fig. 2.4. As seem from Fig.2.4, the moisture content θ tends to become constant which is equal to porosity of soil, n, as soon as $\psi > \psi_{cr}$, i.e., when the suction is less than the air entry value (ψ_{cr}) and D becomes essentially discontinuous as $\partial\psi/\partial\theta \to \infty$. Therefore Eq(2.24) cannot be used for the saturated zone. With this equation, since the movement of water in unaturated

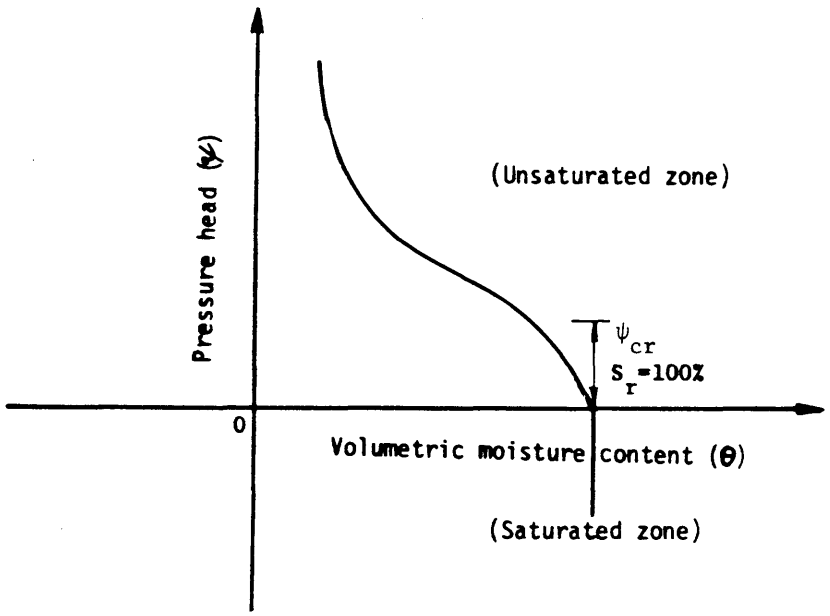

Fig.2.4 Variations in the moisture content

zone must be distinguished from the movement of water in saturated zone, it is quite inconvenient to solve the problem such as advancement of wetting front in the saturated - unsaturated soil media. Although Eq.(2.24) has been used quite often in the flow analysis, solutions are obtained only in the problems for unsaturated zone.[22)23)24)]

Meanwhile, it is known that the volumetric moisture content θ is expressed as

$$\theta = n\, S_w \tag{2.26}$$

where n is the porosity of soil and S_w ($0 \leq S_w \leq 1$) is the degree of saturation. Choosing ψ as only one dependent variable and applying the chain rule of

differentiation to the time derivative on the right hand side of Eq.(2.23), Eq.(2.23) can be transformed to the following equation.

$$\text{div } K(\psi)\vec{\nabla}(\psi + x_3) = \frac{\partial}{\partial t} (n S_w)$$

$$= \frac{d}{d\psi} (n S_w) \frac{\partial \psi}{\partial t}$$

$$= [S_w \frac{dn}{d\psi} + n \frac{dS_w}{d\psi}] \frac{\partial \psi}{\partial t} \qquad (2.27)$$

The two terms on the right hand side of Eq.(2.27) denote two distinct physical phenomena.[25] The first term represents the deformability of the soil skeleton which is anologous to the cosolidation problem expressed by Biot's equation.[26] This term is usually ignored in the problems of flow through porous media by assuming that the porous media is rigid. Here we consider that the soil medium is slightly compressible and also includes the last term which represents the desaturation of the pores, that is, the capacity of the soil to absorb or release moisture due to saturation changes.

Assuming that the porosity n does not change due to the variation of pressure ψ in unsaturated zone, Eq.(2.27) may be resuced to:

$$\text{div } K(\psi) \vec{\nabla} (\psi + x_3) = (C(\psi) + \beta S_s) \frac{\partial \psi}{\partial t} + S \qquad (2.28)$$

where

$$\beta = \begin{cases} 0 & : \text{Unsaturated zone} \\ 1 & : \text{Saturated zone} \end{cases}$$

where S_s denotes the specific storage(defined as the volume of water instantaneously released from storage per unit bulk volume of saturated soil when ψ is lowered by one unit), C (ψ) is the specific moisture capacity (defined as

$d\theta/d\psi$) and S is a sink or source term. In Eq. (2.28), the advantage being that $C(\psi)$ remains finite throughout the range of flow.

$C(\psi)$ attains a maximum value in coarse sand, near the air entry value (ψ_{cr}), where large changes in θ occur at small changes of ψ. It vanishes at suction smaller than the air entry value or for $\psi>\psi_{cr}$ (loosely called, "at saturated soil").

Clearly Eq.(2.28) has the advantage over Eq.(2.24) that is applied for the whole flow region, including saturated and unsaturated flow. So Eq.(2.28) is called "the governing equation for saturated - unsaturated flow through porous media."

2.5 Initial and Boundary Conditions

The supplementary information that, together with the partial differential equation, defines an individual problem should include specifications of:

(a) the geometry of the domain in which the phenomenon being considered takes place,

(b) all physical coefficients and parameters that affect the phenomenon considered (e.g., medium and fluid parameters),

(c) initial condotions which describe the initial state of the system considerd,

(d) the interaction of the system under consideration with surrounding systems, i.e., conditions on the boundaries of the domain in question.

2.5.1 Initial condition

Let us now consider the surface integral in Eq.(2.28). At any instant of time t_o, there is an initial distribution of ψ_o within the flow region boundary by the surface S. This region may be a part or all of the flow region. This distribution of ψ_o forms the initial condition for the transient fluid flow problem.

$$\psi(x_i, 0) = \psi_o(x_i) \tag{2.29}$$

2.5.2 Boundary conditions

The folw region as a whole communicates across its boundaries with its surroundings. The nature of this communication is reflected in the conditions that exist on the boundary of the flow region. The natures of these conditions are termed boundary conditions and, in general, these are four types. In addition, there many exist "mixed boundary conditions" of special types, which will be omitted for the present.

a. No-flow boundary

When no fluid enters or leaves the flow region across its boundary, the boundary is called a no-flow boundary. In fluid flow, an impermeable barrier or a plane of symmetry of flow is an impermeable boundary. Mathematically, this is identical to the condition that there is no gradient in potential across this boundary and hence,

$$\frac{\partial h}{\partial \vec{n}} = \left(K_{ij}(\psi)\frac{\partial \psi}{\partial x_j} + K_{i3} \right) n_i = 0 \tag{2.30}$$

in which $\vec{n}$ denotes the nomal to the boundary.

b. Prescribed flux boundary

It may so happen that the flow region receives fluid from or discharges fluid to its surroundings at a known or prescribed rate. For example, a soil may be receiving rainfall infiltration at a constant rate or a well may be discharging the flow region at a constant or variable rate. Such a condition is

known as a prescribed flux boundary condition. Mathematically, this amounts to saying that, for a unit surface area of the boundary, $\partial h/\partial \vec{n}$ is known, and hence,

$$\left(K_{ij}(\psi)\frac{\partial \psi}{\partial x_j} + K_{i3} \right) n_i = -v(x_i,t) \tag{2.31}$$

Such a condition is called a Neumann problem in potential theory. Indeed, the no flow boundary condition, (a), can be considered as a special case of Neumann problem.

c. Prescribed potential boundary

The third type of boundary condition arises when the flow region interacts with a very large reservoir of the fluid and receives fluid from or discharges fluid into this practically infinite reservoir. In this case, the potential on the boundary will be determined by the fluid potential in the infinite reservoir, which may fluctuate in time in a known, hence,

$$\psi(x_i,t) = \psi_b(x_i,t) \tag{2.32}$$

This type of boundary condition is called a Dirichlet problem in potential theory.

In most problems of practical interest different parts of the boundary of a flow region may experience different typea of boundary conditions and thus these problems are mixed initial-boundary-value problems.

d. Seepage faces

A seepage face is an external boundary of the saturated zone where water leaves the system and ψ is uniformly zero as shown in Fig.2.5. Under transient conditions, the length of the seepage face varies with time in a manner that cannot be predicted a priori. If one treats the seepage face as a prescribed pressure head boundary with ψ=0, the length of this face remains fixed, and

this is contrary to the reality of transient flow. On the other hand, the seepage face cannot be treated as a prescribed flux boundary because the values of Q are generally unknown there.

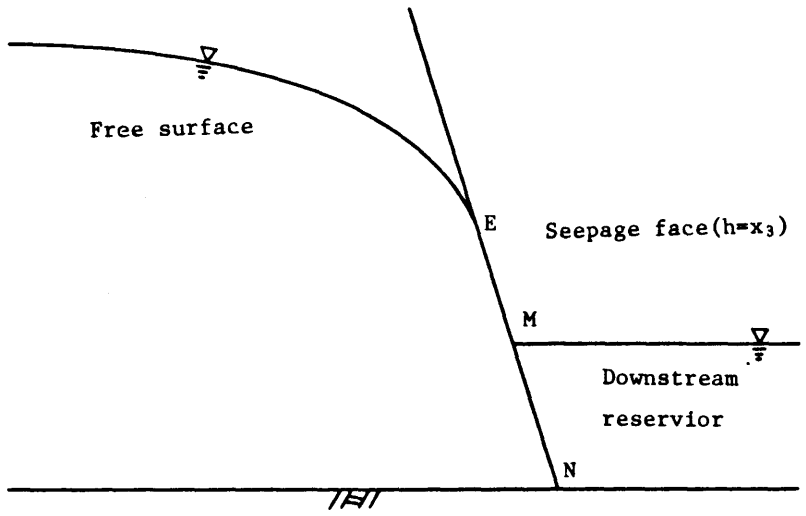

Fig.2.5 Seepage face

Along the seepage face, water emerges from the porous medium into the external space. The emerging water usually trickles down along the seepage face. (Fig.2.5). The seepage face is part of the boundary of the phreatic flow domain. Its geometry is generally known, except for its upper limit, which is also lying on the (*a priori*) unknown free surface. The location of this point is, therefore, part of the required solution.

The seepage face is exposed to the atmospheric pressure (neglecting the thin layer of water flowing above it). Actually, in order for water to emerge from the porous medium domain, the pressure just inside the boundary should be

somewhat higher than atmospheric. With ψ=0 along the seepage face, the boundary condition is described as

$$h = x_3 \qquad \text{on } S_e \tag{2.33}$$

2.5.3 Sources and Sinks

In addition to the movement of fluid that is caused by the initial and boundary conditions, fluid may be arbitrarily extracted from or added to the flow region at one or more locations. Such locations, usually of very small or infinitesimal spatial extent are called sinks or sources. Sources and sinks materially affect the mass balance expressed by Eq.(2.28). Hence their effects would have to be duly incorporated into Eq.(2.28), as will be done subsequently.

References

1) Bird, R.B., W.E.Stewart, and E.N.Lightfoot, Transport Phenomena, John Wiley, New York, 1960.

2) De Wiest: Flow through porous media, Academic Press, 1969, pp.95-96.

3) Bear, J: Dynamics of fluids in porous media, American elsevier Press, 1972, p.105.

4) Whitaker;S.; The equations of motion in porous media, Chem. Engin. Sci.,21, 1966, pp.291-301.

5) Whitaker, S.; Diffusion and dispersion in porous media, Amer, Inst. chem. Engin. Jour., 13, 1967, pp.420-427.

6) Whitaker,S.; Advances in theory of fluid motion in porous media, Industr. Engin. Chem., 61(12), 1969, pp.14-28.

7) Slattery,J.C.; Flow of viscoelastic fluids through porous media, Amer.Inst. Chem. Engin. Jour., 13, 1967, pp.1066-1071.

8) Slattery,J.C.,; Single-phase flow through porous media, Amer. Inst. Chem. Engin. Jour., 15(6), 1969, pp.866-872.

9) Slattery,J.C.; Momentum, Energy, and Mass Transfer in Continua, McGraw-Hill, New York, 1972.

10) Polubarinov-Kochina; Theory of Groundwater movement, Princeton Univ. Press (Princeton), 1962, pp.21-25.

11) Todd, D,K.; Groundwater hydrology, John Wiley Sons, Press,1959, pp47-48.

12) Rose,H.E.; On the resistance coefficient-Reynolds number relationship for fluid flow through a bed of granular material, Proc. Inst. Mech. Engrs., Vol.153, 1945, pp.154-168.

13) Swartzendruber,D.; Non-Darcy behavior in liquid saturated porous media, J.Geophys. Res. 67, 1962, pp.5205-5213.

14) Millor,R.J.,and Low,P.F.; Threshold for water flow in clay systems, Soil Sci. Soc. Amer. Proc. 27, 1963, pp.605-609.

15) Olson,H.W.; Deviations from Darcy's law in saturated clays, Soil. Sci. Soc. Amer. Proc. 27, 1965, pp135-140.

16) Childs,E.C. and Collis-George,N.C.: The Permeability of porous materials, Proceedings, Royal Society A201,1950,pp.392-405.

17) Richards,L.A.: Capillary conduction of liquids through porous systems, Physics, vol.1, 1931, pp.318-333.

18) Miller,E.E. and Miller,R.D.: Theory of capillary flow I, practical implications, Soil Sci.Soc.Amer.Proc.19, 1955, pp.267-271.

19) Miller,E.E. and Miller,R.D.: Theory of capillary flow II, experimental information, Soil Sci.Soc.Amer.Proc. 19, 1955, pp.272-275.

20) Topp,G.C. and Miller,E.E.,Hysteresis moisture characteristic and hydraulic conductivities for glass-bead media, Soil Sci.Soc.Amer.Proc. 30, 1966, pp.156-162.

21) Sokolinikoff,I.S. and R.M. Riedheffer: Mathematics of physics and modern Engineering, McGraw-Hill, New York, 1966.

22) Klute,A.: A numerical method for solving the flow equation for water in in unsaturated materials, Soil Sci.,73,1952,pp.105-106.

23) Ligon,J.T. et al.: Unsteady-state drainage of fluid from a vertical column of porous material, J.Geophys. Res.,67,1962,pp.5199-5204.

24) Philip,J.R.: On solving the unsaturated flow equation; 1, the flux-concentration relation, Soil Sci., 116(5),1973,pp.328-335.

25) Narasimhan,T.N. and P.A.Witherspoon: Numerical model for saturated-unsaturated flow in deformable porous media, part 1;theory, Water Reso. Res., Vol.12,1976,pp.57-64.

26) Biot,M.A.: General theory of three-dimensional consolidation, Jour. Appl. Phys.,1941,pp.12-155.

CHAPTER 3

FINITE ELEMENT ANALYSIS OF FLOW IN SATURATED-UNSATURATED SOILS

3.1. Introduction

The application of the finite element method to flow analysis problems is a relatively recent development but, nevertheless, a significant literature on the topic has already emerged.

The finite difference method has been mainly used before the development of the finite element method in solving the flow problems numerically. One might reasonably inquire what advantages the finite element method has when compared with the finite difference methods. For simple regular mesh networks, the difference equations derived by the two methods are identical. However, for certain complex problems, the finite element method has several advantages. Boundary conditions are handled naturally by the method in contrast to the finite difference method, where special formulas have to be developed for the boundaries in many instances. The mesh size can be varied readily. Small elements may be used in areas of rapid change and large elements may be used where variations are less severe. Also the presence of inhomogeneities and anisotropy is taken into account quite easily.

Although a lot of seepage flow problems have been solved by the finite element method, most of them[1)2)] are merely concerned with ground water in the saturated region, so that the unsaturated region (capillary zone and absorbed water zone) above the free surface is not considered in the calculation. In the movement of the ground water the water content and permeability of the unsaturated region usually play very important roles as well as the storage coefficient and permeability of the saturated region. Particularly in analyzing the problems of the free surface change due to the water rising or infiltration of rain fall, the method which is merely concerned with the saturated

region may not be possible to obtain the satisfactory results.

Problems of seepage in the unsaturated region lead to quasilinear partial differential equations that are extremely difficult to solve by analytical methods. Only one-dimensional flow problems were solved by Youngs[3] and Philip.[4] Many attempts to solve these two- or three-dimensional equations by the finite techniques have been reported in the literature.[5)6)] The finite element method was first applied to problems involving saturated-unsaturated flow in porous media by Neuman[7)8)] but not many researches have been done yet.

Boundary conditions in the form of prescribed heads and non-zero quality of flow can be dealt with easily in the conventional finite element formulation. However, more difficult circumstances arise when there is a free surface in the unconfined flow problem. Free surface for steady flow is determined usually by using iterative procedures. The location of the free surface is first guessed and then modified successively on the basis of the values of fluid heads computed at each step of iteration, and the procedure is carried out until the movements of the free surface become essentially negligible. Location of the transient free surface is more difficult and a number of procedures have been proposed.[1)2)]

But, these methods have fundamental limitations in determination of free surface. The first limitation is that it is impossible to solve the behaviors of flow through an earth dam when water raised at the upstream side in the case which there is no saturated zone at the bottom of earth dam or bank. It is the reason that these methods, as indicating above, treat the ground water in the saturated region, so that only the saturated region is divided into finite elements.

The second limitation is that it is impossible to solve the behavior of flow in an inhomogeneous domain, such as illustrated on Fig.3.1(a). In this case, for example, one solved after these method the change of transient flow

pattern due to the sudden drawdown on the righthand side. The result must become as shown in Fig.3.1(b).

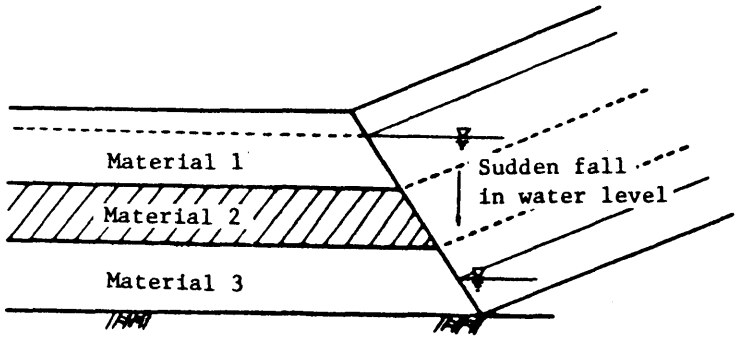

Fig.3.1(a) Flow in an inhomogeneous domain

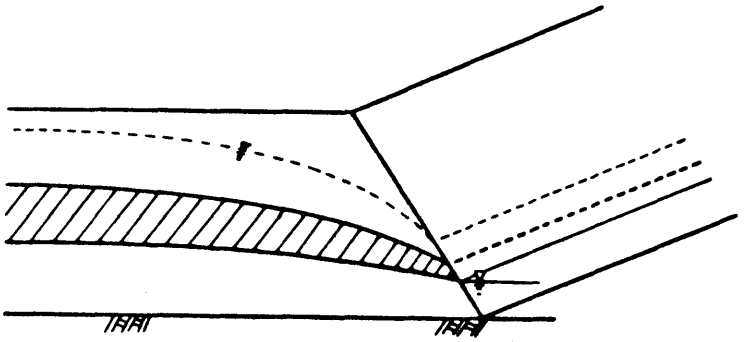

Fig.3.1(b) Result of calculation of Fig.3.1(a)

This result is distinctly in error at the point that the geological conditions are changed in the coordinates. This error is caused by the method of determination of free surface after these method.

On the other hand, the finite element method with saturated-unsaturated flow does not recognize this cumbersome difficulty and can easily handle irregularly shaped flow region. A general procedure proposed by Neuman shows that the so-called free surface is located by finding points where the pressure

head vanishes and the surface of seepage is handled by a special iterative method. With this method one will be able to have a clue to solve the problems, which are almost impossible to be solved by the conventional method, such as behaviors of flow through an earth dam when water raised at the upstream side, flow through an embankment when the water level of a river changed and ground water level fractuation due to water injection to a well.

In this chapter, finite element method will be used to solve the initial-boundary value problems of saturated-unsaturated groundwater motion in two-dimensional, axisymmetric and three-dimensional region.

3.2 Two-Dimensional Finite Element Analysis

3.2.1 Application of Galerkin method

Variational and weighted residual methods have been employed commonly for arriving at a finite element representation. Variational procedures were primarily used in the initial stages of the finite element method. However, weighted residual procedures, particularly the Galerkin method, have been found to be more general for the flow problem which is governed by non-linear equations.[9)10)] The possible advantage of such methods is that:

(a) The search for a 'functional' equivalent to the known differntial equation is made unnecessary.

(b) That the methods can be extended to a range of problems for which a 'functional' may not exist, or has not been discovered.

These approaches will be outlined here. Let us consider a problem of solving approximately a set of differential equations which the unknown function$\{\phi\}$ has to satisfy in the region V.

The governing equation will be written as

$$A(\{\phi\}) = 0 \tag{3.1}$$

and its boundary condition as

$$C\ (\ \{\phi\}\ ) = 0 \tag{3.2}$$

this having to be satisfied on boundary S.

If a trial function which satisfies the boundary conditions is written in the general form

$$\{\phi\}_a = [\ N\ ]\{\phi\} \tag{3.3}$$

in which, as before, [N] are prescribed functions of co-ordinates and $\{\phi\}$ is a set of n parameters, then in general

$$A\ (\ \{\phi\}_a\ ) = R \neq 0 \tag{3.4}$$

The best solution will be one which in some sense reduces the residual R to a least value at all point of V.

An obvious way to achieve this is to make use of the fact that if R is identically zero everywhere, then

$$\int_V WRdV = 0 \tag{3.5}$$

where W is any function of the coordinates. If the number of unknown parameters $\{\Phi\}$ is n then if n, linearly independent, functions W_i are chosen we can write a suitable number of simultaneous equations as

$$\Omega_n(\Phi) = \int_V W_i RdV = \int W_i A([\ N\ ]\{\Phi\})dV = 0 \tag{3.6}$$

from which $\{\Phi\}$ can be found. In other words, the function $\Omega_n(\Phi)$ must vanish for each value of n. W_i is the weighting function.

Galerkin method is that the weighting function is made equal to the shape function defining th approximation, i.e., $W_i=N_i$. This process leads in general to the best approximation.[9)]

Eq.(2.28) is a non-linear differential equation, in which K_{ij} and C are

dependent upon the unknown parameter ψ. And the finite element formulation of this equation may be done most easily with the Galerkin method.

Rewriting Eq.(2.28) in the vector form, this equation becomes,

$$\vec{\nabla}\cdot A\vec{\nabla}h - B\frac{\partial h}{\partial t} = 0 \tag{3.7}$$

where

$$A = K(\psi)$$

$$B = C(\psi) + \beta S_s$$

$$h = \psi + x_3$$

Initial and boundary conditions are also rewitten as follows;

(A) Initial condition

$$h(x_i,0) = H_0(x_i)$$

(B) Boundary conditions

(a) Prescribed head boundary

$$h(x_i,t) = H_b(x_i,t)$$

(b) Prescribed flux boundary

$$\frac{\partial h}{\partial \vec{n}} = V(x_i,t)$$

(3.8)

where H_0, H_b, V are prescribed functions and $\vec{n}$ is the unit outer normal vector.

3.2.2 Formulation by weighted residual procedure

At the beginning, one chooses a trial function h which satisfies the given initial and boundary conditions as follows.

$$h(x_i,t) = N_n(x_i)h_n(t) \qquad (n=1,2,\cdots) \tag{3.9}$$

where $N_n(x_i)$ is a set of linearly dependent coordinates functions and $h_n(t)$

are time-dependent coefficients yet to be determined.

Since Eq.(3.9) may not completely satisfy Eq.(3.7) with Eq.(3.8), substitution of Eq.(3.9) into Eq.(3.7) may produce a residual R such as

$$\vec{\nabla}\cdot A\vec{\nabla}(N_n(x_i)h_n(t)) - B\frac{\partial}{\partial t}(N_n(x_i)h_n(t)) = R \tag{3.10}$$

In order to find the best solution, one must choose a trial function h such that the residual R vanishes everywhere in the flow domain.

Following the weighted residual procedure, integration of Eq.(3.10) over the entire flow domain V with a set of weight functions $W_k(x_i)$ yields

$$\int_V W_k(x_i)RdV = \int_V W_k(x_i)[\vec{\nabla}\cdot A\vec{\nabla}\{N_n(x_i)h_n(t)\} - B\frac{\partial}{\partial t}\{N_n(x_i)h_n(t)\}]dV = 0 \tag{3.11}$$

Since the Galerkin method sets the weight functions $W_k(x_i)$ equal to the shape functions $N_k(x_i)$, Eq.(3.11) becomes

$$\int_V N_n[\vec{\nabla}\cdot A\vec{\nabla}N_m h_m - B\frac{\partial}{\partial t}(N_m h_m)]dV = 0 \tag{3.12}$$

By using Green-Gauss theorem,[11]

$$\int_V A\vec{\nabla}N_n\cdot\vec{\nabla}N_m h_m dV - \oint_S AN_n\vec{\nabla}N_m h_m\cdot\vec{n}d\sigma + \int_V BN_n\frac{\partial N_m h_m}{\partial t}dV = 0 \tag{3.13}$$

where the entire flow domain is discretized into N elements of the finite elements of the finite element mesh, Eq.(3.13) is also applied to the each element (V_n^e) of the mesh, i.e.,

$$V_n^e(h_m N_m^e) = \int_{V^e} N_n^e[\ \vec{\nabla}\cdot A\vec{\nabla}N_m^e h_m - B\frac{\partial N_m^e h_m}{\partial t}\ ]dV \tag{3.14}$$

For the entire flow domain,

$$\sum_{i=1}^{N}\left[\int_{V_i} A_i \vec{\nabla}N_n \cdot \vec{\nabla}N_m h_m dV + \int_{V_i} B_i N_n \frac{\partial N_m h_m}{\partial t} dV - \oint_{S_i} A_i N_n \vec{\nabla}N_m h \cdot \vec{n} d\sigma\right] = 0 \qquad (3.15)$$

At this moment, we define the permeability tensor $K_{ij}(\psi)$ as

$$K_{ij}(\psi) = K^s_{ij} K_r(\psi) \qquad (3.16)$$

where K^s_{ij} is the permeability tensor at the fully saturated condition, $K_r(\psi)$ is a function of pressure head ψ or a function of volumetric moisture content θ and $0 \leq K_r \leq 1$. In saturated region, K_r becomes 1.

It is assumed that the permeability tensor (K^s_{ij}) and the specific storage (S_s) are constant in each element while $K_r(\psi)$ and $C(\psi)$ vary linearly according to

$$K_r = K^r_\ell N^e_\ell \qquad (3.17)$$

$$C = C_\ell N^e_\ell \qquad (3.18)$$

where ℓ stands for the corners of the triangle as shown in Fig.3.2.

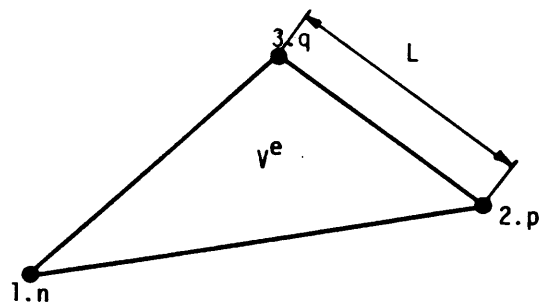

Fig.3.2 Single triangular element

For a triangular element as shown in Fig.3.3, Eq.(3.15) is deduced to a set of quasilinear first-order differential equations

$$A_{nm}\psi_m + F_{nm}\frac{d\psi_m}{dt} = Q_n - B_n - D_n \qquad n,m = 1,2,\cdots,N \tag{3.19}$$

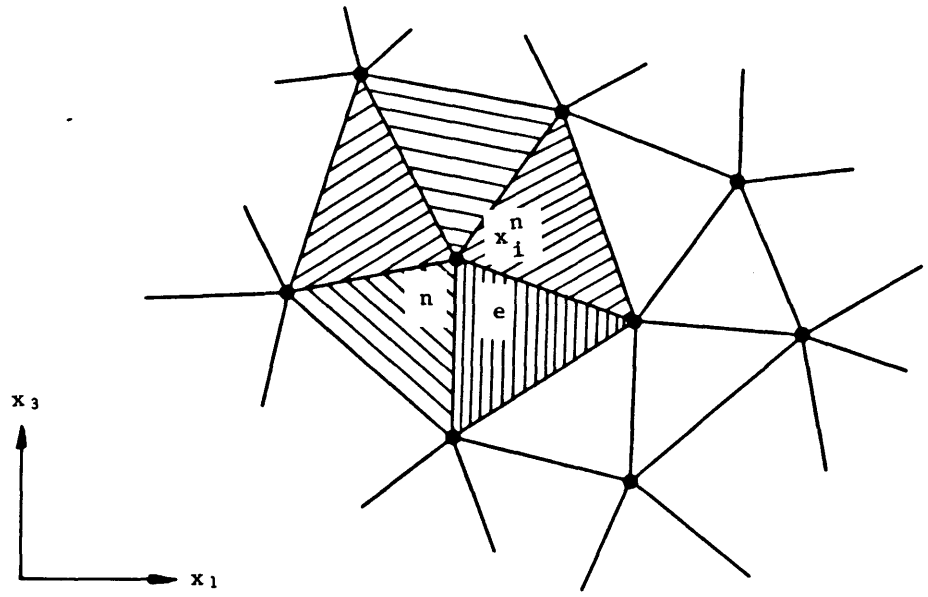

Fig.3.3 Two-dimensional triangular elements

where, for a vertical cross-section described by the coordinates x_1 and x_3,

$$A_{nm} = \sum_{e=1}^{N} K_\ell^r K_{ij}^s \int_V N_\ell^e \frac{\partial N_n^e}{\partial x_i} \cdot \frac{\partial N_m^e}{\partial x_j} dV$$

$$= \sum_e \frac{\alpha}{4\Delta} \bar{K}_r [\, K_{11}^s b_n b_m + K_{13}^s (b_n C_m + b_m c_n) + K_{33}^s c_n c_m \,]$$

(3.20)

$$F_{nm} = \sum_{e=1}^{N} \int_{V^e} (C_\ell N_\ell^e N_n^e + N_n^e \beta S_s) dV$$

$$\left.\begin{aligned} &= \sum_{e} \frac{\alpha\Delta}{12} [(2C_n + C_p + C_q) + 4\beta S_s] \quad : \quad (n=m) \\ &= 0 \qquad\qquad\qquad\qquad\qquad\qquad\quad : \quad (n\neq m) \end{aligned}\right\} \tag{3.21}$$

$$Q_n = -\sum_{e} \phi \int_{S^e} V N_n^e d\sigma = -\sum_{e} \alpha \frac{(LV)_n}{2} \tag{3.22}$$

$$B_n = \sum_{e=1}^{N} K_\ell^r K_{i_3} \int_{V^e} N_\ell^e \frac{\partial N_n^e}{\partial x_i} dV = \sum_{e} \frac{\alpha}{2} \bar{K}^r (K_{i_3}^s b_n + K_{3_3}^s c_n) \tag{3.23}$$

$$D_n = \sum_{e} \int_{V^e} S N_n^e dV \tag{3.24}$$

where b_n and c_n are the values dependent on coordinates. The subscripts n, p, q refer to the three corners of each triangle as shown in Fig.3.2, Δ is the area of the triangle, α=1 for plane flow, $\bar{K}^r$ is the average relative conductivity given by $\bar{K}^r = (K_n^r + K_p^r + K_q^r)/3$. The term $(LV)_n$ represents the flow rate across any side of the triangle, of length L, which includes nodal point n, V is assumed to be uniform along L.

3.2.3 Integration over time

The matrix differential equations obtained in the previous sections are of

a type in which specified values of the functions and, when necessary, of its first time derivatives at the start, uniquely define this function throughout the time interval.

Such a category of problems known as 'initial value' or 'marching' can be solved by writing suitable recurrence relations. From these a step-by-step process allows a full solution of the problems.

The recurrence relation can be established in different ways. For instance, a finite difference scheme may be used directly or the Glerkin weighted residual process applied within each interval. However, since general use of the second process will require further studies, the conventional semidiscretization procedure, i.e., finite difference is adopted to integrate Eq.(3.19) in time domain.

If the entire flow system remains unsaturated at all times, good results can be obtained by employing the time-centered scheme (Crank-Nicolson scheme),[12]

$$\left(A_{nm}^{k+1/2} + \frac{2}{\Delta t^k} F_{nm}^{k+1/2} \right) \psi_m^{k+1} = 2Q_n^{k+1/2} - 2B_n^{k+1/2} - 2D_n^{k+1/2}$$

$$- \left(A_{nm}^{k+1/2} - \frac{2}{\Delta t^k} F_{nm}^{k+1/2} \right) \psi_m^k$$

$$(n,m=1,2,\cdots N) \qquad (3.25)$$

where k represents the time $t=t^k$ and $\Delta t=t^{k+1}-t^k$. In order to evaluate the coefficients in Eq.(3.25), one must know the values of $\psi_n^{k+1/2}$ at $t^{k+1/2}=t^k+\Delta t^k/2$. At the beginning of each time step, these are predicted by linear extrapolation from previously calculated values according to

$$\psi_n^{k+1/2} = \psi_n^k + \frac{\Delta t^k}{2\Delta t^{k-1}} \left(\psi_n^k - \psi_n^{k-1} \right) \qquad (3.26)$$

The resulting set of simultaneous linear algebraic equations is then solved by a highly efficient Gauss elimination method[9] for the values of ψ_n^{k+1} at all nodes.

Due to the nonlinear nature of Eq.(3.25), these results must be improved by an iterative process. At each iteration, the most recent values of ψ_n^{k+1} are used to obtain an improved estimate of $\psi_n^{k+1/2}$ from

$$\psi_n^{k+1/2} = 1/2(\psi_n^k + \psi_n^{k+1}) \tag{3.27}$$

After having reevaluated the coefficients, the equations are again solved by Gauss elimination for improved values of ψ_n^{k+1}. The iterative procedure continues as long as it is necessary to achieve a satisfactory degree of convergence.

If a part of the system is saturated and S_s in this part is zero, the values of F_{nm} corresponding to nodal points in the saturated zone vanish because C is zero, and the governing equations there become elliptic. This means that sudden changes in boundary conditions around the saturated zone have an instantaneous effect on the values of ψ everywhere in this zone, and ψ is no longer a continuous function of time. For example, by imposing a certain boundary condition at time $t=t^k$, all values of ψ in the saturated zone change instantaneously and the values of ψ_n^k at the start of the time step, Δt^k, become unknown. Thus, the right-hand side of Eq.(3.25) is unknown, and the equations cannot be solved.

To overcome this problem, one must adopt a fully implicit backward difference scheme in terms of ψ,

$$\left(A_{nm}^{k+1/2} + \frac{1}{\Delta t_k} F_{nm}^{k+1/2} \right) \psi_m^{k+1} = Q_n^{k+1/2} - B_n^{k+1/2} - D_n^{k+1/2} + \frac{1}{\Delta t^k} F_{nm}^{k+1/2} \psi_m^k \tag{3.28}$$

3.2.4 Treatment of seepage faces

A seepage face is an external boundary of the saturated zone where water leaves the system and ψ is uniformly zero. Under transient conditions, the length of the seepage face varies with time in a manner that cannot be predicted a priori. If one treats the seepage face as a prescribed pressure head boundary with $\psi=0$, the length of this face remains fixed, and this is contrary to the reality of transient flow. On the other hand, the seepage face cannot be treated as a prescribed flux boundary because the values of Q_n there are generally unknown. How, then, should a seepage face be treated?

The inherent difficulty in treating seepage faces has been overcome in the present work owing to the ease with which prescribed pressure head and prescribed normal flux boundary conditions can be assigned at each node with the finite element method. The proposed iterative procedure would be quite cumbersome to use with conventional finite difference techniques, particularly in anisotropic media with irregularly shaped seepage faces, because prescribed flux boundaries are relatively difficult to handle.

Reference is made to all nodes which, at any stage of the calculation, can belong to a given seepage face by having zero values of ψ_n and negative value of Q_n (recall that Q_n is negative when the flow at node n is directed out of the system). Suppose that, knowing the position at time t^{k+1}. During the first iteration, ψ is set equal to zero along the initial length of the seepage face and the latter is treated as a prescribed ψ boundary. At the same time, Q is set equal to zero at all nodes with $\psi<0$ and this segment is treated as a prescribed flux boundary. The solution is expected to yield negative values of Q at nodes where ψ is prescribed to be zero, and negative values of ψ at nodes where Q is prescribed to be zero. If, instead, a positive value of Q is encoun-

tered at a node where ψ=0, the value of Q there is set equal to zero and, in the next iteration, this node is treated as a prescribed flux boundary.

On the other hand, if a positive value of ψ is encountered at a node where Q=0, the value of ψ there is set equal to zero and, in the next iteration, this node is treated as a prescribed pressure head boundary. Experience has shown that in order for the solution to converge, this modification of the boundary conditions should always proceed sequentially from node to node, starting at the saturated end of the seepage face.

In addition, after having set Q equal to zero at any node during a given iteration, Q at all the subsequent nodes must also be set equal to zero. The iterative process continues in the manner described earlier until a sufficient degree of convergence is achieved at each node in the network.

It shoud be noted that due to the ease with which prescribed flux boundary conditions are treated in the finite element method, the handling of seepage faces is considerably more simple than in the finite difference approach.

3.3 Axisymmetric Finite Element Analysis

3.3.1 Finite element discretization

The application of the finite element method to certain axisymmetric saturated-unsaturated flows through porous media is presented in this section. The typical problem of radial flow to a well penetrating an unconfined aquifer is shown in Fig.3.4. The formulation of the general axisymmetric flow problem using finite element analysis will first be discussed, after which the approach will be used to solve the axisymmetric flow to a well.

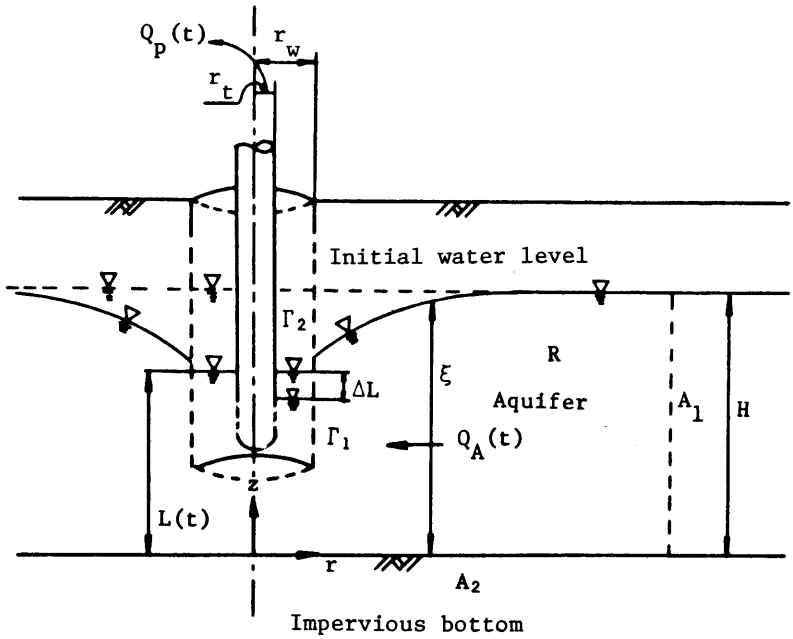

Fig.3.4 Flow through an unconfined aquifer to a well with storage

The physical situation is one of three-dimensional flow with axial symmetry. Thus, cylindrical coordinates are the natural selection. The medium will be devided into concentric rings of constant triangular cross-section in the axisymmetric case (Fig.3.5). In this case, the solution will be a function of only two space coordinates, r and z. As shown in Fig.3.5, Δ represents the cross-section of an axisymmetric annular element of volume V, then, the functions N_n for any given element remain independent of the position of this element. The integral of $N_m N_n$ over the volume of the element in Eq.(3.20) can therefore be written as

$$\int_V N_n N_m dV = \int_0^{2\pi} \left[\int_\Delta N_n N_m d\Delta \right] \bar{r} d\theta = 2\pi\bar{r} \int_\Delta N_n N_m d\Delta \qquad (3.29)$$

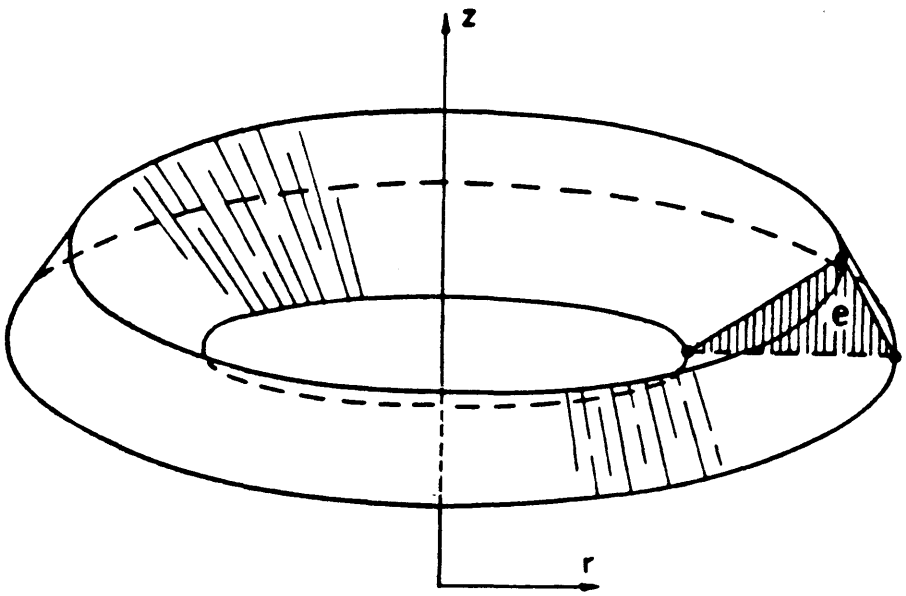

Fig.3.5 Axisymmetric element with constant triangular cross-section.

where $\bar{r}$ is the average value of r for the triangle

$$\bar{r} = \frac{r_1+r_2+r_3}{3} \tag{3.30}$$

this becomes simply

$$\int_V N_n N_m dV = \begin{cases} (2\pi\bar{r})\frac{\Delta}{12} & \text{if } n\neq m \\ (2\pi\bar{r})2\cdot\frac{\Delta}{12} & \text{if } n=m \end{cases} \tag{3.31}$$

then, the finite element analysis for axisymmetric flow is simply formulated by using the factor $\alpha=2\pi\bar{r}$ in Eqs.(3.20),(3.21),(3.22) and (3.23).

3.3.2 Axisymmetric flow to a well

When a well has been completed in an unconfined aquifer and discharges at a rate $Q_p(t)$, flow into the well bore is not uniform along its length. As shown

in Fig.3.6, the boundaries along the well bore consist of an upper segment (Γ_2) across which no water can flow into the well due to the unsaturated state of the porous medium, a seepage face (S), and a boundary (Γ_1) where the total head at any instant of time is uniform and equal to the elevation of the water level, L(t). The total discharge from the pump, $Q_p(t)$, consists of two components, the discharge from the aquifers into the well, $Q_A(t)$, and the amount of discharge contributed from well storage.

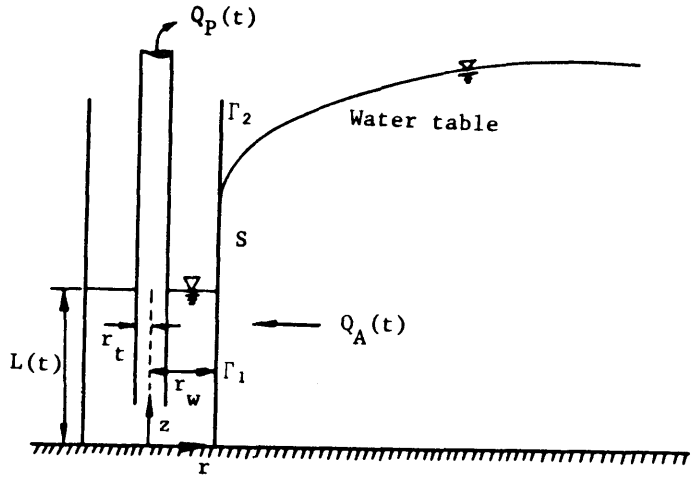

Fig.3.6 Diagram of well in unconfined aquifer.

If one assumes that L, Q_p, and Q_A vary linearly during each time step, then a material balance calculation for the well leads to

$$\Delta L = \frac{\Delta t}{\pi(r_w^2 - r_t^2)} \left(Q_p^{k+1/2} - Q_A^{k+1/2} \right) \tag{3.32}$$

where ΔL is the change in the height of the water level in the well during Δt, r_w is the effective radius of the well, and r_t is the outside radius of the production pipe.

The total discharge from the pump can be regulated at the ground surface

by controling the capacity of the pump. In this case, $Q_p(t)$ is a prescribed function of time and Eq.(3.32) involves only two unknowns, ΔL and $Q_A^{k+1/2}$.

During each time step, an estimate of ΔL for the first iteration is obtained from Eq.(3.32) on the basis of $Q_A^{k+1/2}$ and $Q_p^{k+1/2}$, and $L_{old}^{k+1/2}$ in Eq.(3.33) below is set equal to L^k. The average value of the water level in the well for the time step is then adjusted according to

$$L_{new}^{k+1/2} = \lambda L_{old}^{k+1/2} + (1-\lambda)(L^k+L) \; ; \qquad 0.5 \leq \lambda \leq 1 \tag{3.33}$$

where λ is an under-relaxation factor. Experience has shown that λ should increase as Q_A approaches Q_p and should usually exceed 0.7. During subsequent iterations, Eq.(3.32) is used repeatedly with Eq.(3.33) until a desired degree of convergence is achieved for ψ_n at all nodes. At the end of the time step, the value of L^{k+1} is calculated as $L_{new}^{k+1/2} + \Delta L/2$.

3.4 Three-Dimensional Finite Element Analysis

3.4.1 Isoparametric elements

In sections 3.2, 3.3, emphasis was placed on the solution of the relatively simple two-dimensional problems. However, the method is equally applicable in the more important field of three-dimensional flow. The purpose of this section, therefore, is to consider the extension of the finite element method so that a general three-dimensional saturated-unsaturated aquifer system can be considered. Three-dimensional problems embrace clearly all the practical cases, though for some, the various two-dimensional approximations give an adequate and more economical 'model'.

The simplest two-dimensional continuum element in sections 3.2, 3.3 was a triangle. In three dimensions its equivalent is a tetrahedron, an element with

four nodal corners. But a difficulty not encountered previously is presented. It is one of ordering of the nodal numbers and, in fact, of a suitable representation of a body divided into such elements. It is immediately obvious that the number of simple tetrahedral elements which has to be used to achieve a given degree of accuracy has to be very large. This will result in very large numbers of simultaneous equations in practical problems, which may place a severe limitation on the use of the method in practice. Further the band width of the resulting equation system becomes large leading to big computer storage requirements. Therefore, in case of three-dimensional analysis, isoparametric element is adopted to reduce total computations and data preparation effort. A detailed formulation of the complete family of isoparametric elements is given in the text by Zienkiewicz.[9)13)] Then, only the essentials will be summarised in this section as the element characterictics are later utilized for computing the problem of saturated-unsaturated flow.

The volume defined the flow domain is first subdivided into a number of elements interconnected at a discrete number of points or nodes. In this study cubic isoparametric elements shown in Fig.3.7 are used as these can if desired permit close approximation to curved surface.[14)] Let the variable ψ throughout the domain be approximated by:

$$\psi = \sum_{i=1}^{i=n} N_i \psi_i \qquad (3.34)$$

in which N_i' are the appropriate interpolation functions defined piecewise element by element, ψ_i are the nodal values of ψ in the discretised domain and n is the number of degree of freedom.

These are the very same methods as using in section 3.2 to formulate the governing equations into finite element discretization except for adoptting element shape functions (or interpolation functions).

Consider the cubic isoparametric element shown in Fig.3.7 with positions

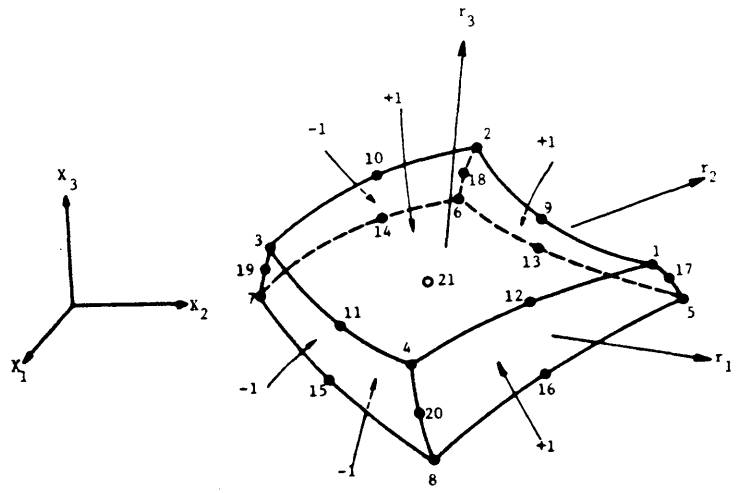

Fig.3.7 Three-dimensional continuum element node numbering convention

defined within it by curvilinear co-ordinates r_i (which take up values of ± 1 on opposite faces). Let these co-ordinates be related to the cartesian x_j by expressions:

$$\{x_j\} = \Sigma N'^{i}(r_k)x_j^i \qquad (i=1,2,\cdots\cdots,21) \tag{3.35}$$

where x_j^i is the nodal co-ordinates and $N'^{i}(r_k)$ are given by known functions of r_k (the interpolation functions corresponding to node i of element listed in Table 3.1[15]).

To perform finite element analysis the matrices A_{nm} in Eq.(3.20), etc., have to be found. These will be of the form

$$E_{nm} = K_{ij}\int_{V^e} K_\ell^r N'^{e}_\ell \frac{\partial N'^{e}_n}{\partial x_i}\frac{\partial N'^{e}_m}{\partial x_j}\,dV^e \tag{3.36}$$

in which the expression $\partial N'^{e}_n/\partial x_i$ depends on derivatives with respect to local co-ordinates.

Table 3.1 Interpolation function

		$\partial h/\partial r_1$	$\partial h/\partial r_2$	$\partial h/\partial r_3$
N'_1	$(1/8)RST$	$(1/8)ST$	$(1/8)RT$	$(1/8)RS$
N'_2	$(1/8)\bar{R}ST$	$-(1/8)ST$	$(1/8)\bar{R}T$	$(1/8)\bar{R}S$
N'_3	$(1/8)\bar{R}\bar{S}T$	$-(1/8)\bar{S}T$	$-(1/8)\bar{R}T$	$(1/8)\bar{R}\bar{S}$
N'_4	$(1/8)R\bar{S}T$	$(1/8)\bar{S}T$	$-(1/8)RT$	$(1/8)R\bar{S}$
N'_5	$(1/8)RS\bar{T}$	$(1/8)S\bar{T}$	$(1/8)R\bar{T}$	$-(1/8)RS$
N'_6	$(1/8)\bar{R}S\bar{T}$	$-(1/8)S\bar{T}$	$(1/8)\bar{R}\bar{T}$	$-(1/8)\bar{R}S$
N'_7	$(1/8)\bar{R}\bar{S}\bar{T}$	$-(1/8)\bar{S}\bar{T}$	$-(1/8)\bar{R}\bar{T}$	$-(1/8)\bar{R}\bar{S}$
N'_8	$(1/8)R\bar{S}\bar{T}$	$(1/8)\bar{S}\bar{T}$	$-(1/8)R\bar{T}$	$-(1/8)R\bar{S}$
N'_9	$(1/4)\overset{*}{R}ST$	$-(1/2)r_1ST$	$(1/4)\overset{*}{R}T$	$(1/4)\overset{*}{R}S$
N'_{10}	$(1/4)\bar{R}\overset{*}{S}T$	$-(1/4)\overset{*}{S}T$	$-(1/2)r_2\bar{R}T$	$(1/4)\bar{R}\overset{*}{S}$
N'_{11}	$(1/4)\overset{*}{R}\bar{S}T$	$-(1/2)r_1\bar{S}T$	$-(1/4)\overset{*}{R}T$	$(1/4)\overset{*}{R}\bar{S}$
N'_{12}	$(1/4)R\overset{*}{S}T$	$(1/4)\overset{*}{S}T$	$-(1/2)r_2RT$	$(1/4)R\overset{*}{S}$
N'_{13}	$(1/4)\overset{*}{R}S\bar{T}$	$(1/2)r_1S\bar{T}$	$(1/4)\overset{*}{R}\bar{T}$	$-(1/4)\overset{*}{R}S$
N'_{14}	$(1/4)\bar{R}\overset{*}{S}\bar{T}$	$-(1/4)\overset{*}{S}\bar{T}$	$-(1/2)r_2\bar{R}\bar{T}$	$-(1/4)\bar{R}\overset{*}{S}$
N'_{15}	$(1/4)\overset{*}{R}\bar{S}\bar{T}$	$-(1/2)r_1\bar{S}\bar{T}$	$-(1/4)\overset{*}{R}\bar{T}$	$-(1/4)\overset{*}{R}\bar{S}$
N'_{16}	$(1/4)R\overset{*}{S}\bar{T}$	$(1/4)\overset{*}{S}\bar{T}$	$-(1/2)r_2R\bar{T}$	$-(1/4)R\overset{*}{S}$
N'_{17}	$(1/4)R\overset{*}{S}T$	$(1/4)\overset{*}{S}T$	$(1/4)R\overset{*}{T}$	$-(1/2)r_3RS$
N'_{18}	$(1/4)\bar{R}\overset{*}{S}T$	$-(1/4)\overset{*}{S}T$	$(1/4)\bar{R}\overset{*}{T}$	$-(1/2)r_3\bar{R}S$
N'_{19}	$(1/4)\bar{R}\overset{*}{S}\bar{T}$	$-(1/4)\overset{*}{S}\bar{T}$	$-(1/4)\bar{R}\overset{*}{T}$	$-(1/2)r_3\bar{R}\bar{S}$
N'_{20}	$(1/4)R\overset{*}{S}\bar{T}$	$(1/4)\overset{*}{S}\bar{T}$	$-(1/4)R\overset{*}{T}$	$-(1/2)r_3R\bar{S}$
N'_{21}	$\overset{***}{RST}$	$-(2)r_1\overset{**}{ST}$	$-(2)r_2\overset{**}{RT}$	$-(2)r_3\overset{**}{RS}$

$R=1+r_1$	$\bar{R}=1-r_1$	$\overset{*}{R}=1-r_1^2$
$S=1+r_2$	$\bar{S}=1-r_2$	$\overset{*}{S}=1-r_2^2$
$T=1+r_3$	$\bar{T}=1-r_2$	$\overset{*}{T}=1-r_3^2$

To evaluate this matrices it must be noted that two transformations are necessary. In the first place as N_i is defined in terms of local (carvilinear) co-ordinates it is necessary to devise some means of expressing the global derivatives of the type occurring in Eq.(3.36) in terms of local derivatives.

In the second place the element of volume (or surface) over which the integration has to be carried out needs to be expressed in terms of the local co-ordinates with an appropriate change of limits of integration.

Consider for instance the set of local co-ordinates r_i and a corresponding set of global co-ordinates x_i. By the usual rules of partial differentiation one can write for instance the r_1 derivative as

$$\frac{\partial N_i}{\partial r_1} = \frac{\partial N_i}{\partial x_1}\frac{\partial x_1}{\partial r_1} + \frac{\partial N_i}{\partial x_2}\frac{\partial x_2}{\partial r_1} + \frac{\partial N_i}{\partial x_3}\frac{\partial x_3}{\partial r_1} \tag{3.37}$$

Performing the same differentiation with respect to the other two co-ordinates and writing in matrix form one has

$$\begin{Bmatrix} \frac{\partial N_i}{\partial r_1} \\ \frac{\partial N_i}{\partial r_2} \\ \frac{\partial N_i}{\partial r_3} \end{Bmatrix} = \begin{bmatrix} \frac{\partial x_1}{\partial r_1}, & \frac{\partial x_2}{\partial r_1}, & \frac{\partial x_3}{\partial r_1} \\ \frac{\partial x_1}{\partial r_2}, & \frac{\partial x_2}{\partial r_2}, & \frac{\partial x_3}{\partial r_2} \\ \frac{\partial x_1}{\partial r_3}, & \frac{\partial x_2}{\partial r_3}, & \frac{\partial x_3}{\partial r_3} \end{bmatrix} \begin{Bmatrix} \frac{\partial N_i}{\partial x_1} \\ \frac{\partial N_i}{\partial x_2} \\ \frac{\partial N_i}{\partial x_3} \end{Bmatrix} = [J] \begin{Bmatrix} \frac{\partial N_i}{\partial x_1} \\ \frac{\partial N_i}{\partial x_2} \\ \frac{\partial N_i}{\partial x_3} \end{Bmatrix} \tag{3.38}$$

In the above, the matrix [J] is known as the Jacobian matrix.

To find now the global derivatives one inverts [J] and writes

$$\begin{Bmatrix} \frac{\partial N_i}{\partial x_1} \\ \frac{\partial N_i}{\partial x_2} \\ \frac{\partial N_i}{\partial x_3} \end{Bmatrix} = [J]^{-1} \begin{Bmatrix} \frac{\partial N_i}{\partial r_1} \\ \frac{\partial N_i}{\partial r_2} \\ \frac{\partial N_i}{\partial r_3} \end{Bmatrix} \tag{3.39}$$

In terms of the shape function defining the co-ordinate transformation [N'], the Jacobian matrix is written

$$[J] = [\Sigma \frac{\partial N^i}{\partial r_k} x^i_j] \tag{3.40}$$

Here, the Jacobian matrix has the following form:

$$J_{kj} = \Sigma \frac{\partial N^i}{\partial r_k} x^i_j \tag{3.41}$$

The inverse of [J] can be found

$$[J]^{-1} = \frac{1}{|J|} \begin{bmatrix} a_{11} & -a_{21} & a_{31} \\ -a_{12} & a_{22} & -a_{32} \\ a_{13} & -a_{23} & a_{33} \end{bmatrix} \tag{3.42}$$

where

$$\begin{aligned} |J| = & (J_{11}J_{22}J_{33} + J_{12}J_{23}J_{31} + J_{13}J_{21}J_{32}) \\ & - (J_{13}J_{22}J_{31} + J_{12}J_{21}J_{33} + J_{11}J_{23}J_{32}) \end{aligned} \tag{3.43}$$

and

$$a_{11} = \begin{vmatrix} J_{22} & J_{23} \\ J_{32} & J_{33} \end{vmatrix} \qquad a_{12} = \begin{vmatrix} J_{21} & J_{23} \\ J_{31} & J_{33} \end{vmatrix} \qquad a_{13} = \begin{vmatrix} J_{21} & J_{22} \\ J_{31} & J_{32} \end{vmatrix}$$

$$a_{21} = \begin{vmatrix} J_{12} & J_{13} \\ J_{32} & J_{33} \end{vmatrix} \qquad a_{22} = \begin{vmatrix} J_{11} & J_{13} \\ J_{31} & J_{33} \end{vmatrix} \qquad a_{23} = \begin{vmatrix} J_{11} & J_{12} \\ J_{31} & J_{32} \end{vmatrix}$$

$$a_{31} = \begin{vmatrix} J_{12} & J_{13} \\ J_{22} & J_{23} \end{vmatrix} \qquad a_{32} = \begin{vmatrix} J_{11} & J_{13} \\ J_{21} & J_{23} \end{vmatrix} \qquad a_{33} = \begin{vmatrix} J_{11} & J_{12} \\ J_{21} & J_{22} \end{vmatrix}$$

Then the inverse of [J] can be given

$$[J]^{-1} = [b_{ij}] \tag{3.44}$$

where

$$b_{ij} = (-1)^{i+j}\frac{1}{|J|}a_{ji}$$

By using Eqs.(3.39) and (3.44), it is possible to devise some means of expressing the global derivatives of the type in terms of local derivatives:

$$\left\{\frac{\partial N_m'}{\partial x_i}\right\} = [b_{ij}]\left\{\frac{\partial N_m'}{\partial r_j}\right\} \tag{3.45}$$

Interporating Eq.(3.45) into Eq.(3.36), the integrand in E_{nm} can be expressed in terms of local co-ordinate.

3.4.2 Numerical integration by Gauss quadrature

The transformation of the variables and region, with respect to which the integration is done, is achieved by the following

$$dx_1dx_2dx_3 = \det[J]dr_1dr_2dr_3 \tag{3.46}$$

which is valid irrespective of the number of co-ordinates used.

By using the inverse of [J], the evaluation of the element properties has been reduced to that of finding integrals of the form of Eq.(3.36). By transformation, this can be written as

$$E_{nm} = K_{ij}\int_{-1}^{1}\int_{-1}^{1}\int_{-1}^{1} K_{\ell}^{r}N_{\ell}'^{e}[b_{ik}]\left\{\frac{\partial N_n'}{\partial r_k}\right\}[b_{jk}]\left\{\frac{\partial N_m'}{\partial r_k}\right\}\det[J]dr_1dr_2dr_3 \tag{3.47}$$

To perform integration of the form indicated in Eq.(3.47), a Gaussian quadrature scheme is used. In this technique a polynomial f(x) of degree 2n-1 may be integrated exactly as the weighted mean of its H_i particular values of specified Gaussian point[16], that is,

$$I = \int_{-1}^{1}\int_{-1}^{1}\int_{-1}^{1} f(r_1,r_2,r_3)dr_1dr_2dr_3$$

$$= \sum_{m=1}^{n}\sum_{j=1}^{n}\sum_{i=1}^{n} H_m H_j H_i f(r_1^m, r_2^j, r_3^i) \qquad (3.48)$$

Table 3.2 shows the positions and weighting coefficients for Gaussian integration.

Table 3.2 Sampling poins and weights in Gauss-Legendre numerical integration

n	r_k^i	H_i
2	±0.57735 02692	1.00000 00000
3	±0.77459 66692	0.55555 55556
	0.00000 00000	0.88888 88889
4	±0.86113 63116	0.34785 48451
	±0.33998 10436	0.65214 51548
5	±0.90617 98459	0.23692 68851
	±0.53846 93101	0.47862 86705
	0.00000 00000	0.56888 88889

References

1) Tayor,G.S. et al.: Computer methods for transient analysis of water-table aquifers, Water Reso. Res., 5(1), 1969, pp.144-152.

2) Neuman,S.P., P.A.Witherspoon: Analysis of non-steady flow with a free surface using the finite element method, Water Reso. Res., 6(5), 1970, pp.889-897.

3) Youngs,E.G.: Moisture profiles during vertical infiltration, Soil Sci., 84, 1957, pp.283-290.

4) Philip,J.R.: The theory of infiltration;1, the infiltration equation and its solution, Soil Sci., 83, 1957, pp.345-357.

5) Rubin,J.: Theoretical analysis of two-dimentional transient flow of water in unsaturated soils, Soil Sci. Am. Proc., 32, 1968, pp.607-614.

6) Freeze,R.A.: Three-dimensional transient saturated-unsaturated flow in a ground water basin, Water Reso. Res., 7(2), 1971, pp.347-363.

7) Neuman,S.P.: Saturated-unsaturated seepage by finite elements, Proc., ASCE HY, Vol.99, No.12, 1973, pp2233-2250.

8) Neuman,S.P.: Galerkin method of analyzing non-steady flow in saturated-unsaturated porous media, Finite Element Method in Flow Problems, edited by C.Taylor, O.C.Zienkiewicz, R.H.Gallagher, John Wiley & Sons, Chap.19, 1974.

9) Zienkiewicz,O.C.: The Finite Element Method in Engineering Science, McGraw-Hill, New York, 1971.

10) Finlayson,B.A.: The Method of Weighted Residuals and Variational Principles, Academic Press, New York, 1972.

11) Sokolnikoff,I.S. and R.M.Riedheffer: Mathematics of Physics and Modern Engineering, McGraw-Hill, New York, 1966.

12) Richtmyer,R.D. and K.W.Morton. : Difference Method for Initial-value Problems. Wiley-Interscience, New York, 1967.

13) Zienkiewicz,O.C. et al.: Iso-parametric and associate elements families for two and three dimensional analysis, chapter 13, in Finite Element Methods in stress Analysis, ed. I.Holand and K.Bell, Techn. Univ. of Norway, Tapir Press, Norway, Trondheim, 1969.

14) Ergatoudis,J., Irons,B.M. and Zienkiewicz,O.C.: Curved isoparametric, "quadrilateral" elements for finite element analysis, Int.J. Solids Struct., 4; 1968, pp.32-42.

15) Bathe,K.J., H.Ozdemir, and E.L.Wilson: Static and dynamic geometric and material nonlinear analysis, Report No.UCSESM 74-4, Univ. of Calif.Berkeley, 1974.

16) Zienkiewicz,O.C., and Y.K.Cheung: The Finite Element Method in Structural and Continuum Mechanics, McGraw-Hill, New York, 1967, p.263.

CHAPTER 4

EXPERIMENTAL STUDY ON DETERMINING UNSATURATED PROPERTY OF SOIL

4.1 Introduction

The hydrologic behavior of soils is to a large extent determined by how the hydraulic conductivity of partially saturated soil varies widely as a function of the volumetric moisture content and/or the pressure head which is also a function of the volumetric moisture content as shown in Fig.4.1. These properties of soils must be known if the analysis of finite element method on flow through porous media is to be applied in field situations.

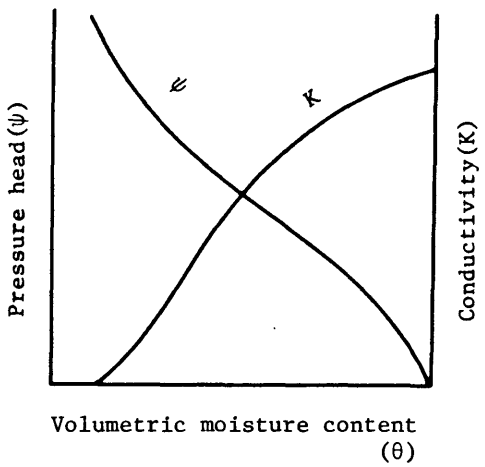

Fig.4.1 Unsaturated property of soil

Since there is no reliable way to predict these values from more fundamental soil properties, these properties must be measured experimentally. A number of techniques for measuring hydraulic conductivities have been reported in the

literature. Most methods are based on the solution of the one-dimensional continuity equation for steady and unsteady flow, with or without the gravity term. In steady flow systems, flux, gradient, and water content are constant with time, while in transient flow systems, they vary. The most commonly used methods are based on steady flow.[1),2),3),4),5)] While many such methods are described in the literature, they are all based on essentially the same procedure. The tested sample, or core, is mounted either in a plexiglass tube or in a pressurized rubber sleeve, and a steady flow of water is established through it. A steady flow, i.e., inflow equals outflow, is reached within 2-40 hours, depending on the sample's permeability and the method used. At this stage the pressures at either end of the sample, the rates of flow and the saturation are determined. But steady-state methods have the disadvantage of requiring relatively long times to establish steady flow. During this time, changes can occur in the hydraulic properties of the sample and the porous end barriers. The use of mercuric chloride, phenol, or thymol in the water to reduce biological activity is customary. If the water that is used in the measurements differs markedly in ionic strength and composition from the soil solution initially present in the pores of the sample, there may be considerable change in the conductivity of soils containing clay during the flow. Therefore steady-state methods are primarily laboratory methods.

Now a widely used transient-flow methods (unsteady-state methods) for measurement of conductivity and diffusivity in the laboratory may be grouped into : (1) outflow methods and (2) instantaneous profile methods.

The outflow method has been used to obtain estimates of the measurement of the volume of water outflow as a function of time from a sample placed in a pressure cell.[6),7)] The slab of soil is placed on a porous plate or membrane and is brought to equilibrium with a certain gas-phase pressure in the cell. By increasing the gas (e.g., air) pressure in the cell by a small increment, water is

forced out through the membrane. The volume of water draining out of the sample is measured as a function of time. The procedure is then repeated by further increasing the gas pressure. These data are then introduced into the solution of the unsteady, one-dimensional continuity equation in which the effect of gravity is neglected. By fitting the experimental outflow-time curve to the theoretical curve, one can obtain a value of the soil water diffusivity that can be associated with the mean water content (or pressure head) of the soil sample during the increment of outflow.

But in many cases the theoretical and experimental outflow curves cannot be matched,[7] indicating that the assumption of negligible membrane resistance in the analysis is not valid.[8] Jackson has examined the method and concluded that it is not practical to use pressure increments small enough to validate the assumption of constant K and C, and that it is extremely difficult to obtain replicated results with the method.

Laboratory measurements of conductivity can also be made on long columns of soil, not only on small samples contained in cells. In such a column, steady-state flow can be induced.[9] If the column is long enough to allow the measurement of pressure gradients and of water-content gradients, the $K(\theta)$ and $K(\psi)$ relationship can be obtained for a considerable range of θ with a single column. If periodic pressure and wetness profiles are measured, the flux values at different time and space intervals can be evaluated by graphic integration between successive moisture profiles. This procedure has been called the "instantaneous profile" method,[10] and it can be applied in the field as well. The theory does not assume uniformity of the hydraulic properties of the flow system, and the boundary conditions do not need to be constant, or known in detail. Methods of this type seem to offer the best possibility for hydraulic characterization of sample or field soils. In the laboratory, pressures are measured by pressure transducer tensiometers.[11),12),13),14] Moisture content may be measured by a gamma-ray attenuation

11),13),14).15) 16)
system, by a neutron scattering device.

The purposes of this chapter are to propose a rational basis of getting experimental relationships between moisture content(θ) and hydraulic conductivity $K(\theta)$ and between pressure head(ψ) and volumetric moisture content(θ) by the instantaneous profile method by using the source of low-energy gamma-ray attenuation and pressure transducer tensiometer.

4.2 Instantaneous Profile Analysis

In essence, the method of instantaneous profiles consists of determining down the column the profiles of the macroscopic flow velocity, the potential gradient, and the volumetric moisture content at any instant of time after the commencement of drainage or infiltration. Once these are known for a particular time, it is then possible to find the instantaneous hydraulic conductivity for each elevation by dividing the appropriate velocity value by the potential gradient value.

The continuity equation which already has been given Eq.(2.22) in section 2.3 may be applied to one-dimensional flow system as

$$\left(\frac{\partial \theta}{\partial t} \right)_z = -\left(\frac{\partial V}{\partial z} \right)_t \qquad (4.1)$$

where V is the flow velocity (cm/sec), θ is the volumetric moisture content (cc/cc), and z is the elevation above the datum plane defined as positive in the upward direction as sketched in Fig.4.2. In the case of drainage, the curves presented in Fig.4.3 which will be obtained from the experimental information give the variations of water content with time for several column elevations. Using this information, it is a straightforward matter to find the relation between $\partial\theta/\partial t$ and z at several required times as shown in Fig.4.4.

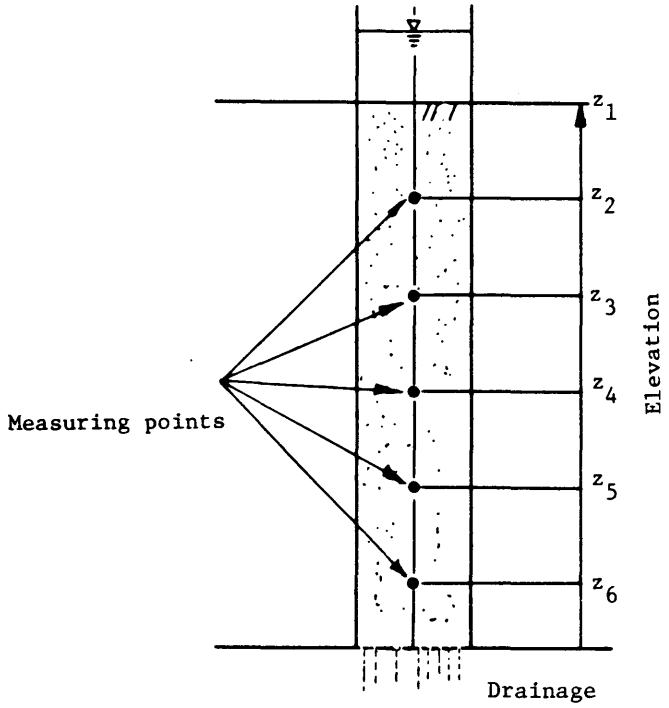

Fig.4.2 Schematic picture of vertical drainage

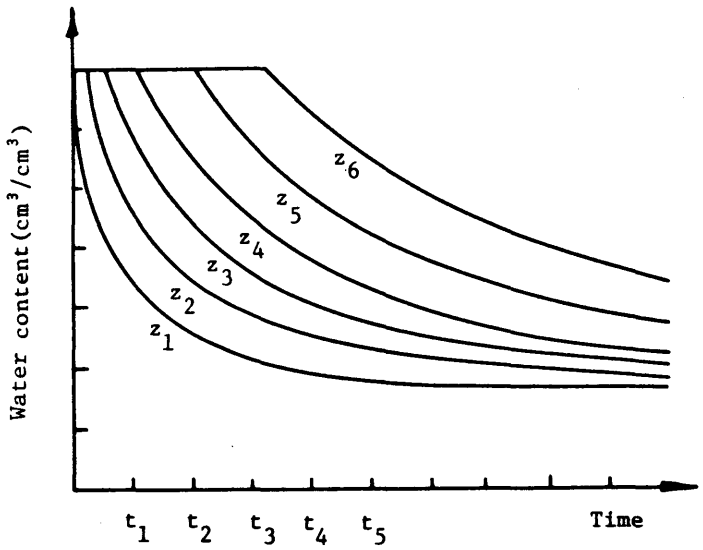

Fig.4.3 Variation of moisture content with time at several column elevations (after Watson[11])

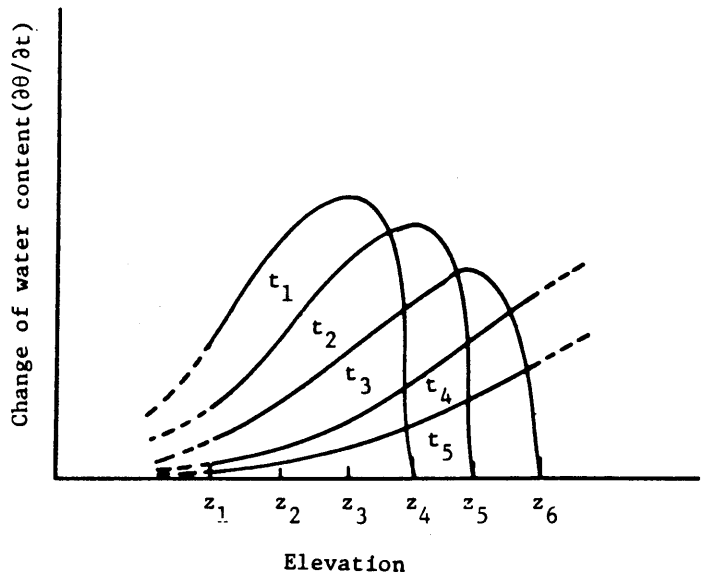

Fig.4.4 Changes of water content at each elevations with time

Integration of Eq.(4.1) with respect to z yields:

$$\int \frac{\partial \theta}{\partial t} dz = -V + C(t) \qquad (4.2)$$

It should be noted the velocity is zero at the surface, then Eq.(4.2) becomes

$$-V(z,t) = \int_{z_s}^{z} \frac{\partial \theta}{\partial t} dz \qquad (4.3)$$

where V(z,t) is the velocity at position z and z_s is the elevation of surface. The velocity profiles are obtained by integrating graphically with respect to

z-$\partial\theta/\partial t$ profile curves, and the resulting velocity profiles are given in Fig. 4.5. These profiles represent the instantaneous velocities down the column at time stated.

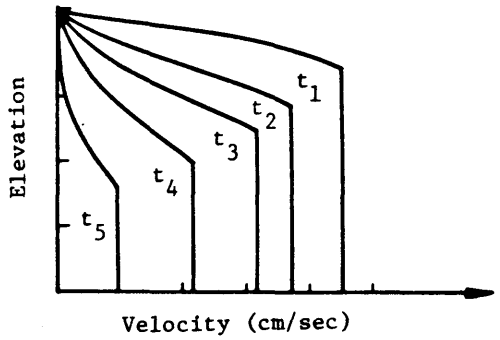

Fig.4.5 Instantaneous velocity profiles

The first part of the method is the determination of the pressure head(ψ) profile with time at several elevations in the column as shown in Fig.4.6. Since the total potential h is equal to the negative pressure head(ψ) (in the case of drainage) and the gravitational component z, the total potential profiles at each time may be readily plotted and are presented in Fig.4.7. These curve may then be differentiated graphically to give the positive potential gradient ($\partial h/\partial z$) profiles as shown in Fig.4.8.

From Fig.4.5 and Fig.4.8, it is a relatively simple matter to determine the instantaneous hydraulic conductivity for any elevation and time from Darcy's law which already has been given Eq.(2.18) in section 2.2.

$$K = \frac{(V)_{z,t}}{(\frac{\partial h}{\partial z})_{z,t}} \qquad (4.4)$$

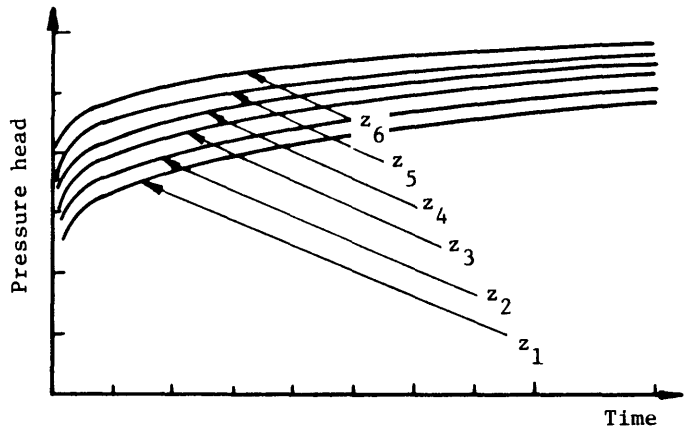

Fig.4.6 Variation of soil water suction with time at several column elevations

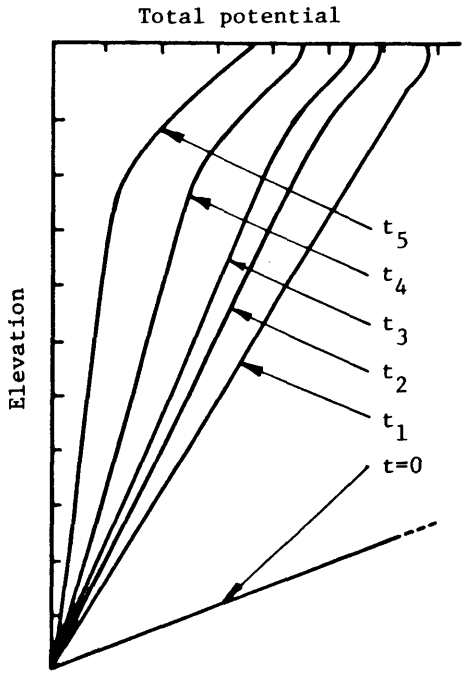

Fig.4.7 Instantaneous total potential profiles

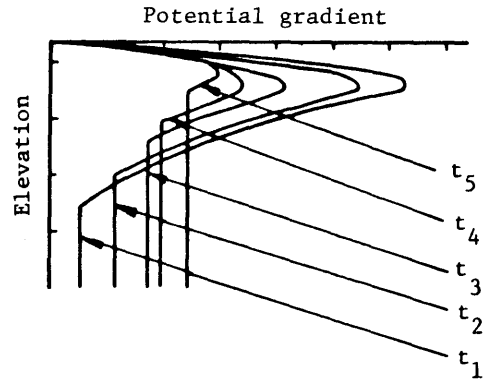

Fig.4.8 Instantaneous potential profiles

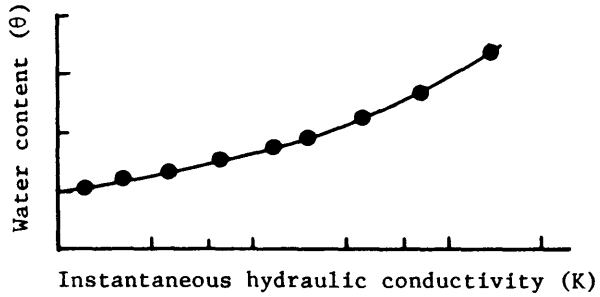

Fig.4.9 The water content-instantaneous hydraulic conductivity relation showing the computed values

The last step of the method is the plotting of the curve relating the values of the instantaneous hydraulic conductivity and the water content. This relationship is given in Fig.4.9, where the conductivity scale is logarithmic to enable the lower conductivities to be presented accurately.

4.3 Experimental Apparatus and Procedure

4.3.1 Measurement of moisture content by gamma ray attenuation

In the determination of unsaturated permeability of columns of soil, some experimental methods of measuring the distribution of soil water content along the length of the column have been reported.[17),18)] Gravimetric sampling is the common method used. This disturbs the system so that information about water distribution as a function of time must be put together from measurements made on replicated systems. Because of undetected density gradients, cracks and other flaws which may occur, true replicated systems are difficult to produce; thus, serious errors may result in water distribution-time studies.

Then, some methods of nondestructive measurement are desirable. Methods involving measuring electrical or thermal properties of porous blocks are secondarily applied,[19)] however, these methods have the following limitations:

(1) lag in following water content changes

(2) insufficient range

To conquest these limitations, two radioactive techniques have been used for measuring soil water content, the neutron-scattering method and the gamma ray absorption method. In the neutron-scattering method, the region of neutron scattering is very wide, and so it is difficult to get an accurate coordinate of measuring point. While, the gamma ray method enable accurate measurement of soil density and water content at given positions in a column of soil,[20)] based on the fact that scattering and absorption of gamma rays are related to the density of matter in their path.

The method is not specific for water, as in the case of the neutoron-scattering method. However, it has the advantage that gamma rays may be collimated by suitable geometry and shielding to a narrow beam which gives resolution in position at which readings are taken. As neutrons are not readily collimated,

and as the counting technique commonly used counts the scattered neutrons rather than the unscattered, the neutron method is more suited to water-content measurements of a large bulk of soil.

To use the gamma ray method to determine water content, the soil density must be known to the same degree of accuracy. This may readily be determined at a fixed value of water content and used for subsequent determinations of water content provided the soil density remains unchanged thereafter. Then, the method has one major limitation which restricts its use in measuring soil water content. A change in density which occurs in the soil because of shrinking and swelling will affect gamma absorption. Hence, use of the method is restricted to conditions where bulk density changes are negligible compared with changes in moisture density to be measured, or where independent measurements permit correction for changes in bulk density. Then, in this study, the water content was measured by using gamma ray attenuation, following the procedure of Davidson et al.[21], Watson.[11] However, in contrast to previous works as indicated in Table 4.1, low-energy gamma radiation (100μ curies of cobalt 60) rather than cesium 137 or americium 241 was used as the source of gamma photons.

Table 4.1 Summary of gamma attenuation method

Reference	Gamma ray source	
Gurr.C.G[22]	25 millicuries of C_s^{137}	1962
H.Ferguson et al.[23]	20 millicuries of Cesium^{137}	1962
Davidson et al.[21]	200 millicuries of C_s^{137}	1963
Topp G.C et al.[24]	200 millicuries of Cesium^{137}	1966
G.C.Topp et al.[25]	100 millicuries of Cesium^{137}	1967
Yen et al.[26]	200 millicuries of C_s^{137}	1968
Topp[27]	200 millicuries of C_s^{137}	1969
G.Vachaud et al[13]	100 millicuries of americium^{241}	1971
R.S.Saksena[28]	100 millicuries of C_s^{137}	1974

The arrangement of the source and detector is shown schematically in Fig.4.10. The C_o^{60} source holder was made of lead bricks arranged in a cube about 6.0 cm on a side. The source was placed in the center of one of the block faces in such a way that it was about 2 cm from the face.

The total thickness of the lead collimator was 5.0 cm, and the collimator slit was 7.0 cm high and 0.6 cm wide. The detector was inserted in a lead annular ring with the front of the probe flush against the rear of the collimator so that the collimation slit was centered on the face of the probe. Thus, with minor exception, the probe detects only those gamma rays which pass directly from the source through the sample and collimation hole to the probe.

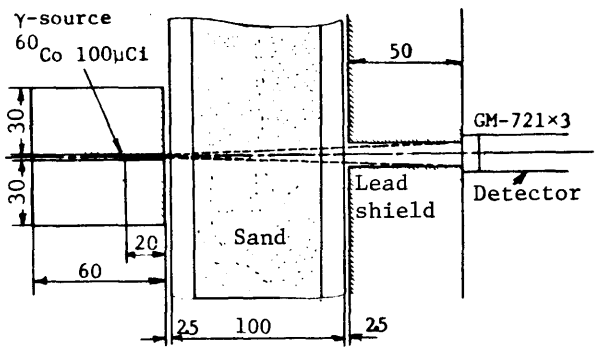

Fig.4.10 Schematic position of the gamma beam

(Schematic representation of the gamma source holder, collimation and probe)

A small conveyor was placed on a vertical guide track between the source holder and the collimator in such a way that the conveyor could be moved vertically through the stationary gamma beam. The guide track maintained the conveyor at a constant position with regard to the collimator face. During a run, soil through which water was moving was placed on the conveyor in such a way that

the gamma beam passed through the soil in a direction perpendicular to the direction of water movement. By moving the conveyor it was possible to pass the beam through any vertical section of soil.

It was necessary to calibrate counts against moisture content. The various content soils were packed with same dry density (γ_d = 1.5g/cm^3) in acrylic rectangular boxes 7.0 cm high, 10.0 cm wide, and 20.0 cm long. The cuve as shown in Fig.4.11 was obtained by plotting the record of the counts per 10 seconds obtained at a particular moisture content. This graph of moisture content against counts was used to transform the counts obtained during a run to moisture content.

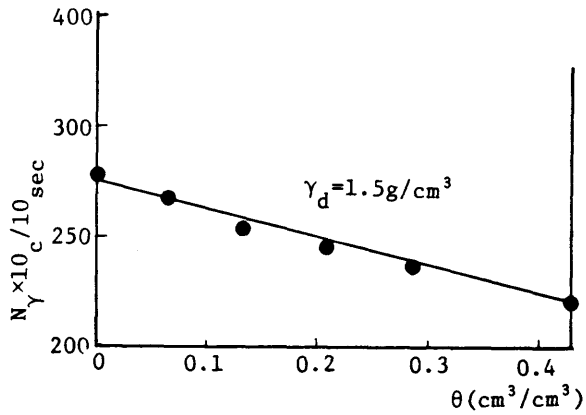

Fig.4.11 Calibration curve for sand

4.3.2 Measurement of pore water pressure

To know the relation of moisture content and pore water pressure, it is necessary to measure pore water pressure at the same time. The satisfactory use of a pressure transducer for pressure head measurements requiring rapid response has been previously reported by Klute,[29)30)] and Watson.[31)]

Then, in this experiment, pressure head was measured at the same time for 5 different depths in the column by using tensiometers and transducers (the range of measuring from -100g/cm^2 to +100g/cm^2), each tensiometer was connected to its own transducer. Five tensiometers were arranged vertically along the column at 10 cm intervals as shown in Fig.4.12. The active area of each tensiometer was a ceramic plate which has a bubbling pressure of approximately 2000 cm of water. The tensiometer units, illustrated in Fig.4.13, are screwed directly into the acrylic box. Each transducer was connected by a multichannel data acquisition system.

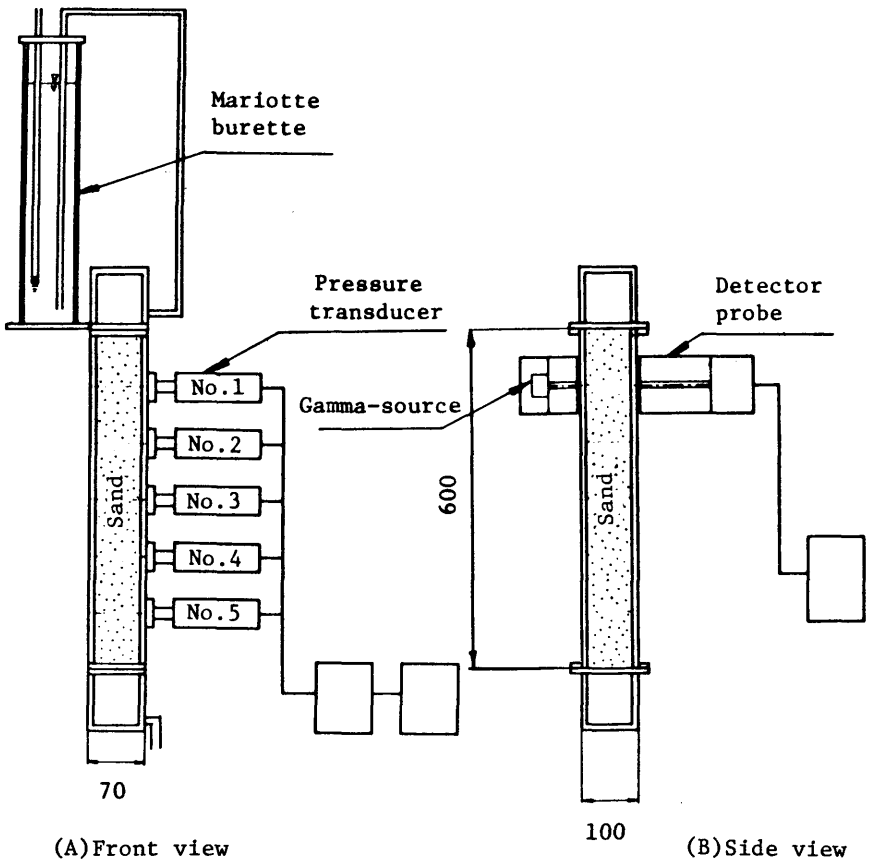

Fig.4.12 A schematic representation of the experimental apparatus: (A) front view showing relative position of the gamma system, (B) side view showing relative positions of tensiometers

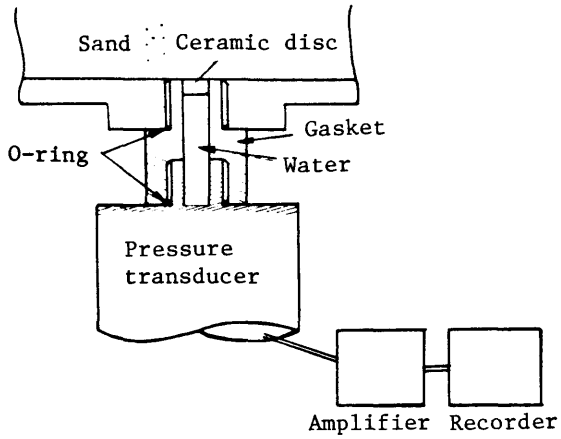

Fig.4.13 Pressure transducer assembly details

4.3.3 Experimental procedure

The soil sample used in the experiment was Toyoura standard sand with a specific gravity of 2.65. The material was carefully packed into the acrylic ractangular box 7.0 cm heigh, 10.0 cm wide, and 60.0 cm long with a particular dry density(γ_d=1.50g/cm^3) using a tremie to prevent segregation and tamped frequently to produce a tight packing. The mode of packing was identical in all experiments. Both ends of column were made of fine screen through which water moved into soil.

A. Series 1 (Water applied on top of the column)

Test 1-1. The air-dried column of sand at an initial uniform water content (0.01cm^3/cm^3) had water applied on top of the surface by keeping a head of water 8.5 cm in height as shown in Fig.4.12. The quantity of water entering the column was measured by using a Mariotte burette as shown in Fig.4.12.

Pore water pressure was measured by pressure transducers. The use of this equipment permitted accurate ($\pm$0.5 mm of water) pressure measurements to be made on a dynamic system.

To measure moisture content 10-second counts was made at each 10 cm interval along the column. The conveyor was then positioned to the place where the first water measurement was desired water flow into the soil was started, and a 10-second count was made.

Both the count and the time at which it was started were recorded. Because of the rapid entry of water into the air-dry soil, counts were made as frequently as possible during the early part of the run. As water moved into the soil, the conveyor was moved to whatever position a water determination was desired. In this way a record of counts per 10seconds as a function of time was obtained at various positions along the soil column.

Infiltration occurred for 16minutes after which the wetting front reached the bottom (z=0). Infiltration examined for a period of 25 minutes.

Test 1-2. At the end of Test 1-1, to obtain the hydraulic conductivity K_s ($S_r \doteqdot 100\%$) in saturated state constant-head permeability test was performed. Fig. 4.14 shows the setup. The lowest elevation in the sand column was thus a fixed piezometric surface; this surface was taken as datum in gradient measurements. Under these conditions the hydraulic gradient was known and, from measuring the rate of volume outflow from the bottom of the column, the saturated hydraulic conductivity (K_s) could be determined.

Test 1-3. In the third test of experiments, the columns were first allowed to become saturated by infiltrating water, keeping the surfaces saturated, until water drained from the bottom. Since the flow condition was that of drainage of the saturated column to atmosphere at its base, the base of the column was constructed so that air at atmospheric pressure was always maintained during an experiment on the under side of the screen supporting the sand.

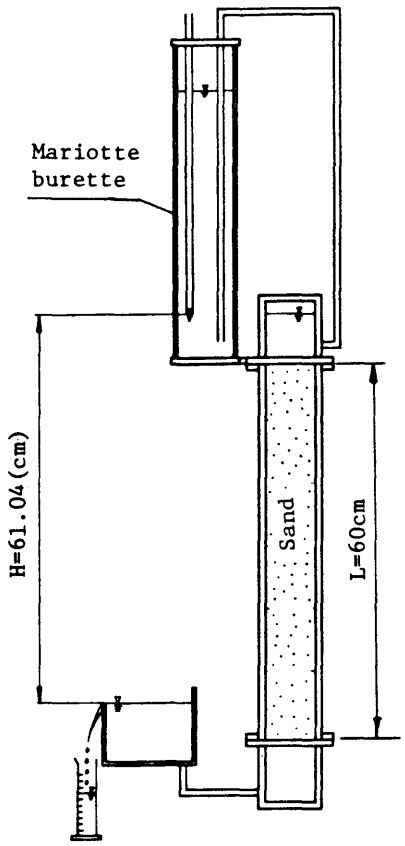

Fig.4.14 Setup for constant-head permeability test

The drainage process commenced the moment the ponded water disappeared through the upper soil surface. Drainage examined for a period of 35 hours measuring the variations of pressure head and volumetric moisture content to obtain the relationship during the drying process.

Test 1-4. A fourth test of experiments was initiated at the end of Test 1-3. The soil column was submitted to another cycle of infiltration and redistribution to obtain a scanning curve. On rewetting, water was ponded constantly on the soil surface to a depth of 8.5 cm, but the initial water content distribution in the soil column was that obtained at the end of the Test 1-3 redistribution and was very close to a static equilibrium water profile. Infiltration occurred for 22 minutes.

B. Series 2 (Water applied from the base of the column)

Test 2-1. The air-dried column of sand at an initial uniform water content ($0.01 cm^3/cm^3$) had water applied from the base of the column by a constant head of water 31.5cm. in height as shown in Fig.4.15. So the lower end of the column was then immersed under a free water surface. The rate of infiltration was reduced to slower constant rates by means of capillaries fed from a constant head, and the moisture profiles were allowed to attain their equilibrium conditions. In this test, the variations of pressure head and volumetric moisture content were measured.

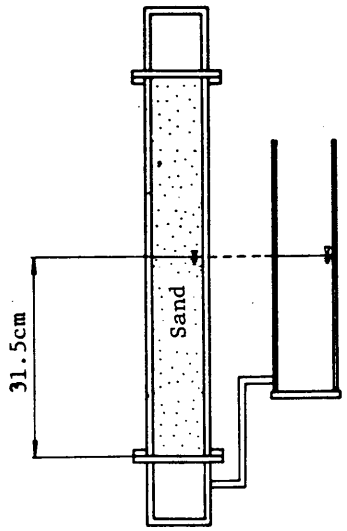

Fig.4.15 Setup for water applied from the base

Test 2-2. At the end of Test 2-1, the initial water content distribution in the soil column was obtained. The potential head was suddenly lowered to a head of water 15.2 cm in height at the bottom. The pressure head and volumetric moisture content was changed by this process. These variations were measured for a long period of time.

4.4 Experimental Results and Discussions

4.4.1 Relationships between hydraulic conductivity (K), volumetric moisture content (θ) and pressure head (ψ)

The results relative to Test 1-1 are reported in Fig.4.16 (a), Fig.4.16 (b). Fig.4.16 indicates the variation of the volumetric moisture content (θ) with time at five elevations in the column for the 25 minutes of infiltration. These values of the moisture content (θ) were obtained by using the calibration curve in Fig.4.11.

As it is clear from Fig.4.16, the moisture content at the wetting front changed so rapidly that it is difficult to obtain hydraulic conductivity at low moisture contents. Therefore the results relative to drainage process (Test 1-3) was mainly used to determine the relationships between hydraulic conductivity (K) and volumetric moisture content (θ).

The experimental information obtained from Test 1-3 has been summarized in Figs.4.17, 4.18, and 4.19. Fig.4.18 indicates the volumetric moisture content variation with time for each depth. If these lines are replotted with time as the parameter, as shown in Fig.4.18, useful soil-water relations may readily be calculated. It is possible to calculate moisture flux through each depth increment by integrating moisture-time curve with respect to depth. The slope ($d\theta/dt$) is measured at particular points in time.

In a similar manner, Fig.4.19 gives pressure head changes with time at the same column elevations. From this results hydraulic head profiles can be calculated by adding pressure head to depth for each tensiometer. By using Eq.(4.4), the hydraulic conductivity can be calculated by dividing fluxes by the corresponding hydraulic gradient values. The gradients are obtained by measuring the slopes of hydraulic head versus elevation. Correlating each time the value of K with the mean water content $\bar{\theta}$ obtained in z_j during the mean time $(t_{K+1}-t_K)/2$ permitted us to obtain the $K(\theta)$. The results are given in Fig.4.20.

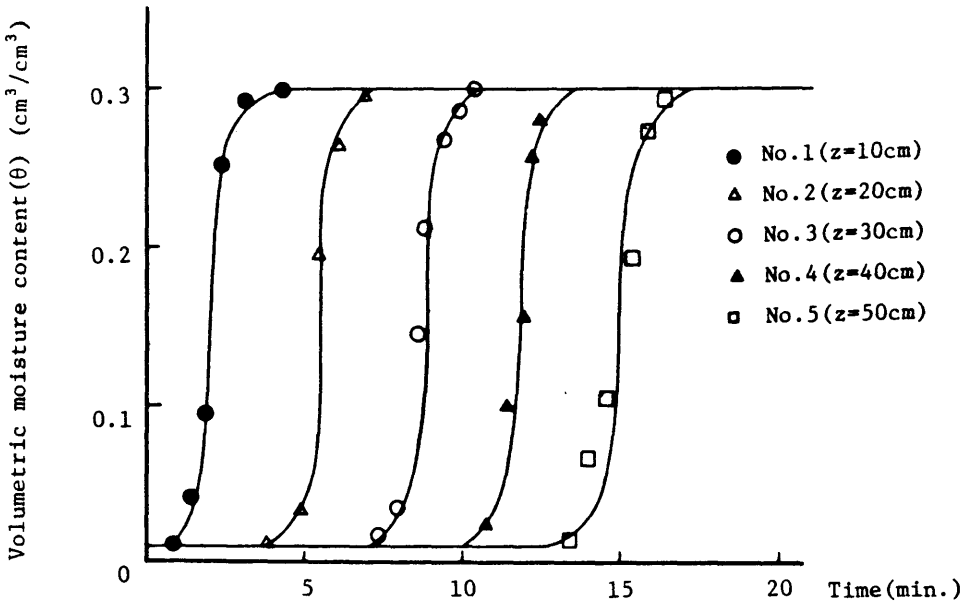

Fig.4.16 (a) Change of moisture content with time during infiltration (Test 1-1)

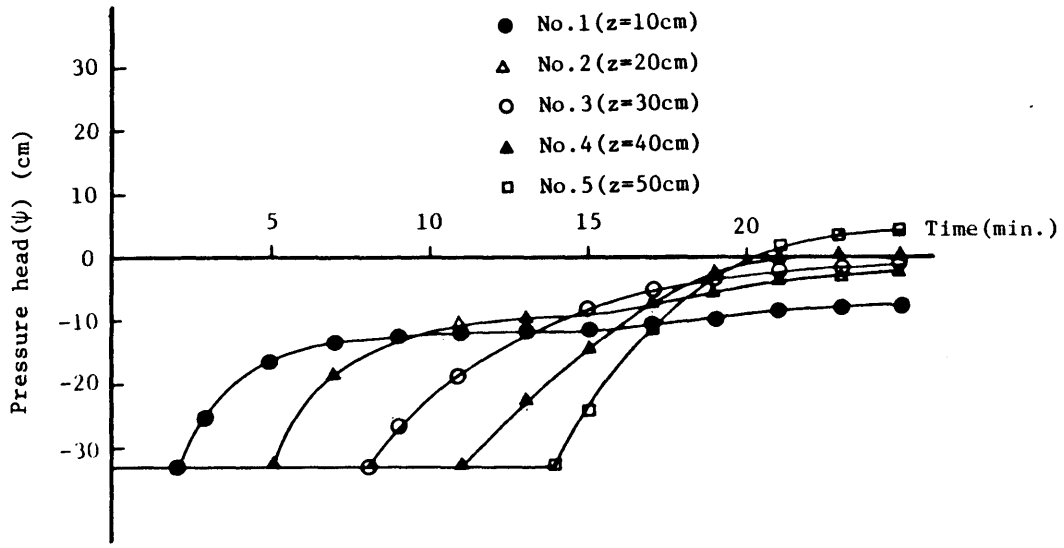

Fig.4.16 (b) Change of pressure head with time at five column elevations during infiltration (Test 1-1)

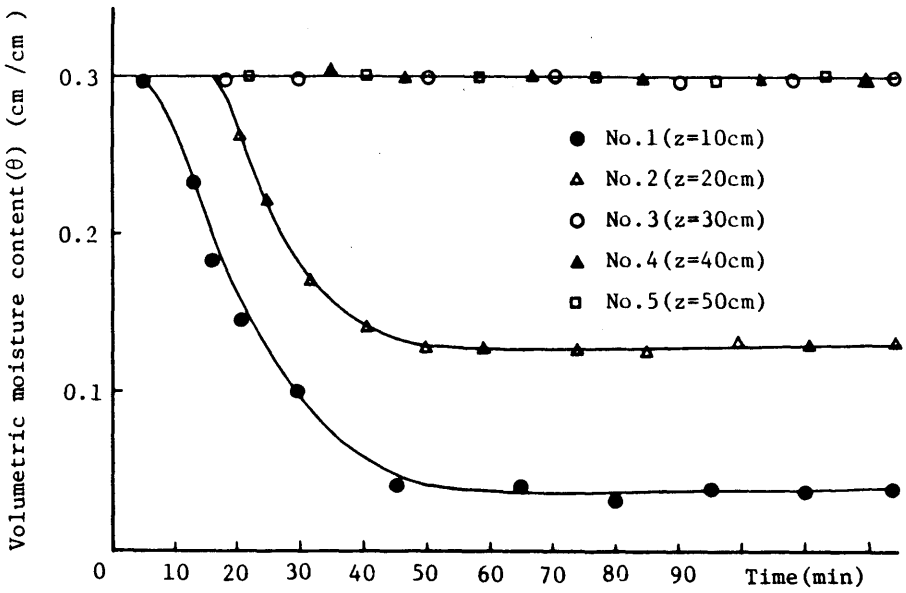

Fig.4.17 Change of moisture content with time during drainage
(Test 1-3)

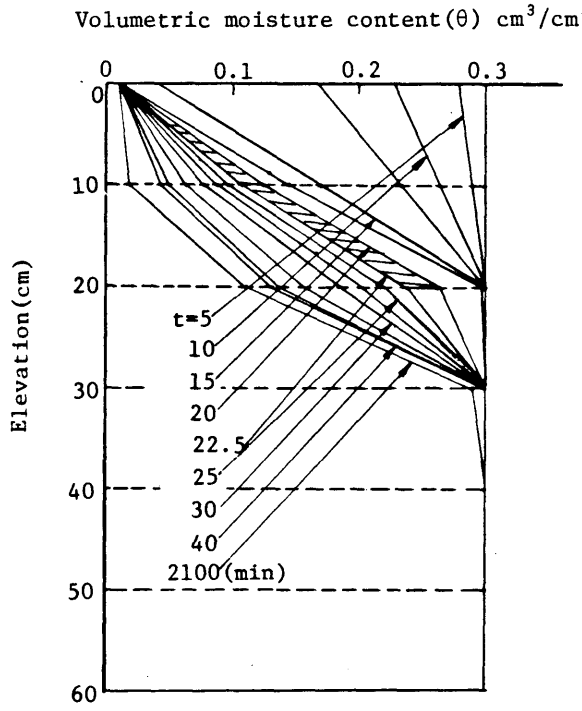

Fig.4.18 Distribution of water content for sand during drainage
(Test 1-3)

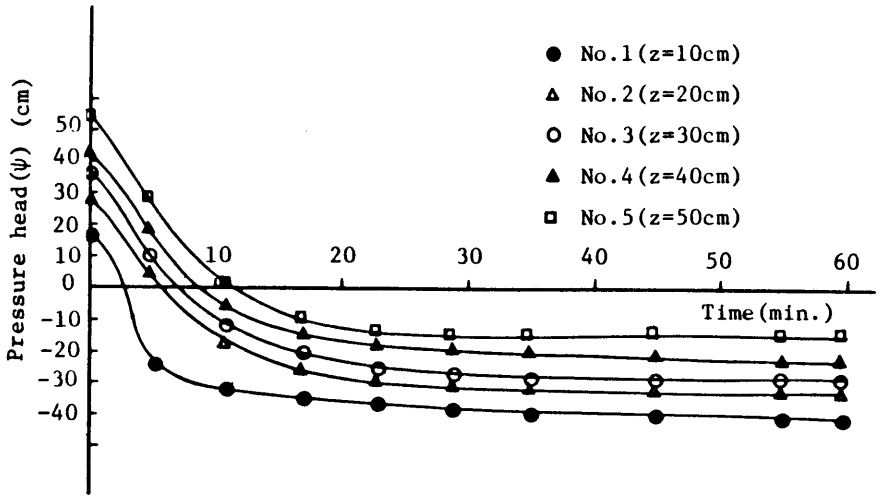

Fig.4.19 Change of pressure head with time at five column elevations during drainage (Test 1-3)

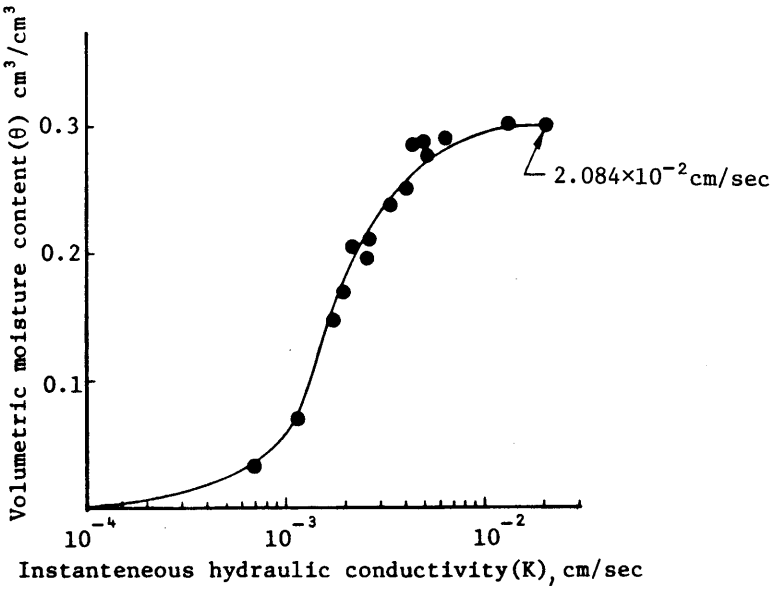

Fig.4.20 The moisture content - instantaneous hydraulic conductivity relation for sand (Test 1-3)

The hydraulic conductivity which was obtained from the results of constant-head permeability test of Test 1-2 was $K_s = 2.084 \times 10^{-2}$cm/sec.

In Fig.4.20, the relation between K-θ is shown. On the other hand, the relations between K and ψ was sometimes used heretofore. Various empirical equations for that relation of conductivity to pressure head (ψ) or moisture content (θ) have been proposed by many researchers as indicated in Table 4.2. In Table 4.2, the empirical parameters are depend upon the liquid, the soil, and the capillary pressure history of the system and the values of the parameters must be determined experimentally. And then no fundamentally based equation of general validity is available for the relation, and existing knowledge does not allow the reliable prediction of unsaturated conductivity from basic soil properties.

There is general agreement that the relation of conductivity to pressure head depends upon hysteresis, and is thus different in a wetting than in a drying soil.[15),24)] Namely, if Fig.4.21 is compared with Fig.4.22, of which results are obtained in the same condition, it is clear that the relation of conductivity to moisture content is affected by hysteresis to a much lesser degree. One may thus neglect any hysteresis in K(θ) and use a unique relationship.

Table 4.2 Empirical equations for the relation of hydraulic conductivity of unsaturated soil to pressure head or moisture content

Empirical equation	Reference
$K = \frac{a}{(-\psi)^m + b}$	Gardner,W.R[32]
$K = K_0 (a/\psi)^m$	Schleusener,R.A. and A.T.Corey[33] Scott,V.H. and A.t.Corey[34]
$K = a \left[\frac{\cosh[(\psi/b)^m] - 1}{\cosh[(\psi/b)^m] + 1} \right]$	King,L.G.[35]
$K = K_0 \exp(m\psi)$	Gardner,W.R.[36] Philip,J.R.[37]
$K = a\theta^m$	Ahuja,L.R.[38]
$K = K_0 \left(\frac{\theta - \theta_r}{\theta_s - \theta_r} \right)^3$	Kroszynski,V.[39]
$K = K_0 + a\theta + b\theta^2$	Bruch,J.C. and G.Zyvoloski[40]

where

a,b and m : Empirical parameters depending upon the liquid, the soil, and the capillary pressure history of the system.

K_0 : The hydraulic conductivity in saturated state.

θ_s : Volumetric moisture content in saturated state.

θ_r : Residual volumetric moisture content.

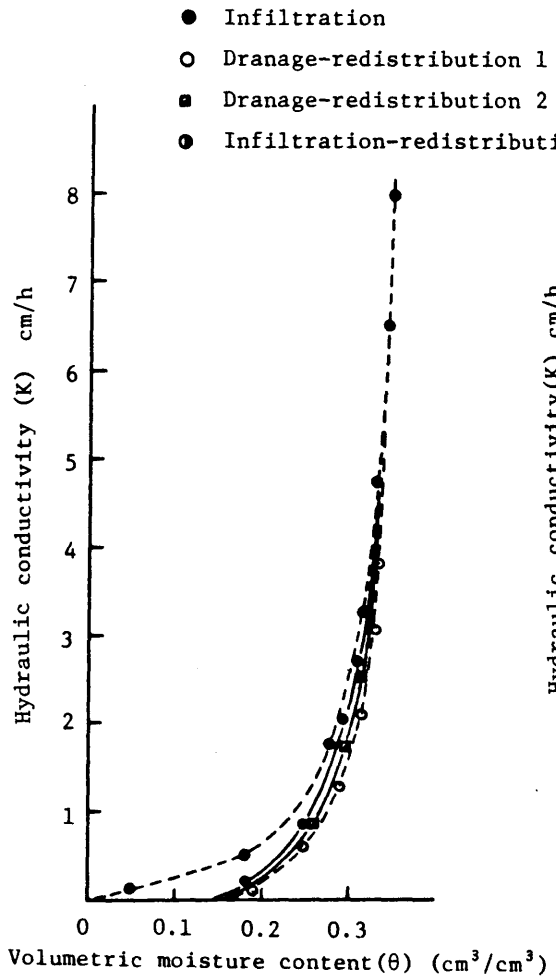

Fig.4.21 K(θ) relationship for different flow conditions (after Varchard)[15)]

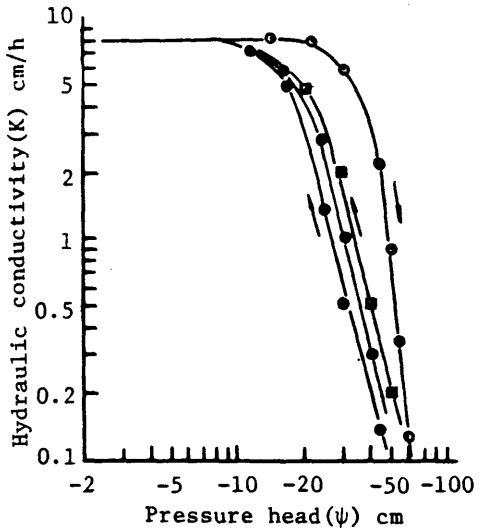

Fig.4.22 K(ψ) relationship for different flow conditions (after Varchard)[15)]

4.4.2 Relationships between pressure head (ψ) and volumetric moisture content (θ)

To get the relationships between pressure head (ψ) and volumetric moisture content (θ), the variation of the volumetric moisture content and that of the pressure head with time are used.

The results from Test 1-1 are reported in Fig.4.16 (a) and Fig.4.16 (b) and those from Test 1-3 are shown in Fig.4.17 and Fig.4.19. Using the these figures, it should be noted that a relationship (θ-ψ) is obtainable by plotting, for any elevation, the pressure head at successive times. When this process was carried out for different elevations, the relationship (θ-ψ) on the sand was defined as shown in Fig.4.23.

In Fig.4.23, data points (closed squares) for the scanning curves which is obtained from selections of data from Test 1-4 for rewetting, the tensiometer position at 20 cm from the top of the column, are added and line was drawn by eye as a best fit.

In soil science, the curves in Fig.4.23 are called "retention curves", as they show how water is retained in the soil by capillary forces against gravity. Some authors refer to the drying retention curve as a "desorption curve" and to the wetting curve as a "sorption curve".

It is evident from Fig.4.23 that hysteresis in the relationship between pressure head and volumetric moisture content exists in soils. The reasons why the hysteresis loop exists in the retention curve may be as follows.[41)]

(1) The geometry of the void space of soil with many bottlenecks, i.e., the ink bottle effect.

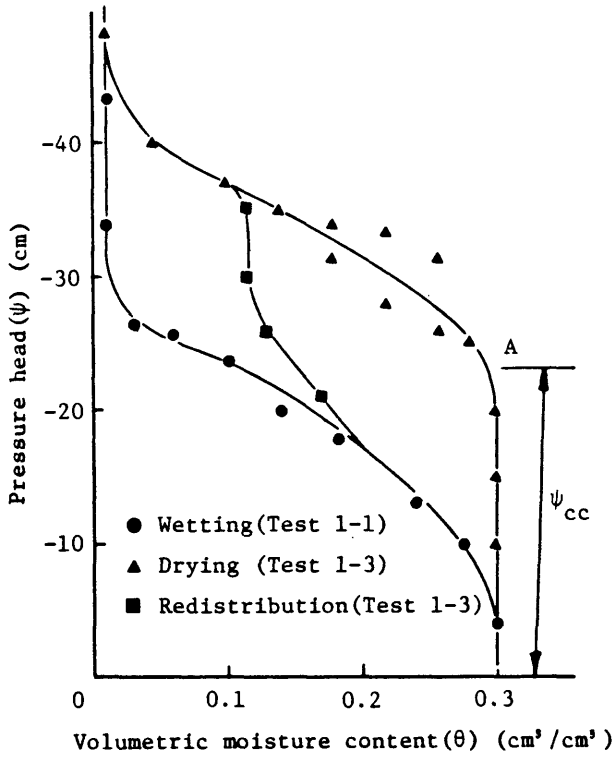

Fig.4.23 Relationships between volumetric moisture content and pressure head

(2) The angle of contact α_c is a function of the direction of the displacement, α_c may have different values if equilibrium is approached by advancing or receding over a face. Fig.4.24 shows this phenomenon for an air-water interface.

(3) The air in the void space may be trapped in the process of water advancing.

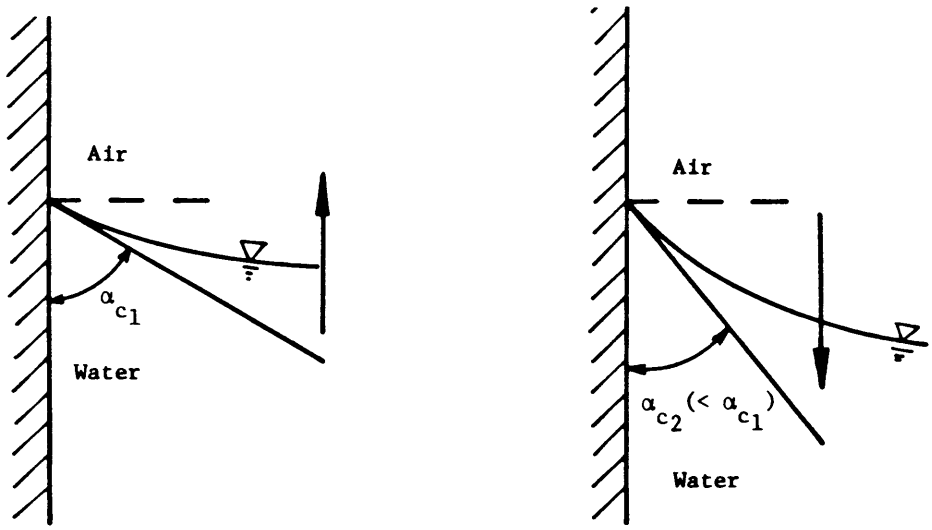

(a) Water wetting (b) Water drying

Fig.4.24 Contact angle between a water-air interface and a solid

Point A in Fig.4.23 is the critical capillary head ψ_{cc}. If the drainage process is start from a saturated sample, no water will leave the sample until the critical capillary head is reached. As the value of ψ_{cc} is increased, the initial small reduction in θ is associated with the retreat of the air-water meniscii into the pores at the external surface of the sample. Then, at the

critical value ψ_{cc} the larger pores begin to drain.

The reason of this phenomenon may be the time lag in air entry into soil. The soil pores are probably smaller at the soil surface than they are in the interior of soil mass. There is a "skin effect" due to the smaller surface soil pores. When the surface soil pores are emptied, the water declines in the capillaries for a considerable distance downward, since the soil pores are larger beneath the soil surface. The soil water tension at the soil surface would very quickly increase. The entry of air into the soil would occur shortly after the water table reached the bottom of the soil column; assuming that the length of the column is such that the air-entry value of the soil is exceeded.

In same manner of the relations (K-θ), various empirical equations for the relations of pressure head to moisture content have been proposed, as indicated in Table 4.3.

Table 4.3 Empirical equations for the relation of pressure head to moisture content

Empirical equation	Reference
$\frac{\theta - \theta_r}{\theta_s - \theta_r} = \exp[\, a(\psi - b)]$	Kroszynski,U[39]
$\theta = a[\frac{\cosh[(\psi/b)^m + c\,] - d}{\cosh[(\psi/b)^m + c\,] + d}\,]$	King,L.G.[35]
$\theta = a + b \log_e(\psi - c\,)$	Rogowski,A.S[42]

where

a,b,c,d, and m : empirical parameters

The main loops in Fig.4.23, drying curve and wetting curve which are obtained by making the air-dried soil saturated and the saturated soil dried respectively, are unique for a given soil and can be determined experimentally. However, if, at any point on the drying (or wetting) curve the process is reversed, hysteresis, as shown by the scanning curve in Fig.4.23, is exhibited. In the wetting process the θ versus ψ relation moves along the scanning curve until it meets the wetting curve and then moves up the wetting curve. The drying and the wetting curves form the boundary of the "hysteresis loop", within which the soil can assume any value of saturation and ψ , depending on the past history of the process. Although a number of analyses which took into account the phenomenon of this hysteresis have been done for the unsaturated soil[43),44),45),46)], all of them have used experimental hysteresis data directly and their procedures are very complex.

On the other hand, several attempts to estimate any hysteresis loop from the main drying and wetting curves have been proposed. The most of them are same methods in applying " independent domain theory " which was formulated by Everett[52)]. Among them, Mualem's method[51)] seems to be the simplest and the most efficient. In this study his method has been used whenever the hysteresis had to be taken into account in the flow analyses in Chapter 5.

4.4.3 Evaluation and discussion on Green and Ampt model and pressure distribution at equilibrium condition

A. Green and Ampt model

The Green and Ampt model of infiltration[53)] has been the subject of considerable attention in recent literature[54)55)56)57)] with the need to model simply the infiltration component in hydrological studies.

The model is based on the following form of Darcy-type equation[58)] for a uniform profile in vertical infiltration as depicted in Fig.4.25,

$$q = K_s \frac{H_0 - H_c + z_f}{z_f} \qquad (4.5)$$

where q is the rate of the infiltration into the soil; K_s is the hydraulic conductivity (which is a uniform soil under ponding approximates the saturated conductivity); H_o is constant depth of ponded water at the soil surface; z_f is the distance from the surface to the weting front (i.e., the length of the wetted zone); H_c is negative pressure head at the wetting front.

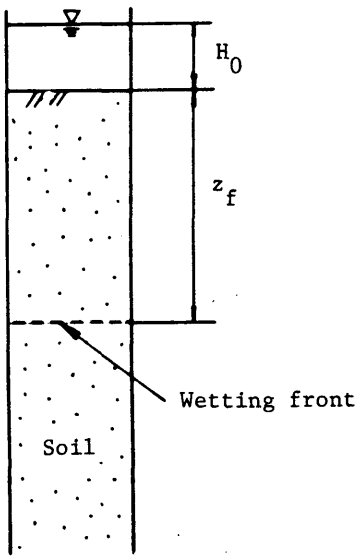

Fig.4.25 Vertical infiltration

This model assumes that the flow of water occurs in a uniformly saturated region on account of a hydraulic head gradient caused by a constant soil water pressure head at the wetting front and gravity. The advancing wetting front is thus a precisely defined surface boundary above which the soil is saturated and

below which the soil is unsaturated. These assumptions simplify and linearize the flow equation, making it amenable to analytical solution.

In order to find the model to be satisfactory for infiltration through an unsaturated soil, the result of the advancing wetting front with respect to Test 1-1 is shown in Fig.4.26. By using Figs.4.16(b) and 4.26, the distributions of total head ($h=\psi+z_f-z$) are shown in Fig.4.27.

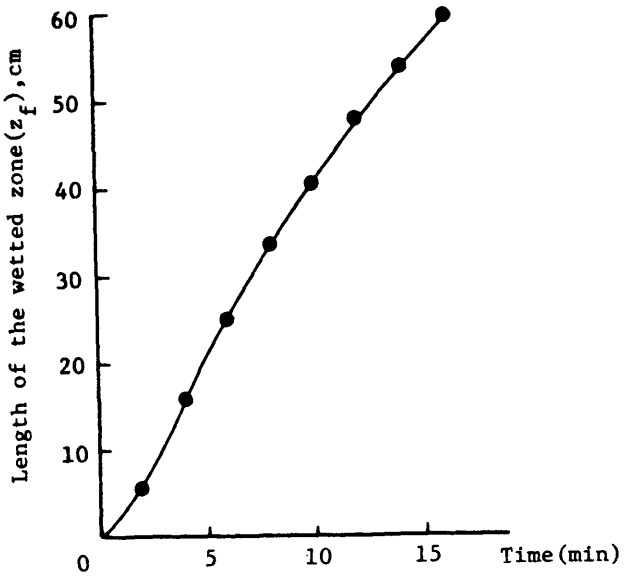

Fig.4.26 Advancing of wetting front with time

It is obvious in Fig.4.27 the graduate of total head is constant in the wetting zone for each time,and H_c is equal to the initial pressure head of air-dry soil. Fig.4.28 shows the infiltration (Q) plotted as a function of time. According to Fig.4.16, it is evident that behind the wetting front, the soil is uniformly wet. Since an uniformly wetted zone can be assumed to extend all the way to the

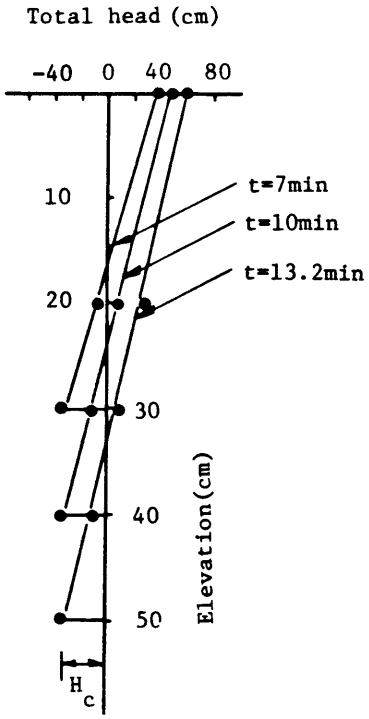

Fig.4.27 Distributions of total head with time

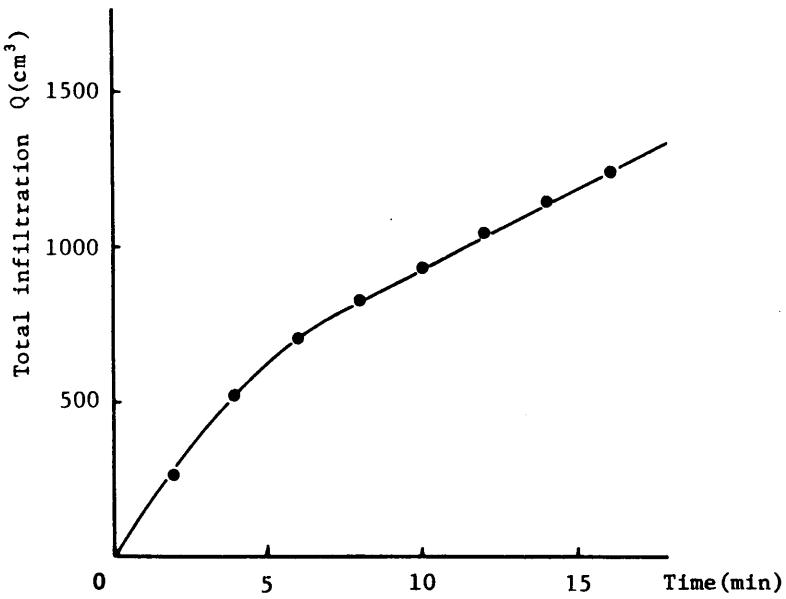

Fig.4.28 Infiltration Q plotted as a function of time

cumulative infiltration Q should be equal to the product of the wetting front depth z_f and the wetness increment $\beta=\theta_t-\theta_i$ (where θ_t is the transmission-zone wetness during infiltration and θ_i is the initial profile wetness which prevails beyond the wetting front):

$$Q = A\beta z_f \qquad (4.6)$$

where A is the area in cross section of soil column. Therefore,

$$\beta = \frac{Q}{Az_f} \qquad (4.7)$$

By using Fig.4.26 and Fig.4.28, the average value of β was obtaind as 0.31, and this value is nearly equal to the value getted by gamma ray attenuation.

The infiltration rate is thus seen to be inversely related to the cumulative infiltration. Rearranging Eq.(4.5), next equation is obtained:

$$q = \frac{dQ}{dt} = K_s \frac{H_0 - H_c + z_f}{z_f} \qquad (4.8)$$

Then the value of K_s for each time can be calculated by using the both results of Q versus t and z_f versus t. The average value of K_s is obtained as 1.9×10^{-2} cm/sec. This value also well agrees with the value obtained by Test 1-2. Thus it can be understood that attempts to reconcile the Green and Ampt model with the classical flow equation is successful for the infiltration through the air dry sandy soil. However, in actual field conditions, particularly where the initial moisture content is not uniform, H_c may be undefinable. In many real situations, the wetting front is too diffuse to indicate its exact location at any particular time. Then this model remains a quasi-empirical method founded

on crude theory.

B. Pressure distribution at equilibrium condition

In order to perform the nonsteady numerical analysis of flow through porous media, the distribution of initial pressure head ψ_o in the entire flow domain must be used as the initial condition. Test 2-1 was carried out to obtain this distribution and infiltration from the base of the column occurred for 2 days Fig.4.29 gives the advances of capillary zone.

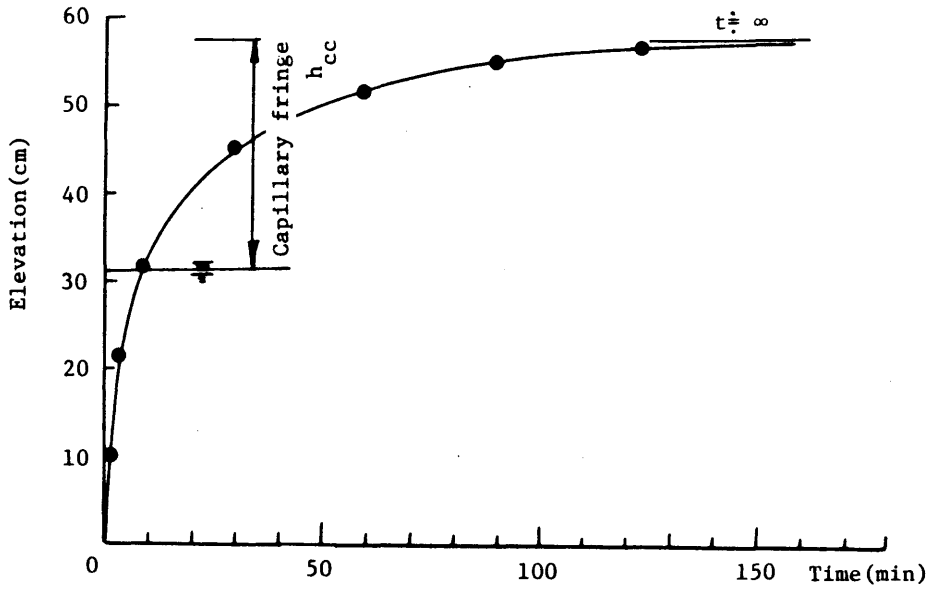

Fig.4.29 Advances of capillary zone

As this phenomenon is analogous to rise in capillary tube where the water rises to a certain height above the free surface with a full saturated tube below the meniscus, the nearly saturated zone above the free surface is called the capillary fringe. This h_{cc} in Fig.4.29 is the capillary rise for this soil and its

value became about 25 cm .

Fig.4.30 shows the change of moisture distribution above the free surface with respect to time, and after 2 days this change reached the near static equilibrium condition. Fig.4.31 represents the distribution of pressure head at this condition. In Fig.4.31, as z increases upward, so decreases ψ and the ultimate straight line was gotton as the relationship (ψ-z) in the capillary fringe. Then, in this zone the total potential (h) may be

$$h = \psi + z = 0 \qquad (4.9)$$

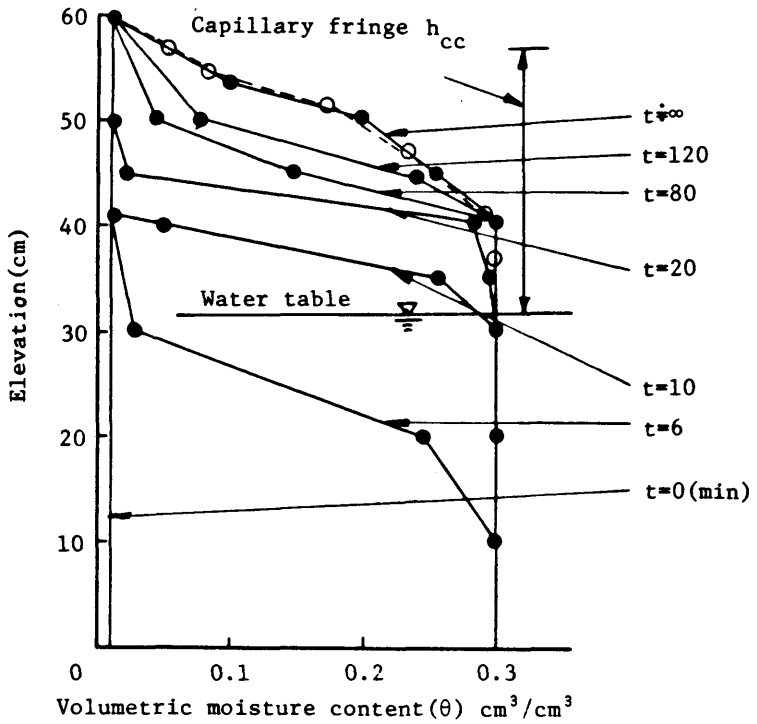

Fig.4.30 Distribution of water content for standard sand during infiltration from bottom (Test 2-1)

The distribution of pressure head above the capillary fringe must be ψ_o which is initial pressure head of air dry soil because the volumetric moisture

content did not change during this successive time.

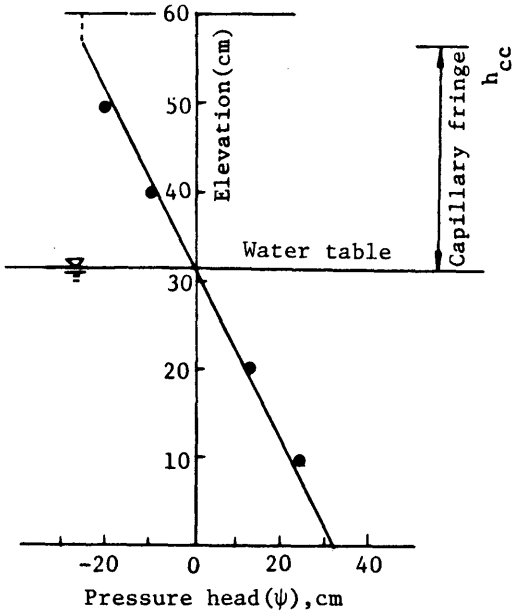

Fig.4.31 Pressure head distribution in capillary fringe at equilibrium condition

By the way, the open circles points in Fig.4.30 were plotted of the value of moisture content from the wetting curve of Fig.4.23 with considering the value of pressure head is equivalent to the height above free surface. From this result, the equilibrium moisture profile can therefore be applicable to the retention curve of wetting process.

4.5 Conclusions

In this chapter, the need for determining the hydraulic properties of soil profiles was pointed out and available methods are reviewed. Experimental tests

have been performed to determine the hydraulic properties of unsaturated soil during the flow of water in a vertical soil column and a technique for handling the data was systematically described and illustrated. Throughout of this chaper, the following main conclusions are obtained.

(1) The instantaneous profile method for determining soil hydraulic properties based on simultaneously monitoring the changing moisture content and pressure head profiles during internal drainage is outlined and this method is probably easier to carry out than altanative methods.

(2) A technique for using a low-energy gamma radiation apparatus for measuring water content in the column of soil has been described. Although its use in limited to porous materials which do not shrink or swell upon wetting, it does provide a means for accurate measurement of water content without disturbing the system into which water is moving. Furthermore rapid measurement of water content becomes possible at any position in a soil so that water content changes with time may easily be followed.

(3) The tensiometer-transducer system provides a most valuable means of measuring pressure head with rapid response and with provision of a complete record of the pressure head changes with time.

(4) The hydraulic conductivity in relation to volumetric moisture content of the sand was obtained.

(5) Different flow conditions have been imposed to map out conveniently the hysteresis domain in $\psi(\theta)$.

(6) Applications of the Green and Ampt infiltration equation were discussed and good agreements between the model and experimental data were shown, then it was found that the Green and Ampt approach is satisfactory for infiltration through the air-dry sand column where the initial moisture content is uniform.

(7) The distribution of pressure head and moisture content above the free sur-

face was obtained at the equilibrium conditon in order to apply this distribution to the numerical analysis of drainage and infiltration in soil as a initial conditon.

References

1) Nielsen,D.R. and Phillips,R.E.: Small fritted glass bead plates for determination of moisture retention, Soil Sci. Soc. Amer. Proc., 22: 1958, pp.574-575.

2) Elrick,D.E. and Bowman.D.H.: Improved apparatus for soil moisture flow measurements. Soil Sci. Soc. Amer. Proc., 28, 1964, pp.450-453.

3) Smiles,D.E. and Towner.G.D.: The steady-state measurement of the relation between hydraulic conductivity and moisture content in soils., Water Reso. Res. 4, 1968. 1029-1030.

4) Childs,E.C.: The Physical Basis of Soil Water Phenomena, John Wiley & Sons, New York, 1969.

5) Watson,K.K.: The measurement of the hydraulic conductivity of unsaturated porous materials using a zone of entrapped air, Soil Sci. Soc. Amer. Proc. 31, 1967, pp.716-721.

6) Gardner,W.R.: Calculation of capillary conductivity from pressure plate outflow data, Soil Sci. Soc. Amer. Proc. 20, 1956, pp.317-320.

7) Kunze,R.J. and Kirkham,Don.: Simplified accounting for membrane impedance in capillary conductivity determinations. Soil Sci. Soc. Amer. Proc. 26, 1962, pp.421-426.

8) Jackson,R.D., Van Bavel,C.H.M., and Reginato,R.J.,: Examination of the pressure plate outflow method for measuring capillary conductivity, Soil Sci. 96, 1963, pp.249-256.

9) Youngs,E.G.: An infiltration method of measuring the hydraulic condutivity

of unsaturated porous materials. Soil Sci. 97, 1964, pp.307-311.

10) Van Bavel,C.H.M., Stirk,G.B., and Brust,K.J.: Hydraulic properties of a clay loam soil and the field measurement of water uptaken by roots. I. Interpretation of water content and pressure profiles. Soil Sci. Soc. Amer. Proc. 32, 1968, pp.310-317.

11) Watson,K.K.: An instantaneous profile method for determinig the hydraulic conductivity of unsaturated porous materials. Water Reso. Res. 2, 1966, pp.709-715.

12) Weeks,L.V. and Richards,S.J.: Soil water properties computed from transient flow data, Soil Sci. Amer. Proc. 31, 1967, pp.721-725.

13) Vachaud,G. and Thony,Jean-Louis.: Hysteresis during infiltration and redistribution in a soil column at different initial water content. Water Reso. Res. 7, 1971, pp.111-127.

14) Rogers,J.S. and Klute,A.: The hydraulic conductivity water content relationship during non-steady flow through a sand column, Soil Sci. Soc. Am. Proc. 35, 1971, pp.695-700.

15) Vachaud,G.: Determination of the hydraulic conductivity of usnaturated soils from an analysis of transient flow data. Water Reso. Res. 3. 1967, pp.697-705.

16) McHenry,J.R.: Theory and application of neutron scattering in the measurement of soil moisture, Soil Sci. No.5, 95, 1963, pp.294-307.

17) Bruce,R.R., Klute,A.: The measurement of soil moisture diffusivity, Soil Sci. Soc. Am. Proc. 20, 1956. pp.458-462.

18) Nielsen,D.R., Biggar,J.W. and Davidson,J.M.: Experimental consideration of diffusion analysis in unsaturated flow problems, Soil Sci. Soc. Am. Proc. Vol.26, 1962, pp.107-111.

19) Uno,T.: Studies on unsteady seepage flow through soil and water level fluctuations, Doctor Thesis, Civil Eng., Kyoto Univ., (in Japanese) 1970.

20) Van Bavel,C.H.M.,Underwood,N., and Ragar,S.R.: Transmission of gamma radiation by soils ans soil densitometry. Soil Sci. Soc. Am. Proc. 21, 1957, pp.588-591.

21) Davidson,J.M., D.R.Nielsen, and J.W.Biggar: Gamma-radiation attenuation for measuring density and transient water flow in porous media, J.Geophys. Res., 68(16), 1963, pp.4777-4783.

22) Gurr,C.G.: Use of gamma-rays in measuring water content and permeability in unsaturated columns of soil, Soil Sci., 94, 1962, pp.224-229.

23) Ferguson,A.H., and W.H.Gardner: Water content measurement in soil columns by gamma-ray absorption, Soil Sci. Soc. Am. Proc., 26, 1962, pp.11-14.

24) Topp,G.C.,and E.E.Miller: Hysteretic moisture characteristics and hydraulic conductivities for glass beads media, Soil Sci. Soc. Am. Proc., 30, 1966, pp.156-162.

25) Topp.G.C., A.Klute and D.B.Peters: Comparison of water content- pressure head data obtained by equilibrium, steady-state, and unsteady-state methods, Soil Sci. Soc. Am. Proc., 31, 1967, pp.312-314.

26) Yen,W.W.G, J.B.Franzini: Moisture movement in a horizontal soil column under the influence of an applied pressure. J.Geophys. Res., 73(16), 1968, pp.5151 -5157.

27) Topp.G.C.: Soil-water hysteresis measured in a sandy loam and compared with the hysteretic domain model, Soil Sci. Soc. Am. Proc., 33, 1969, pp.645-651.

28) Saksena,R.S., S.Chandra and B.P.Singh: A gamma transmission method for the determination of moisture content in soils, J.Hydrol., 23, 1974, pp.341-352.

29) Klute,A., and D.B.Peters: A recording tensiometer with a short response time, Soil Sci. Soc. Am. Proc., 26, 1962, pp.87-88.

30) Klute,A. and W.R.Gardner: Tensiometer response time, Soil Sci., 93, 1962, pp.204-207.

31) Watson,K.K.: Some operating characteristics of rapid response tensiometer

system, Water Resour. Res., 1(4), 1965, pp.577-586.

32) Gardner,W.R.: Some steady-state solutions of the unsaturated moisture flow equation with applocation to evaporation from a water table, Soil Sci. Vol. 85, 1958, pp.228-232.

33) Schleusener,R.A., and A.T.Corey: The role of hysterisis in reducing evaporation from soils in contact with a water table, Geophys. Res. Vol.64, 1959, pp.469-475.

34) Scott,V.H. and A.T.Corey: Pressure distribution during steady flow in unsaturated sands, Soil Sci. Socie. Proc. 1961, pp.270-274.

35) King,L.G: Description of soil chracteristics for partially saturated flow, Soil Sci. Soci. Proce, 1965, pp.359-362.

36) Gardner,W.R.: Solutions of the flow equation for the drying of soils and other porous media, Soil Sci. Socie. Proc. 1959, pp.183-187.

37) Philip,J.R.: Steady infiltration from buried point sources and spherical cavities, Water Resour. Res. Vol.4, 1968, pp.1039-1047.

38) Ahuja,L.R.: Unsaturated hydraulic conductivity from cumulative inflow data, Soil Sci. Soc. Amer. Proc. Vol.38, 1974, pp.695-699.

39) Kroszynski,U.: Flow in a vertical porous column drained at its bottom at at constant flux, Journal of Hydrology, Col.24. 1975, pp.135-153.

40) Bruch,J.C. and G.Zyvoloski: Solution of equation for vertical unsaturated flow of soil water, Soil Sci., Vol.116, No.6, 1974, pp.417-432.

41) Bear,J.: Dynamics of Fluids in Porous Media, Elsevier, 1972, pp.447-448.

42) Rogowski,A.S.: Watershed physics: model of the soil moisture characteristic, Water Reso. Res., Vol.7, No.6, 1971, pp.1575-1582.

43) Whisler,F.D. and Klute,A.: A numerical analysis of infiltration, considering hysteresis into a vertical soil column at equilibrium under gravity, Soil Sci. Soc. Proc., 29(5), 1965, pp.489-494.

44) Ibrahim,H.A. and Brutsaert,W.: Intermittent infiltration into soils with

hysteresis. ASCE, HY, 94, 1968, pp.113-137.

45) Staple,W.J.: Comparison of computed and measured moisture redistribution following infiltration, Soil Sci. Soc. Amer. Proc.,33, 1969, pp.840-947.

46) Bresler,E., W.D.Kemper, and R.J.Hanks: Infiltration, redistribution, and subsequent evaporation of water from soil, Soil Sci. Soc. Amer. Proc., Vol.33, 1969, pp.832-840.

47) Poulovassilis,A.: Hysteresis of pore water an application of the concept of independent domains, Soil Sci., 93, 1964, pp.405-412.

48) Philop,J.R.: Similarity hypothesis for capillary hysteresis in porous material, J.Geophys. Res., 69(8), 1964, pp.1553-1562.

49) Everett,D.H.: Absorption hysteresis, solid gas interface, Vol.2. edited by E.A.Flood, Maree Dekker, New York, Chap.36, 1967, pp.1055-1113.

50) Topp,G.C.: Soil-water hysteresis, the domain theory extended to pore interaction condition, Soil Sci. Soc. Amer. Proc., 35, 1967, pp.219-225.

51) Mualem,A.: A conceptual model of hysteresis, Water Reso. Res., 10(3), 1974, pp.514-520.

52) Everett,D.H.: A general approach to hysteresis,4, An alternative formulation of the domain model, Trans, Faraday Soc., 51, 1955, pp.1551-1557.

53) Green,W.H., and G.A.Ampt: Studies on soil physics, 1, the flow of air and water through soils, J.Agr. Sci., 4, 1911, pp.1-24.

54) Bouwer,H.: Unsaturated flow in ground-water hydroulics, ASCE, 90(HY5), 1964, pp.121-129.

55) Hillel,D., and W.R.Gardner: Transient infiltration into crust-topped profiles, Soil Sci., Vol.109, 1970, pp.69-76.

56) Ahuja,L.R.: Applicability of the Green and Ampt approach to water infiltration through surface crust, Soil Sci. 118, 1974, pp.283-288.

57) Neuman,S.P., Wetting front pressure head in the infiltration model of Green and Ampt, Water Reso. Res. Vol.12, No.3, 1976, pp.564-566.

58) Childs,E.C.: An Introduction to the Physical Basis of Soil Water Phenomena, John Wiley, New York, 1969, pp.275-277.

CHAPTER 5

COMPARISON OF EXPERIMENTAL AND NUMERICAL RESULTS

5.1 Introduction

In order to investigate the validity and the accuracy of the numerical analysis solution, in general two methods are used, i.e., numerical results are compared with the analytical results of simple problems for which rigorous analytical solutions are available and numerical results are compared with the experimental results.

The flow problem in this thesis involves so complex conditions, that is, the saturated-unsaturated flow region and the nonlinear equation, that there is no analytical solution to the author's knowledge. Then in this chapter to check the validity of the two-or three-dimensional finite element analysis on the saturated-unsaturated flow problems, and its applicability to practical problems of flow, laboratory experimental studies on infiltration and drainage for two- or three-dimensional sand box were carried out. Numerical results are compared with the experimental results using as input data the pressure head-moisture content relationship and the hydraulic conductivity-moisture content relationship that were obtained in Chapter 4.

5.2 Experimental Study on Flow through Sand Model

5.2.1 Experimental apparatus and its procedure for two-domentional sand model.

A. Experimental apparatus

The experimental sand box was constracted of 3 cm acrylic. The sand box

measures 80cm long, 50cm tall and 10cm deep as shown in Fig.5.1. The left hand and the right hand side of the sand box are free to enable entry and exit of water, while the remaining three sides are rendered impermeable.

The pressure heads were regularly measured with the help of 15 piezometers set up at the bottom of sand box. In addition, the levels of the free surface were also measured with the help of 8 porous tubes set up at the face of front side. Air-dry sand which is the same sand used in Chapter 4 was carefully packed into this box with an approximately constant dry density (γ_d=1.5g/cm^3).

B. Experimental procedure

a. Infiltration

Before the start of the experiment, t<0, the water tables was brought to a height of 7cm above the base, by letting the water levels on the left hand side and on the right hand side of the model stand at that elevation for a long period of time (about 24 hours). At t=0, the water level on left hand side was suddenly raised to an elevation of 47cm , creating a raise of 40cm , and was maintained at that elevation through the duration of the experiment.

During the course of this experiment, lasting over 3 hours, the pressure heads were measured at the bottom, and the levels of the free surface were also measured.

b. Drainage

At the end of infiltration experiment, the water tables were brought to a height of 47cm above the base, by letting the water levels on the left hand side and on the right hand side of the model stand at that elevation for 2 days. At t=0, the water level on the right side was suddenly lowered to an elevation of 7cm , creating a drawdown of 40cm , and was maintained at that elevation through

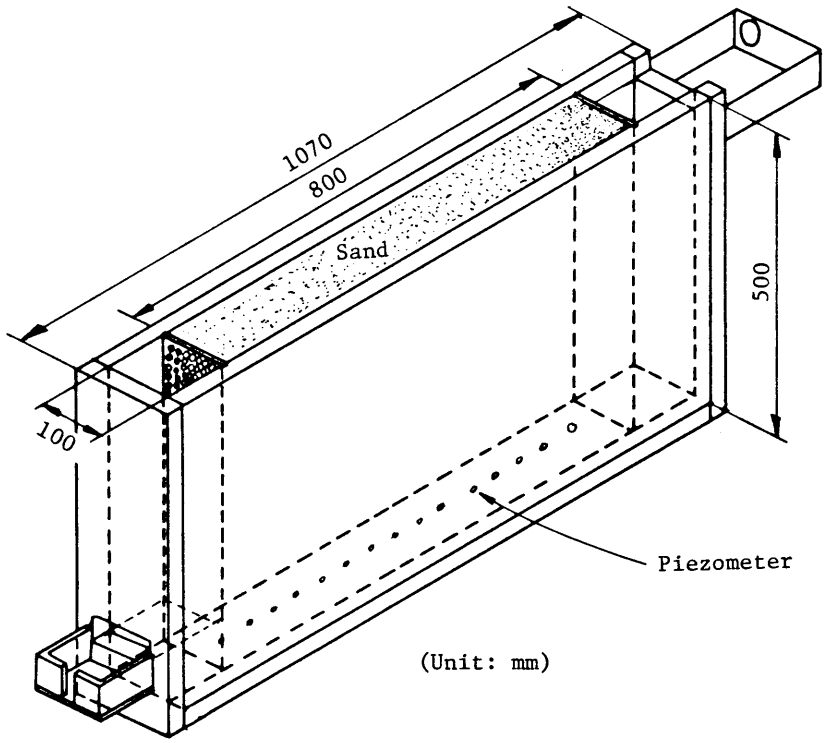

Fig.5.1 Schematic figure of sand box (for two-dimentional flow)

the duration of the experiment.

During the course of the experiment, lasting over 3 hours, the pressure heads, the levels of free surface and the quantity of water removed from storage were measured as a function of time.

5.2.2 Experimental apparatis and its procedure for three-dimensional sand model

A. Experimental apparatus

The experimental sand box measures 106cm long, 100cm tall and 82cm deep as shown in Fig.5.2. The right hand side of the sand box is free to enable entry and exit of water, while the remaining three sides are rendered impermeable. Impermeable wall (CDGH in Fig.5.2) was set at the center of the sand box, then if water is supplied at the face of ABCD (the letters locate in Fig.5.2), the flow through sand may occour following the arrow in Fig.5.2, and the flow may remove from the face of CDEF. This is a three-dimensional flow behaviour.

The pressure heads were measured with the help of 72 piezometers set up at the bottom of sand box. In addition, the levels of the free surface were also measured with the help of 26 porous tubes set up at the three impermeable sides. The soil used in this experiment was the same sand in Chapter 4. The air dry sand was carefully packed into the sand box 50cm height, 100cm wide, and 106cm long with an approximately constant dry density (γ_d=1.50g/cm^3).

B. Experimental procedure

a. Infiltration

The outlines of this experimental procedure are same methods of the two-dimensional experiment. Namely before the start of the experiment the water tables were brought to a height of 7cm above the base, by letting the water levels on the ABCD side and on the CDEF side of the model stand at that elevation

for a long period of time (about 24 hours). At t=0, the water level on the ABCD side was suddenly raised to an elevation of 47cm , creating a raise of 40cm , and was maintained at that elevation through the duration of the experiment.

During the course of this experiment, lasting over 2 hours, the pressure heads were measured at the bottom, and the levels of the free surface were also measured.

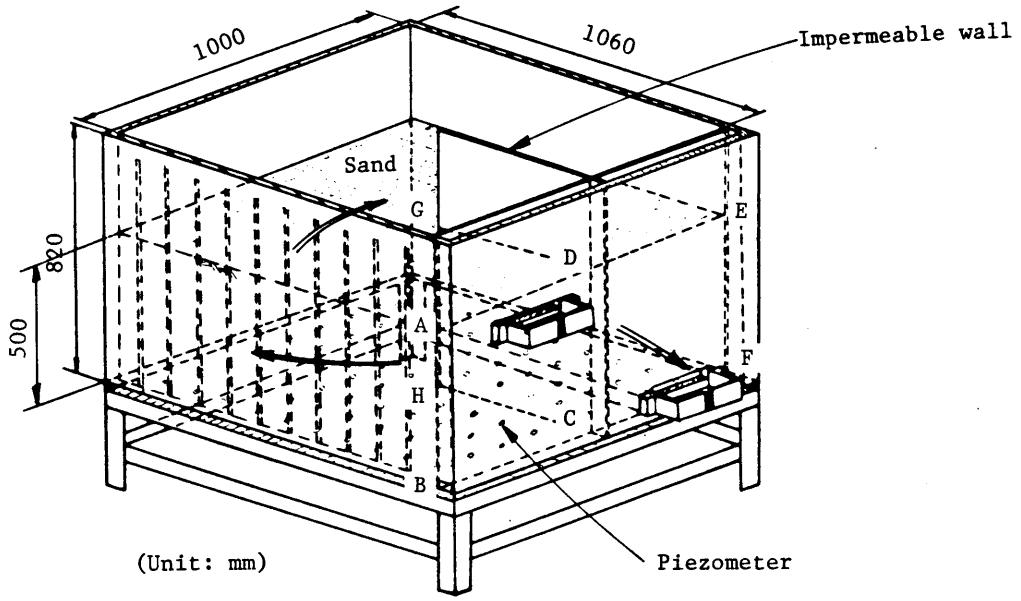

Fig.5.2 Schematic figure of sand box (for three-demensional flow)

b. Drainage

At the end of the infiltration experiment, the water tables were brought to a height of 47cm above the base of sand box, by letting the water levels on ABCD side and on CDEF side stand at that elevation for the long period of time. The

sand in the sand box was initially saturated, at zero time the water level on CDEF side was suddenly lowered to an elevation of 7cm , creating a drawdown of 40cm , and was maintained at that elevation through the duration of the experiment.

During the course of this experiment, lasting over 1 hour, the pressure heads, the levels of free surface and the quantity of water removed from storage were measured as a function of time.

5.3 Material Properties and Initial-Boundary Conditions

5.3.1 Material properties

The data required to solve the flow problem in saturated-unsaturated soil by using the finite element method with Eq.(2.28) are as follows.

(1) Specific storage S_s and permeability coefficient K_s in saturated condition.

(2) Effective porosity n_e of constitutive material.

(3) Functional relationship between the volumetric moisture content θ and permeability coefficient K_r in unsaturated condition.

(4) Functional relationship between θ and pressure head ψ in unsaturated condition.

These properties have been already obtained from the experiments in Chapter 4, and then in this simulation following values were adopted.

(1) For the flow problem in unconfined aquifer, it is a valid approximation to ignore changes in the deformation of the water and porous media. Consequently the specific storage can be neglected (i.e., $S_s=0$). The permeability in the saturated zone was measured to be $K_s=2.08\times10^{-2}$cm/sec.

(2) The porosity of the sand medium was also measured to be n=0.428 since the bulk density used was $1.50g/cm^3$. However, it is evident from Fig.4.23 that the value of effective porosity of this sand was measured to be $n_e=0.30$. This difference from n to n_e is the cause of trapped air existing in sand.

(3) The experimentally observed relations between volumetric moisture content and pressure head, for both the drying process and the wetting process, as well as those between relative conductivity (K_r) and pressure head are shown in Fig.5.3.

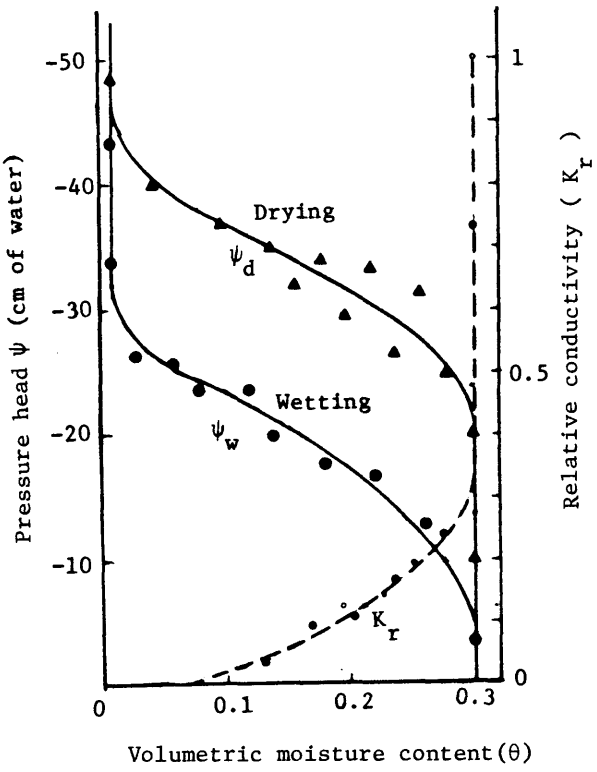

Fig.5.3 Unsaturated property of soil

As noted in Chapter 2, the specific moisture capacity $C(\theta)$ that appears in Eq.(2.28) can be computed from the slope of the moisture content-pressure head curve. For saturated flow ($\psi \geq 0$), $C(\theta)$ was set equal to zero, and K_r equal to 1. Both functions $K(\theta)$ and $\psi(\theta)$ were stored in computer memory as a series of line segment representation with linear interpolation between the co-ordinate points.

Where as hysteresis in the relationship between the pressure head ψ and the volumetric moisture content θ is important to some applications and numerical procedures must be used and have been very successful.[1),2),3),4)] These numerical methods take into account hysteresis, which must then be measured independently.[5),6),7),8),9)] In principle the relationship should be known for any possible scanning curve. Since there is an infinite number of them, some interpolation must be used in practice between two consecutive scanning curves. To simplify the problem even further, it would be useful to know a priori the minimum number of scanning curves that are necessary to predict accurately any other scanning curve. To answer this question, a physical understanding of hysteresis is necessary. Some researches clarified greatly the qualitative concepts that underlie the phenomenon of capillary hysteresis. The applicability of the independent domain theory was exploited to soil physics.[5),10)] Further developments in the theory are discussed also derived a rational interpolation formula that predicts all scanning curves within a loop from the knowledge of the boundaries of the loop alone.[11),12)] As it is pointed out by Mualem,[11)] other models exist at present, but to use the author's own words "these models need more measured data and this fact, as well as their complexity, makes them on little practical use." The fundamental achievement of Mualem's analysis is to yield a simple formula that can be used accurately in many practical case. Then in this study his analysis has been used. A detailed analysis is given in his report,[12)] so only the essentials will be summarised in this section. The various scanning curves are obtained as follows:

(1) The primary drying scanning curve is given by

$$\theta\left(\begin{matrix}\psi_1\\ \psi_{min}\end{matrix}\ \psi\right) = \theta_w(\psi) + \frac{[\theta w(\psi_1) - \theta w(\psi)]}{[\theta_u - \theta_w(\psi)]}[\theta_d(\psi) - \theta_w(\psi)] \qquad (5.1)$$

The scanning curve is obtained inside the main loop as it should be, because $(\theta_d-\theta_w)$ is multipled by a factor smaller than unity.

(2) The primary wetting scanning curve is given by

$$\theta\begin{pmatrix}\psi_{max} & \psi\\ & \psi_1\end{pmatrix} = \theta_w(\psi) + \frac{[\theta_u - \theta_w(\psi)]}{[\theta_u - \theta_w(\psi_1)]}[\theta_d(\psi_1) - \theta_w(\psi_1)] \tag{5.2}$$

As follows from Eq.(5.2), the scanning curves approach the main wetting curve during the process.

(3) Wetting after a series of alternating process of drainage and imbibition is given by

$$\theta\begin{pmatrix}\psi_1 & \cdots\cdots & \psi\\ \psi_{min} & \psi_2 & \psi_N\end{pmatrix} = \theta_w(\psi)$$

$$+[\theta_w(\psi_{N-1}) - \theta_w(\psi)]\frac{\theta_d(\psi_N) - \theta_w(\psi_N)}{\theta_u - \theta_w(\psi_N)}$$

$$+\sum_{j=1}^{(N/2)-1}[\theta_w(\psi_{2j-1}) - \theta_w(\psi_{2j+1})]\frac{\theta_d(\psi_{2j}) - \theta_w(\psi_{2j})}{\theta_u - \theta_w(\psi_{2j})} \tag{5.3}$$

(4) Drainage after a series of alternating processes of drainage and imbibition is given by

$$\theta\begin{pmatrix}\psi_1 & \cdots\cdots & \psi_N\\ \psi_{min} & \psi_2 & \psi\end{pmatrix} = \theta_w(\psi)$$

$$+[\theta_w(\psi_N) - \theta_w(\psi)]\frac{\theta_d(\psi) - \theta_w(\psi)}{\theta_u - \theta_w(\psi)}$$

$$+\sum_{j=1}^{(N-1)/2}[\theta_w(\psi_{2j-1}) - \theta_w(\psi_{2j+1})]\frac{\theta_d(\psi_{2j}) - \theta_w(\psi_{2j})}{\theta_u - \theta_w(\psi_{2j})} \tag{5.4}$$

In all cases the dependence of θ on ψ is expressed as a simple function of $\theta_w(\psi)$ and $\theta_d(\psi)$. Eq.(5.1) gives the primary drying scanning curve by way of example the curve from a point A in Fig.5.4 and similarly Eq.(5.2) gives the curve from a point B for a wetting process.

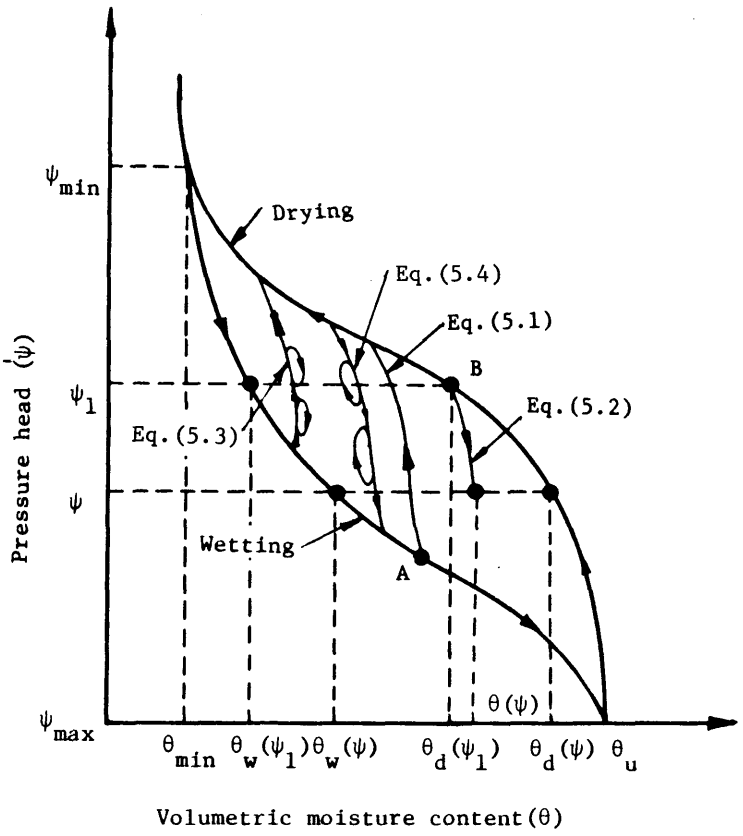

Fig.5.4 Hysteresis in the volumetric moisture content - pressure head and showing the method of Maulem

Parameters in Eqs.(5.1)-(5.4) are indicated in Fig.5.4. The value of θ_u must be equal to the effective porosity n_e.

5.3.2 Initial and boundary conditions

A. Boundary conditions

a. Two-dimentional sand model

The size of the entire flow domain and the finite element mesh are shown in Fig.5.5. This model is composed of 221 nodal points, 192 elements. The boundary conditions were imposed as follows. In Fig.5.5 AH is an impermeable boundary and CDEF is also an effective impermeable boundary in the absence of rainfall or evaporation because water cannot flow out of this domain. FG is a no-flow boundary as long as $\psi<0$ but becomes at constant head boundary (seepage face), allowing outflow, once ψ attains the value $\psi=0$. The boundary conditions can be specified in the total pressure.

Along AH and CDEF

$$\frac{\partial h}{\partial z} = 0$$

Along AC

$$h = 47\text{cm} \qquad \text{(constant)}$$

Along GH

$$h = 7\text{cm} \qquad \text{(constant)}$$

Along FG

$$\begin{cases} \dfrac{\partial h}{\partial \vec{n}} = 0 & \psi<0 \\ h = z & \psi=0 \quad \text{(seepage face)} \end{cases}$$

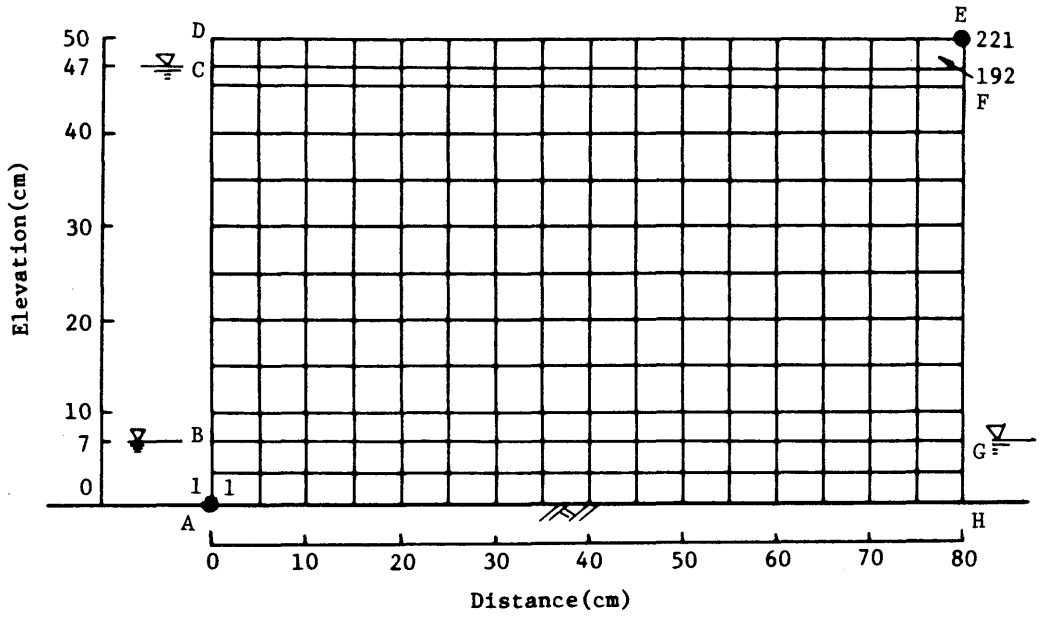

Fig.5.5 Finite element network

b. Three-dimensional sand model

Fig.5.6 gives the three-dimensional finite element subdivision of the entire flow region by using 867 nodes and 576 lower-order elements. The boundary conditions by reference to this domain can be set down. At the upper and lower boundaries of this domain, there is no vertical flow, and the quantity $\frac{\partial h}{\partial z}$ is equal to zero. In Fig.5.6 the boundary conditions are as follows.

Along the faces of ABKJ, AFPJ, and FENP

$$\frac{\partial h}{\partial x} = 0 \quad \text{or} \quad \frac{\partial h}{\partial y} = 0$$

Along the impermeable wall CDGHLMPQ

$$\frac{\partial h}{\partial x} = 0 \quad \text{or} \quad \frac{\partial h}{\partial y} = 0$$

More detailed figure of the face BENK is shown in Fig.5.7.

On the face of KSTL

$h = 47\text{cm}$ (constant)

On the face of XMNW

$h = 7\text{cm}$ (constant)

On the face of UXWV

$\frac{\partial h}{\partial \vec{n}} = 0$ $\psi<0$

$h = z$ $\psi=0$ (seepage face)

On the faces of BSTC and DUVE

$$\frac{\partial h}{\partial x} = 0$$

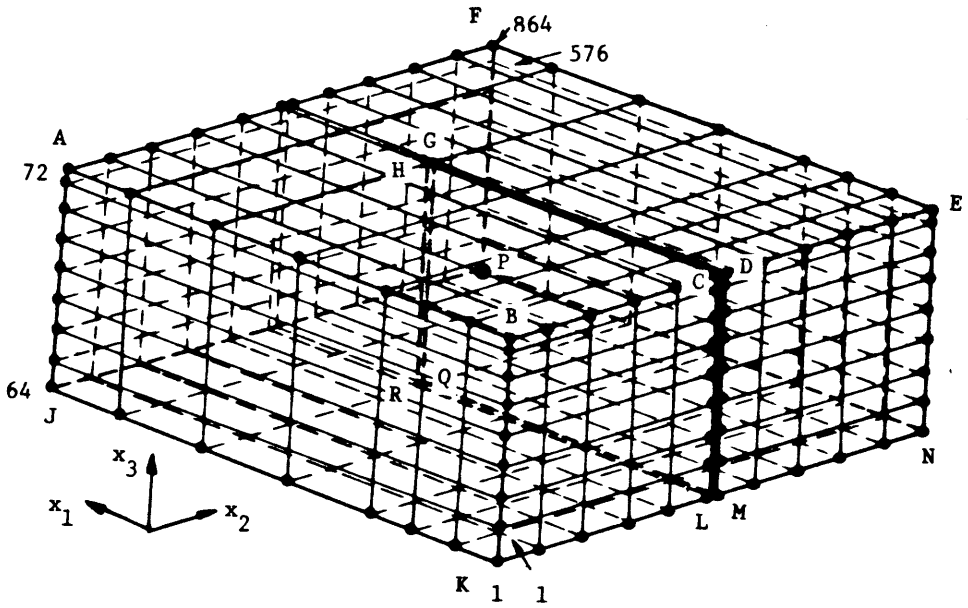

Fig.5.6 Subdivision of the entire flow region for three-dimensional finite element formulation

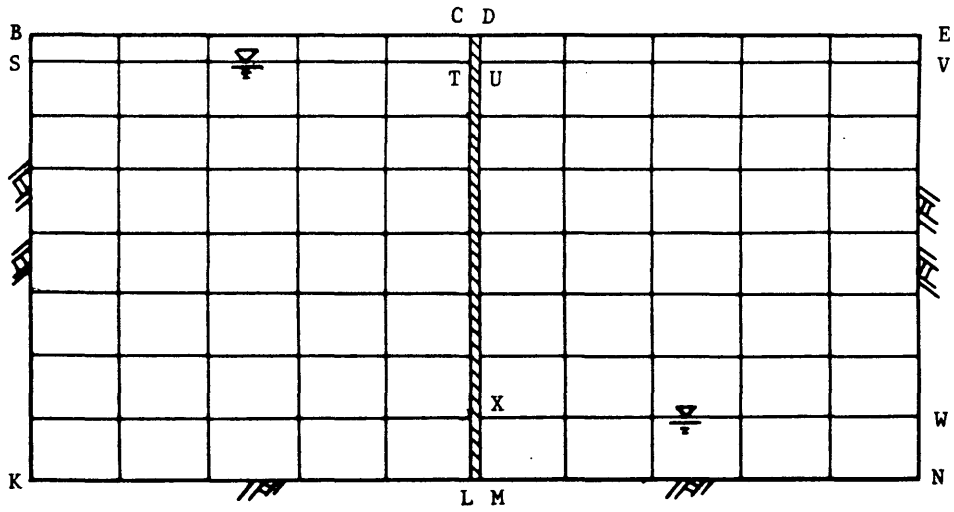

Fig.5.7 Cross section of the domain

B. Initial Conditions

The aim of the numerical simulation was to use a distribution of initial pressure head ψ_0 in the entire flow domain. In the experiment sand was carefully packed in the box with the bulk densities γ_d=1.5g/cm^3. Scatter of the bulk densities may be exist, for puruose of numerical simulation, however, the sand was assumed to be homogeneous. According to the results of the experiment in Chapter 4, hydrostatic equilibrium was initially obtained as indicated by the profiles of pressure head for infiltration and drainage experiment in Fig.5.8 and Fig.5.9 , respectively. These prefiles of pressure head were applied to numerical analysises of two-dimensional and three-dimensional flow model as initial conditions. In Fig.5.8 the initial condition was established by setting the negative value of the pressure head(ψ) at the top of capillary fringe equal to the elevation head and linearly increasing the head to zero at the free surface.

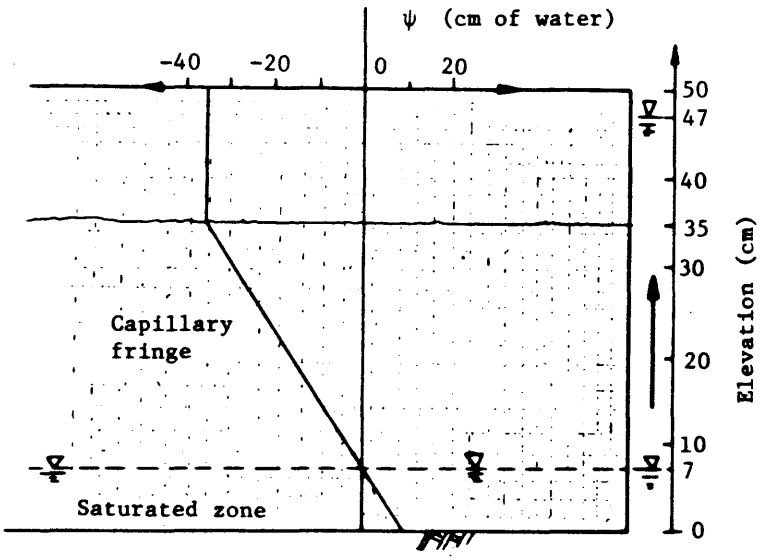

Fig.5.8 Initial distribution of pressure head(ψ) for infiltration used in the simulation

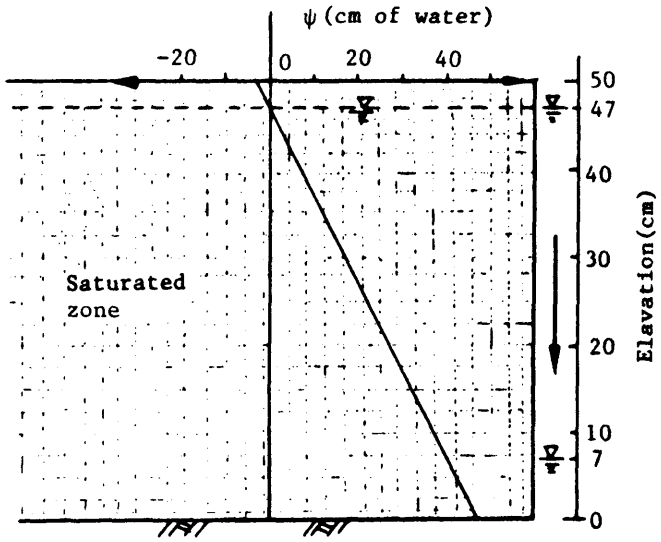

Fig.5.9 Initial distribution of pressure head(ψ) for drainage used in the simulation

5.4 Comparisons of Experimental data with Numerical Results and Discussions

5.4.1 Two-dimensional sand model

A. Infiltration

As a first step in comparison of experimental and numerical results, the computed positions of the free surface, ψ=0, at various times are shown in comparison with the experimental results of infiltration in Fig.5.10. In the classical approach the free surface is treated as a moving material boundary, whereas in the present work it is merely an internal isobar which happens to separate the saturated and unsaturated portions of the flow domain. At t=3600sec, the zero-pressure surface (free surface) attains a quasi-steady configuration, and the saturated zone reaches a state of near equilibrium. The computed pressure head

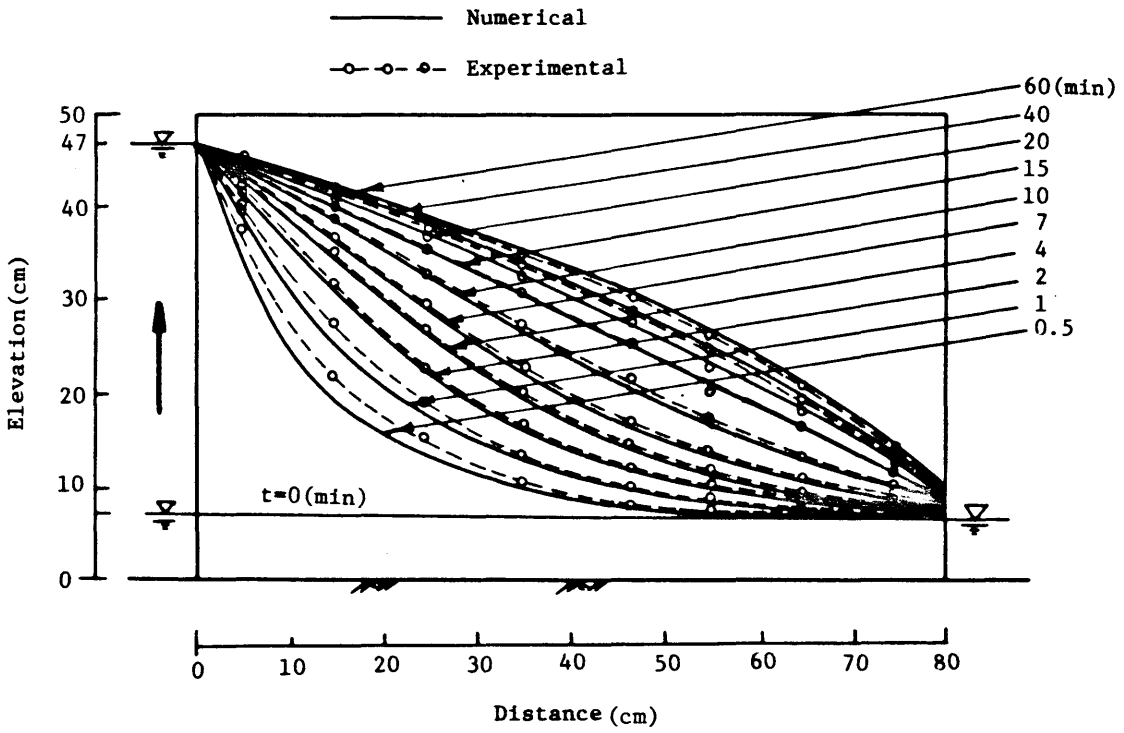

Fig.5.10 Comparison of numerical and experimental results of free surface (for wetting)

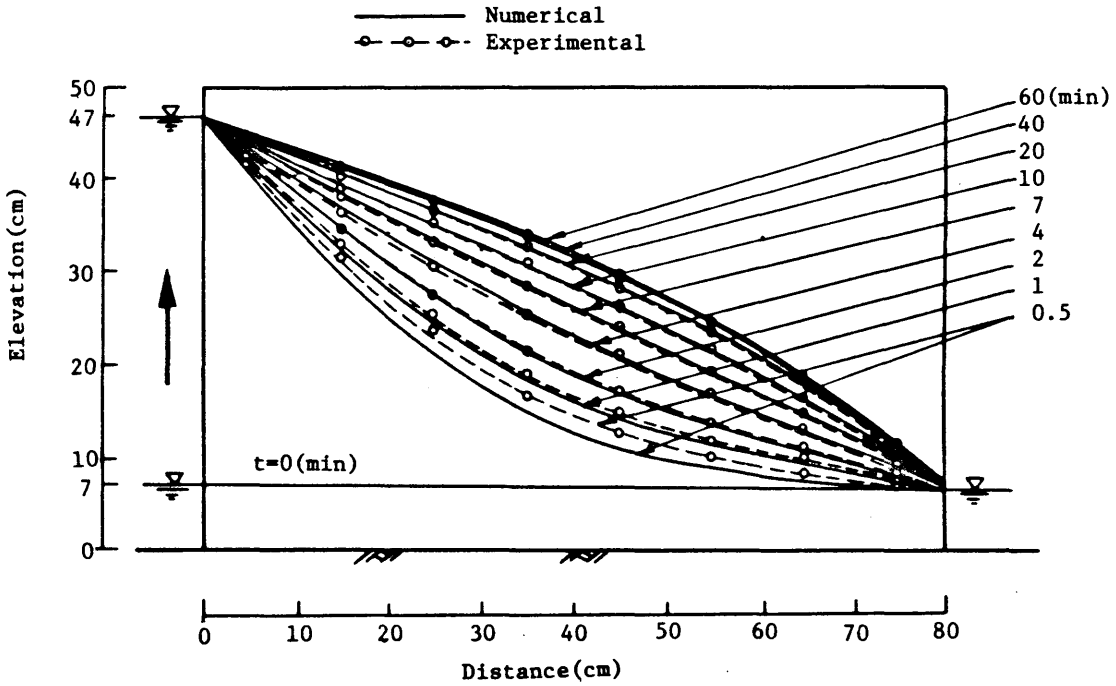

Fig.5.11 Comparison of numerical and experimental results of pressure head on the bottom (for wetting)

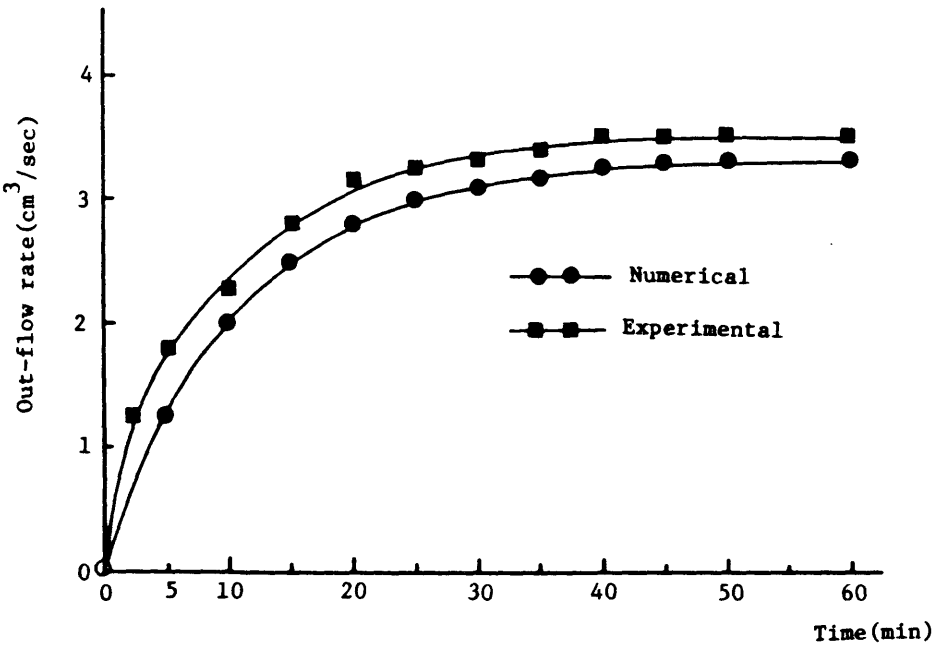

Fig.5.12 Comparison of numerical and experimental results of out-flow rate (for wetting)

distributions on the bottom at various times are shown in Fig.5.11, which also shows experimental results of infiltration. The numerals on the curves in both figures represent time in minutes from the start of infiltration. The agreement between computed and measured profiles in Figs.5.10 and 5.11 for standard sand was considered satisfactory for both points of free surface positions and pressure heads at bottom. These agreements show that the independent measurements of $\psi(\theta)$ and $K(\theta)$ must have been essentially correct for this soil. Furthermore these agreements improve the accuracy of this numerical analysis solution and would suggest that if the hydrologic characteristics of the porous material are accurately known, then the computer solution of the differential flow equation developed for this study would enable the pressure head profiles to be easily obtained.

Fig.5.12 presents computed and experimental out-flow rate with respect to time for the case of infiltration. The computed results do not exactly equate to the experimental data. This deviation is probably due to the expected error in region with a fairly coarse mesh on seepage face.

This simulation period was 120 minutes, the total computer time use was 352 seconds. A fully backword difference scheme was used to solve for ψ during a time increment. Convergence was measured in terms of the maximum absolute change in $\Delta\psi_n$ at any node during an iteration. Usually between 2 to 10 iterations were required during each time step to reduce max $|\Delta\psi_n|$ below 0.01cm before advancement to next time increment.

B. Drainage

Fig.5.13 shows the comparison between the behavior of the computed free surface and that of the experimental results in the case of drainage. Fig.5.14 also presents the pressure head distribution at the bottom for different times with comparison of experimental data. In this computation the time increment

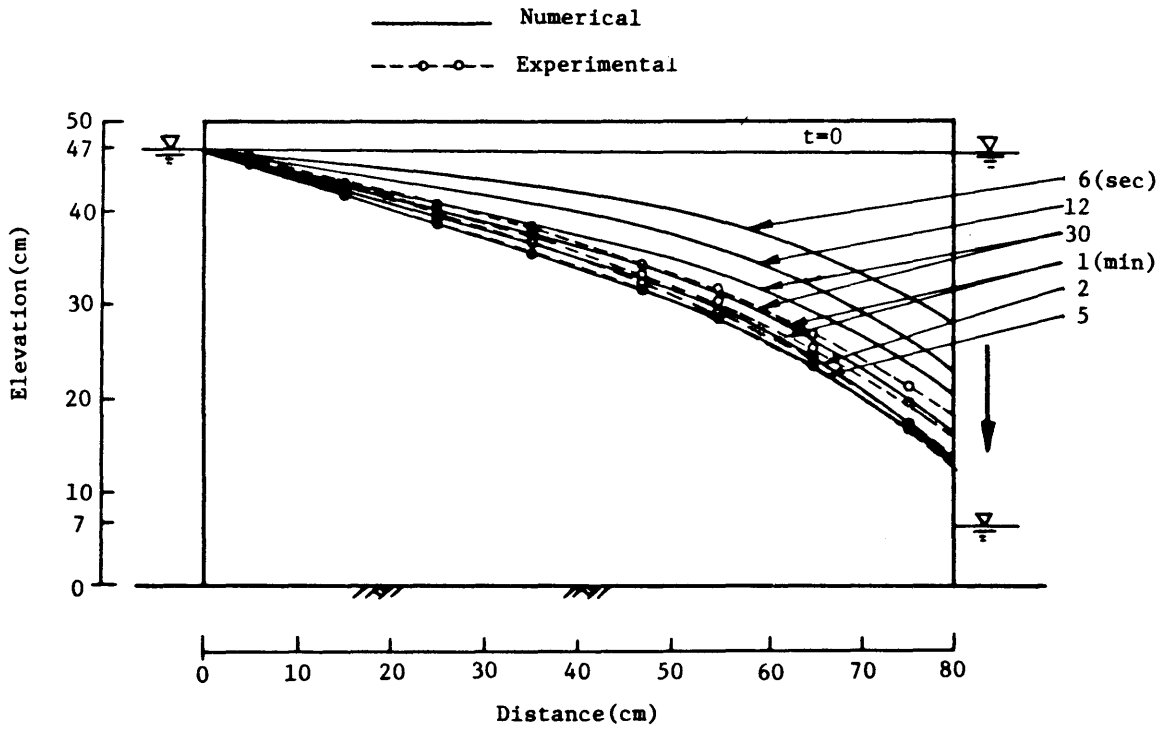

Fig.5.13 Comparison of numerical and experimental results of free surface (for drainage)

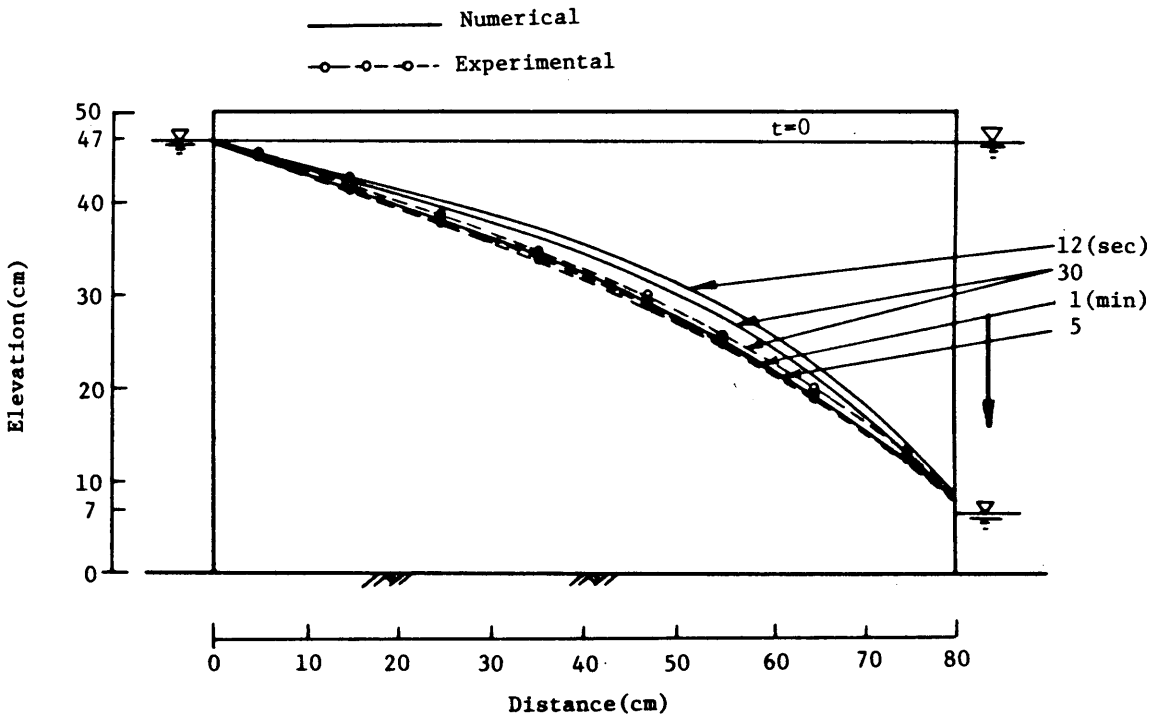

Fig.5.14 Comparison of numerical and experimental results of pressure head on the bottom (for drainage)

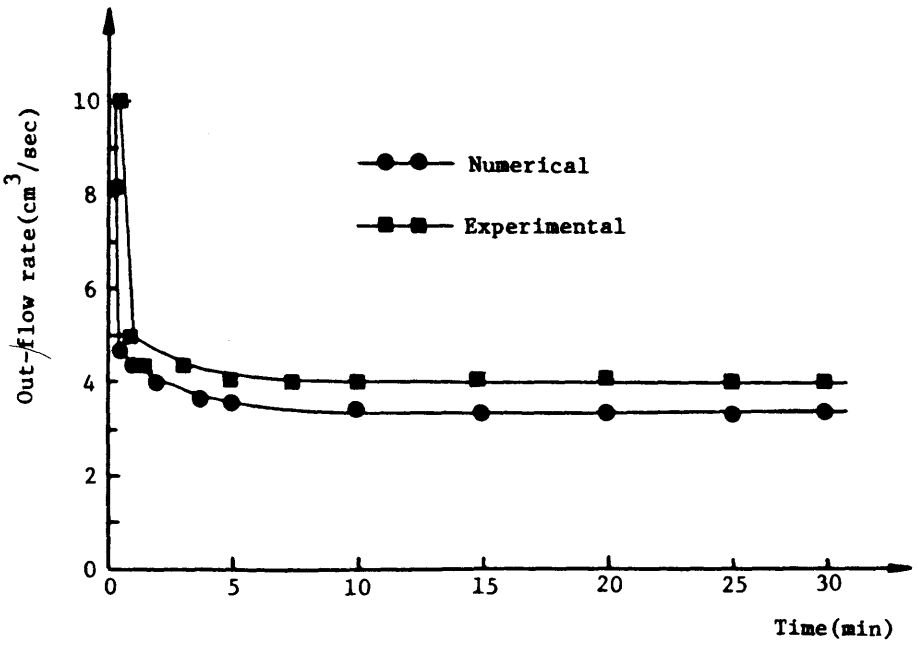

Fig.5.15 Comparison of numerical and experimental results of out-flow rate (for drainage)

was varied, ranging from 0.1 seconds during initial time steps to as much as 10 minutes after 120 minutes of drainage have elapsed. It can be seen from Fig. 5.13 that there is some difference between the two results at early time, with the computed position remaining slightly above the observation position. The observed potentials are falling more rapidly than the computed potentials and hence the experimental model is approaching steady-state much more rapidly than the numerical model. The departure attenuated at large values of time and the system attained steady-state after about 10 minutes. Thus the numerical and the experimental models appear to tend toward the same steady-state conditon, but follow different transient paths in attaining steady-state. However, a careful comparison in Fig.5.13 reveals the fact that the magnitudes of the differences between the computed values of potentials and those actually measured are less than 2cm at all times and all locations. These departures are small and can be ignored.

That the numerical model can be approaching steady-state rapidly is led by using the drying curve of material properties in Fig.5.3 in the calculations, that is, in near saturated region the drying curve may be providing relatively high values of hydraulic conductivity K and relatively low values of specific moisture capacity ($\partial\theta/\partial\psi$). Fig.5.15 presents computed and experimental outflow with respect to time. In spite of the rapid change of experimental data, a good agreement exists between computed and measured outflow.

5.4.2 Three-dimentional sand model

A. Infiltration

The results of the three-dimentional finite element analysis are compared with the experimental results of three-dimentional seepage for infiltration at

sections ABKJ and FENP (the letters locate the relative position of Fig.5.6) in Figs.5.16 and 5.17.

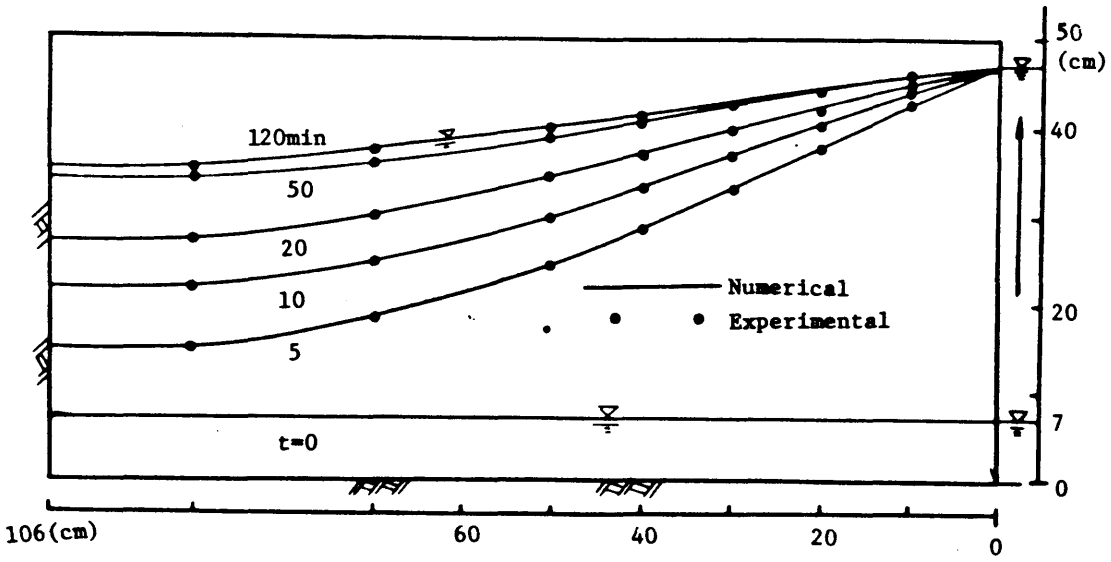

Fig.5.16 Comparison of numerical and experimental results (for wetting) along the cross section of ABKJ in Fig.5.6

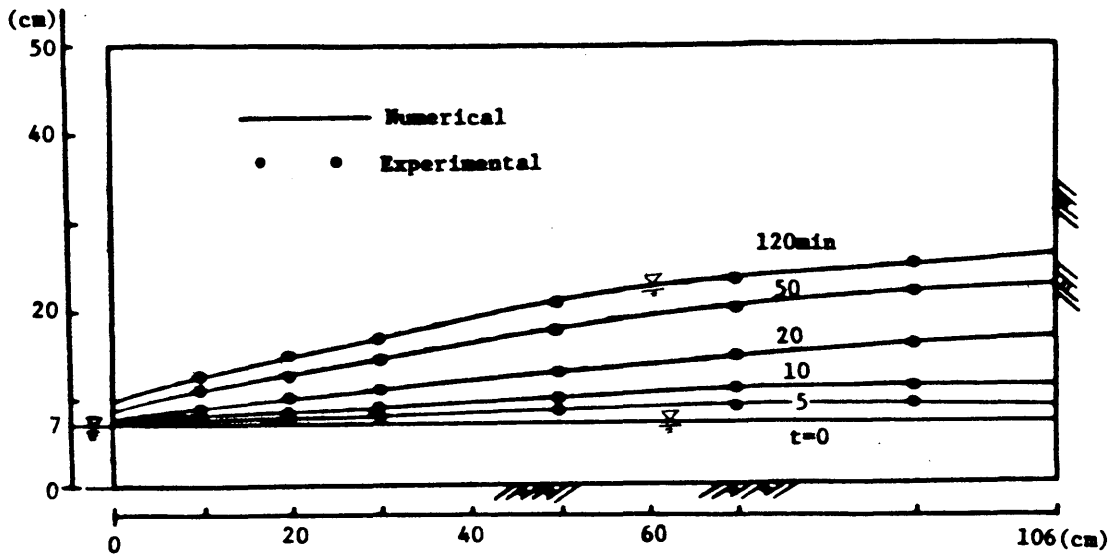

Fig.5.17 Comparison of numerical and experimental results (for wetting) along the cross section of FENP in Fig.5.6

The defference in curvature of the profiles at the two sections considered is clearly evident. In this experiment, steady-state conditions were attained after about 120 minutes and Fig.5.18 gives computed and experimental steady-state results of the position of free-surface. Over all, the agreement between the computed solution and the experimental determined values is good.

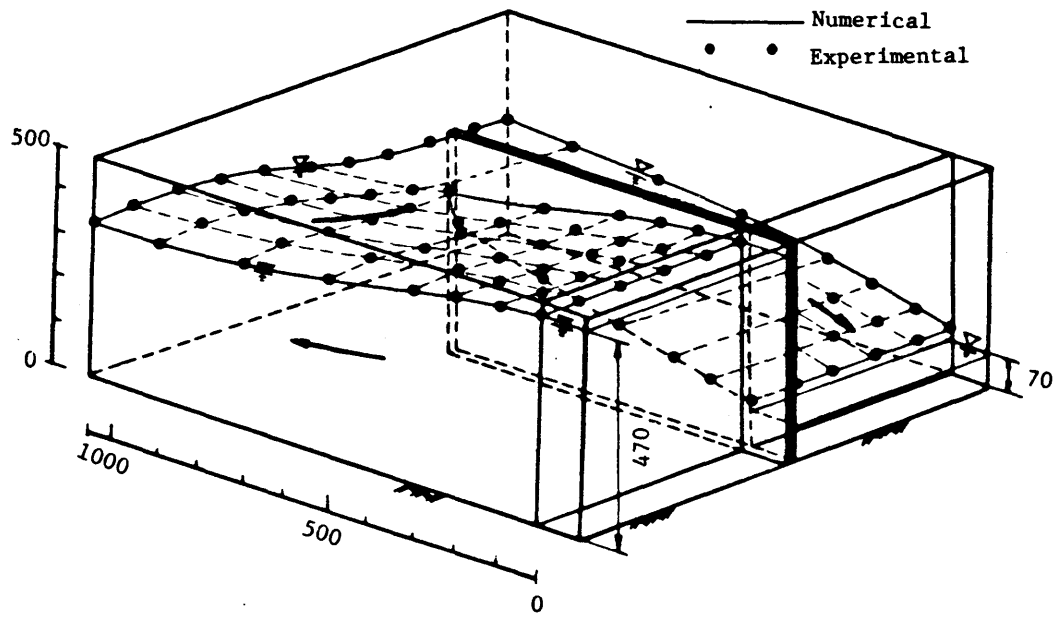

Fig.5.18 Comparison of numerical and experimental results (for wetting) of steady state

B. Drainage

Figs.5.19a and 19b show both results of experiment and numerical analysis at sections ABKJ and FENP for a few drainage times. Steady-state condition was attained after about 60 minutes. Fig.5.20 also shows computed and experimental outflow with respect to time for infiltration and drainage. There are also good agreements between computed and measured positions of free surface and these good agreements are extremely encouraging and suggest that it is valid to apply this three-dimensional finite element model to an actual analysis of a field problem. But its possibilities of application for field problems are limited by the size of the computers available. This simulation required 110k words of core storage and 2 hours of computer time for 15 time steps. In each time step, the iterative procedure was necessary to achieve a satisfactory degree of convergence on an average to 0.01cm usually between 2 to 10 times. To reduce the core storage and computer time, some techniques have been proposed.[13),14)] For example, a disk or tape is used to store data reading from cards or Jacobian matrix for each elements. But this techniques can be used only for steady-state and linear problemes and if this techniques is too applied, the drastic increase in computational time is largely, then it is very difficult problem at the point of view of cost. It must be, however, emphasized that consideration of economy is strongly in favour of numerical methods which yield more comprehensive results faster and at less cost than alternative techniques.

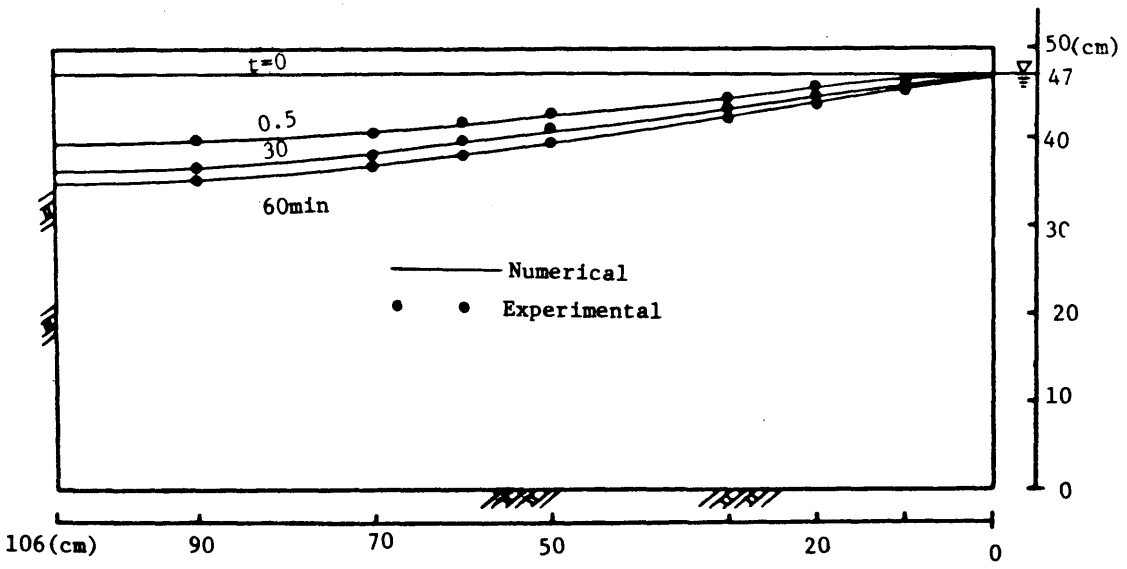

Fig.5.19a Comparison of numerical and experimental results (for drying) along the cross section of ABKJ in Fig.5.6

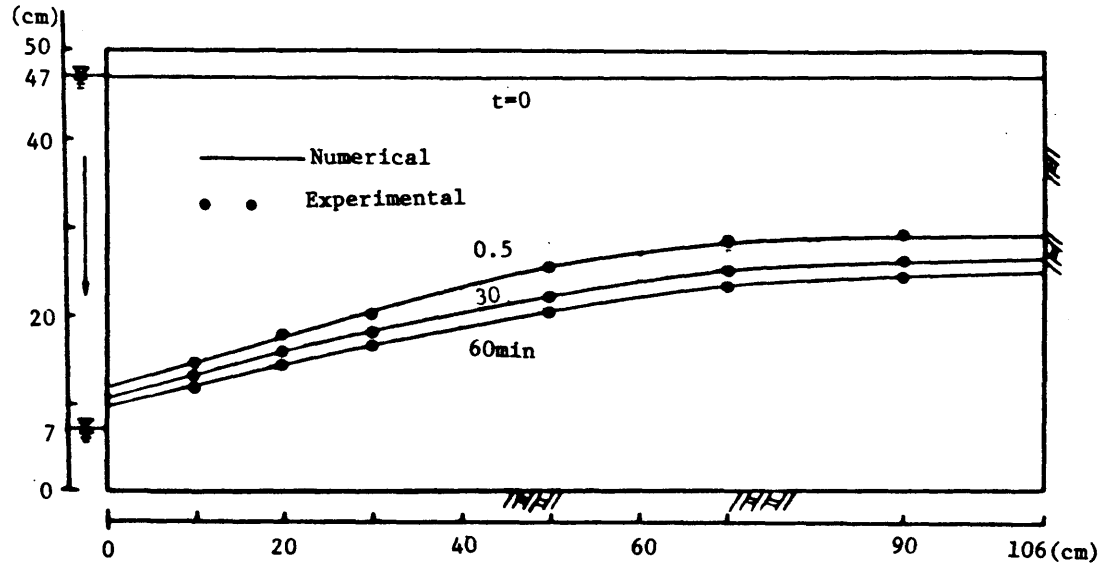

Fig.5.19b Comparison of numerical and experimental results (for drying) along the cross section of FENP in Fig.5.6

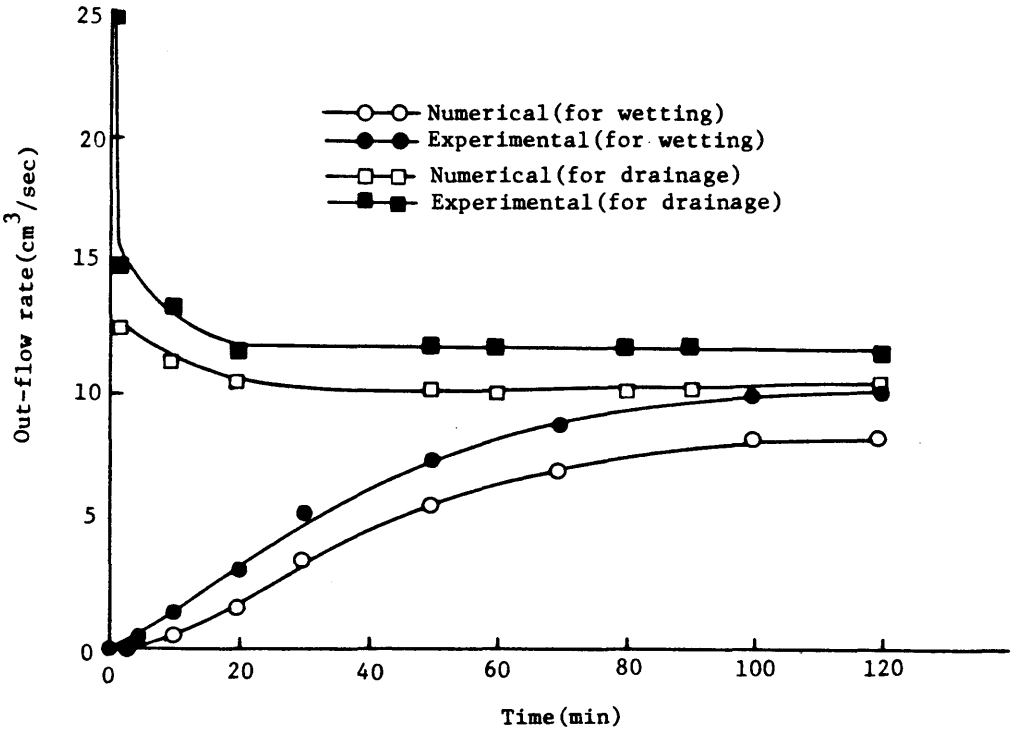

Fig.5.20 Comparisons of numerical results out flow rate

5.4.3 Effects of initial conditions and hysteresis of retening curve

In order to investigate the further validity and applicability of the finite element analysis in the saturated-unsaturated flow problem mainly for two-dimension, numerical results were compared with the experimental results obtained by Akai and Uno[15]. A watertank used in the experiment is 400cm long, 25cm wide and 50cm high and its front panel was made by a thick glass. Sand, whose average grain size was 1.5mm was packed in the watertank and a sand model with porosity of 0.44 was constructed. The water pressures in the sand model were measured by pressure transducers at many points.

Among the many experimental results, the following five cases are chose for comparison with the finite element analysis.

Case 1. Change of transient flow pattern due to the sudden water raise

(a) The base rock is permeable and the initial water level is 10cm above the base.

(b) The base rock is permeable and the initial water level is on the base.

(c) The base rock is impermeable and no water exists.

Case 2. Change of transient flow pattern due to the sudden drawdown

Case 3. Change of transient flow pattern due to the sudden water raise with the hysteresis phenomenon

The finite element mesh is shown in Fig.5.21. The permeability in the saturated zone and the porosity of the sand medium were measured to be 0.33cm/sec and 0.44 respectively. Since the relationship between θ and ψ, and also the relationship between θ and K_r were not available unfortunately, these relationships had to be assumed as shown in Fig.5.22 from the experimental data in which θ=0.44 in the saturated state and θ=0.0085 when the capillary tension (pressure head) was -8cm.

Figs.5.23,5.24, and 5.25 show the results of the finite element analysis (solid lines) and the experiments (dotted lines with open circles), when the water rise was 20cm. In these figures, it is noted that the initial condition of water produces the significant influence of the flow pattern. When the water exist initially in the sand medium (Figs.5.23 and 5.24), the water front advances in the convex form, while it advances in the concave form when the water does not exist initially. Such complex flow behaviors are well analyzed by the finite element method.

Figs.5.26 (a) and (b) are for case 2, in which the water level was reduced 20cm down from the initial level of 30cm. Fig.5.26 (a) shows the comparison between the experimental result and the saturated-unsaturated finite element analysis. The saturated-unsaturated finite element analysis was compared with the conventional saturated finite element analysis in Fig.5.26 (b). Fig.5.26 (a) indicates the both results agree very well. Fig.5.26 (b) shows

that the change of the free surface by the conventional method is faster than by the new method. This is because the effective porosity n_e was used in the conventional method, in which it is assumed discharge of water with the amount of n_e occurs instantaneously when the elevation of free surface was down. However, in reality, the water discharge occurs gradually and the saturated medium transfered to the unsaturated state with a long time. In order to take into account the delayed effect, very complex methods have been proposed.[16] The saturated-unsaturated finite element method described in this thesis can treat this complex phenomenon easily and can solve much more complicated problems.

Fig.5.27 is for the case 3 and an example of hysteresis analysis. The water retention curve was assumed as shown in Fig.5.28 and the hysteresis loops are estimated by Maulem's method.

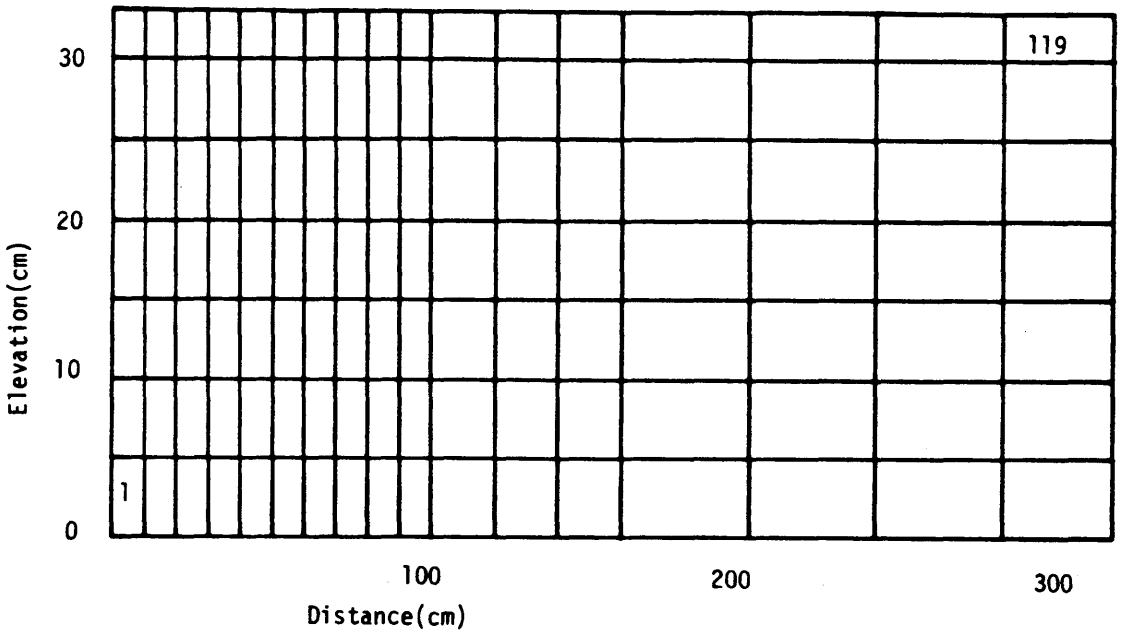

Fig.5.21 Finite element network

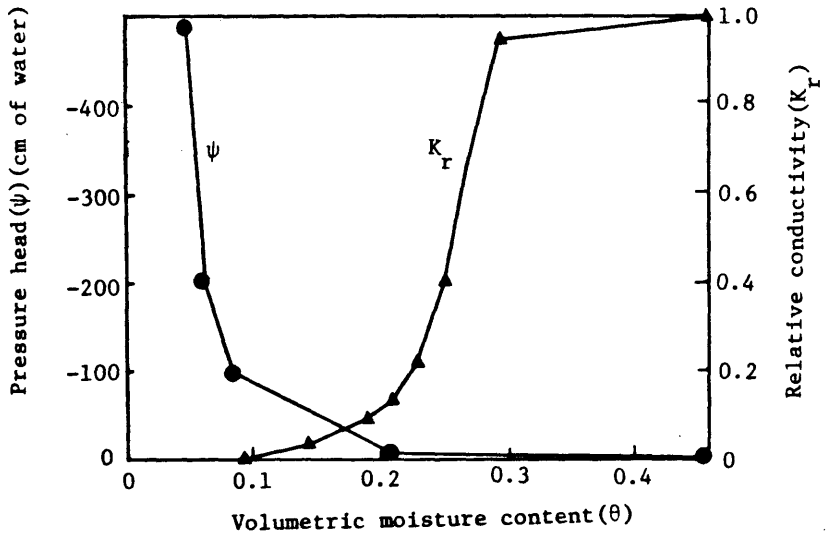

Fig.5.22 Unsaturated property of soil

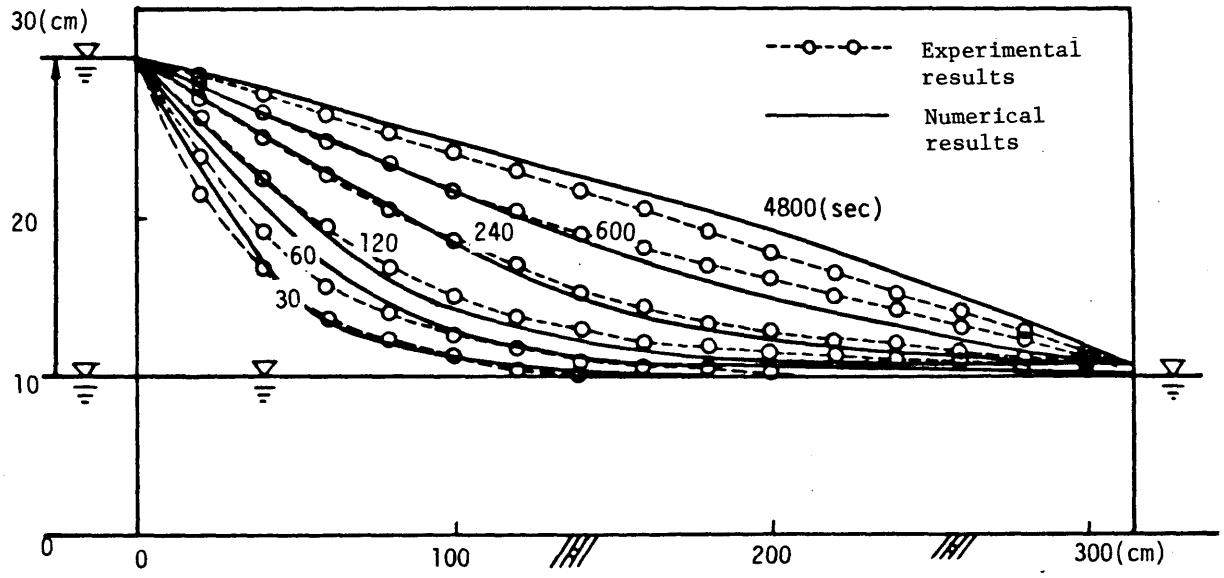

Fig.5.23 Comparison of numerical and experimental results (for wetting)

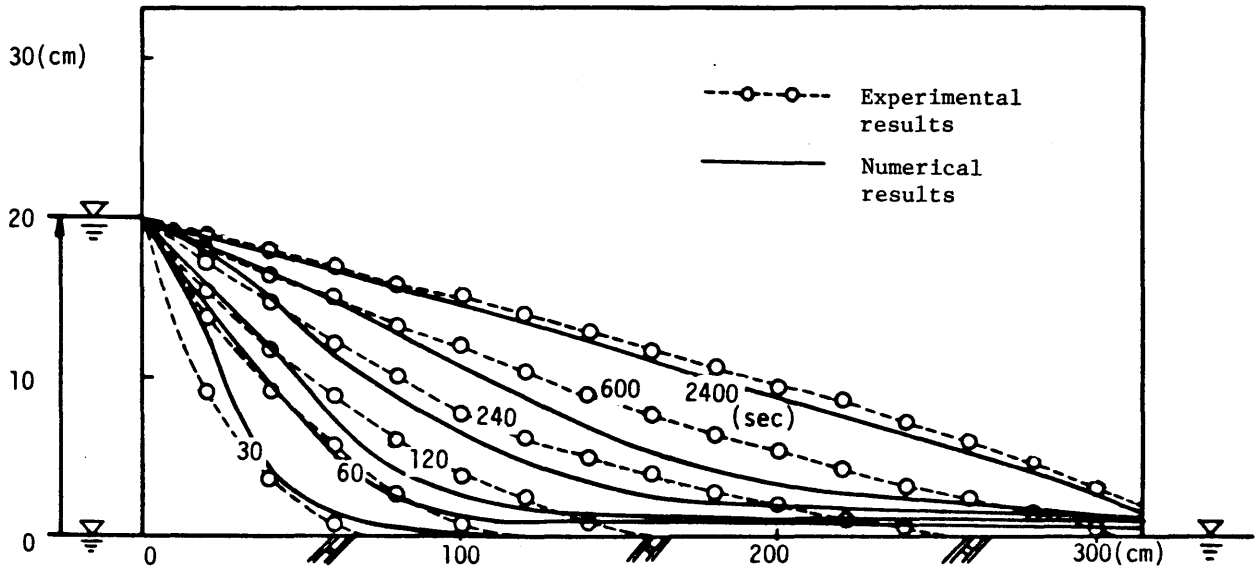

Fig.5.24 Comparison of numerical and experimental results (for wetting)

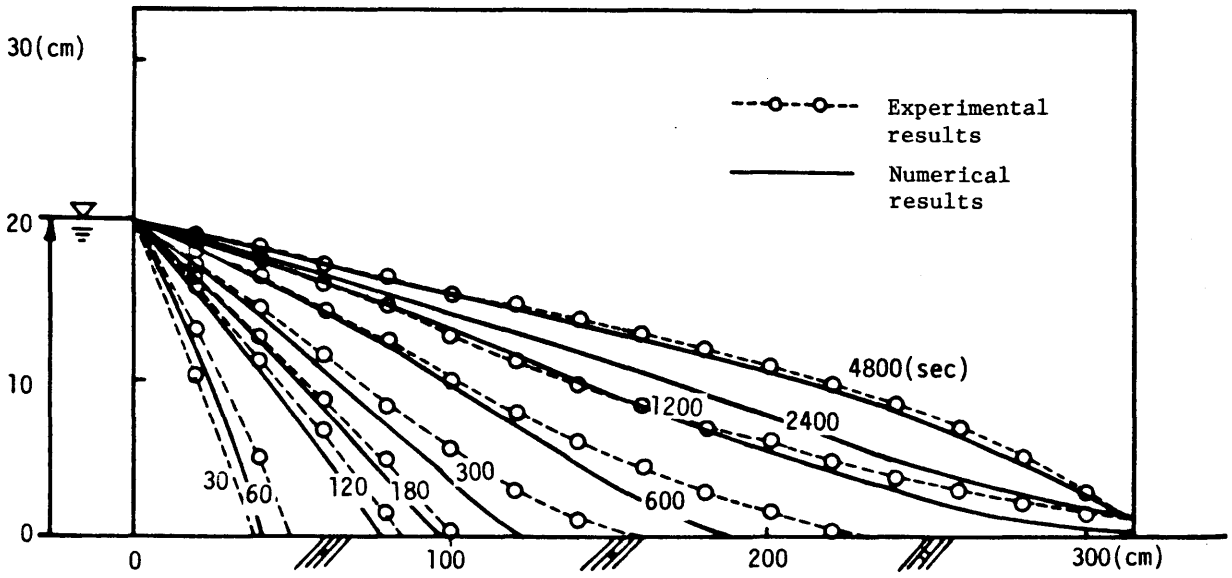

Fig.5.25 Comparison of numerical and experimental results (for wetting)

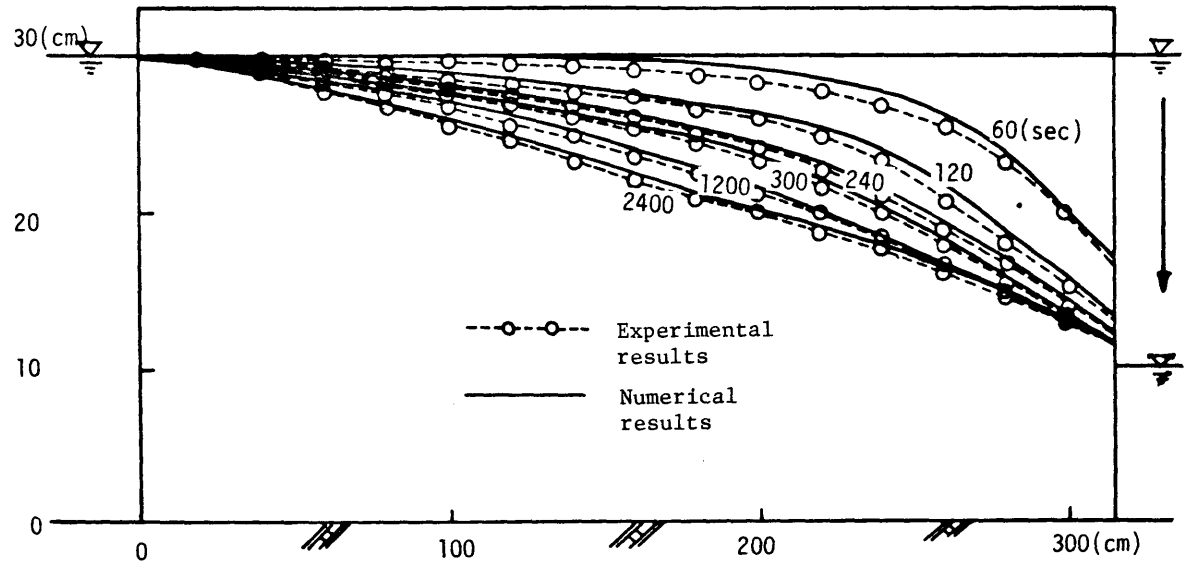

Fig.5.26 (a) Comparison of numerical and experimental results (for drying)

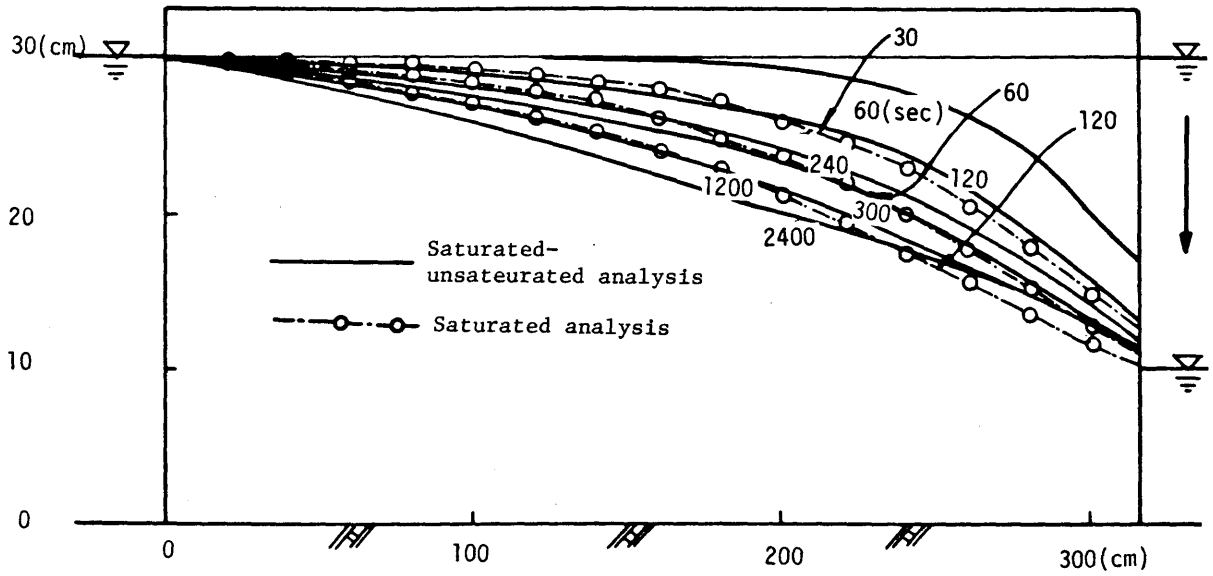

Fig.5.26 (b) Comparison of the saturated-unsaturated analysis and saturated analysis (for drying)

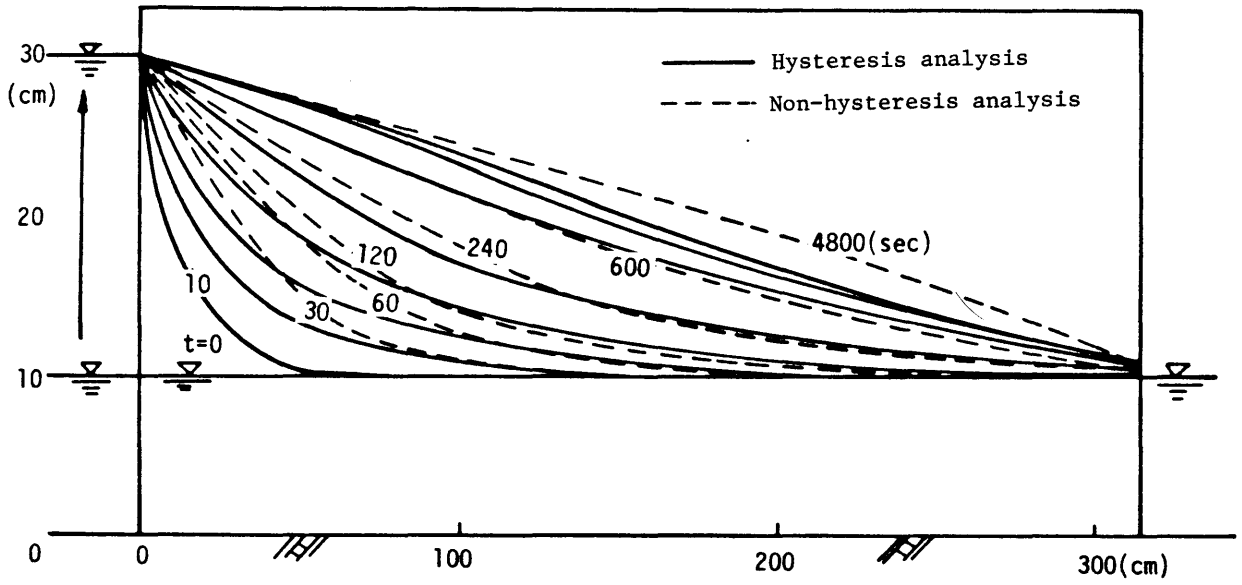

Fig.5.27 The numerical results in considering hysteresis

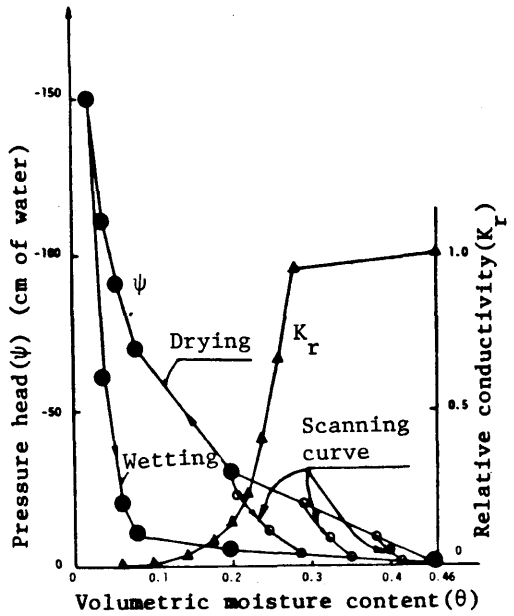

Fig.5.28 Unsaturated property of soil (considering hysteresis)

5.5 Conclusions

The validity and the accuracy of the two-and three-dimensional saturated-unsaturated finite element approach which has been descrived in Chapter 3 have been investigated to compare the numerical results with the experimental data. The results were that the good agreements between computed and measured pressure head profiles have been obtained. It should be remarked that the saturated-unsaturated finite element analysis for two-and three-dimensional model is very powerful for the problems of transient flow throught soil and offers a realistic representation of actual nature and applications to a wide range of problems. In addition an advantage which has not been demonstrated herein in the case with which seepage through nonhomogeneous and anisotropic regions can be included. The moisture content field can be determined from the pressure head field by using the $\psi(\theta)$ relationship. All computer runs were carried out on a ACOS-700.

The main conclusions in this chapter are as follows:

(1) The laboratory experiments on infiltration and drainage for two-or three-dimensional sand box were carried out with measuring pressure head and outflow rate.

(2) The problems of infiltration and drainage for same models were simulated by numerical analysis.

(3) The relationships of pressure head (ψ) - volumetric moisture content (θ) and hydraulic conductivity (K) - volumetric moisture content that have been obtained in Chapter 4 were used as input data to gets numerical results.

(4) The pressure head distribution at the hydrostatic equilibrium condition according to the results of experiments in Chapter 4 was also applied to the numerical simulation as an initial condition.

(5) The results of two-and three-dimensional finite element analysis were compared with the laboratory model tests. The numerical results showed the very good agreements with the experimental data. These agreements suggest that if the hydrologic characteristics of porous material are accurately known, then the numerical solution of the differential flow equation developed in this study would enable the pressure head profiles to be easily obtained.

(6) The saturated-unsaturated finite element method was applied to the various problems whose initial conditions were different and found to be very effective to detect the realistic changes of the flow pattern.

(7) The numerical analysis to take into account of the complex phenomenon of hysteresis is shown to be possible by using Maulem's method.

References

1) Hanks,R.J., A.Klute, and E.Bresler: A numerical method for estimating infiltration, redistribution, drainage, and evaporation of water from soil, Water Reso. Res., 5, 1969, pp.1064-1069.

2) Rubin,J.: Numerical method for analyzing hysteresis-affected, post-infiltration redistribution of soil moisture, Soil Sci. Soc. Amer. Proc., 31, 1967, pp.13-20.

3) Staple,W.J.: Infiltration and redistribution of water in verical columns of loam soil, Soil Sci. Soc. Amer. Proc., 33, 1969, pp.840-847.

4) Whisler,F.D., and A.Klute: The numerical analysis of infiltration considering hysteresis into a vertical column of soil at equilibrium under gravity, Soil Sci. Soc. Amer. Proc., 29, 1965, pp.489-494.

5) Poulovassilis,A.: Hysteresis of pore water, an application of the concept of

independent domains, Soil Sci., 93, 1962, pp.405-412.

6) Poulovassilis,A.: Hysteresis of pore water in granular porous bodies, Soil Sci. 109, 1970, pp.5-12.

7) Topp,G.C.: Soil water hysteresis measured in a sandy loam compared with the hysteretic domain model, Soil Sci. Soc. Amer. Proc., 33, 1969, pp.645-651.

8) Topp,G.C.: Soil water hysteresis in silt loam and clay loam soils, Water Resour. Res., 7, 1971, pp.914-920.

9) Topp,G.C., and E.E.Miller: Hysteretic moisture characteristics and hydraulic conductivities for glass-bead media, Soil Sci. Soc. Amer. Proc., 30,1966, pp.156-162.

10) Miller,E.E., and R.D.Miller: Theory of capillary flow: 1, practical implications, 2. experimental information, Soil Sci. Soc. Amer. Proc., 19, 1955, pp.267-275.

11) Mualem,Y.: Modified approach to capillary hysteresis based on a similarity hypothesis, Water Resour. Res., 9, 1973, pp.1324-1331.

12) Mualem,Y.: A conceptual model of hysteresis, Water Resour. Res., 10, 1974, pp.514-520.

13) Gupta,S.K. and K.K.Tanji: A three-dimensional Galerkin-finite element solution of flow through multi-aquifers in Sutter Basin, California, Water Resour. Res. 12(2), 1976, pp.155-162.

14) Gupta,S.K. and K.K.Tanji: A new approach to reduce core storage and computational time in finite element solution and its applications. "Finite Element in Water Resources", Edited by W.G.Gray, G.F.Pinder and C.A.Brebbia, Pentech Press, 1976, pp.2.179-2.194.

15) Akai,K. and Uno,T.: The study on quasi-one-dimensional non-steady seepage flow of ground water, Proc.JSCE, No.127, 1966, pp.14-22,(in Japanese).

16) Boulton,N.S.: Analysis of data from non-equilibrium pumping test allowing for delayed yield from srorage, Proc. ICE, 26, 1963, pp.469-482.

CHAPTER 6

DRAWDOWN TEST METHODS FOR DETERMINING AQUIFER CHARACTERISTICS

6.1 Introduction

Many complicated field flow problems can now be solved by applying finite element method. However, the reliability of the results obtained by this method depends largely on the accuracy of the numerical values of the hydraulic characteristics of aquifers and also on properly assumed boundary condition. It is obvious that the result of any ground water flow computation will be erroneous when these values and boundary conditions are insufficiently known.

No matter how carefully laboratory permeability tests are made, they represent only minute volumes of soil at individual points in large masses. Their value in solving field seepage and drainage problems depends on how well they represent masses of materials that actually exist in the field. When used with careful consideration of field conditions, laboratory methods can be of considerable value. Nevertheless, in important projects it is often advisable to require field tests that measure the hydraulic characteristics of large masses of soil in situ.

A drawdown test is one of the most useful means of determining hydraulic properties of aquifers. It may yield reliable results which, in general, are representative of a larger area than are single point observations. Based on the work of Darcy, Theis' or Jacob's formula have been commonly applied. To obtain the hydraulic characteristics of an aquifer to be computed by pumping a well and observing the effect of this pumping in a number of other wells in the vicinity. These formulas for the analysis of pumping test data are based on certain assumptions and generalizations. Erroneous results of the computations of the hydraulic characteristics of an aquifer are sometimes ascribed to

incorrectness of the formula applied, whereas the actual case of error is the fact that field conditions did not satisfy the assumptions on which the formula is based. Therefore, in this chapter special attention is paid to the conditions and limitations of these methods of analysis and new methods for the analysis of drawdown test data will be shown.

Firstly, it is not always possible to install the well screen over the whole thickness of the aquifer. In such a case the well is partially penetrating. Around a partially penetrating well, the flow lines in the aquifer are no longer horizontal but are radial in a vertical sense. Therefore it is necessary to understand the effect of partial penetration. In section 6.2 formulas and methods are described to avail in evaluating the data from drawdown tests under partially penetrated aquifers, with some illustrative examples.

Secondly, drawdown tests sometimes have to be performed near the boundary of the aquifer. In such instances, the assumption that the aquifer is of infinite areal extent is no longer valid. Therefore, formulas and methods of evaluating drawdown test results in aquifers with circular constant head boundaries are presented in section 6.3.

Each formula is developed in a nonsteady-state and for confined and unconfined aquifer.

6.2 Analysis of Drawdown Test Data for Pratially Penetrating Wells

6.2.1 Introduction

To obtain the formation constants from drawdown test data, Theis' Method or Jacob's Method is commonly used. However , we are often confronted with the case in which we can not obtain the formation constant, using these methods. For this problem, it is necessary to consider again the assumption on which Theis'and Jacob's Methods stand as follows;

(1) Flow within the porous medium obeys Darcy's law.

(2) The layer is homogeneous and isotropic with respect to permeability.

(3) Storage coefficient is time independent.

(4) The system is considered to be of infinite radial extent with the well at its center.

(5) Only single phase (or saturated) flow occurs in the aquifer.

(6) The well is assumed to have no surface of seepage.

(7) Head losses through the well screen are neglected.

(8) The pumping well is totaly penetrated in the aquifer.

It seems that some assumptions of those do not satisfy the conditions of actual field drawdown test. In this conception, we consider that it is quite common in developing aquifer storage projects not to open up the entire aquifer thickness. In other words, the last assumption does not satisfy the conditions of drawdown test. Therefore, it is necessary to understand the effects of partial penetration and to consider the deviations from simple radial flow.

In the case of partially penetrating well, water moving toward the pumping well has to converge in some manner into the open well from all parts of the aquifer. This diversion of flow lines from the horizontal leads to a more complicated pressure distribution pattern around the pumping well than is the case with complete penetration. The produces pressure changes in the aquifer

that many by substantially above or below those that would be predicted using the Theis' solution.

There may be situations where the total thickness of the aquifer is not known. As will be discussed below, the effects of partial penetration may be used to determine the thickness of the aquifer or, that part of the total thickness that is responding to the drawdown test, and may be considered the anisotropy of permeability. Therefore, the drawdown test with partially penetrating well would be more useful than that with completely penetrating well.

In this section, methods of handling partially penetration problems are disccussed.

6.2.2 Analytical solution for partially penetrating well in a confined aquifer

Wells, of which the water-entry section is less than the aquifer they penetrate, are called partially penetrating wells. Unlike the flow toward completely penetrating wells where the main flow takes place essentially in planes parallel to the bedding planes of the formation, the flow toward partially penetrating wells is three-dimensional. Consequently, the drawdown observed in partially penetrating wells will depend, among other variables, on the length and space position of the screened portion (water-entry section) of the observation wells, as well as on that of the pumping or flowing well.

In aquifer where the horizontal conductivity is several times greater than the vertical, the yield of partially penetrating wells may be appreciably smaller than that of equivalent wells in isotropic aquifer.

In treating the problem of flow toward partially penetrating well (Fig. 6.1), the following assumptions are made.

(1) The aquifer is homogeneous, anisotropic and extends infinitelly with impermeable clay layers above and below.

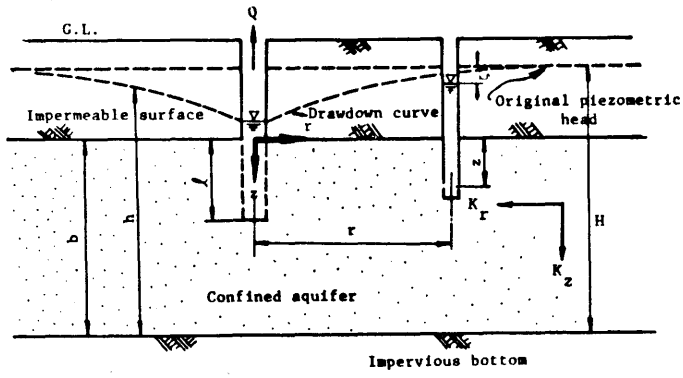

Fig.6.1 Partially penetrating wells in a confined aquifer

(2) The aquifer is also considered to be horizontal and water saturated at all times.

(3) The conductivities of main aquifer in the horizontal and vertical directions have different, but constant values, k_r, k_z, respectively.

(4) The well is of a vanishingly small radius and discharging at a constant rate.

A. Basic equation and solution

The differential equation that describes the fluid movement is given by

$$k_r \frac{\partial^2 h}{\partial r^2} + k_r \frac{1}{r} \frac{\partial h}{\partial r} + k_z \frac{\partial^2 h}{\partial z^2} = S_s \frac{\partial h}{\partial t} \qquad (6.1)$$

where r and z are co-ordinates as shown in Fig.6.1, t is time, and S_s is the specific storage. Then the hydraulic head, $h(=\psi+z)$, is now a function of r, z, and t. The initial and boundary conditions to be imposed on the solution are as follows:

$$h(r,z,0) = H \quad \text{(head initially constant)} \tag{6.2}$$

$$h(\infty,z,t) = H \quad \text{(head at infinity remains constant)} \tag{6.3}$$

$$\frac{\partial h}{\partial z}(r,0,t) = 0 \quad \text{(no flow across upper boundary)} \tag{6.4}$$

$$\frac{\partial h}{\partial z}(r,b,t) = 0 \quad \text{(no flow across lower boundary)} \tag{6.5}$$

$$\lim_{r\to 0} 2\pi k_r r\int_{b-\ell}^{\ell}\frac{\partial h}{\partial r}dz = -Q \quad \text{(flow rate into well of zero radius remains constant)} \tag{6.6}$$

Hantush has studied this problem for a more complicated situation where there is also clay leakage into the aquifer that was being pumped.[1),2)] By imposing the condition of no clay leakage, i.e,Eqs.(6.4), (6.5), the Hantush's solution can be simplified to

$$\zeta_r^* = W(u_r) + f^r(u_r, r^*/b, \ell/b, z/b) \tag{6.7}$$

where

$$\zeta_r^* = \frac{4\pi k_r b}{Q}\zeta \quad , \quad \zeta = H-h, \quad u_r = \frac{(r^*)^2}{4(k_r/S_s)t}, \quad r^* = \sqrt{k_z/k_r}\, r \tag{6.8}$$

and ζ is the drawdown of piezometric surface at any time and at any point in aquifer, b is the thickness of aquifer.

Noting that

$$W(u_r) = \int_{u_r}^{\infty}\frac{e^{-\omega}}{\omega}d\omega \quad \text{(so called well function)} \tag{6.9}$$

and

$$f^r(u_r, r^*/b, \ell/b, z/b) = \frac{2b}{\pi\ell}\sum_{n=1}^{\infty}\frac{1}{n}\cos\left(\frac{n\pi z}{b}\right)\sin\left(\frac{n\pi\ell}{b}\right) \cdot\int_{u_r}^{\infty}\exp\left[-\omega - \frac{(n\pi r^*)^2}{4\omega b^2}\right]\frac{d\omega}{\omega} \tag{6.10}$$

describing another form of the Hantush's solution

$$\zeta_r^{**} = \int_{u_r}^{\infty}\frac{e^{-\omega}}{\omega}\left[\sum_{n=1}^{\infty}\left\{\operatorname{erf}\frac{(2nb+\ell+z)\sqrt{\omega}}{r^*} - \operatorname{erf}\frac{(2nb-\ell-z)\sqrt{\omega}}{r^*} + \operatorname{erf}\frac{(2nb+\ell-z)\sqrt{\omega}}{r^*} - \operatorname{erf}\frac{(2nb-\ell+z)\sqrt{\omega}}{r^*}\right\} + \operatorname{erf}\frac{(\ell+z)\sqrt{\omega}}{r^*} - \operatorname{erf}\frac{(\ell-z)\sqrt{\omega}}{r^*}\right]d\omega \tag{6.11}$$

where

$$\zeta_r^{**} = \frac{8\pi k_r \ell}{Q}\zeta$$

For infinite aquifer thickness ($b \to \infty$),

$$\zeta_r^{**} = \int_{u_r}^{\infty} \frac{e^{-\omega}}{\omega} \{\mathrm{erf}\frac{(\ell-z)\sqrt{\omega}}{r^*} + \mathrm{erf}\frac{(\ell+z)\sqrt{\omega}}{r^*}\}\, d\omega \qquad (6.12)$$

Substituting $k_r=k_z=k$ in Eq.(6.7), the solution for an isotropic aquifer is obtained as follows:

$$\zeta^* = W(u) + f(u, r/b, \ell/b, z/b) \qquad (6.13)$$

where

$$\zeta^* = \frac{4\pi kb}{Q}\zeta \qquad (6.14)$$

$$u = \frac{r^2}{4(k/S_s)t} \qquad (6.15)$$

Javandel shows in some detail how Eq.(6.13) can be derived and has used a heat transfer model as an independent means of verifying the solution.[3] By comparing Eq.(6.13) with the Theis' solution for the pumping well with complete penetration, it is evident that f (u, r/b, ℓ/b, z/b) is simply added to the exponetial integral to describe the effects of partial penetration. For full penetration, ℓ is equal to b in Eq.(6.13) and the result is the same of the Theis' solution. Therefore, Eqs.(6.7), (6.13) are defined as general solutions for drawdown test in a confined aquifer.

For relatively large values of time, the function $f^r(u_r, r^*/b, \ell/b, z/b)$

can be replaced by $2K_0(n\pi r^*/b)$ for all practical purposes in which case Eq.(6.10) becomes independent of time as follows:

$$f^r(u_r, r^*/b, \ell/b, z/b) \doteqdot f_s^r(r^*/b, \ell/b, z/b) = (4b/\ell\pi)\sum_{n=1}^{\infty}(1/n) \times K_0(n\pi r^*/b)\cos(n\pi z/b)\sin(n\ell\pi/b) \qquad (6.16)$$

where K_0 is the zero-order modified Bessel function of the second kind.

Similarly for relatively large values of time, the function Eq.(6.9) becomes

$$W(u_r) \doteqdot \ln(t/r^{*2}) - \ln(S_s/2.25k_r) \qquad (6.17)$$

From Eqs.(6.16), (6.17), the approximate solution of drawdown (ζ) becomes for relatively large values of time

$$\zeta = (Q/4\pi k_r b)[\ \ln(t/r^{*2}) - \ln(S_s/2.25k_r) + f_s^r(r^*/b, \ell/b, z/b)] \qquad (6.18)$$

if an aquifer is isotropic ($k_r=k_z=k$, i.e. $r=r^*$), Eq.(6.18) becomes Hantush' [1] solution as follows:

$$\zeta = \frac{Q}{4\pi kb}[\ \ln(t/r^2) - \ln(S_s/2.25k) + f_s(r/b, \ell/b, z/b)] \qquad (6.19)$$

$$\zeta = \frac{2.3Q}{4\pi kb}[\ \log(t/r^2) - \log(S_s/\exp(f_s)\times 2.25k)] \qquad (6.20)$$

$$f_s = \frac{4b}{\pi\ell}\sum_{n=1}^{\infty}\frac{1}{n}K_0\left(\frac{n\pi r}{b}\right)\sin\left(\frac{n\pi\ell}{b}\right)\cos\left(\frac{n\pi z}{b}\right) \qquad (6.21)$$

Moreover if the pumping well completely penetrated ($\ell=b$), Eq.(6.18) becomes to be equal to the Jacob's approximate solution. Eq.(6.18) is rewritten with common logarithms

$$\zeta = (2.30Q/4\pi k_r b)\ [\ \log(t/r^2) - \log(S_s k_z \exp(-f_s^r)/2.25k_r^2)] \qquad (6.22)$$

It is evident that the third term in Eq.(6.18) is the effect of partial penetration of the pumping well.

B. Effects of partial penetration

The effects of partial penetration on the drawdown around a pumping well is shown in Figs.6.2a, 6.2b and 6.2c. The variation is for a vicinity of well in an isotropic aquifer ($k_r=k_z$). Regardless of the location of the wells and the space position of their screens, the time-drawdown curves, at relatively large values of time ($t>S_s/kr^2$), will have approximately the same slope. This slope is the same as would obtained if the pumping well completely penetrates the aquifer. In other words, the effect of partial penetration has attained its maximum value.

If the observation well is relatively apart (r/b>0.5), the drawdown is given by the Theis' formula. In other words, the drawdown in such a well is not affected by partial penetration; it is the same as though the pumping well completely penetrated in the aquifer. Hantush has also discussed the wells located at r/b>1.5, regardless of the space position of its screen.[1)]

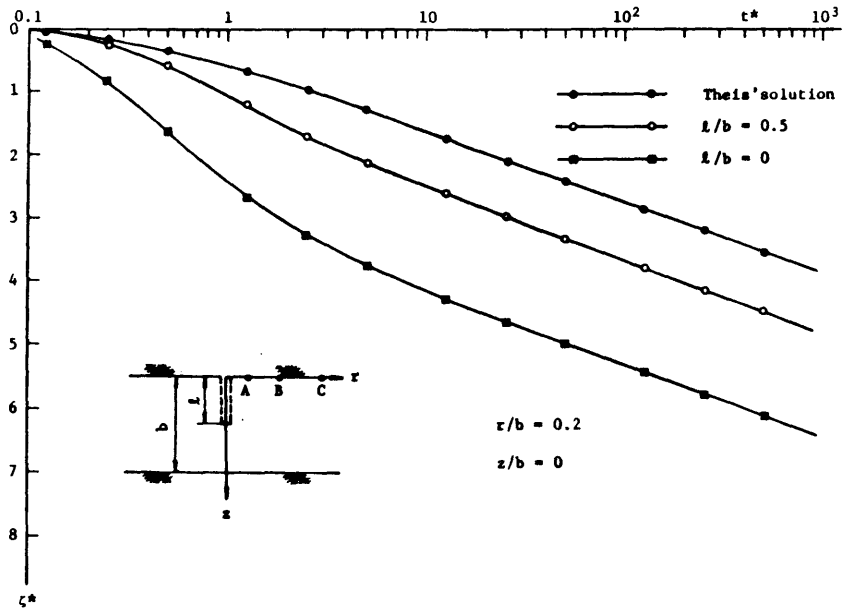

Fig.6.2a Drawdown characteristics for partially penetrating well in a confined aquifer.

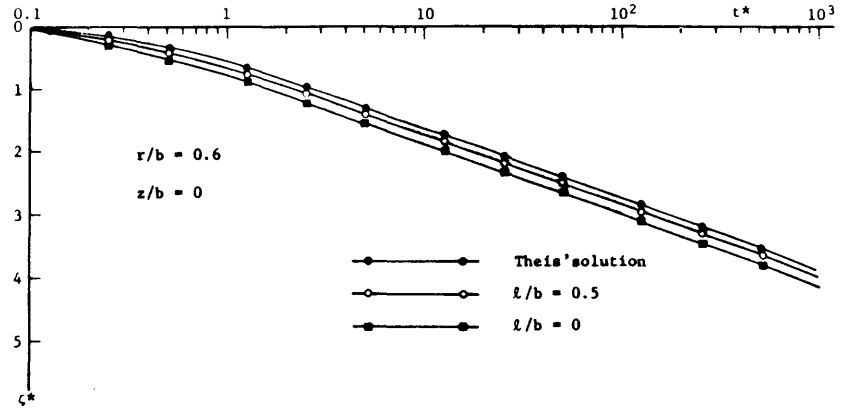

Fig.6.2b Drawdown characteristics for partially penetrating well in a confined aquifer

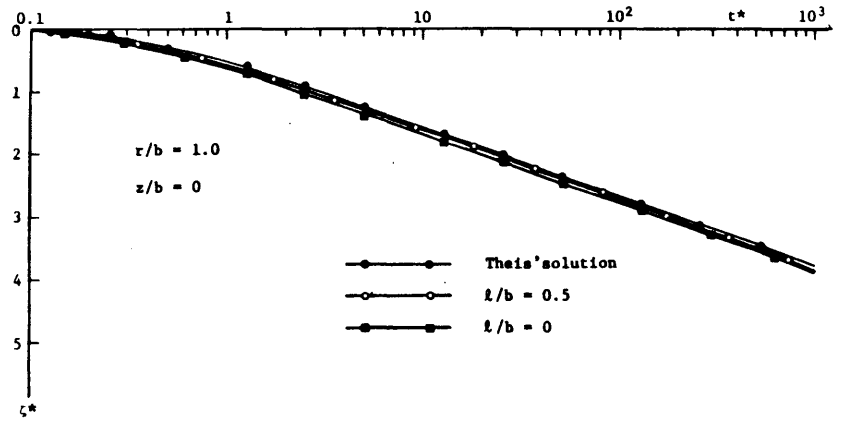

Fig.6.2c Drawdown characteristics for partially penetrating well in confined aquifer

Fig.6.3 compares the drawdowns observed in two equaly distance wells, one of zero penetration and the other screened throughout its depth of penetration.

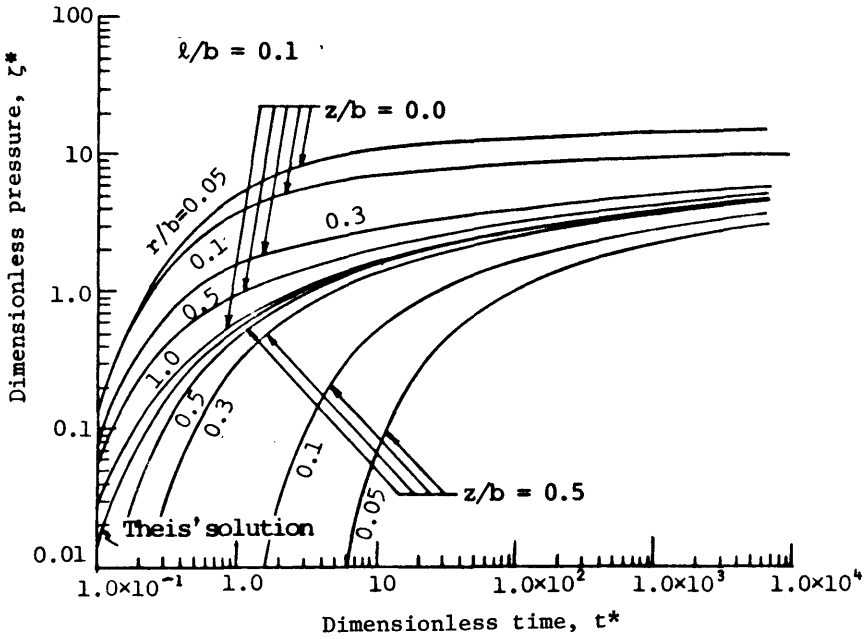

Fig.6.3 ζ^* versus t^* from Eq.(6.13) for infinite radial case with tenth penetration in pumping well

Noticing it shows that two wells equally distant from a partially penetrating pumping well may register two different drawdowns. In fact, depending on the length and the relative positions of the screens, it is possible for a more distant well to reflect a greater drawdown.

A partially penetrating well will discharge less than a completely penetrating well if the two are operated at the same pumping level, other conditions controlling the flow remaining constant. If they are pumped at the same rate, however, the pumping level of the former will be lower than that of the latter.

Pumping at the same level, the yield of partially penetrating well in an anisotropic aquifer ($k_r \neq k_z$) will decrease with decreasing k_z/k_r, other conditions being the same. The effect of the anisotropy decreases as the well penetration increase, as shown in Fig.6.3. Note in Fig.6.3 that the following dimensionless time is used for the abscissa.

$$t^* = \frac{1}{4u} = (k/S_s)(t/r^2) \qquad (6.23)$$

If k_r/k_z does not differ greatly from unity, the anisotropy will not be of particular consequence except for very small penetration. On the other hand, should k_z/k_r be very small, the anisotropy of the aquifer may cause an appreciable decrease in the yield of the partially penetrating well. If k_z should actually vanish, the flow toward the well will become purely radial, confined to the part of the aquifer in which the well is screened.

C. Methods of analyzing field data

In evaluating the results of drawdown test data where partial penetration must be considered, i.e., where $r/b<0.5$, one needs to know the geological conditions of the aquifer under investigation. In drilling the exploration wells, a considerable number of cores well often be taken, and an analysis of the poro-

sity of these samples provides valuable data on the nature of the aquifer. Such cores, of course, provide only a very small sample of the total aquifer system. Thus, the results of a drawdown test can be very helpful in providing an additional source of reliable data.

In the field of hydrology, basic methods of analyzing field data have been developed; Log-Log Method, Log-Log Distance Drawdown Method, which will be discussed below. In addition, Jacob's Method Adjusted for Partial Penetration, which is a variation of Jacob's Method, and Modified Jacob's Method Adjusted for Partial Penetration for anisotropic aquifer will also be presented.

All of the above methods require data that are measured in observation wells at some distance from the pumping well. If one could measure fluid levels in the pumping well itself, similar analysis could be made but it is rarely possible to keep the pumping rate exactly constant. Thus, the fluid levels may fluctuate rapidly, making it difficult to get reliable data. The depth to the pumping fluid level will, of course, be much greater than in the observation wells, and this may make it difficult to obtain accurate measurements. For these reasons, an analysis of the drawdown data in the pumping well is not often made.

a Log-Log Method

In the Log-Log Method, one can use graphical methods similar to Theis' Method. Knowing the values of ℓ/b and z/b one can prepare a graph of log ζ^* versus log t^* ($t^*=1/4u$) for the appropriate r/b between pumping and observation wells. As is evident in Fig.6.3, separate curves will have to be prepared for each observation well, unless the values of the three ratios (ℓ/b, z/b, r/b) are identical.

When the drawdown data from each observation well has been plotted on

log-log paper with the same dimensions per cycle as used above, one can match the field results to the theoretical curve in the same manner as is done when using the Theis' curve. When the curves are matched, one can read the dimensionless parameters that correspond to each point of field data. It will be found that one can also choose any point of the curve of field data and still obtain the same result by using the appropriate values of ζ^* and t^* for that particular point.

An equivalent value ζ^* can be determined for any ζ measured in the observation well and as equivalent value of t^*, for the corresponding value of real time, t. The permeability can be calculated from Eq.(6.14)

$$k = \frac{Q\zeta^*}{4\pi b\zeta} \tag{6.24}$$

and the compressibility factor from Eq.(6.23)

$$S_s = (k/t^*)(t/r^2) \tag{6.25}$$

The compressibility obtained in this manner should give a value that is of the same order as the compressibility of water. At the reservoir conditions that will generally prevail in water storage operation, the compressibility of water is about $4.6\times10^{-11}cm^{-1}$.

b. Log-Log Distance Drawdown Method

When the aquifer is considered anisotrpic, the permeability must be evaluated k_r and k_z, respectivery. In this case, it is necessary to develop a new method and the "Log-Log Distance Drawdown Method" is a variation of the Log-Log method. Knowing the values of ℓ/b and z/b, one can prepare a graph of

log ζ_r^* versus log t_r^* similar to that shown in Fig.6.4, and

$$t_r^* = \frac{1}{4u_r} = (k_r/S_s)(t/r^{*2}) \qquad (6.26)$$

As is evident from Fig.6.4, separate curves will have to be prepared for each r*/b. Here, as r* is dependent on a horizontal conductivity k_r and a vertical conductivity k_z, estimating the values of $\sqrt{k_z/k_r}$, separate curves of r*/b will have to be prepared for each observation well.

When the drawdown data from each observation well have been plotted on log-log paper with the same dimensions per cycle as used above, one can match the field results to the theoretical curve in the same manner as is done when using the Theis' curve. One obtains a graphical solution by placing the field results on top of the theoretical solution and shifting the plots, keeping the axes parallel, until the field data fall on the theoretical curves, when the curves are matched, one can read the dimensionless parameters that correspond to each point of field data and still obtain the same result by using the appropriate of ζ_r^* and t_r^* for that particular point.

At any datum point, one therefore reads the drawdown ζ, and its corresponding value of ζ_r^*. The horizontal conductivity k_r, of the aquifer being pumping may be calculated from

$$k_r = \frac{Q\zeta_r^*}{4\pi b\zeta} \qquad (6.27)$$

Having obtained the horizontal conductivity, one reads from the same data point used above, the radial distance r, of an observation well and the dimensionless parameter r*. The vertical conductivity k_z, may be calculated from

$$k_z = k_r\left(\frac{r^*}{r}\right)^2 \qquad (6.28a)$$

The compressibility factor may be calculated using the elapsed pumping time t and its corresponding value of t_r^*, and the above determined vertical permeability from

$$S_s=(k_r/t^*)(t/r^{*2}) \qquad (6.28b)$$

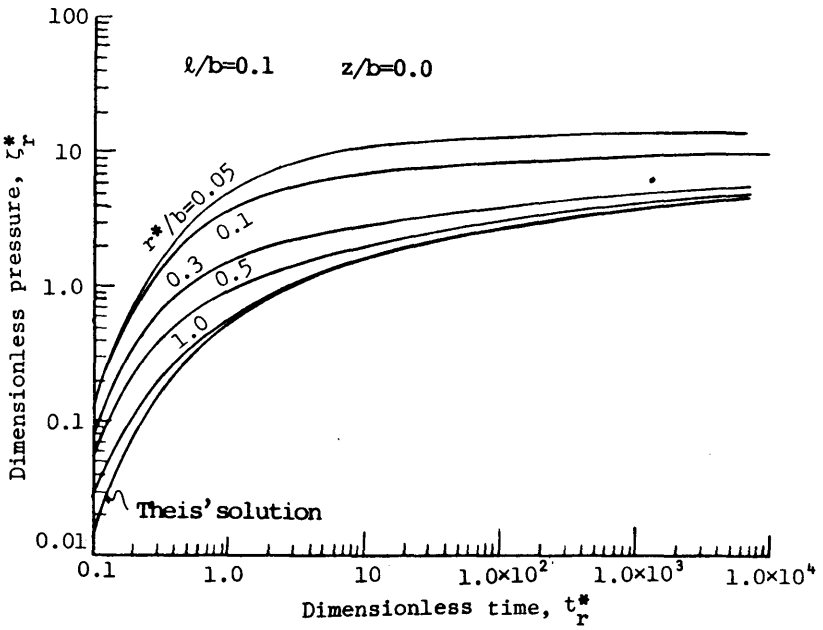

Fig.6.4 ζ_r^* versus t_r^* from Eq.(6.7) for each r*/b.

c. Jacob's Method Adjusted for Partial Penetration

During the time period in which the ultimate semilogarthmic straight line forms, the drawdown is given, depending on the well observed, by Eq.(6.19) or Eq.(6.20). Because the second term of these equations are constant with time, it is clear that Jacob's method can be applied if the numerical value of this constant can be obtained. The procedure is as follows:

(1) On the observed semilogarithmic plot, construct the ultimate straight line and extend it to the zero-drawdown axis.

(2) Obtain the slope, ($m=\Delta\zeta$/cycle) of this line and its time intercept, (t/r^2) on the zero-drawdown axis.

(3) The permeability can be calculated from Eq.(6.20)

$$k=\frac{2.3Q}{4\pi bm} \qquad (6.29)$$

(4) Compute $\exp(f_s)$ from Eq.(6.21) interpolating r/b, ℓ/b, z/b as shown in Fig.6.5.

(5) Then calculate the compressibility factor from

$$S_s=[\frac{2.25kt}{r^2}]\cdot\exp(f_s) \qquad (6.30)$$

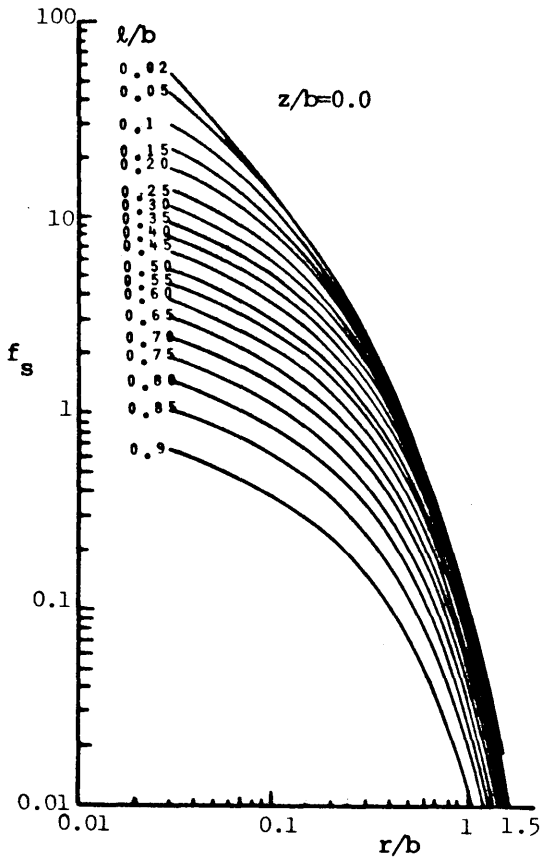

Fig.6.5
The relation of f_s versus r/b.

d. Modified Jacob's Method Adjusted for Partial Penetration

This method is an improved one of "Jacob's Method Adjusted for Partial Penetration" to determine anisotropic coefficients of permeability.

The procedure to determine the formation constants is as follows.

(1) Horizontal permeability coefficient (k_r)

Plotting drawdown data obtained in each observation well on the common semilogarithmic paper, the ultimate straight lines are gotten for relatively large values of time. If the confined aquifer is homogeneous these lines become

parallel as shown in Fig.6.6. To obtain the slope (m = $\Delta\zeta$/cycle) of these lines the horizontal permeability can be calculated from Eq.(6.22).

$$k_r = 2.30Q/4\pi bm \tag{6.31}$$

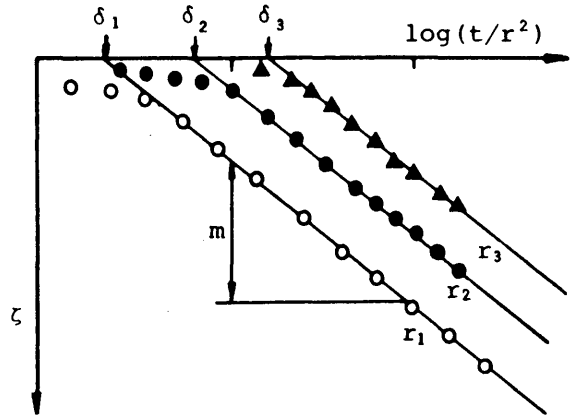

Fig.6.6 Semi-log plot of drawdown data

(2) Vertical permeability coefficient (k_z)

Extending these lines to the zero-drawdown axis, one can obtain their time intercepts ($\delta_i = t/r_i^2$) for each observation well on the zero-drawdown axis as shown in Fig.6.6.

From Eq.(6.22) these values of δ_i are described

$$\begin{aligned} \delta_1 &= \alpha\exp(-f_{s1}^r) \\ \delta_2 &= \alpha\exp(-f_{s2}^r) \\ \delta_3 &= \alpha\exp(-f_{s3}^r) \end{aligned} \tag{6.32a}$$

where $\alpha = S_s k_z/2.25k_r^2$.

The ratio of above values can be written

$$\beta_{12} = \delta_2/\delta_1 = \exp(f_{s1}^r - f_{s2}^r)$$
$$\beta_{13} = \delta_3/\delta_1 = \exp(f_{s1}^r - f_{s3}^r) \qquad (6.32b)$$

Interpolating known factors (ℓ/b, z/b,r/b) in Eq.(6.16), one can prepare a graph of f_s^r versus k_z/k_r for each observation well as shown in Fig.6.7. Since in most anisotropic aquifers, the horizontal coefficient of permeability is larger than the vertical one, then can be treated as $k_z/k_r<1$.

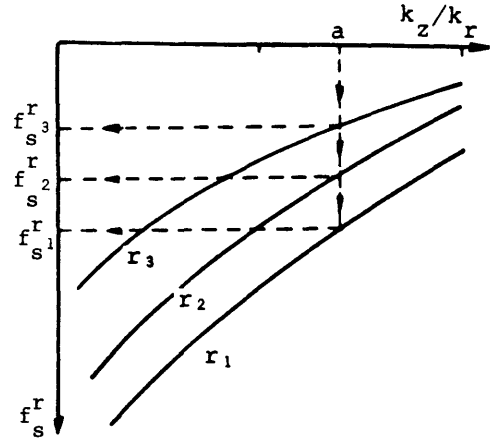

Fig.6.7 Relation of f_s^r versus k_z/k_r

Calculating the values of exp($f_{si}^r - f_{sj}^r$) versus k_z/k_r the graph of β_{ij} versus k_z/k_r can be gotten as shown in Fig.6.8.

From the gotten values of time intercepts (δ_i) and in Eq.(6.32b) the point of β_{ij} can be easily decided on the ordinate of the graph, as a result, the ratio (a) of k_z/k_r can be determined. Having obtained the horizontal conductivity and the ratio k_z to k_r, the vertical conductivity k_z may be calculated from

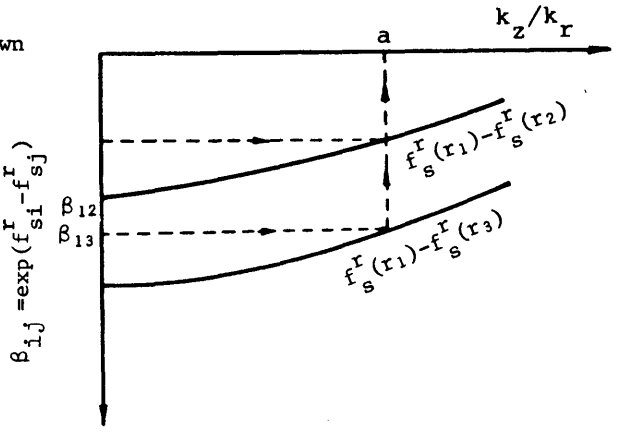

Fig.6.8 Relation of β versus k_z/k_r

$$k_z = ak_r \qquad (6.33a)$$

(3) Specific storage (S_s)

By using the ratios (a) of k_z to k_r in Fig.6.7, one can get a value of f_{si} for each observation well and determine the specific storage (S_{si}) from following equation

$$S_{si} = 2.25 \left(k_r^2/k_z \right) \delta_i \exp\left(f_{si}^r \right) \qquad (6.33b)$$

e. Trial and Error Method for Unknown Aquifer Thickness

In general, the thickness of aquifer is assumed from the boring logs that have been obtained from boring a pumping well and observation wells. But sometimes one problem that has arisen in connection with the aquifer being pumped is that the total thickness may not be known precisely from the boring logs. The question has therefore been raised how drawdown test results can be used to determine the total thickness of the aquifer that is responding to the pressure disturbances caused by the water removal.

Since there are normally several wells available for observation purposes at the time of the drawdown test, it is quite likely that one or more of these wells will be located for enough from the pumping well so that the distance r will exceed 0.5 times the aquifer thickness b. In this event, one should first analyze the drawdown behavior of the distant observation wells where it is reasonably certain that r>0.5b. In this case, the Theis' solution can be employed directly because the effects of partial penetration should be nil. Once one has obtained a match between field data and the Theis' curve, the total effective permeability-thickness can be calculated from

$$T=kb= \frac{Q}{4\pi} \frac{\zeta^*}{\zeta} \qquad (6.34)$$

On the basis of the core analysis results from wells that have been completed in the aquifer, one should have an approximate idea of the average per-

meability, and thus the first estimate of b can be determined from the value of kb obtained in Eq.(6.34). Appropriate curves of ζ^* versus t^* can then be prepared for each well where r<0.5b since the necessary ratios (ℓ/b,z/b,r/b) can all be calculated. If the observed field data make a satisfactory fit to these curves of dimensionless values, one can again calculate kb and compare with the results previously obtained for wells with r>0.5b. However, if the field data do not give a good match because they lie above (or below) the theoretical curve, the assumed value of b must be reduced (or increased). This process can be repeated on a trial and error basis until a satisfactory match is obtained. In this manner, both b and k can be determined.

D. Analysis of drawdown test data

The following discussion is on example calculations for the methods given above, except " Log-Log Distance Drawdown Method ". The drawdown test data are taken from a real aquifer project that is located in Okayama City. The geologic conditions obtained from well logs is shown in Fig.6.9. The water level of the sand-gravel layer under G.L.-13m is different from that of the upper gravel layer; therefore, the sand-gravel layer is revealed a confined aquifer. A test well to check the thickness of the sand-gravel layer was penetrated into the depth of G.L.-30m, thickness could not be ascertained though. The pumping test data are taken from a hypothetical case where both pumping and observation wells partially penetrate the aquifer of unknown thickness. The depth of penetration in each observation well is 20m and that of penetration in the pumping well is 25m, as shown in Fig.6.9.

The drawdown test was performed on this project using an average rate of 30 hours. Water levels were measured in observation wells.

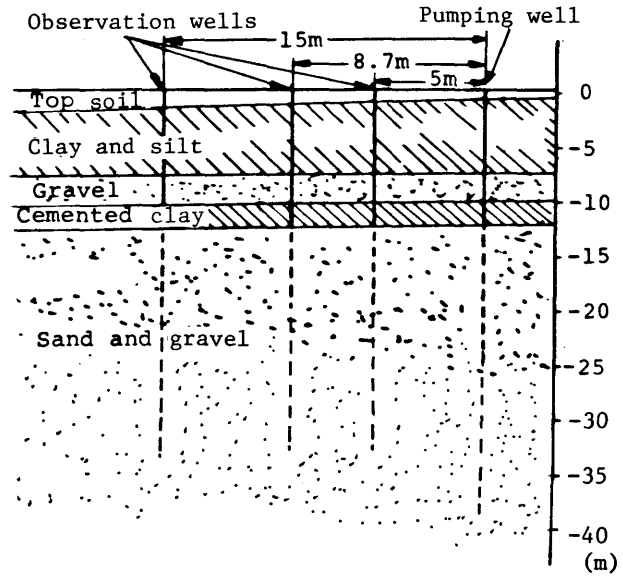

Fig.6.9
The geologic conditions of the field

a. Log-Log Method and Trial and Error Method

As a first trial in analyzing the drawdown data of this drawdown test, b=100m was assumed, trial curves were compared with the drawdown data. Trial curves did not give a satisfactory fit to the field data, indicating the assumed aquifer thickness of 100m is too high.

A second trial curve of ζ^* versus t^* was constructed on the assumption that b=30m. Trial curves again did not fit the field data.

A third trial of b=50m was assumed. The parameter ℓ/b is obtained for the pumping well

$$\ell/b=25/50=0.5$$

wells also have penetrations of 20m, then z/b is obtained

$$z/b=20/50=0.4$$

and radial distances of each well to obtain

No.1 $r_1/b=5.0/50=0.1$

No.2 $r_2/b=8.7/50=0.17$

No.3 $r_3/b=15/50=0.3$

No.4 $r_4/b=26/50=0.52$

One can interpolate the results to construct the curve of ζ^* versus t^* for $\ell/b=0.5$, $z/b=0.4$ and each r/b curves are compared with the drawdown data as shown in Fig.6.10, they can be matched satisfactorily to the field data.

At the match point where $\zeta^*=3.1$, $t^*=1.3\times10^3$, one reads $\zeta=1\times10^2$cm and $t/r^2=1\times10^{-3}$sec/cm^2. From Eq.(6.24), the permeability can be calculated

$$k=\frac{Q\zeta^*}{2\pi b\zeta}=\frac{7.0\times10^3\times3.1}{(2\times3.14)\cdot(5.0\times10^3)\cdot(1.0\times10^2)}=6.91\times10^{-3}\text{cm/sec}$$

From Eq.(6.25), the compressibility factor can be calculated

$$S_s=(\frac{k}{t^*})(\frac{t}{r^2})=(6.91\times10^{-3})\times(1\times10^{-3})/(1.3\times10^3)=5.32\times10^{-9}\text{cm}^{-1}$$

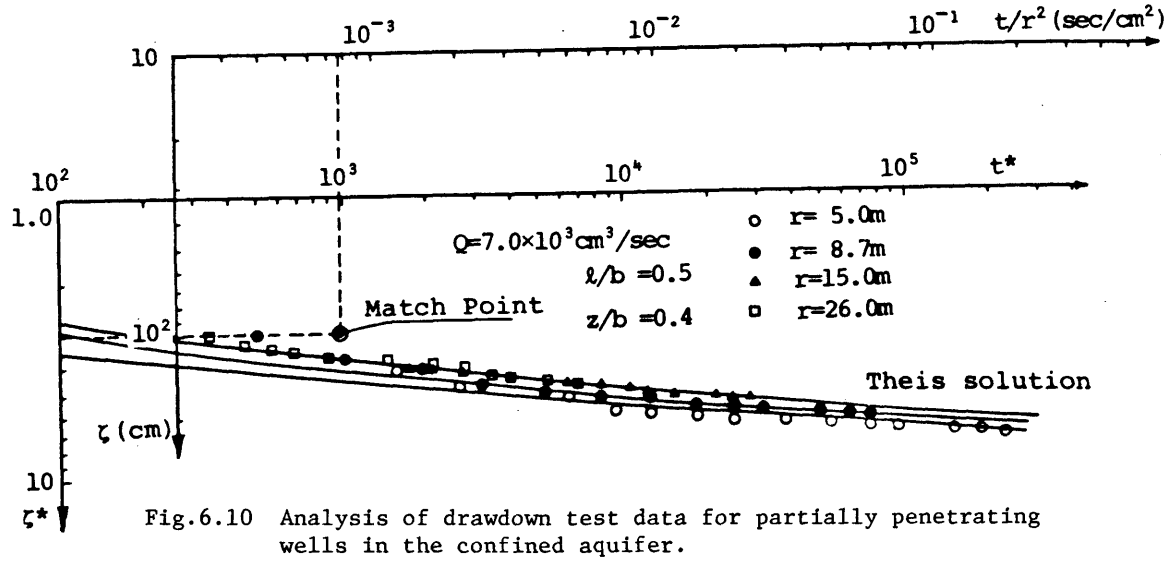

Fig.6.10 Analysis of drawdown test data for partially penetrating wells in the confined aquifer.

b. Jacob's Method Adjusted for Partial Penetration

The same data are analysised by the Jacob's Method Adjusted for Partial Penetration, the values of the slope for each observation well are nearly same as shown in Fig.6.11, therefore the permeability can be obtained from the slope of straight lines and Eq.(6.29)

$$k = \frac{2.30Q}{4\pi bm} = \frac{2.30\times 7.0\times 10^{3}}{4\times 3.14\times 5.0\times 10^{2}\times 40} = 6.41\times 10^{-3}\text{cm/sec}$$

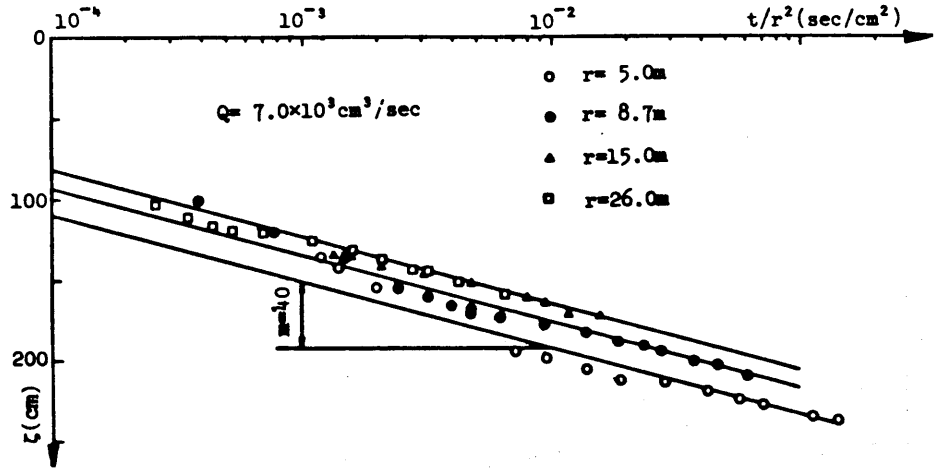

Fig.6.11 Semi-log plot of drawdown data for partially penetrating wells in the confined aquifer (for $Q=7.0\times 10^{3}cm^{3}/sec$).

The compressibility factor can be calculated from the time (t/r^2) intercept on the zero-drawdown axis, but for the effect of partial penetration, different values of t/r^2 are obtained from respective data of the observation well, as indicated in Table 6.1.

Table 6.1 (for $Q=7.0\times 10^{3}cm^{3}/sec$)

r(m)	5.0	8.7	15.0	26.0
r/b	0.10	0.17	0.30	0.52
ℓ/b	0.5	0.5	0.5	0.5
z/b	0.4	0.4	0.4	0.4
f_s	1.486	0.833	0.392	0.147
t/r^2 (sec/cm^2)	2.3×10^{-7}	6.3×10^{-7}	1.5×10^{-6}	1.5×10^{-6}
S_s (cm^{-1})	1.47×10^{-8}	2.03×10^{-8}	3.20×10^{-8}	2.51×10^{-8}

Interpolating the parameter ℓ/b, z/b, r/b in Eq.(6.21), the values f_s(r/b, ℓ/b, z/b) are obtained for each observation well by numerical calculation. Using Eq.(6.30), the compressibility factor can be calculated as indicated in Table 6.1 and its average value is $2.32\times10^{-8}cm^{-1}$.

In the same field the drawdown test was performed using an average rate of $Q=4.33\times10^{3}cm^{3}/sec$ for a period of 30 hours. In this case, the permeability can be obtained from the slope of straight lines in Fig.6.12.

$$k=\frac{2.30Q}{4\pi bm}=\frac{2.30\times4.33\times10^{3}}{4\times3.14\times5.0\times10^{3}\times33}=4.81\times10^{-3}cm/sec$$

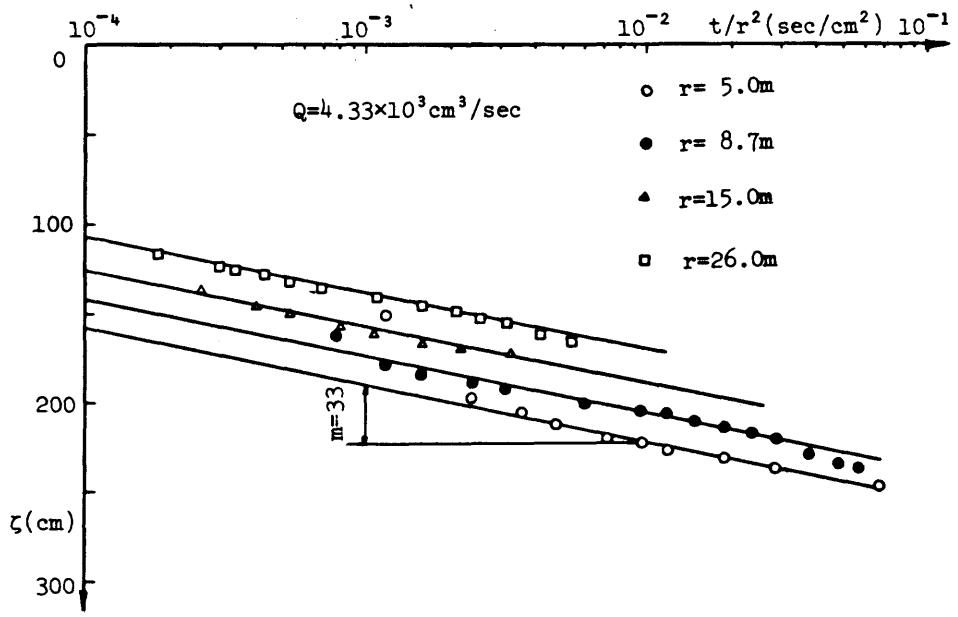

Fig.6.12 Semi-log plot of drawdown data for partially penetrating wells in the confined aquifer (for $Q=4.3\times10^{3}cm^{3}/sec$).

The compressibility factor can be calculated as indicated in Table 6.2, its average value is $1.97\times10^{-10}cm^{-1}$. This value is very small compared with the value of the pumping test using an average rate of $7.0\times10^{3}cm^{3}/sec$. This discrepancy is discussed in paragraph E.

Table 6.2 (for $Q=4.333\times10^{3}cm^{3}/sec$)

r(m)	5.0	8.7	15.0	26.0
r/b	0.10	0.17	0.30	0.52
ℓ/b	0.5	0.5	0.5	0.5
z/b	0.4	0.4	0.4	0.4
f_s	1.486	0.833	0.392	0.147
t/r^2 (sec/cm^2)	2.0×10^{-9}	5.0×10^{-9}	1.2×10^{-8}	3.0×10^{-8}
S_s (cm^{-1})	9.56×10^{-11}	1.24×10^{-10}	1.92×10^{-10}	3.76×10^{-10}

c. Modified Jacob's Method Adjusted for Partial Penetration

The parameters ℓ/b, z/b are obtained for the pumping well and the observation wells

$$\ell/b = 25/50 = 0.5$$

$$z/b = 20/50 = 0.4$$

and (r/b) can be calculated with radial distances from the pumping center to each well

No.1 $r_1/b = 5.0/50 = 0.1$

No.2 $r_2/b = 8.7/50 = 0.17$

No.3 $r_3/b = 15/50 = 0.3$

Fig.6.13 shows the result of pumping data plotted on the semilogarithmic paper. Horizontal permeability can be determined from Eq.(6.31)

$$k_r = 2.30Q/4\pi bm = (2.30\times7.0\times10^{3})/(4\times3.14\times5.0\times10^{3}\times40) = 6.41\times10^{-3} \ (cm/sec)$$

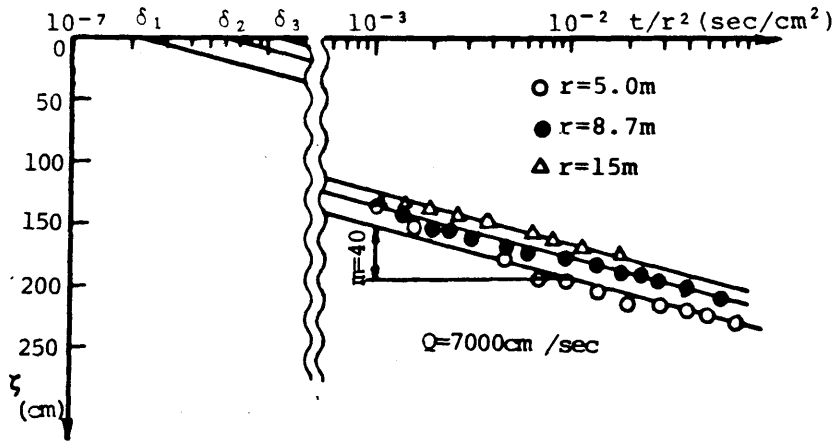

Fig.6.13 Semi-log plot of drawdown data

The values of time intercepts (δ_i) for each observation well are obtained as follows:

$\delta_1=2.3\times10^{-7}$sec/cm^2
$\delta_2=6.3\times10^{-7}$sec/cm^2
$\delta_3=1.5\times10^{-6}$sec/cm^2

From these values the ratios (β_{ij}) are

$$\beta_{12} = \delta_2/\delta_1 = 2.74$$

$$\beta_{13} = \delta_3/\delta_1 = 6.52$$

Interpolating known factors (ℓ/b, z/b, r_i/b) in Eq.(6.16), Fig.6.14 can be prepared for each observation well, and the graph of β_{ij} versus k_z/k_r can be easily gotten as shown in Fig.6.15. By using values of β_{12}, β_{13}, the ratio (a) of k_z to k_r can be determined on Fig.6.15, i.e. $a = k_z/k_r = 0.105$, then the vertical permeability coefficient is calculated with Eq.(6.33a) as following,

$$k_z = 0.105 \times 6.41 \times 10^{-3} \text{cm/sec} = 6.73 \times 10^{-4} \text{cm/sec}$$

Deciding the ratio (a) on the abscissa in Fig.6.14, the value of f_{si}^r for each observation well and the specific storage (S_{si}) are determined from Eq.(6.33b). The average value of S_s is

$$S_s = 9.73 \times 10^{-7} \text{cm}^{-1}$$

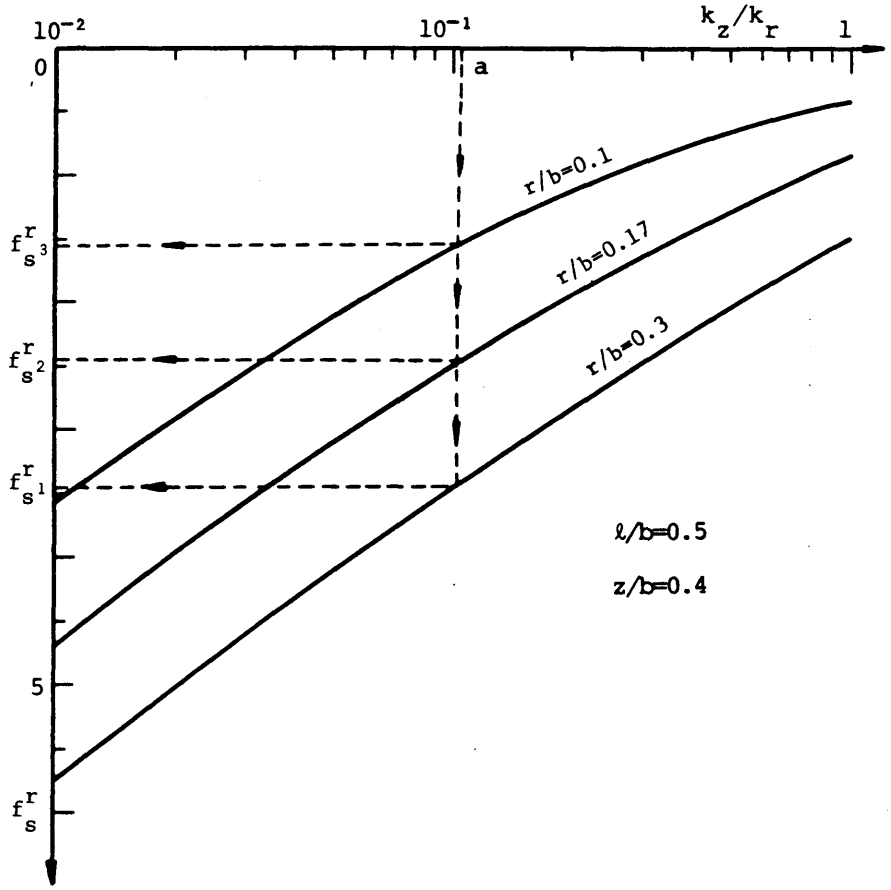

Fig.6.14 Relation of f_s^r versus k_z/k_r

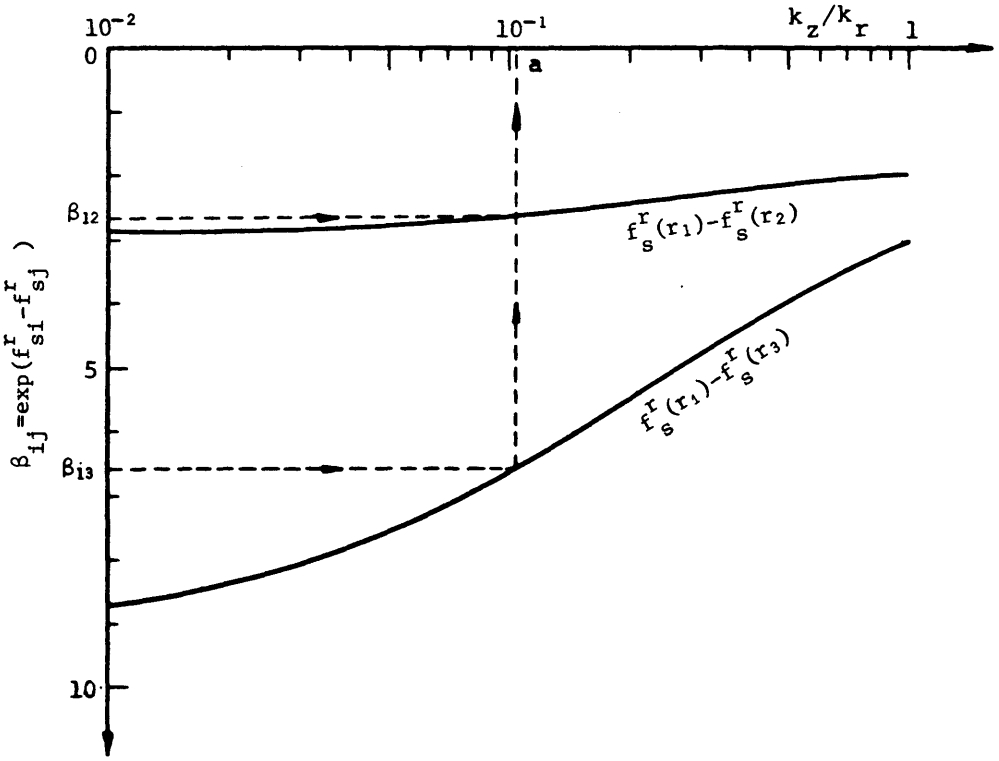

Fig.6.15 Relation of β versus k_z/k_r

E. Discussion of analysis of drawdown test data

In section C, some methods of analyzing field data are given and in section D the example calculations for the methods are shown. Comparing these methods with Theis' and Jacob's methods, which can evaluate an anisotropy of permeability and the aquifer thickness, proved that they would be more effective than Theis' and Jacob's methods.

Using Jacob's Method, various values of compressibility factor for each observation well are obtained. Therefore the constant compressibility factor can not be calculated. Sometimes, Jacob's method results a big variation for a compressibility factor of second to third power in difference.

In section D, different compressibility factors are obtained for each average pumping rate, that is, $S_s=2.32\times10^{-8}cm^{-1}$, $S_s=1.97\times10^{-10}cm^{-1}$ are obtained from $Q=7.0\times10^{3}cm^{3}/sec$, $Q=4.33\times10^{3}cm^{3}/sec$, respectively. This discrepancy is considered as follow.

General behavior between of the effective stress (σ')-volumetric strain (ε_v) is shown in Fig.6.16. From Fig.6.16 it is evident that the compression factor is small as the average pumping rate is small.

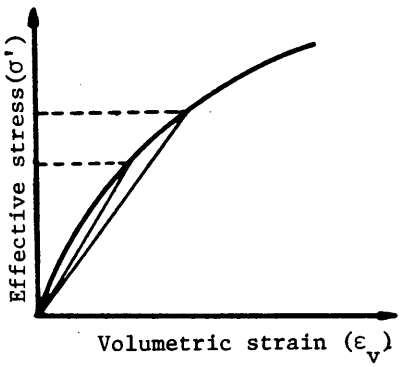

Fig.6.16 Behavior of σ'-ε_v.

A drawdown test aimes at finding coefficients of an aquifer before a ground excavation. In the actual excavation the drainage rate of water is larger than the drawdown test. Thus, the compression factor must be assumed a larger value than that obtained from drawdown test.

For example consider the confined aquifer as shown in Fig.6.17. In this case the drawdown for unsteady state is obtained as follows;[4)]

where
$$\frac{\zeta}{\zeta_0} = \mathrm{erfc}(\xi) \qquad (6.35)$$
$$\xi = x/2\sqrt{k/S_s}\,t \qquad (6.36)$$

and ζ is drawdown, ζ_0 is drawdown at the face of excavation, and erfc(ξ) is the complementary error function, i.e,

$$\mathrm{erfc}(\xi)=1-\mathrm{erf}(\xi) \qquad (6.37)$$

The numerical result of Eq. (6.35) is shown in Fig.6.18. If a small S_s is given in Eq.(6.36) the value of ξ becomes a small value, then from Fig.6.18 the drawdown ζ at the distance x from the excavation face becomes large.

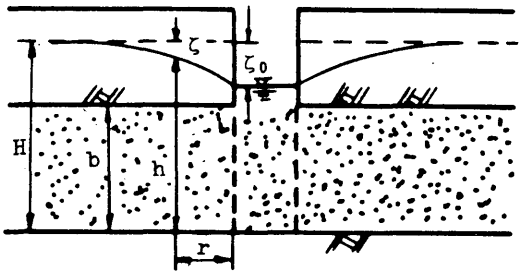

Fig.6.17
Excavation trench in a confined aquifer.

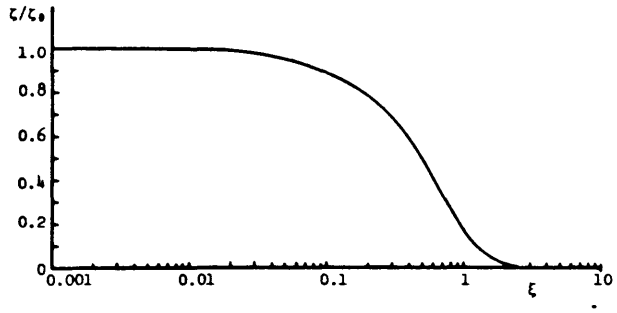

Fig.6.18
Numerical solution of erfc(ξ)

For this reason if the value S_s obtained from small pumping rate is used in the analysis of the ground excavation, the larger result of the analysis must be obtained comparing with the actual drawdown.

In the actual excavation analysis, sometimes this discrepancy has happened. For this cause in traditional notion, it has been considered that the permeability coefficient obtained from drawdown test is larger than that of the aquifer. Therefore the compressibility factor has not been watched. However, from the above evaluation, it becomes clear that the drawdown in the actual excavation is smaller than that of the analysis.

On the other hand, it can be considered that the permeability coefficient is independent of the pumping rate from the analysis in section D.

6.2.3. Analytical solution for partially penetrating well in an unconfined aquifer

The subject of this investigation is the flow toward a single well, partially penetrating an unconfined aquifer that is infinite in lateral extent. The saturated region is unconfined, possesing a free surface that is initially horizontal. The velocity distribution in time and space within the porous aquifer is obtained for various piezometric head functions in the well. Then it is possible to relate quantities, such as free surface drawdown, well discharge flow rate, and piezometric head with aquifer parameters and answer some pertinent questions regarding the behavior and characteristics of this physical system.

First, certain physical assumptions about the problem need to be made. Each one restricts in some way the applicability of the final solution to the real physical problem and determines the nature of the mathematical model of the situation.

(1) Flow within the porous medium obeys Darcy's Law.

(2) The water is assumed to be incompressible and the porous matrix rigid. This assumption is suitable for unconfined aquifers where storage yield corresponds to a lowering of the free surface with essentally no compression of the porous matrix or volumetric expansion of water.

(3) Only single phase (or saturated) flow occurs in the aquifer.

(4) Capillarity is neglected at the free surface.

(5) The porous medium has homogeneous, constant, anisotropic permeability.

(6) The effective porosity or specific yield of the aquifer is assumed to be uniform and constant.

(7) The well is assumed to have no surface of seepage.

(8) Head losses through the well screen are neglected.

A. Basic equation and solution

The physical situation is one of three-dimensional flow with axial symmetry as shown in Fig.6.19. Thus cylindrical co-ordinates are the natural selection. The origin is taken to be on the well axis at the level of the horizontal free surface at time zero.

Darcy's law gives

$$V_r = -k_r \frac{\partial h}{\partial r} \quad , \quad V_z = -k_z \frac{\partial h}{\partial z} \tag{6.38}$$

Applying the equation of continuity for incompressible flow yields Laplace's equation for the potential,

$$k_r \frac{\partial^2 h}{\partial r^2} + k_r \frac{1}{r} \frac{\partial h}{\partial r} + k_z \frac{\partial^2 h}{\partial z^2} = 0 \tag{6.39}$$

at all points of the saturated aquifer.

The boundary conditions for this problem are as follows:

(1) The free surface is a boundary whose location in space and time is unknown before the problem is solved. Therefor, let $z=\zeta(r,t)$ designate the free surface. Since atomospheric pressure over the free surface is taken to be

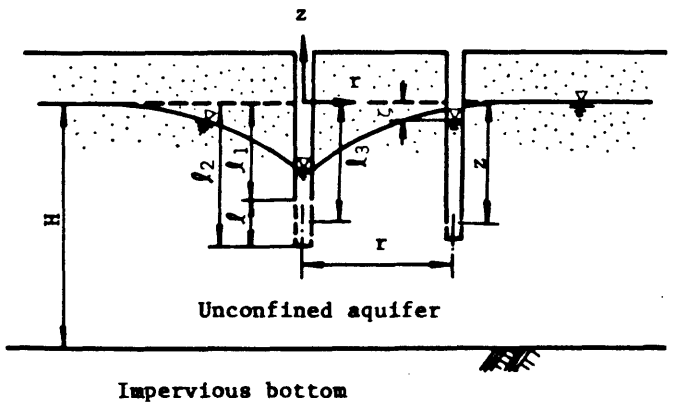

Fig.6.19

Partially penetrating wells in unconfined aquifer.

zero, the defining equation for h becomes

$$h(r,z,t)_{z=\zeta} = \zeta \qquad (\text{at } z=\zeta) \tag{6.40}$$

The kinematic boundary condition comes from the fact that particle initially on the free surface remains on the free surface as the surface moves. Mathematically, this means that the derivative following the motion of the equation defining the free surface must equal zero. Thus, the nonlinear, kinematic, free-surface boundary condition,

$$S_y \frac{\partial h}{\partial t} + k_z \frac{\partial h}{\partial z} + k_r \left(\frac{\partial h}{\partial r}\right)^2 + k_z \left(\frac{\partial h}{\partial z}\right)^2 = 0 \qquad (\text{at } z=\zeta) \tag{6.41}$$

where S_y is the effective porosity or specific yield.

(2) On the no flow across lower boundary,

$$\partial h/\partial z = 0 \tag{6.42}$$

(3) Along the well $(-\ell_2 < z < -\ell_1)$,

$$\lim_{r \to 0} 2\pi k_r r \int_{-\ell_2}^{-\ell_1} \frac{\partial h}{\partial r} dz = -Q \tag{6.43}$$

Initially the free surface is horizontal. Thus,

$$h(r,t) = H \qquad (t=0) \tag{6.44}$$

This is a mixed boundary-value problem with a non-linear boundary condition at the free surface. Note that time appears only in the boundary conditions and not in the partial differential equation.

It is now appropriate to introduce dimensionless variables

$$h^*=h/H,\ z^*=z/H,\ \zeta^*=\zeta/H,\ t^*=t/t_0,\ Q^*=Q/(k_r H^2),\ \ell^*=\ell/H \tag{6.45}$$

and

$$r^* = \frac{r}{H}\sqrt{k_z/k_r} \tag{6.46}$$

t_0 is the time scale factor.

Writing the system equations in dimensionless from gives the following set:

Differential equation

$$\frac{\partial^2 h^*}{\partial r^{*2}} + \frac{1}{r^*}\frac{\partial h^*}{\partial r^*} + \frac{\partial^2 h^*}{\partial z^{*2}} = 0 \tag{6.47}$$

Boundary conditions

$$\frac{\partial h^*}{\partial t^*} + \varepsilon\frac{\partial h^*}{\partial z^*} + \varepsilon\left(\frac{\partial h^*}{\partial r^*}\right)^2 + \varepsilon\left(\frac{\partial h^*}{\partial z^*}\right) = 0 \quad (\text{at } z^* = *) \tag{6.48}$$

$$\zeta^* = h^*\left(r^*, z^*, t^*\right)_{z^*=\zeta^*} \tag{6.49}$$

$$\frac{\partial h^*}{\partial z^*} = 0 \tag{6.50}$$

$$\lim_{r^* \to 0} r^*\frac{\partial h^*}{\partial r^*} = \frac{Q^*}{2\pi\ell^*} \tag{6.51}$$

$$h^* = 1 \qquad r^* \to \infty \tag{6.52}$$

Initial condition

$$h^* = 1 \qquad (\text{at } t^*=0) \tag{6.53}$$

The parameter ε is defined as

$$\varepsilon = \left(t_0 k_z\right)/(S_y H) \tag{6.54}$$

When ε is small, perturbation expansion techniques may be used to linearize the problem. The dimensionless drawdown ζ^{**} is solved.[5),6)]

$$\zeta^{**} = \frac{1}{\pi\ell^*}\left[\frac{1}{4}\log\frac{\ell_3^*+\ell^*/2+z^*+\left\{\left(\ell_3^*+\ell^*/2+z^*\right)^2+r^{*2}\right\}^{1/2}}{\ell_3^*-\ell^*/2+z^*+\left\{\left(\ell_3^*-\ell^*/2+z^*\right)^2+r^{*2}\right\}^{1/2}} \cdot \frac{\ell_3^*+\ell^*/2-z^*+\left\{\left(\ell_3^*+\ell^*/2-z^*\right)^2+r^{*2}\right\}^{1/2}}{\ell_3^*-\ell^*/2-z^*+\left\{\left(\ell_3^*-\ell^*/2-z^*\right)^2+r^{*2}\right\}^{1/2}}\right.$$

$$-\int_0^\infty \frac{\cosh\lambda(1+z^*)\cdot\sinh\lambda(\ell^*/2)\cdot\cosh\lambda(1-\ell_3^*)}{\lambda\sinh\lambda\cdot\cosh\lambda}\exp(-\lambda t^{**}\tanh\lambda)\cdot J_0(\lambda r^*)\,d\lambda$$

$$\left.+\int_0^\infty \frac{\sinh\lambda(\ell^*/2)\cdot\cosh\lambda\ell_3^*\cdot\cosh\lambda z^*}{\lambda\sinh\lambda}\cdot\exp(-\lambda)\cdot J_0(\lambda r^*)\,d\lambda\right] \tag{6.55}$$

where

$$\zeta^{**}=\zeta^{*}/Q^{*}=\zeta k_r H/Q \tag{6.56}$$

$$t^{**}=\varepsilon t^{*}=k_z t/S_y H \tag{6.57}$$

Substituting $k_r=k_z=k$ in Eq.(6.55), the solution for an isotropic aquifer is obtained as the same form of Eq.(6.55).

B. Effects of partial penetration

Considering the shallower the penetration of a pumping well is the more superior the effect of partial penetration becomes, the effect of partial penetration on the drawdown around a pumping well for $\ell/H=0.2$ is shown in Fig.6.20. The variations are around a well in an isotropic aquifer ($k=k_r=k_z$). If the observation well is at relatively large distance ($r/H>1.2$), the time-drawdown is given by the Theis' formula. In other words, the drawdown in such well is not affected by partial penetration; it is the same as though the pumping well completely penetrated the aquifer. The same result is obtained from Fig.6.21 in the case of $\ell/H=0.4$.

In Figs.6.22a,6.22b, the effect of well penetration is shown. It is clear that for the observation well set in relatively small distance ($r/H=0.3$), the effects of partial penetration is striking. On the other hand, for the observation well set at $r/H=0.6$ its effect is not so striking.

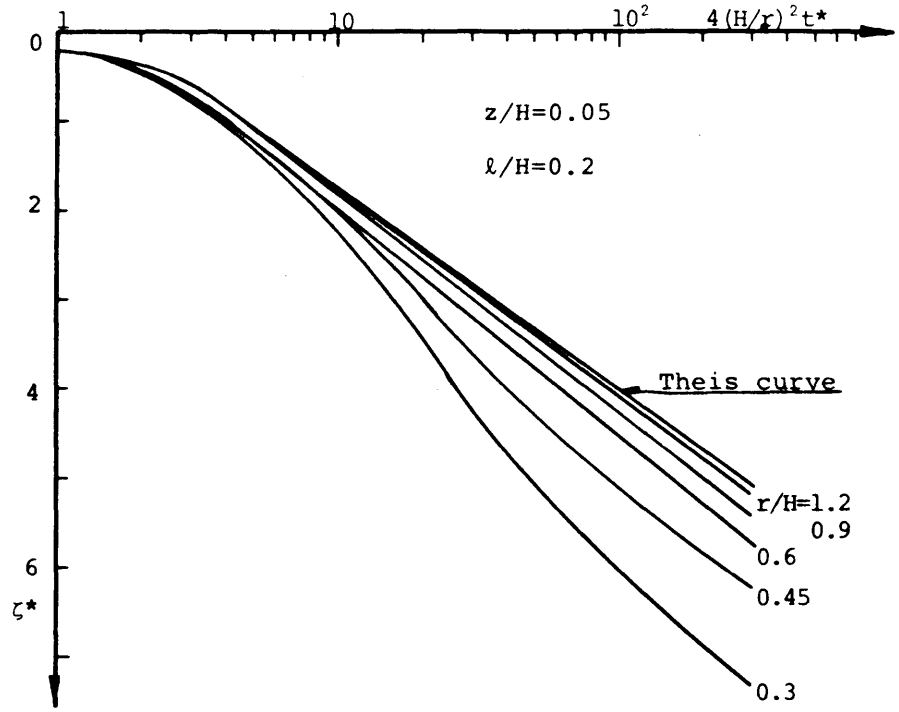

Fig. 6.20

Drawdown characteristics for partially penetrating well in an unconfined aquifer

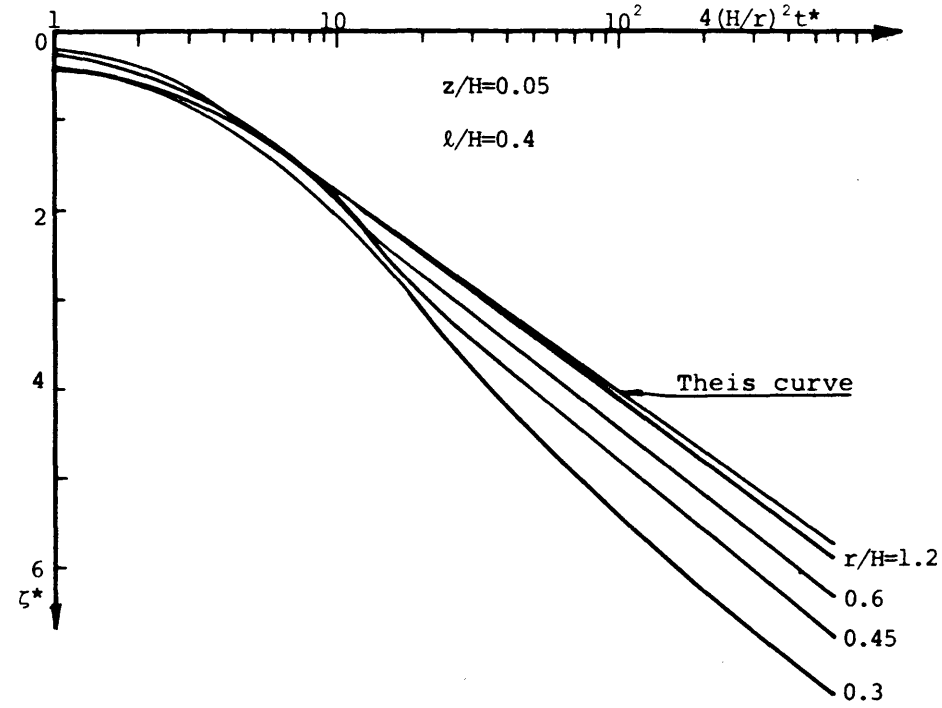

Fig. 6.21

Drawdown characteristics for partially penetrating well in an unconfined aquifer

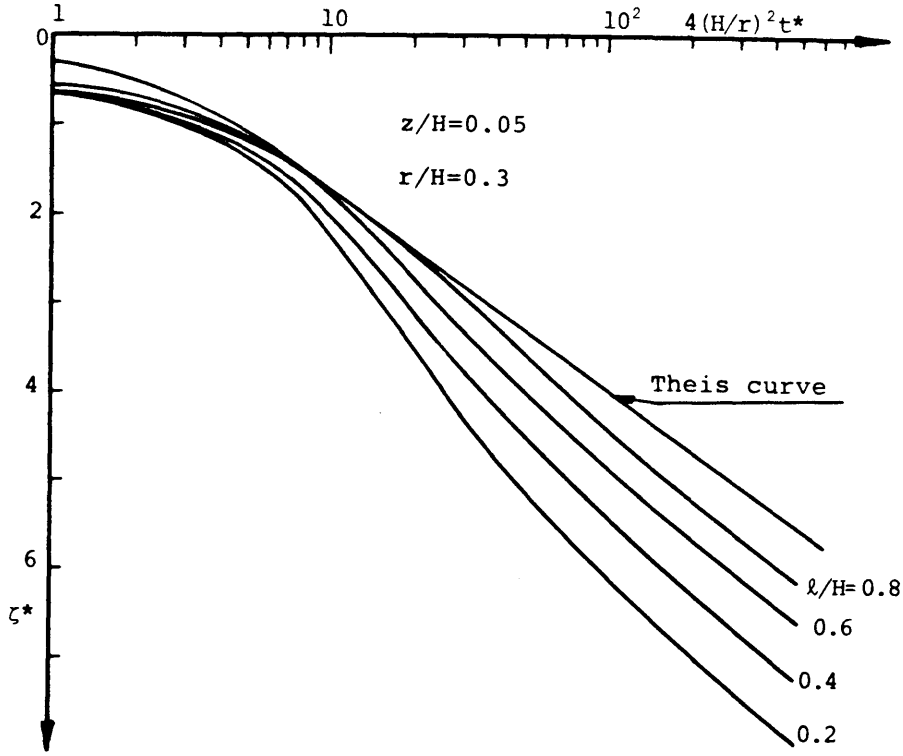

Fig. 6.22a

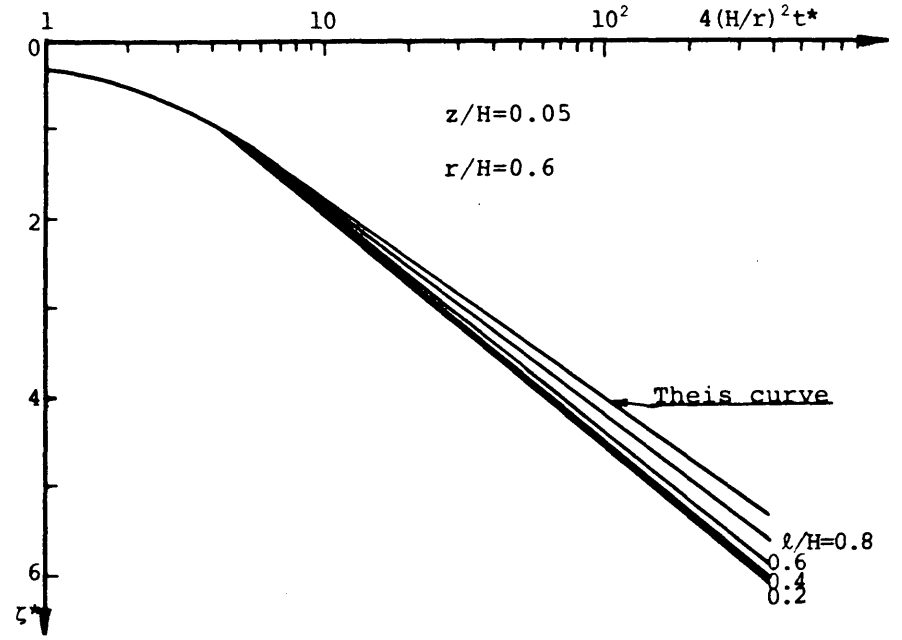

Fig. 6.22b
Drawdown characterstics for partially penetrating well in an unconfined aquifer

C. Method of analyzing field data

In evaluating the results of a drawdown test where partial penetration must be considered, i.e., where $r/H<1.2$, one needs to know the geological conditions of the aquifer under investigation.

In the field of hydorology, basic methods of analyzing field data have been developed; " Log-Log Method " for an isotropic aquifer and " Log-Log Distance Drawdown Method " for an anisotropic aquifer.

Both of the above methods require data that are measured in observation wells at some distances from the pumping well.

a. Log-Log Method

In the Log-Log Method, one can use graphical method similar to Theis' method. Knowing the values of $\ell/H, \ell_3/H$ and z/H, one can prepare a graph of $\log\zeta^{**}$ versus $\log t^{**}$ for the appropriate r/H between pumping and observation wells from Eq.(6.55). As is evident from Fig.6.23 separate curves will have to be prepared for each observation well, unless the values of the three rations $(\ell/H, z/H, r/H)$ are identical.

When the drawdown data from each observation well have been plotted on log-log paper with the same dimensions per cycle as used above, one can match the field results to the theoretical curve in the same manner as is done when using the Theis curve.

When the curves are matched, one can read the dimensionless parameters that correspond to each point of field data. It will be found that one can also choose any point of the curve of field data and still obtain the same result by using the appropriate values of ζ^{**} and t^{**} for that particular point.

An equivalent value of ζ^{**} can be determined for any ζ, measured in the

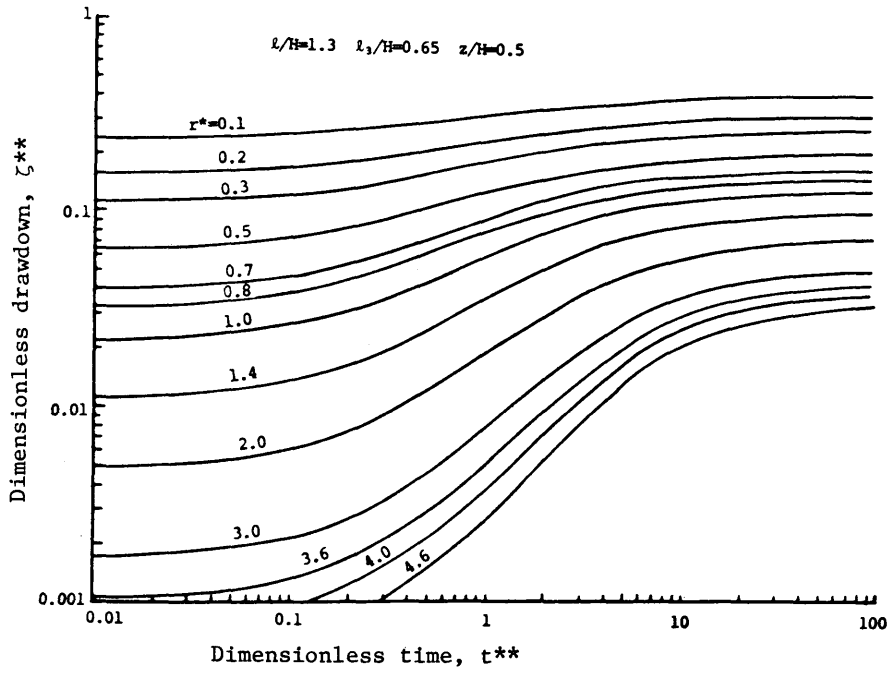

Fig.6.23 Relation of log ζ** versus log t** from Eq.(6.55)

observation well and an equivalent value of t**, for the corresponding value of real time,t. The permeability can be calculated from Eq.(6.56)

$$k = \zeta^{**}Q/\zeta H \tag{6.58}$$

and the effective porosity from Eq.(6.57)

$$S_y = kt/t^{**}H \tag{6.59}$$

b. Log-Log Distance Drawdown Method

" Log-Log Distance Drawdown Method " is a variation of " Log-Log Method ".

The characteristics of the aquifer k_r,k_z and S_y may be obtained by matching the measured drawdowns and the theoretical curve from Eq.(6.55).

For this purpose the values of ℓ*,ℓ$_3^*$ (pumping well) and z* (observation

well) have to be inserted in Eq.(6.55); ζ^{**} becomes a function of t^{**} and r^{*}. A set of couves ζ^{**}-t^{**} for different constant r^{*} are to be drawn on a log-log paper. Since most anisotropic aquifers have $k_z/k_r<1$, r^{*} has to be smaller than r/H.

The measured drawdowns have to be represented on a similar logarithmic paper. By matching them with one of the curves of the set, five values are obtained from the best fitting curve, an equivalent value of ζ^{**} can be determined for any ζ, measured in the observation well and an equivalent value of t^{**}, for the corresponding value of real time t. Since r,H and Q are known, the values of k_r,k_z and S_y may be easily found from next equations.

$$k_r = \zeta^{**}Q/\zeta H \tag{6.60}$$

$$k_z = (r^{*}H/r)^2 k_r \tag{6.61}$$

$$S_y = tk_z/t^{**}H \tag{6.62}$$

D. Analysis of drawdown test data

The following discussion gives example calculations for the methods discussed above. The pumping test data are taken from real aquifers project that is located in Kyoto City.

a. Log-Log Method

The geological condition obtained from well logs is shown in Fig.6.24. The water level in the sandy layer is G.L.-11m and the aquifer of sandy layer is revealed as an unconfined aquifer. A test well to check the thickness of the sandy layer was penetrated into the depth of G.L. -30m, however, the thickness

could not be ascertained. The drawdown test data are taken from a hypothetical case where both pumping and observation wells partially penetrate the aquifer of unknown thickness. The depth of penetration in each observation well is 5m and that of penetration in the pumping well is 13m, as shown in Fig.6.24.

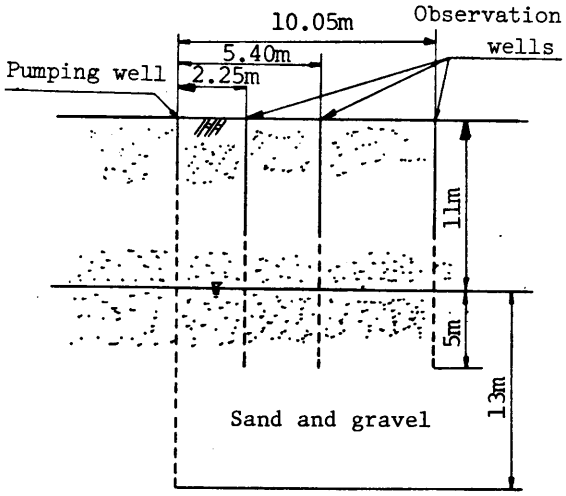

Fig.6.24
The geological condition of the field

The drawdown test was performed on this project using an average rate of $7.0\times10^{3}cm^{3}/sec$ for a period of 5 hours.

As a first trial in analyzing the drawdown data of this drawdown test, H= 50m was assumed, trial curves were compared with the drawdown data. Trial curves did not give a good match.

A second trial curves of ζ^{**} versus t^{**} was constructed on the assumption that H=10m. Trial curves again did not fit the field data.

A third trial of H=20m was assumed, the parameter ℓ^{*},ℓ_{3}^{*} are obtained for the pumping well

$$\ell^{*}= \ell/H= 13/20 =0.65$$

$$\ell_{3}^{*}= \ell_{3}/H= 6.5/20= 0.325$$

Observation wells also have penetration of 5m,

$$z^{*}= z/H= 5/20= 0.25$$

and radial distances of each well to obtain

No.1 $r_1^* = 2.25/20 = 0.113$

No.2 $r_2^* = 5.40/20 = 0.270$

No.3 $r_3^* = 10.05/20 = 0.50$

One can interpolate the results to obtain the curve of ζ^{**} versus t^{**} for ℓ^*, ℓ_3^*, z^* and each r_i^*. Curves are compared with the drawdown data as shown in Fig. 6.25; they can be matched satisfactorily to the field data.

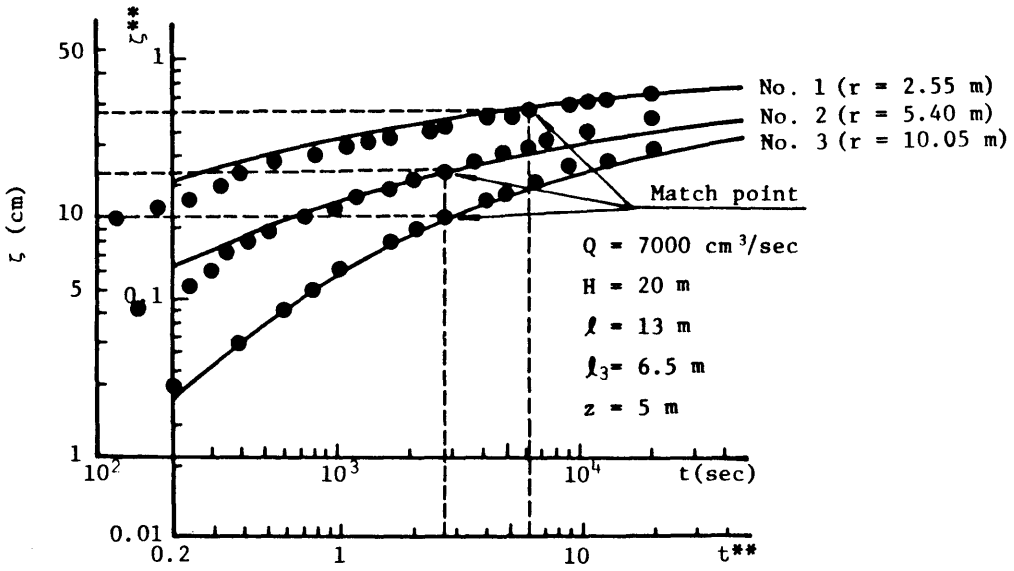

Fig.6.25
Analysis of drawdown test data for partially penetrating wells in the unconfined aquifer(isotropic)

Using the match point and Eqs.(6.58),(6.59), the permeability and the effective porosity can be calculated as indicated in Table 6.3.

By the way, the same drawdown test data was analyzed by Jacob's method as shown in Fig.6.26. The permeability obtained from the slope of straight lines is as follows:

$$k = \frac{2.30 \times 7.0 \times 10^3}{4 \times 3.14 \times 2.0 \times 10^3 \times 13.5} = 4.75 \times 10^{-2} \quad (\text{cm/sec})$$

Table 6.3
Analysis of drawdown test data for partially penetrating wells in the unconfined aquifer(isotropic)

r(m)	2.55	5.40	10.05
ζ(cm)	27.5	15.5	10.0
t(sec)	6.2×10^{3}	2.75×10^{3}	2.75×10^{3}
ζ^{**}	0.60	0.34	0.22
t^{**}	6.00	2.65	2.65
k(cm/sec)	7.64×10^{-2}	7.68×10^{-2}	7.63×10^{-2}
S_y	3.95×10^{-2}	3.99×10^{-2}	3.96×10^{-2}

But the various effective porosities for each observation well are obtained as indicated in Table 6.4. The major cause for this discrepancy must be the effect of partial penetration.

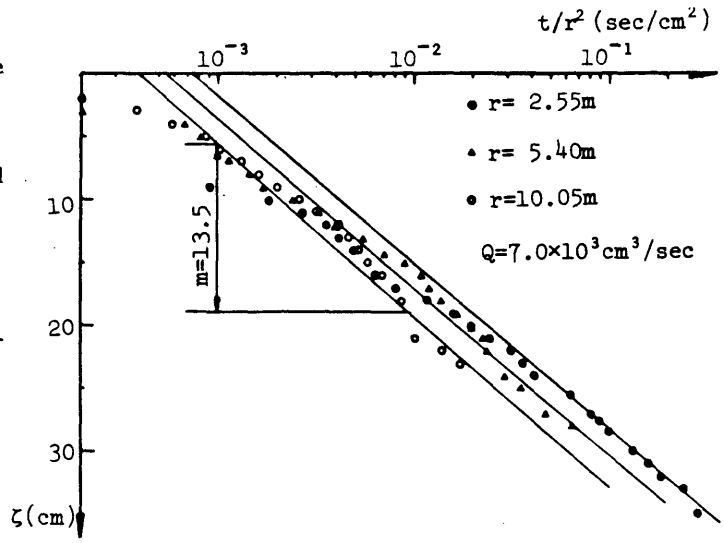

Fig.6.26 Semi-log plot of drawdown data for partially penetrating wells in the unconfined aquifer.

b. Log-Log Distance Drawdown Method

The geological condition obtained from well logs is shown in Fig.6.27. The water level in the sandy layer is G.L.-11.47 m and the aquifer of sandy layer is revealed an unconfined aquifer. A test well to check the thickness of the

Table 6.4
Effective porosity from Jacob's Method

r(m)	2.55	5.40	10.05
t/r^2(sec/cm^2)	3.9×10^{-4}	5.4×10^{-4}	7.2×10^{-4}
S_y	8.3×10^{-2}	1.2×10^{-1}	1.5×10^{-1}

sandy layer was penetrated into the depth of G.L.-40.4 m . From the result of well logs, the thickness of sandy layer is revealed H=23.2 m . This assumption is based on that the clay layer that is regarded as an impermeable layer lies at G.L.-34.67 m.

The depth of penetration in each observation well is 4.23m and that of penetration in the pumping well is 6.93m, as shown in Fig.6.27.

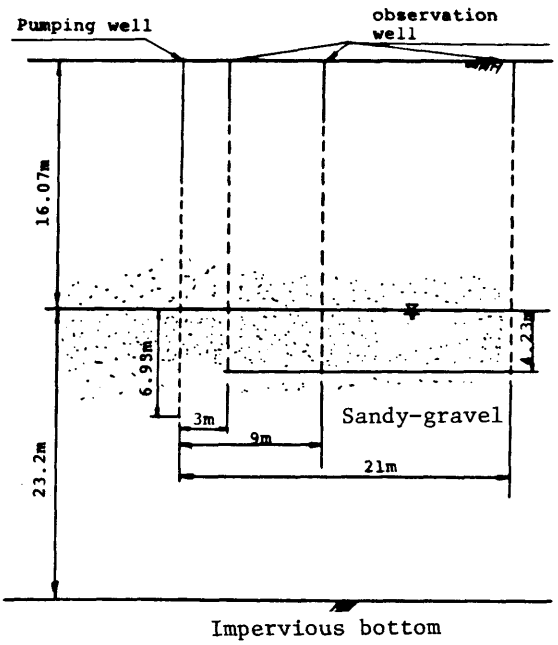

Fig.6.27
The geological condition of the field

The drawdown test was performed on this project using an average rate of $Q=3.23\times10^{3}cm^{3}/sec$ for a period of 24 hours.

The parameters ℓ^*, ℓ_3^* are obtained

$$\ell^* = \ell/H = 6.93/23.2 = 0.299$$

$$\ell_3^* = \ell_3/H = 3.46/23.2 = 0.149$$

Observation wells also have penetration of 4.23m

$$z^* = z/H = 4.23/23.2 = 0.182$$

One can interpolate these paremeters in Eq.(6.55), curves relating ζ^{**} ($= \zeta k_r H/Q$) versus t^{**} ($tk_z/S_y H$) at different value of r^* ($=(r/H)\sqrt{k_z/k_r}$) have been computed numerically on a logarithmic paper as shown in Fig.6.28. The drawdown ζ as function of t have drawn on similar logarithmic paper and the

measured points and theoretical curves have been match in Fig.6.28. The values of $r^*, \zeta^{**}, t^{**}, r, \zeta$ and t at the matching points are presented in Table 6.5. The results show an average anisotropy of $k_z/k_r=0.32$ and $k_r=1.92\times10^{-1}$cm/sec, $k_z=6.04\times10^{-2}$cm/sec.

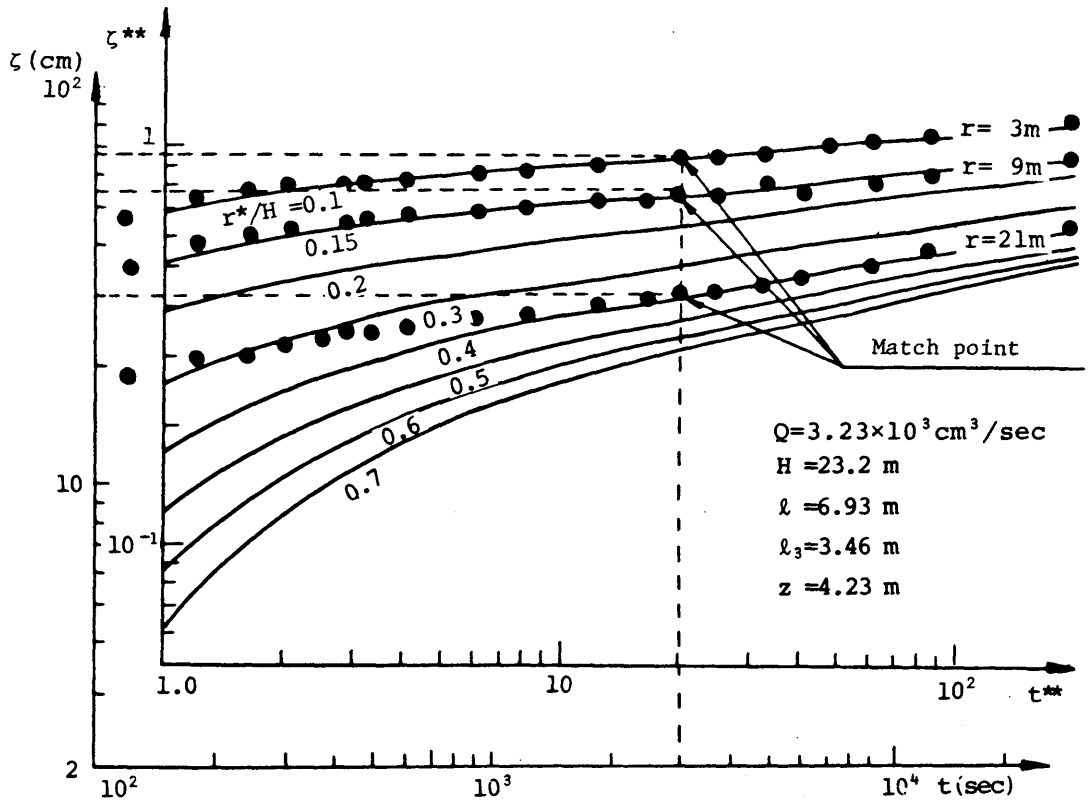

Fig.6.28
Analysis of drawdown test data for partially penetrating wells in the unconfined aquifer(anisotropic)

Same data is analysised by the Jacob's method, the values of the slopes for the each obsevation well are nearly same as shown in Fig.6.29, therefore the permeability can be obtained from the slope of the straight lines;

$$k=\frac{2.30Q}{4\pi Hm}=\frac{2.30\times3.23\times10^3}{4\times3.14\times2.32\times10^3\times12}=2.12\times10^{-1}\text{cm/sec}$$

Table 6.5
Analysis of drawdown test data for partially penetrating wells in the unconfined aquifer(anisotropic)

r(cm)	300	900	2100
r*	0.10	0.15	0.40
ζ**	0.91	0.75	0.42
t**	20	20	20
ζ(cm)	66	54	30.5
t(sec)	2.90×10^{3}	2.90×10^{3}	2.90×10^{3}
k_r(cm/sec)	1.92×10^{-1}	1.93×10^{-1}	1.92×10^{-1}
k_z(cm/sec)	1.15×10^{-1}	2.89×10^{-2}	3.74×10^{-2}
S_y	7.18×10^{-3}	1.81×10^{-3}	2.34×10^{-3}

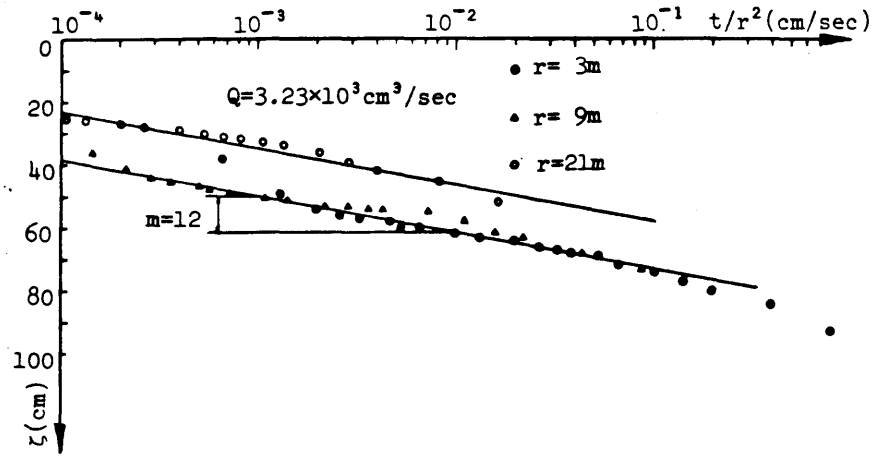

Fig. 6.29
Semi-log plot of drawdown data for partially penetrating wells in the unconfined aquifer.

The effective porosity can be calculated from the time(t/r^2) intercept on the zero-drawdown axis, but for the effect of partial penetration, different valuea of t/r^2 are obtained from respective data of the observation well, as indicated in Table6.6. This discrepancy is very large.

Table 6.6
Effective porosety from Jacob's Method

r(m)	3	9	21
t/r^2 (sec/cm^2)	4.30×10^{-8}	4.30×10^{-8}	1.00×10^{-6}
S_y	4.76×10^{-5}	4.76×10^{-5}	1.11×10^{-3}

E. Discussion of analysis of drawdown test data

In section C two methods of analyzing field data are given and in section D the example calculations for the methods are shown.

Comparing these methods with Theis' and Jacob's methods, as these methods can also evaluate an anisotropy of the permeability and the aquifer thickness as same as the methods for a confined aquifer, therefore, they would be more effective than Theis' and Jacob's method.

6.3 Transient flow in Groundwater to Wells in Island Model Aquifer

6.3.1 Introduction

In Theis' or Jacob's method, the assumption has been made that the horizontal extent of the aquifer was so great that for mathematical purposes it could be considered as an infinite radial system. However, adjusting drawdown test data gotten within relatively large time, the drawdowns in an observation well are often no longer dependent of time and their behaviors become nearly in steady state. It is difficult to explain this behavior by using Theis' assumption that water is supplied from an infinite radial region.

To give an explanation of this reason, it is considered that the drawdown within relatively large time becomes to keep the equilibrium with surrounding water supply, that is, the existence of an influence region of which radial distance keeps the balance against the pumping rate must be considered. Namely, the head around this region is equal to the initial head of groundwater.

This conception in which that model is named "Island Model" has been applied for the model of analysis in steady state drawdown test for a long time, but not the analysis of Island Model in unsteady state has been yet.

The Island Model is as same as the practical situation bounded in some manner, e.g.,by a river or a reservior. In this situation, the analysis of drawdown test has been solved by the method of images for boundary. This method, however, is confined to the assumption that the groundwater supply from many sourses, that is, from river-bed water or neighboring ground water is regarded as only one point well.

In this section, first, the solutions of unsteady phreatic flow due to drawdown test are derived in the conception of "Island Model" that the shape of groundwater level is fixed by the circular water supply which is equilibrium with the pumping rate.

By using these solutions, the methods of analyzing drawdown test data in a confined aquifer and in an unconfined aquifer are given and the effect of influence region is evaluated. Furthermore, the analyses which have been separated in each cases of steady state and unsteady state pumping test are consolidated.

In this section, the analyses stand on following assumptions.

(1) Flow within the porous medium obeys Darcy's law.

(2) The aquifer is homogeneous and isotropic with respect to permeability.

(3) Storage coefficient is time independent.

(4) Only single phase (or saturated) flow occurs in an aquifer.

(5) The well is assumed to have no surface of seepage.

(6) The pumping well used in the testing operations will also be assumed to be fully penetrating and to operate at a constant rate of withdrawal.

6.3.2 Analytical solution for Island Model drawdown test in a confined aquifer

Indicating in section 6.3.1, the Theis' analytical solution heretofore in use was derived on the assumption that water is supplied from the region of infinite distance in drawdown test. Yielding this assumption, the radial distance (r) from drawdown test well to the observation well and the time (t) since pumping starts are always treated in the form of (t/r^2) or the inverse form of that, and drawdown test data performed in ideal conditions can be plotted on a curve independently of the position of wells.

But when drawdown data, which were obtained within large pumping time, are adjusted according to Theis' or Jacob's method, the results for each observation well are on the curve of Theis-Jacob's analytical solution untill some time, and then they depart from that curve, that is, each curve of them becomes parallel to the abscissa independently of time.

To explain this reason, it is able to consider that there is a constant

head boundary in finite radius (R) as shown in Fig.6.30. In this section, the solution of unsteady radial flow in a confined aquifer will first be derived, after which the method of analyzing drawdown test data will be given.

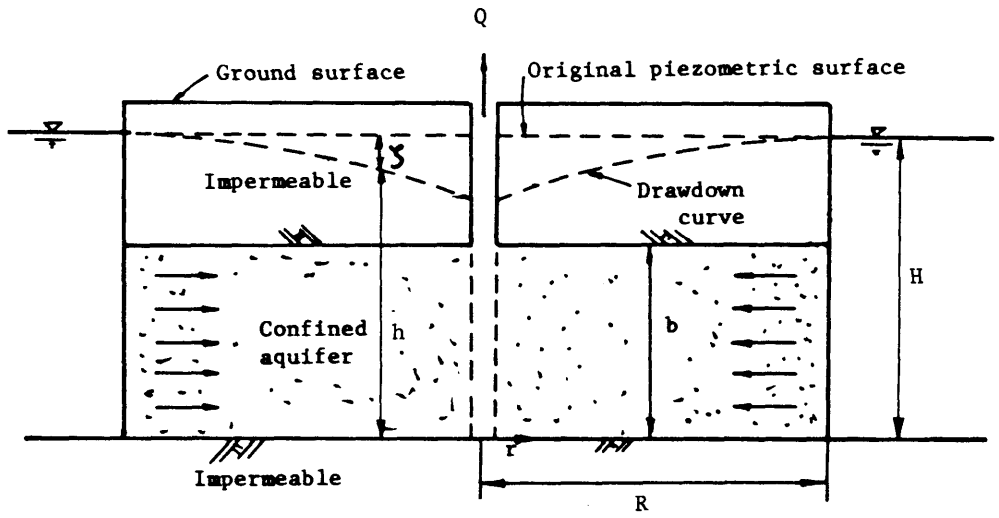

Fig.6.30 Nonsteady radial flow to a well penetrating a confined aquifer on an island

A. Basic equation and solution

The partial differential equation that describes the fluid movement in this system is again

$$\frac{\partial^2 \zeta}{\partial r^2} + \frac{1}{r}\frac{\partial \zeta}{\partial r} = \frac{1}{\alpha_s}\frac{\partial \zeta}{\partial t} \tag{6.63}$$

where α_s is hydraulic diffusivity of aquifer ($=K/S_s$) and ζ is drawdown in aquifer ($=H-h$).

Eq.(6.63) must be solved subject to following conditions,

$$\zeta(r,0) = 0 \qquad \text{(head initially constant)} \tag{6.64}$$

$$\zeta(R,t) = 0 \qquad \text{(constant head at water boundary)} \tag{6.65}$$

$$\lim_{r\to 0} r\frac{\partial \zeta}{\partial r} = -\frac{Q}{2\pi Kb} \qquad \text{(flow rate into well of zero radius remains constant)} \tag{6.66}$$

To solve the initial boundary value problem given by Eqs.(6.64),(6.65), and (6.66), Laplace transformation is applied to Eq.(6.63) using initial condition Eq.(6.64)

$$\frac{\partial^2 \bar{\zeta}}{\partial r^2} + \frac{1}{r}\frac{\partial \bar{\zeta}}{\partial r} - q^2\bar{\zeta} = 0 \qquad (0<r\leq R) \tag{6.67}$$

where $q^2=p/\alpha_s$, p is the parameter of Laplace transform and $\bar{\zeta}$ is Laplace transform of ζ.

The boundary conditions Eq.(6.65) and Eq.(6.66), treated in the same way, give

$$\bar{\zeta}(R,p) = 0 \tag{6.68}$$

$$\lim_{r\to 0} r\frac{\partial \bar{\zeta}}{\partial r} = -\frac{Q}{2\pi Kb}\frac{1}{p} \tag{6.69}$$

The solution of Eq.(6.67) will be of the form

$$\bar{\zeta} = AI_0(qr) + BK_0(qr) \tag{6.70}$$

where $I_0(qr)$ is the zeroth order modified Bassel function of the first kind and $K_0(qr)$ is the zeroth order modified Bessel function of the second kind. Substituting Eq.(6.70) in Eqs.(6.68), (6.69) and solving for A and B, $\bar{\zeta}$ is gotten finally.

$$\bar{\zeta} = \frac{Q}{2\pi Kb}\{\bar{g}_1 - \bar{g}_2\cdot\bar{g}_3\} \tag{6.71}$$

where

$$\bar{g}_1 = K_0(qr)/p \tag{6.72}$$

$$\bar{g}_2 = K_0(qR) \tag{6.73}$$

$$\bar{g}_3 = I_0(qr)/pI_0(qR) \tag{6.74}$$

Eqs.(6.72),(6.73), and (6.74) are now respectively, determined by the Inversion Theorem.

$$g_1 = \frac{1}{2}\int_{r^2/4\alpha_s t}^{\infty} \frac{e^{-u}}{u}\,du \tag{6.75a}$$

$$g_2 = \frac{1}{2t}\exp(-R^2/4\alpha_s t) \tag{6.75b}$$

$$g_3 = 1 - \frac{2}{R}\sum_{n=1}^{\infty} \exp(-\alpha_s \alpha_n{}^2 t)\times J_0(r\alpha_n)/\alpha_n^3 J_1(R\alpha_n) \tag{6.75c}$$

where α_n are the roots of the characteristic equation

$$J_0(r\alpha_n) = 0 \tag{6.76}$$

By using the Duhamel Formulas and combining these results the solution of $\bar{\zeta}$ is derived,

$$\zeta = \frac{Q}{4\pi Kb}\left[\int_{r^2/4\alpha_s t}^{\infty} \frac{e^{-\lambda}}{\lambda}d\lambda - \int_{R^2/4\alpha_s t}^{\infty} \frac{e^{-\lambda}}{\lambda}d\lambda\right]$$

$$+ \frac{Q}{2\pi KbR}\int_0^t \frac{1}{\tau}\exp\left[-R^2/4\alpha_s\tau\right] \sum_{n=1}^{\infty}\exp[-\alpha_s\alpha_n^2(t-\tau)]$$

$$\times \frac{J_0(r\alpha_n)}{\alpha_n^3 J_1(r\alpha_n)}\,d\tau \tag{6.77}$$

If R becomes an infinite radial distance in Eq.(6.77), the result is the same of Theis' solution.

In general the value of permeability (K) is $K=1\times10^{-2} \sim 10^{-3}$(cm/sec) and the value of specific storage (S_s) is $S_s=1\times10^{-5} \sim 10^{-6}(cm^{-1})$, then the value of the ratio ($\alpha_s=K/S_s$) becomes about $\alpha_s=10^2 \sim 10^4(cm^2/sec)$. Therefore, on the right hand side of Eq.(6.77), the third term is as small as negligible comparing with the first and second terms, and so the approximate solution of drawdown (ζ) is given by

$$\zeta \doteqdot \frac{Q}{4\pi Kb}\left[\int_{r^2/4\alpha_s t}^{\infty}\frac{e^{-u}}{u}du - \int_{R^2/4\alpha_s t}^{\infty}\frac{e^{-u}}{u}du\right]$$

$$= -\frac{Q}{4\pi Kb}\left[E_i(-r^2/4\alpha_s t) - E_i(-R^2/4\alpha_s t)\right]$$

$$= \frac{Q}{4\pi Kb}\left[W(r^2/4\alpha_s t) - W(R^2/4\alpha_s t)\right] \qquad (6.78)$$

where $E_i(x)$ is the exponential integral and W(x) is the well function. It can be expanded as a convergent series so that W(x) becomes

$$W(x) = -0.5772 - \ln(x) + x - \frac{x^2}{2\cdot 2!} + \frac{x^3}{3\cdot 3!} \cdots\cdots\cdots \qquad (6.79)$$

For large values of time (t), x is small, so that the series terms in Eq.(6.79) become negligible after the first two terms. As a result, the drawdown can be expressed by the asymptote

$$\zeta \doteqdot \frac{2.30Q}{4\pi Kb}\left[(\log_{10}(t/r^2) - \log_{10}(S_s/2.25K)\right.$$
$$\left.-(\log_{10}(t/R^2) - \log_{10}(S_s/2.25K))\right]$$
$$= \frac{2.30Q}{2\pi Kb}\log_{10}(R/r) \qquad (6.80)$$

Eq.(6.80) is the solution of the model shown in Fig.6.30 for steady state flow.

B. Effects of constant head at outer boundary

Eq.(6.78) is used to evaluate ζ^* as a function of t^* for values of R^* ranging from 1.5 to 100, in which

$$\zeta^* = 4\pi Kb\zeta/Q \tag{6.81}$$

$$t^* = (K/S_s)(t/r^2) \tag{6.82}$$

$$R^* = R/r \tag{6.83}$$

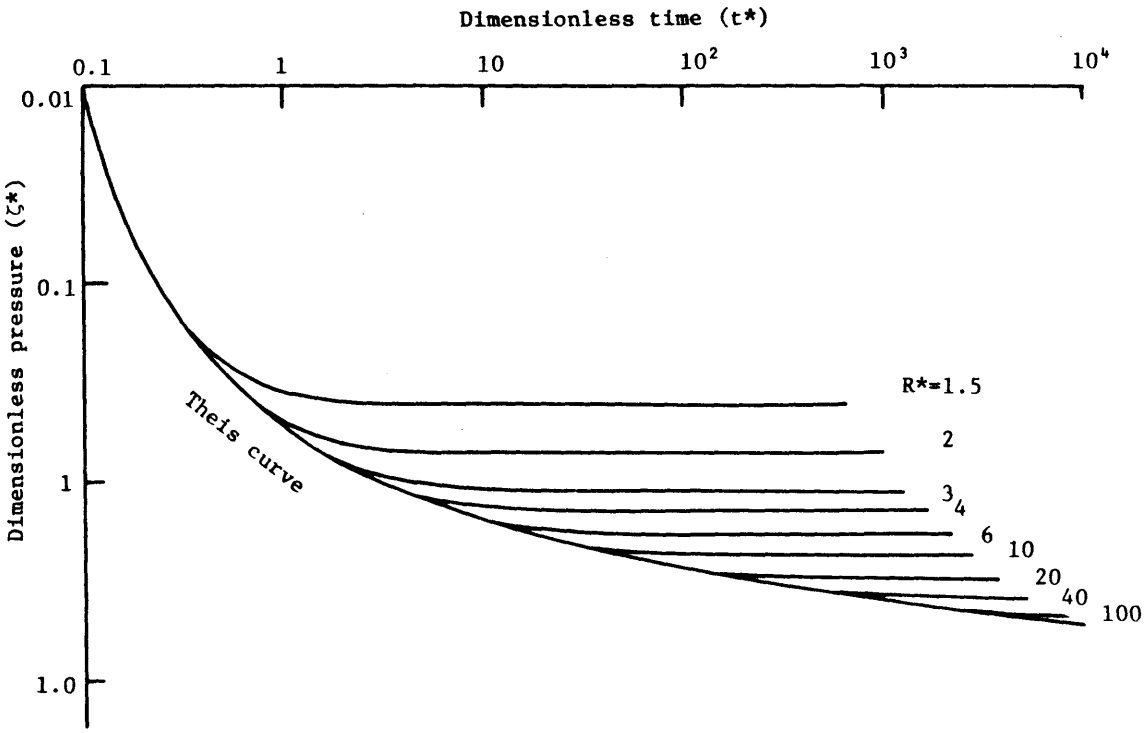

Fig.6.31 ζ^* versus t^* for limited aquifer with constant head boundary

Fig.6.31 shows the resulting family of curves for several values of R*. The type curves depart from the Theis curve in pairs with the point of departure depending on the value of R*, and it is distinct that the drawdown in the aquifer bounded by constant head becomes steady state earlier than that in the infinite extent aquifer. From Fig.6.31 it is also obvious that if the value of R* is larger than 100, the effects of the influence region is negligible. In other words, the drawdown in such a condition is not affected by constant head boundary. An interesting way of looking at this result has been suggested by Mononobe for steady state well problem. To use his own words[7] " In actual problem, the influence region extends since pumping starts, whereas, by reason of the extent of aquifer, the effects of other wells, and the infiltration of rain, the head at circular boundary does not have to be constant. Therefore the influence region is not always expanding into the infinite region.

If a large pumping rate is continued the groundwater around well may be dried up. In general, it would be safe to calculate the drainage rate assuming the influence region must be within the range from 500 meters to 1000 meters ". We perform the pumping test at the condition that the observation wells are set within about 20 meters of the radial distance from pumping well. And so the value of R*>100 means that the influence region must be within 2000 meters. This is a theoritical explanation of the assumption based on experiences.

C. Method of analyzing field data

The engineer wishes to determine the values of the aquifer constants (K, S_s) and the radial distances of the influence region, (R). The properties of the aquifer will presumably to known from earlier drawdown tests, and the approximate radial distances of the influence region will have been predicted by geological reconnaissance.

The basic Log-Log Method of interpreting time versus drawdown data have been discussed in section 6.2 in relation to infinite aquifers. In this section, the differences that appear in the data, and the adaptations that must be made to the methods of interpretation, due to the presence of boundary will be given.

Log-Log Method

The presence of a suspected circular boundary within the region of influence of the drawdown test may be indicated by the inability to match the log-log field data plot on time versus drawdown with the Theis' method. Eq.(6.78) is rewritten by using dimensionless drawdown (ζ^*) and time (t^*)

$$\zeta^* = -E_i(-r^2/t^*) + E_i(-R^2/t^*) \tag{6.84}$$

where

$$\left.\begin{aligned} \zeta^* &= 4\pi Kb\zeta/Q \\ t^* &= 4\alpha_s t \end{aligned}\right\} \tag{6.85}$$

It is necessary to assume the value of R for calculating Eq.(6.84) in numerical method. As indicating in section (6.3.1), the value of R is defined by the conditions of the pumping rate and that of hydrology.

If a drawdown test is run for a relatively long time, the drawdown will become in steady state. In this state the drawdown is given by Eq.(6.80), the value of R can be calculated as follows:

$$R = r \cdot \exp(2\pi Kb\zeta/Q) \tag{6.86}$$

In Eq.(6.86), the values of r, ζ, b, and Q are known from the relatively long time pumping test. The permeability (K) is obtained from the application of Jacob's method. With this method, an observation well near the pumping well is needed. Such a well will have a high value of $R^*(=R/r)$, and as reference to

Fig.6.31 shows, deviation from the Theis curve due to the effect of the boundary will not occur until considerable pumping time has elapsed. A rough estimate of permeability (K) can be calculated on the basis of the early drawdown data from such a well. A rough calculation of the value of R is gotten. Knowing the values of R, one can prepare a graph of $\log\zeta^*$ versus $\log t^*/r^2$ depending on the value of r from Eq.(6.84). When the drawdown data from each observation well has been plotted log-log paper with the same dimensions per cycle as used above, one matches the field results to the theoretical curve in the same manner as in section 6.2.

When the curves are matched, one can read the dimensionless parameters that correspond to each point of field data. An equivalent value ζ^* can be determined for any ζ measured in the observation well and an equivalent value of t^*/r^2, for the corresponding value of real time, t/r^2. The permeability can be calculated from Eq.(6.85)

$$K = \frac{Q\zeta^*}{4\pi b\zeta} \tag{6.87}$$

and the compressibility factor can be calculated from Eq.(6.85)

$$S_s = 4K(t/r^2)/(t^*/r^2) \tag{6.88}$$

Moreover by the data of drawdown for a rlatively large time, the permeability can be obtained from Eq.(6.80) in the another method.

$$K = \frac{2.30Q}{2\pi b\zeta} \log_{10}(R/r) \tag{6.89}$$

D. Analysis of drawdown test data

The following discussion gives example calculations of the method given above. The drawdown test data are taken from a real aquifer project that is located near Lake Shinji, Shimane Pref. in Japan.

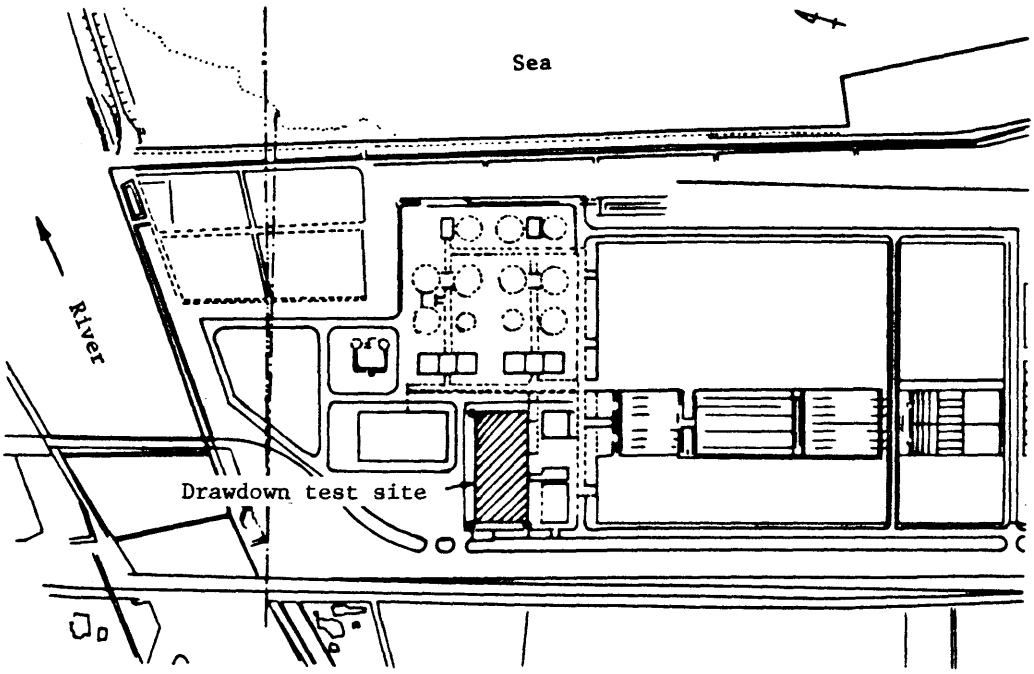

Fig.6.32 Plane view of the drawdown test site

The plane view of this region is shown in Fig.6.32. This region is bounded by the river on the west and by sea on the north. The geological condition obtrained from well logs is shown in Fig.6.33.

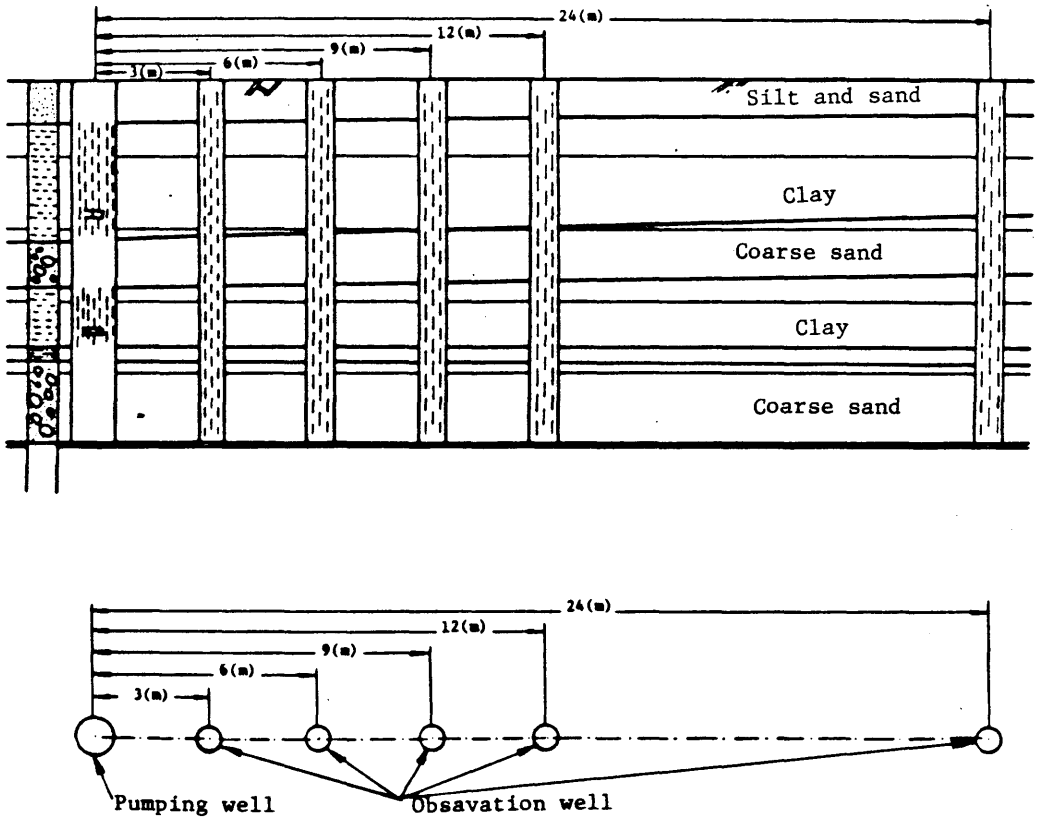

Fig.6.33 Hydrogeological cross-section through the experimental group of wells

Two sand-gravel layers revealed as confined aquifers exist in this region.

Firstly the drawdown test performed in the lower part confined aquifer is going to be analyzed for example using an average rate of $Q=4.17\times10^{3}cm^{3}/sec$. The thickness of this aquifer is revealed b=5.2m. The drawdown test data is analyzed by Jacob's method as shown in Fig.6.34, a rough estimate of permeability is obtained $K=5.78\times10^{-2}cm/sec$. For the relatively large time (4 hours) drawdown test data of the observation well (r=12m), the drawdown which is regarded as steady state is $\zeta=52cm$. Interpolating these parameters in Eq.(6.86). The rough calculation of the value of R is gotten

$$R = r\cdot\exp(2\pi kb\zeta/Q) \doteqdot 126m$$

The radial distance from pumping well to the river and sea is about 175m. From these results the value of R is estimated the four cases, that is, 100m, 125m, 150m, and 175m. Matching the field results to the theoretical curves for each value of R, the field data make a satisfactory fit to the theoretical curves for R=150m as shown in Fig.6.35. At the match point where $\zeta^{*}=5.0$, and $t^{*}/r^{2}=2.3\times10^{3}$, one reads $\zeta=5.2\times10cm$ and $t/r^{2}=10^{-2}sec/cm^{2}$ for r=12m. From Eq.(6.87), the permeability can be calculated

$$K = \frac{5.0\times4.17\times10^{3}}{4\times\pi\times520\times5.2\times10} = 6.14\times10^{-2}(cm/sec)$$

From Eq.(6.88), the compressibility factor can be calculated

$$S_{s} = \frac{4\times6.14\times10^{-2}\times10^{-2}}{2.30\times10^{3}} = 1.07\times10^{-6}cm^{-1}$$

Interpolating these calculated values in Eq.(6.78), the result of comarison of theoretical curves with drawdown test data is shown in Fig.6.36. It is

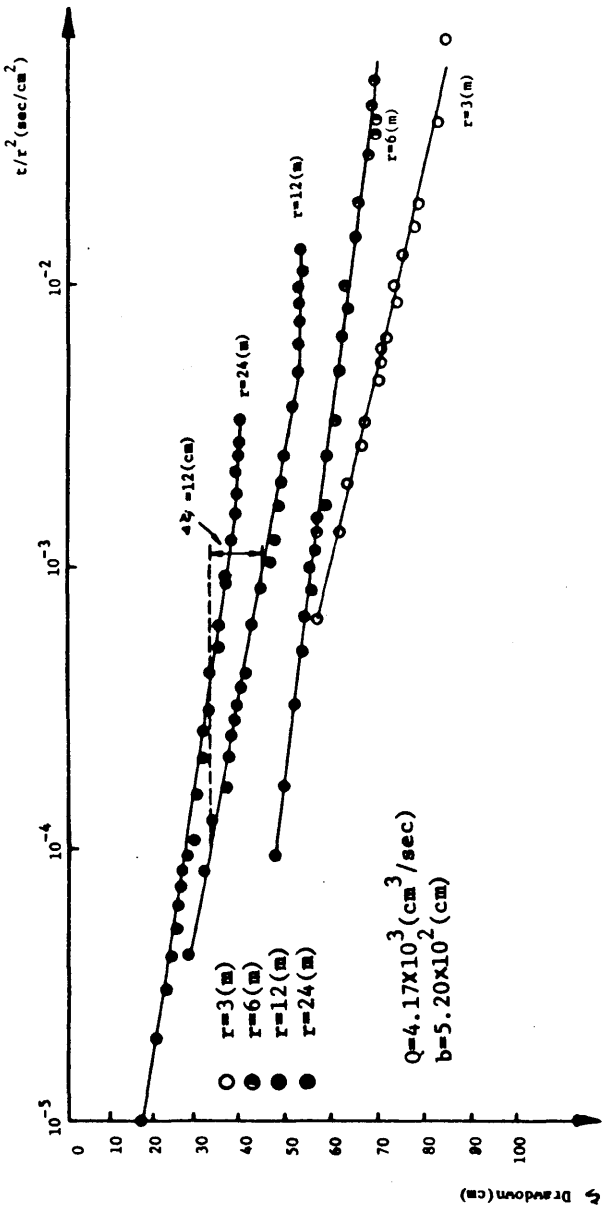

Fig.6.34 Method of Jacob's analysis(ζ-t/r^2)

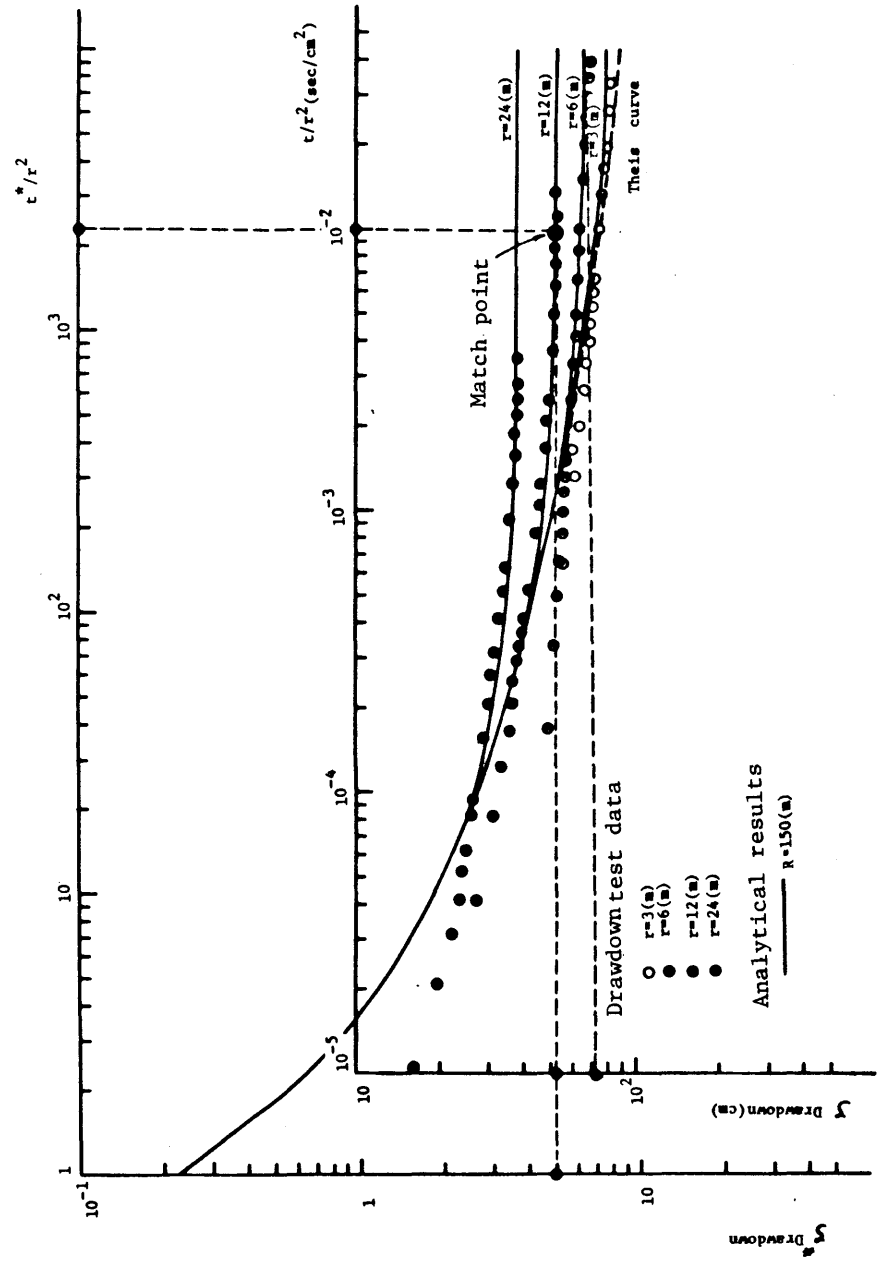

Fig.6.35 Method of superposition for finite region solution

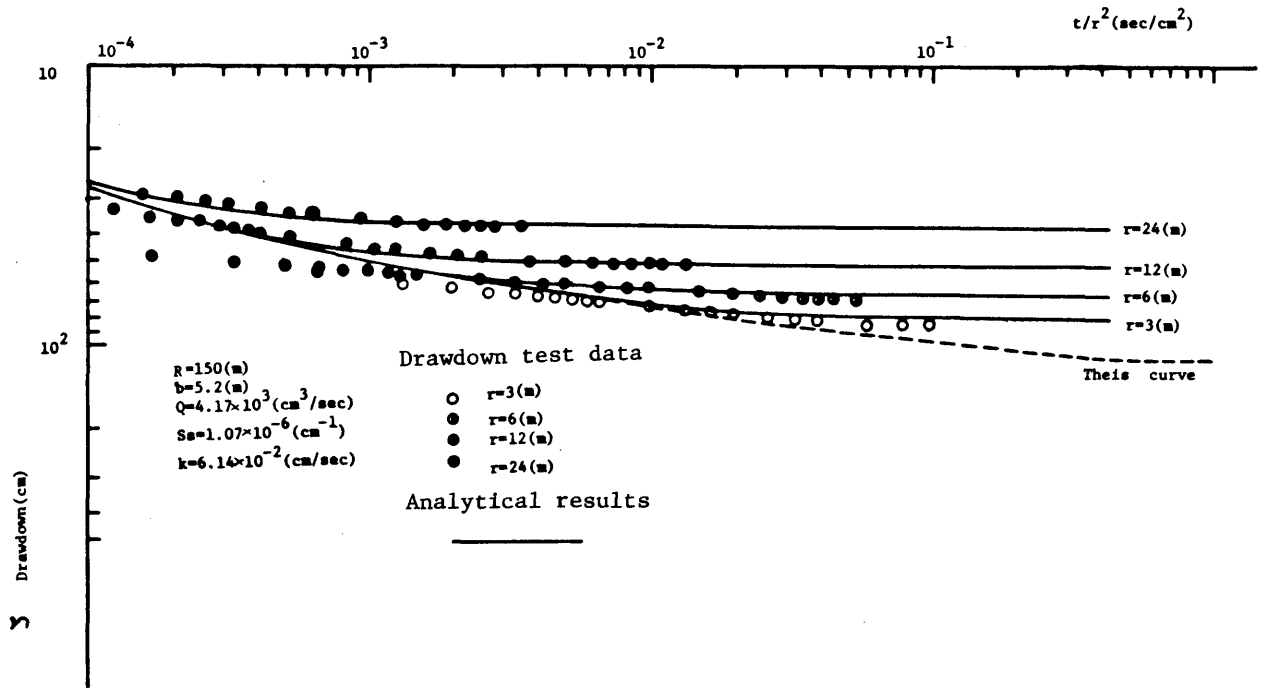

Fig.6.36 Comparision of the analytical results and drawdown test data

definite that theoretical curves give a good match with the drawdown test data.

From the steady state data, the permeability can be calculated from Eq.(6.89) interpolating R=150m, r=12m, ζ=52cm, Q=4.17×10^{3}cm^3/sec, b=5.2m

$$K = \frac{2.30\times4.17\times10^3}{2\times\pi\times520\times52}\log_{10}(150/12) = 6.20\times10^{-2}(\text{cm/sec})$$

Secondly the drawdown test performed in the upper part confined aquifer is going to be analyzed for the second example using an average rate of Q=3.69×10^2 cm^3/sec. The thickness of this aquifer is revealed b=2.10m. With the same way of the first example, R is estimated R=13.5m. At the match point where ζ^*=2.2×10^{-1} and t^*/r^2=13, one reads ζ=4.0cm, t/r^2=10^{-2}sec/cm^2 as shown in Fig.6.37. From Eqs.(6.87), (6.88) the permeability and the compressibility factor

$$K = \frac{369\times2.2\times10^{-1}}{4\times\pi\times210\times4.0} = 7.69\times10^{-3}(\text{cm/sec})$$

$$S_s = \frac{4\times7.69\times10^{-3}\times10^{-2}}{13} = 2.37\times10^{-5}(\text{cm}^{-1})$$

Interpolating these values into Eq.(6.78), the result of comparison of theoretical curves with the drawdown test data is shown is Fig.6.38. In this case theoretical curves also give a good match with the drawdown test data.

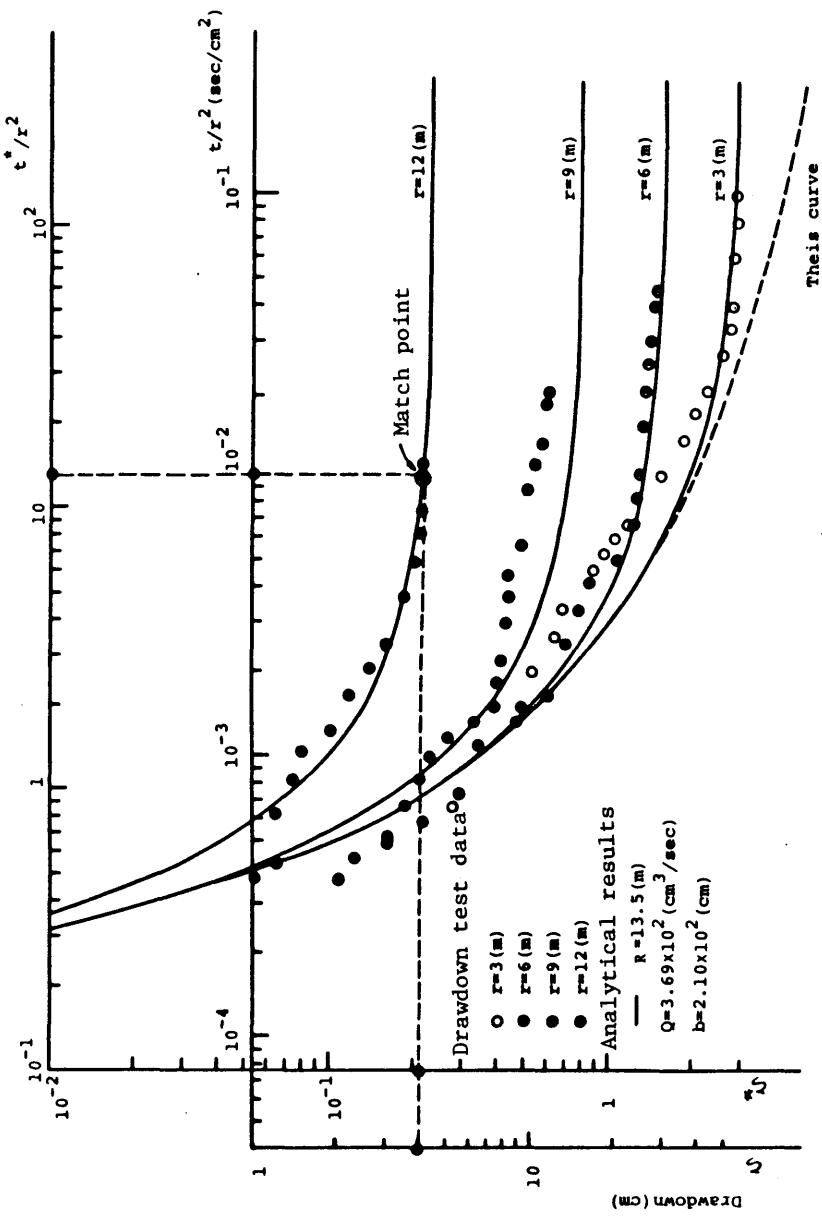

Fig.6.37 Method of superposition for finite region solution

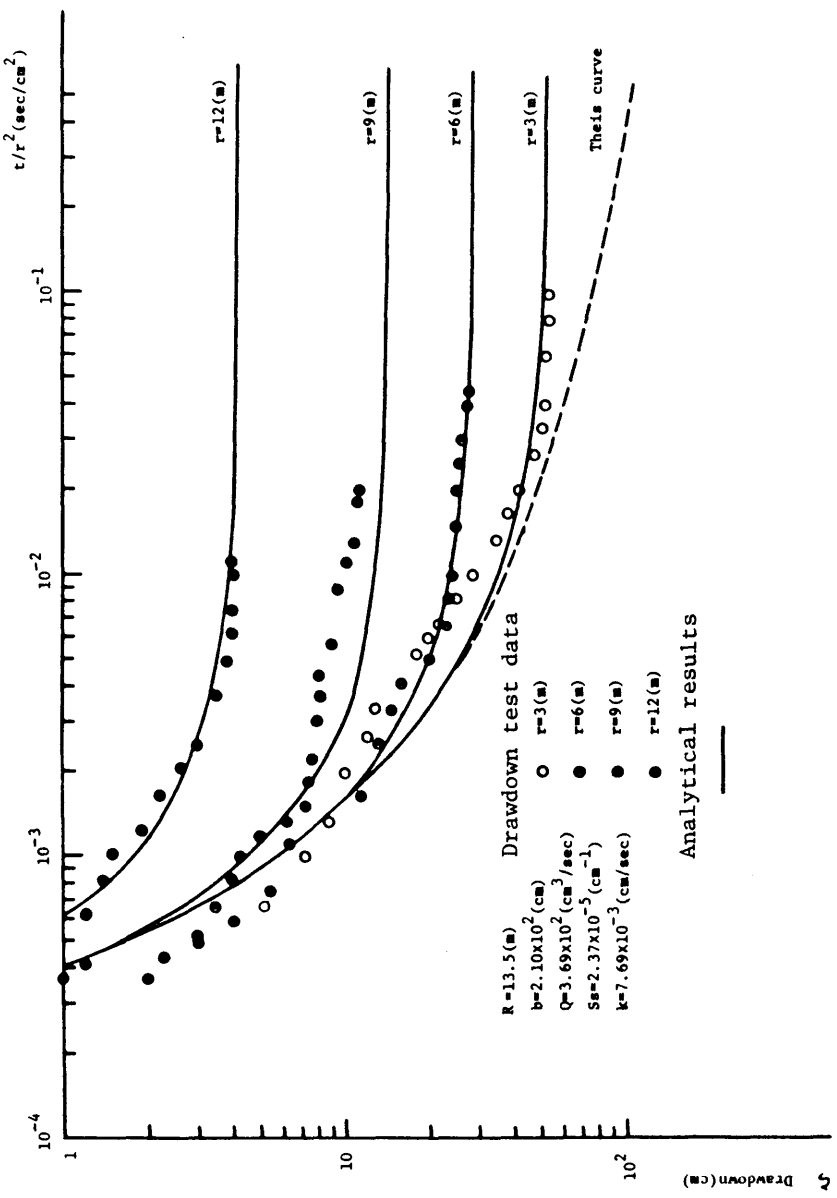

Fig.6.38 Comparison of the analytical results and drawdown test data

6.3.3 Analytical solution for Island Model drawdown test in an unconfined aquifer

In section 6.3.2, the analytical solution on a confined aquifer has been derived and example calculations are given.

In this section, consider an unconfined aquifer of finite lateral extent that rests on an impermeable horizontal layer such as that shown schematically in Fig.6.39. A well completely penetrating the aquifer discharges at a constant rate Q, and water is released from storage by gravity drainage at the free surface, neglecting the storage by compaction of the aquifer material expansion of the water.

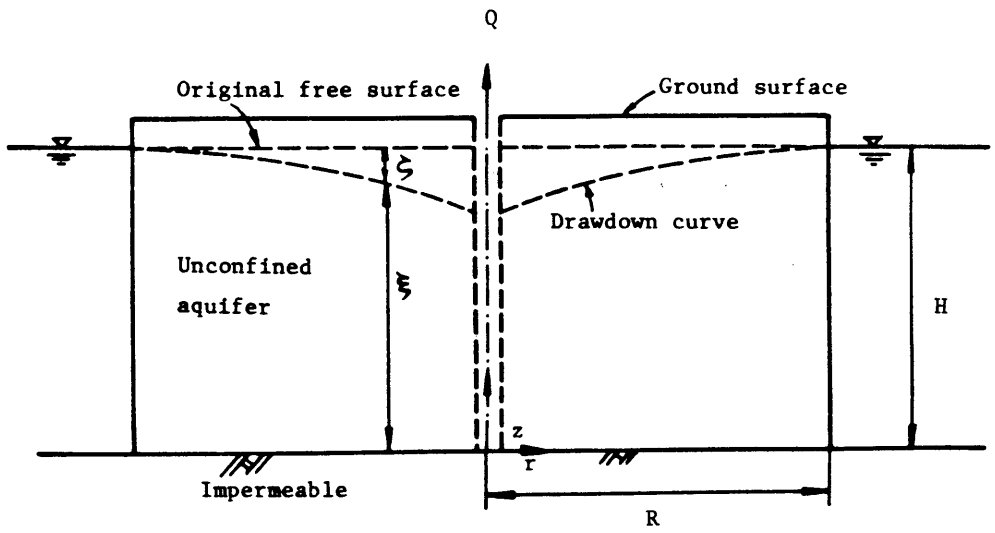

Fig.6.39 Nonsteady radial flow to a well penetrating a unconfined aquifer on an island

A. Basic equation and solution

With the assumptions which are described in section 6.3.1, the governing partial differential equation are given

$$\frac{\partial^2\zeta}{\partial r^2} + \frac{1}{r}\frac{\partial\zeta}{\partial r} + \frac{\partial^2\zeta}{\partial z^2} = 0 \quad (\ 0<z<\xi,\ 0<r<R) \tag{6.90}$$

Eq.(6.90) must be solved subject to following conditions

$$\left.\begin{aligned}\zeta(r,z,0) &= 0\\ \xi(r,0) &= H\end{aligned}\right\} \quad \text{(head initially constant)} \tag{6.91}$$

$$\zeta(R,z,t) = 0 \quad \text{(constant head at out boundary)} \tag{6.92}$$

$$\frac{\partial\zeta}{\partial z}(r,0,t) = 0 \quad \text{(on the no flow across lower boundary)} \tag{6.93}$$

$$\lim_{r\to 0}\int_0^{\xi} r\frac{\partial\zeta}{\partial r}dz = -\frac{Q}{2\pi K} \quad \text{(at the well-bore)} \tag{6.94}$$

$$\left.\begin{aligned}&\frac{\partial\zeta}{\partial r}n_r + \frac{\partial\zeta}{\partial z}n_n = \frac{S_y}{K}\frac{\partial\zeta}{\partial t}n_z\\ &\xi(r,t) = H - \zeta(r,\xi,t)\end{aligned}\right\} \quad \text{(on the free-surface boundary)} \tag{6.95}$$

where n_r, n_z is the component of unit outer nomal vector in r direction and in z direction respectively. S_y is the effective porosity or specific yield.

Eqs.(6.90)-(6.95) can be linearized by using a perturbation technique similar to that described by Dagan,[8),9)] provided the aquifer is thick enough and ζ remains much smaller than ξ. Here this technique leads to a first order linearized approximation, obtained simply by shifting the boundary condition from the free surface to the horizontal plane z=H.

This eliminates ξ from Eqs.(6.90)-(6.95), one obtains

$$\frac{\partial^2 \zeta}{\partial r^2} + \frac{1}{r}\frac{\partial \zeta}{\partial r} + \frac{\partial^2 \zeta}{\partial z^2} = 0 \tag{6.96}$$

$$\zeta(r,z,0) = 0 \tag{6.97}$$

$$\zeta(R,z,t) = 0 \tag{6.98}$$

$$\frac{\partial \zeta}{\partial z}(r,0,t) = 0 \tag{6.99}$$

$$\lim_{r \to 0} r \frac{\partial \zeta}{\partial r} = -\frac{Q}{2\pi KH} \tag{6.100}$$

$$\frac{\partial \zeta}{\partial z}(r,H,t) = -\frac{1}{\alpha_y}\frac{\partial \zeta}{\partial t}(r,H,t) \tag{6.101}$$

where $$\alpha_y = K/S_y \tag{6.102}$$

In solving the initial boundary value problem posed by (6.97)-(6.101), it is convenient to divide ζ into two components

$$\zeta = \zeta_1(r,t) + \zeta_2(r,z,t) \tag{6.103}$$

Although both ζ_1 and ζ_2 satisfy Eqs.(6.96)-(6.99), there is a change in boundary conditions Eqs.(6.100) and (6.101), which now take the form

$$\frac{\partial^2 \zeta_1}{\partial r^2} + \frac{1}{r}\frac{\partial \zeta_1}{\partial r} = 0 \tag{6.104}$$

$$\zeta_1(R,0) = 0 \tag{6.105}$$

$$\zeta_1(R,t) = 0 \tag{6.106}$$

$$\lim_{r \to 0} r \frac{\partial \zeta_1}{\partial r} = \frac{-Q}{2\pi KH} \tag{6.107}$$

$$\frac{\partial^2\zeta_2}{\partial r^2} + \frac{1}{r}\frac{\partial\zeta_2}{\partial r} + \frac{\partial^2\zeta_2}{\partial z^2} = 0 \tag{6.108}$$

$$\zeta_2(R,z,0) = 0 \tag{6.109}$$

$$\zeta_2(R,z,t) = 0 \tag{6.110}$$

$$\frac{\partial\zeta_2}{\partial z}(r,0,t) = 0 \tag{6.111}$$

$$\lim_{r\to 0} r\frac{\partial\zeta_2}{\partial r} = 0 \tag{6.112}$$

$$\frac{\partial\zeta_2}{\partial z}(r,H,t) = -\frac{1}{\alpha_y}\frac{\partial(\zeta_1+\zeta_2)}{\partial t}(r,H,t) \tag{6.113}$$

When Laplace transform is applied to Eqs.(6.104)-(6.113) with respect to ζ_1 and ζ_2, Eqs.(6.104)-(6.113) are given as follows;

$$\frac{\partial^2\overline{\zeta}_1}{\partial r^2} + \frac{1}{r}\frac{\partial\overline{\zeta}_1}{\partial r} = 0 \tag{6.114}$$

$$\overline{\zeta}_1(R,p) = 0 \tag{6.115}$$

$$\lim_{r\to 0} r\frac{\partial\overline{\zeta}_1}{\partial r} = \frac{1}{p}\frac{-Q}{2\pi KH} \tag{6.116}$$

$$\frac{\partial^2\overline{\zeta}_2}{\partial r^2} + \frac{1}{r}\frac{\partial\overline{\zeta}_2}{\partial r} + \frac{\partial^2\overline{\zeta}_2}{\partial z^2} = 0 \tag{6.117}$$

$$\overline{\zeta}_2(R,H,p) = 0 \tag{6.118}$$

$$\frac{\partial\overline{\zeta}_2}{\partial z}(r,0,p) = 0 \tag{6.119}$$

$$\lim_{r\to 0} r\frac{\partial\overline{\zeta}_2}{\partial r} = 0 \tag{6.120}$$

$$\frac{\partial\overline{\zeta}_2}{\partial z}(r,H,p) = -\frac{1}{\alpha_y}(\overline{\zeta}_1+\overline{\zeta}_2)p \tag{6.121}$$

The solution of Eq.(6.114) with respect to $\bar{\zeta}_1$ can be obtained with the conditions, Eqs.(6.115),(6.116).

$$\bar{\zeta}_1 = -\frac{Q}{2\pi Kb}\frac{1}{p}\ln(r/R) \tag{6.122}$$

The solution of Eq.(6.117) with respect to $\bar{\zeta}_2$ will be of the form

$$\bar{\zeta}_2 = A\, e^{\alpha z} J_0(\alpha r) + B\, e^{-\alpha z} J_0(\alpha r) \tag{6.123}$$

where $J_o(x)$ is the Bessel function of order zero of the first kind. From the condition (6.119), Eq.(6.123) becomes

$$\bar{\zeta}_2 = A\cosh(\alpha z) J_0(\alpha r) \tag{6.124}$$

To satisfy the boundary condition Eq.(6.118) α must be an infinite number of real positive roots

$$J_o(\alpha_n R) = 0 \tag{6.125}$$

$\alpha_n R$ is defined as λ_n, then Eq.(6.124) can be rewritten as

$$\bar{\zeta}_2 = \sum_{n=1}^{\infty} A_n \cosh(\lambda_n z/R) J_0(\lambda_n r/R) \tag{6.126}$$

The constant value A_n can be obtained from the condition Eq.(6.121),

$$\sum_{n=1}^{\infty} A_n (\lambda_n/R)\sinh(\lambda_n H/R) J_0(\lambda_n r/R)$$
$$= -(p/\alpha_y)[(Q_0/p)\ln(r/R) + \sum_{n=1}^{\infty} A_n \cosh(\lambda_n H/R) J_0(\lambda_n r/R)] \tag{6.127}$$

and the expression above can be rewritten as

$$\sum_{n=1}^{\infty} A_n C_n J_0(\lambda_n r/R) = \ln(r/R) \tag{6.128}$$

where now

$$C_n = -(\alpha_y/Q_0)[\ (\lambda_n/R)\sinh(\lambda_n H/R) + (p/\alpha_y)\cosh(\lambda_n H/R)] \tag{6.129}$$

and

$$Q_0 = -\ Q/(2\pi kH) \tag{6.130}$$

On a given interval $0<r\leq R$ the right-hand side of Eq.(6.128) is expanded in the form of Fourier-Bessel series,

$$\ln(r/R) = \sum_{n=1}^{\infty} a_n J_0(\lambda_n r/R) \tag{6.131}$$

the Fourier constants a_n of $\ln\frac{r}{R}$ in Eq.(6.131) are

$$a_n = \frac{2}{R^2 J_1^2(\lambda_n)} \int_0^R r[\ln(r/R)]\ J_0(\lambda_n r/R)dR \tag{6.132}$$

Integrating over r from 0 to R, one finds

$$a_n = -2/(\lambda n^2\ J_1^2(\lambda_n)) \tag{6.133}$$

From Eqs.(6.128), (6.131) and (6.133), the constants A_n are

$$A_n = a_n/C_n \tag{6.134}$$

Interpolating Eq.(6.134) into (6.127) and using (6.122), adding the transforms of both components gives

$$\bar{\zeta} = \bar{\zeta}_1 + \bar{\zeta}_2 = (Q_0/p)\ln(r/R) + \sum_{n=1}^{\infty}(a_n/C_n) \times\cosh(\lambda_n z/R)J_0(\lambda_n r/R) \tag{6.135}$$

The inversion of the Laplace transform of $\bar{\zeta}$ is accomplished, one obtains the first order approximation to the original initial boundary value problem. The final solution is expressed as follows;

$$\zeta = -\frac{Q}{2\pi KH}\Big[\ln(r/R) + \sum_{n=1}^{\infty}\frac{2J_0(\lambda_n r/R)\cosh(\lambda_n z/R)\exp[-t(\lambda_n K/RS_y)\tanh(\lambda_n H/R)]}{\lambda_n^2 J_1^2(\lambda_n)\cosh(\lambda_n H/R)}\Big] \tag{6.136}$$

In Eq.(6.136), let t become infinite the result becomes

$$\zeta = -\frac{Q}{2\pi KH}\ln(r/R) \tag{6.137}$$

this is just the steady state solution of the model shown in Fig.6.39.

B. Effects of constant head at outer boundary

To illustrate the analytical results, a computer program that permits to determine the dimensionless ratio $\zeta^*(=2\pi KH\zeta/Q)$ as a function of the dimensionless time $t^*(=Kt/RS_y)$ for given dimensionless values of $r^*(=r/R)$, $z^*(=z/R)$ and $H^*(=H/R)$, according to follow expression of Eq.(6.136) has been prepared.

$$\zeta^* = -\ln(r^*) - \sum_{n=1}^{\infty}\frac{2J_0(\lambda_n r^*)\cosh(\lambda_n z^*)\exp[-\lambda_n t^*.\tanh(\lambda_n H^*)]}{\lambda_n^2 J_1^2(\lambda_n)\cosh(\lambda_n H^*)} \tag{6.138}$$

The program has been run for various combinations of the paramaters.

In Fig.6.40, drawdown curves at (z^*=1) observation wells (r/R=100,20,10,5,4, and 2) are presented for R/H=10. The abscissa $t^*/(r^*)^2$ ($=\frac{RKt}{S_y r^2}$) is the independent variable in the Theis formula, whose drawdown curve has also been represented in Fig.6.40.

The type curves depart from the Theis curve in pairs with the point of departure depending on the value of $R^*(=\frac{R}{r})$. It is noted on Fig.6.40, as same as the confined condition, that the drawdown in the aquifer bounded by constant head becomes steady state earlier than the drawdown in the infinite extent aquifer.

C. Method of analyzing field data

In an unconfined aquifer, the engineer wishes to determine the value of the aquifer constants (K, S_y) and the radial distances of the influence region (R) in the same way of the case in the confined aquifer. The geological condition of the aquifer is known from the well logs. Here, an analysis of the drawdown data in the observation wells is shown.

Log-Log Method

To prepare a graph of drawdown $\log\zeta^*$ versus $\log t^*$ for the appropriate r^* ($=r/R$) between pumping well and observation wells from Eq.(6.138), it is necessary to obtain the values of R, H. The thickness (H) of the aquifer can be obtained from the well logs and the measuring the existent ground water level. The value of R is assumed from the same way of confined aquifer, namely, if a drawdown test is run for relatively long time, the drawdown will become in steady state, and in this state the drawdown is given by Eq.(6.137). From that equation, the value of R can be calculated

$$R = r \cdot \exp(2\pi KH\zeta/Q) \qquad (6.139)$$

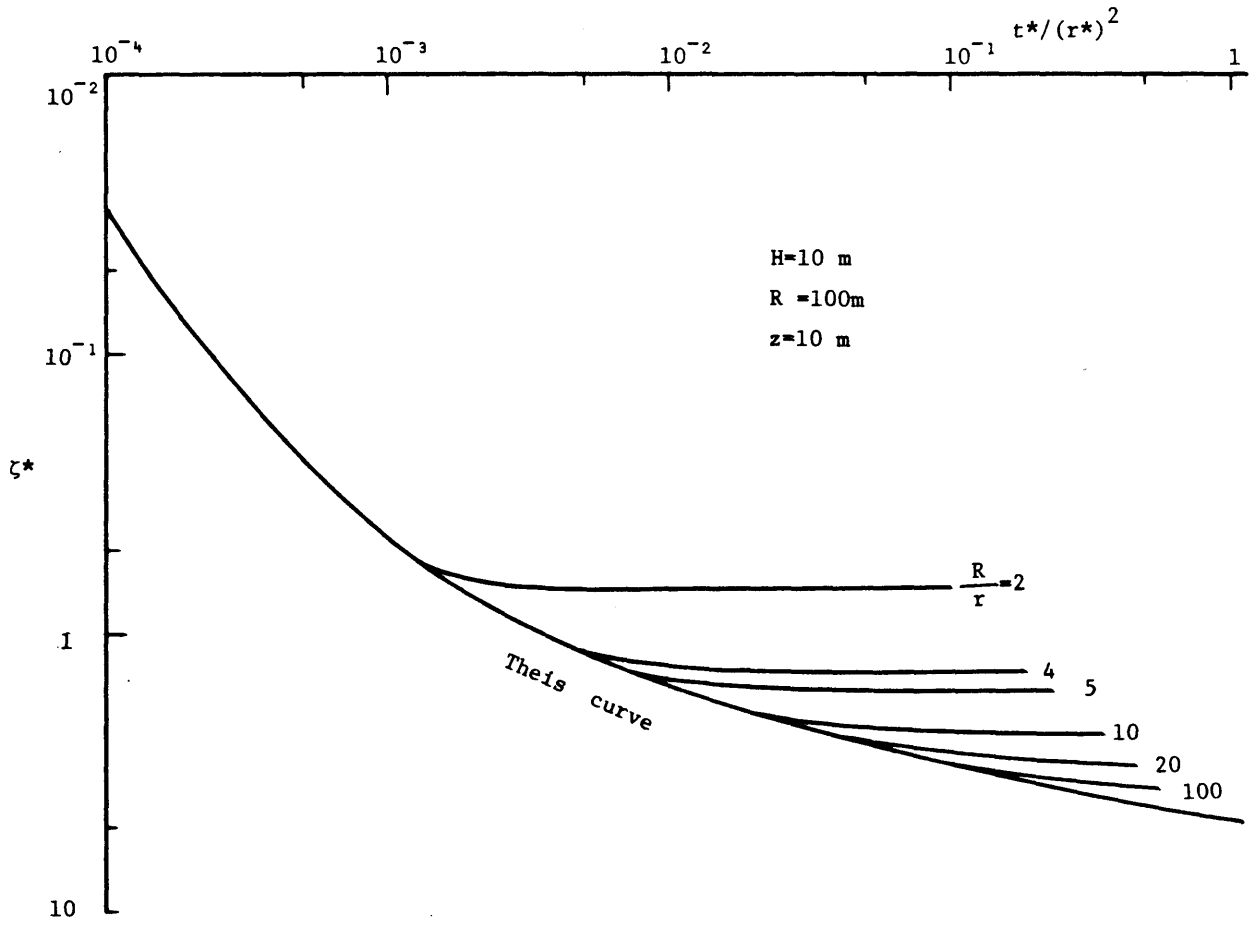

Fig.6.40 Analytical results for radii of flow region

In Eq.(6.139), though the known values are H, ζ, and Q, the permeability (K) is unknown value. The permeability (K) is obtained from the application of Jacob's method. With this method, an observation well near the pumping well is needed. Such a well will have a high value of $R^*(=R/r)$, and as reference to Fig.6.40 , devistion from the Theis curve due to the effect of the boundary will not occur until considerable pumping time has elapsed. A rough estimate of permeability (K) can be calculated on this basis of the early drawdown data from such a well. Interpolating these parameters in to Eq.(6.139), a rough calculation of the value of R can be gotten. Getting the values of R, one can prepare a graph of $\log\zeta^*$ versus $\log t^*/r^2$ depending on the value of r from Eq.(6.138), in that equation

$$\zeta^* = 2\pi KH\zeta/Q \tag{6.140}$$

$$t^* = (K/S_y)\cdot t \tag{6.141}$$

By using the match point method, one can read the dimensionless parameters that correspond to each point of field data.

An equivalent value ζ^* can be determined for any ζ measured in the observation well and an equivalent value of t^*/r^2, for the corresponding value of real time, t/r^2. The permeability can be calculated from Eq.(6.140)

$$K = (Q/2\pi H)(\zeta^*/\zeta) \tag{6.142}$$

and the effective porosity can be calculated from Eq.(6.141)

$$S_y = K(t/t^*) \tag{6.143}$$

D. Analysis of drawdown test data

The drawdown test data are taken from a real aquifer project that is located near Goshyo, Kyoto City in Japan. The geological condition obtained from well logs is shown in Fig.6.41. The drawdown test performed in the unconfined aquifer is going to be analyzed for example using an average rate of $Q=2.67\times10cm^3/sec$. The thickness of this aquifer is revealed H=2.17m. The result of the drawdown test data analyzed by Jacob's method is shown in Fig.6.42. From this result a rough estimate of the permeability is obtained as $K=1.12\times10^{-3}cm/sec$. For the relatively large time (t=20 hours) drawdown test data of the observation well(r=15.7m), the drawdown which is regarded as steady state is $\zeta=17.5cm$. Interpolating these values into Eq.(6.139), the rough calculation of the value of R is gotten

$$R = r\cdot\exp(2\pi KH\zeta/Q)$$
$$= 1.57\times10^3\exp(2\times3.14\times1.12\times10^{-3}\times2.17\times10^2\times17.5/2.67\times10^3)$$
$$=42.4m$$

Though the Kamo river that is regarded as the constant head boundary exists at the distance R=1000m from the pumped well, for the reason that the pumping rate is small and the ground water supply is large because the region is the center of the Kyoto Basin, the value of the influence is estimated for cases, that is, R=25m, 30m, 40m, and 50m. All observation wells have penetrations of z=2m and radial distance of each well is shown in Fig.6.40. Then, interpolating these values (z, R, r_i, H) into Eq.(6.138), the theoretical curves are gotten.

Matching the field results to the theoretical curves for each value of R, the field data make a satisfactory fit to the theoretical curves for R=30m, as shown in Fig.6.43.

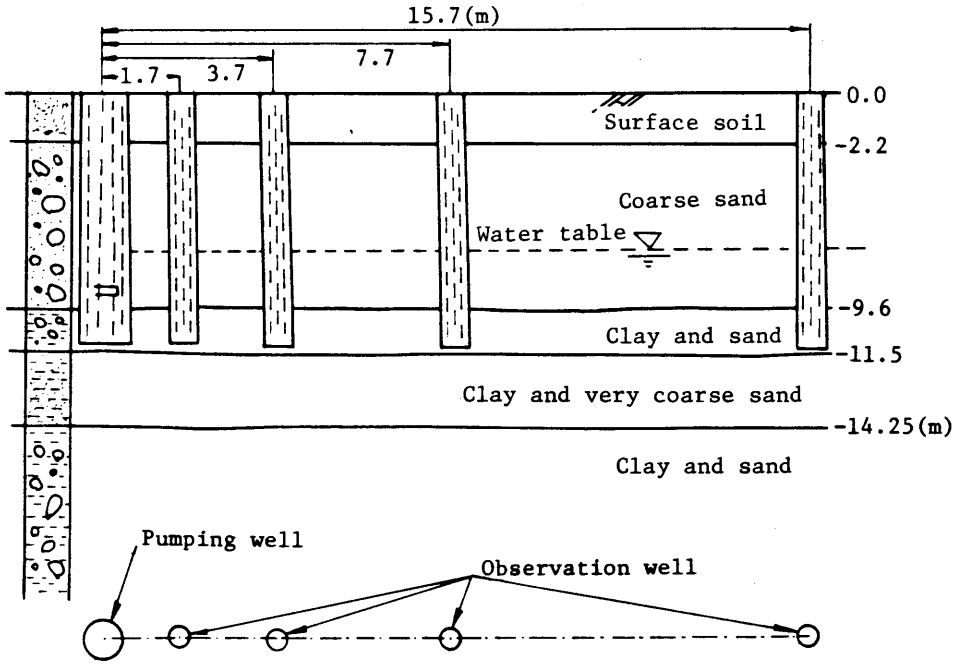

Fig.6.41 Hydrogeological cross-section of the drawdown test site

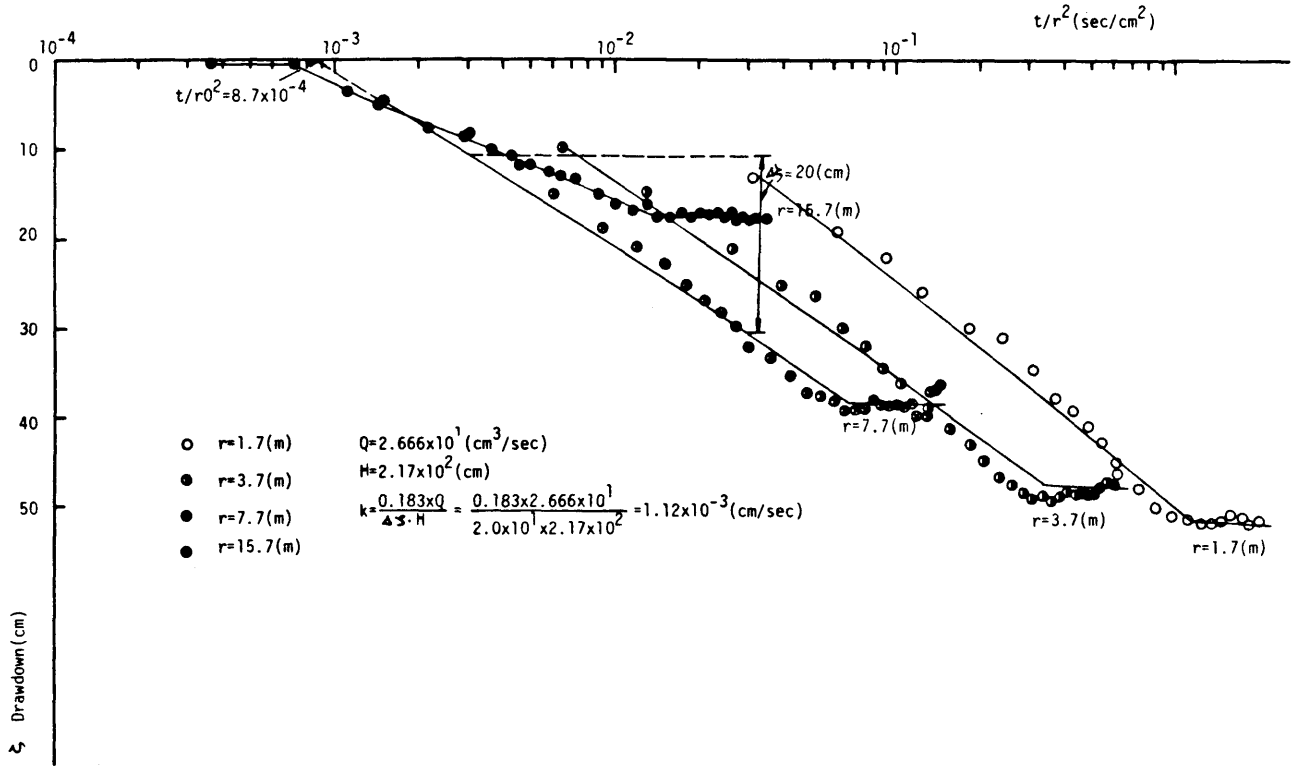

Fig.6.42 Method of Jacob's analysis(ζ-t/r^2)

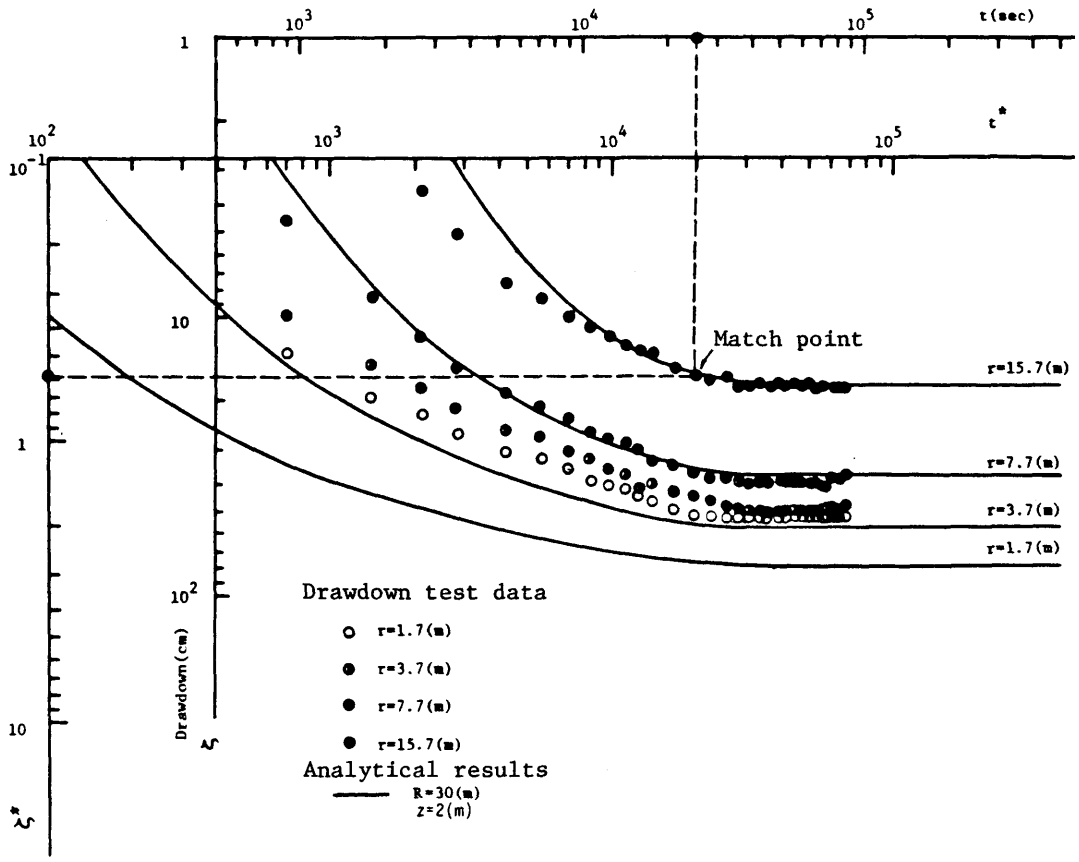

Fig.6.43 Method of superposition for finite region solution

At the match point where $\zeta^*=5.9\times10^{-1}$, and $t^*=2\times10^4$, one reads ζ=16cm and t=2.55 $\times10^4$sec for r=15.7m. From Eq.(6.142) the permeability can be calculated

$$K=\frac{26.66\times5.9\times10^{-1}}{2\times\pi\times217\times16}=7.21\times10^{-4}(cm/sec)$$

From Eq.(6.143), the effective porosity can be calculated

$$S_y=\frac{7.2\times10^{-4}\times2.55\times10^4}{2\times10^4}=9.19\times10^{-4}$$

Interpolating these calculated values in Eq.(6.136), the result of comparison of theoretical curves with drawdown test data is shown in Fig.6.44. It is definite that theoretical curves give good match with the drawdown test data.

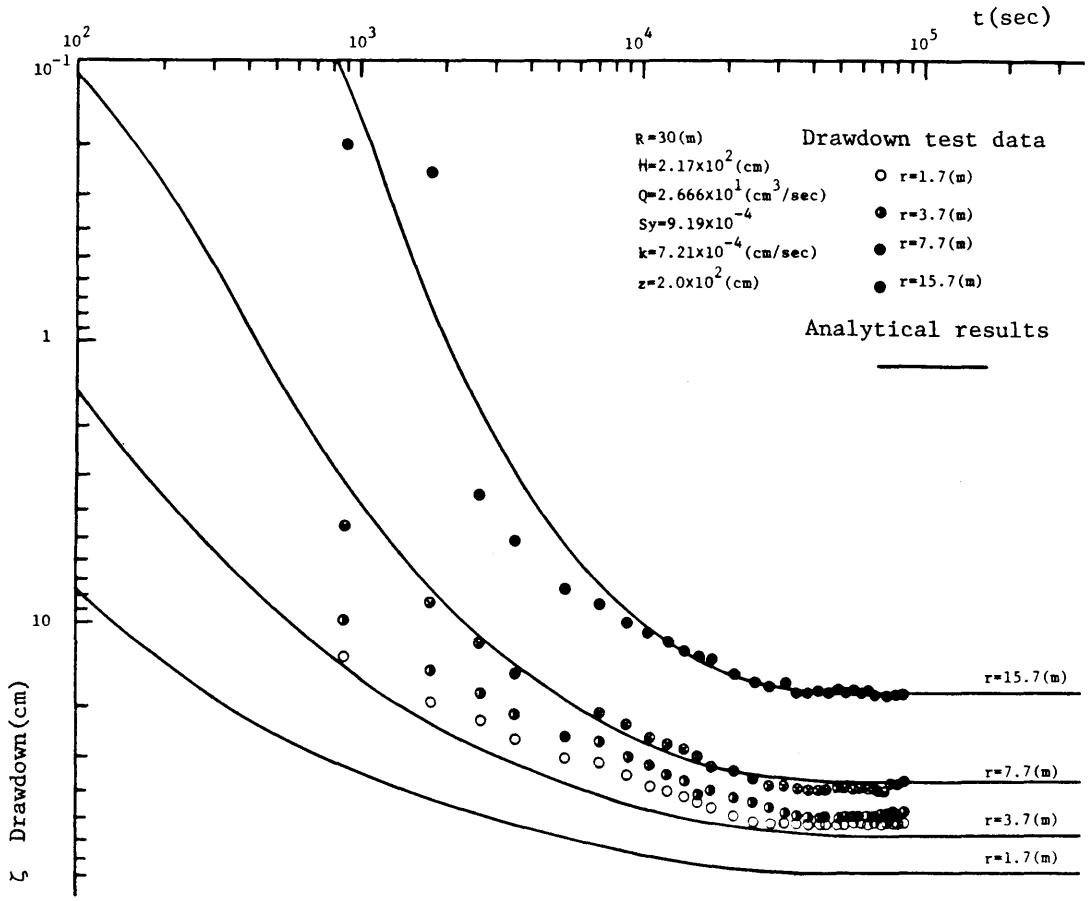

Fig.6.44 Comparison of the analytical results and drawdown test data

6.4 Conclusions

In this chapter formulas and methods available to evaluate the data from pumping tests under two special conditions have been developed. Namely, firstly, analyses of pumping test data for partially penetrating well in a confined and an unconfined aquifers have been shown to determine anisotropic hydraulic conductivities and a storage coefficient. Secondly, to analyze drawdown test data obtained in the much groundwater supplied region, a conception of "Island Model" has been applied in unsteady state. The results of this study can be used to analyze drawdown tests in order to measure the two aquifer parameters K and S. These analytical solutions are very complex, but they can be recognized that they have greater generality than previous solution.

The conclusions obtained in this chapter are as follows;

(1) The unsteady analytical solution of phreatic flow to partially penetrating well in a confined aquifer is shown. By using this solution, four methods are provided to evaluated the anisotropy of permeability and the compressibility factor (or specific storage) of confined aquifer.

(2) For an unconfined aquifer the unsteady analytical solution of phreatic flow to partially penetrating well was obtained and to determine anisotropic permeabilities and an effective porosity (or storage yield) two methods were developed.

(3) The limitations of adapting Theis'and Jacob's methods for partially penetrating well test were described.

(4) For each method the practical application was shown.

(5) The unsteady analytical solutions of phreatic flow due to drawdown test are derived in the conception of "Island Model" that the shape of groundwater level is fixed by the circular water supply both for confined and unconfined aquifer.

(6) By using these solutions, the methods of analyzing drawdown test data

performed in confined and unconfined aquifer are given.

(7) The effect of influence region is evaluated, and a theoretical explanation of the assumption based on experiences was given.

(8) The example analysis to determine permeability and storage coefficient are shown.

(9) The propriety of the solutions is verified comparing the analytical results with the drawdown test data taken from a real aquifer project.

References

1) Hantuch,M.S.: Drawdown around a partially penetrating wells, Trans. ASCE, 127, 1962, pp.268-283.

2) Hantush,M.S.: Aquifer tests on partially penetrating wells, Trans. ASCE, 127, 1962, pp.284-308.

3) Javandel,I.: Verification of analytic solution for partial penetration wells by mathematical and heat transfer models, M.S.Thesis, U.C.Berkeley, 1965.

4) Carslaw,H.S. and Jaeger,J.C.: Conduction of heat in solids, Oxford Univ. Press, 1959, pp.75.

5) Dagan,G.: A method of determining permeability and effective porosity of unconfined, anisotropic aquifers, Water Resources Res., 3,4, 1967, pp.1059-1071.

6) Akai,K. et al.: The unsteady analysis of drawdown due to pumping in vartical and horizontal well, 10th Conf. JSSMFE, 1975, pp.619-622, (in Japanese).

7) Mononobe,T.: Hydraulics, Iwanami Syoten, 1950, pp.472, (in Japanese).

8) Dagan,G.: The solution of the linearized equations of free-surface flow in porous media, Journal de Mecanique. Vol.5, No.2, 1966, pp.207-215.

9) Dagan,G.: Second order linearized theory of free surface flow in porous media, La Houille Blanche, Grenoble, France, 8, 1964, pp.901-910.

CHAPTER 7

APPLICATION TO FIELD PROBLEMS

7.1 Introduction

The validity and the accuracy of the saturated-unsaturated finite element method has been investigated in Chapter 5 by comparing with laboratory experimental results. It can be concluded, with a sense of confidence, that the numerical methods can provide reliable basis for design analysis. In this chapter, some application of models to field situation will be demonstrated. To simulate a practical flow problem in the field following data and conditions must be required.

(1) Hydraulic properties of soils that constitute a flow domain.

(2) Initial conditions in a flow domain.

(3) Boundary conditions of a flow domain.

In simulating the model of laboratory experiment, these data and conditions are relatively easily obtained. In many practical situations, however, one may encounter these data and conditions that are impossible to be defined.

The purpose of this chapter is twofold: before progressing into the various levels of applications, (1) to discuss and evaluate the above data and conditions; and (2) to describe two example applications for both two- and three-dimensional field problems.

7.2 Hydraulic Characteristics of Soil in Field

The decision as to whether it is necessary to include consideration of the unsaturated zone in the analysis of seepage through porous media involves a tradeoff between the possible additional accuracy and the definite additional complexity. As mentioned in Chapter 5, the method requires an increased amount

of input data in the form of the characteristic ψ-θ-K curves which are strongly dependent on soil texture. The concept of soil characteristics that vary with moisture content is not common in soils engineering but is well established in the solution of irrigation and drainage problems in agricultural engineering. These data are not commonly collected, nor are they familiar to most civil engineers. The curves can be determined in the laboratory by the techniques that are well established in Chapter 4. Data for compacted soils, on the other hand, are almost nonexistent and undoubtedly the relationships are more complex. It is clear from compaction theory[1] that saturated permeability is heavily influenced by soil density, compactive effort, and moisture content at compaction. This conclusion undoubtedly holds for the unsaturated curves as well and results suffer from the usual suspicions as to their applicability to actual field sites. It is encouraging to note that research is proceeding in the soil physics field in developing direct field measurement techniques. Because of the paucity of data on the unsaturated properties of compacted soils, it is difficult to vouch for the suitability of the soil properties, especially in cases of similitude extrapolation. Rather, the emphasis has been on examining the possible implications of the complete analysis.

A number of methods are now available for measuring the unsaturated hydraulic conductivity function of soil profiles in situ. The purpose of this section is to survey the various methods available for the measurement of hydraulic conductivity and water retention characteristics and to identify the principles advantages and disadvantages of each. There are mainly two kinds of method to estimate the hydraulic characteristics of unsaturated soil in situ:

(1) Direct measurement of the hydraulic conductivity function.

(2) Calculation of conductivity from water retention data.

In the former, many laboratory methods have been applied in the field.[2] It is generally much more difficult to set steady flow regimes in the field than in

the laboratory. Infiltration techniques have been proposed based on a steady application rate by sprinkling[3] or based on ponding infiltration through an impeding crust.[4),5] In unsteady-state methods, the "instantaneous profile" techniques which have already been described in Chapter 4 seem to offer the best possibility for hydraulic characterization of field soils. The theory does not assume uniformity of the hydraulic properties of the flow system, and the boundary conditions do not need to be constant, or known in detail. Because in this method a diffusivity in an internally draining profile is measured. Several variations in the method of experimental procedure have been employed. The water content distributions were measured by using neutron[6),7),8)] or gamma ray[9),10)] or gravimetric sampling.[11),12)] The pressure head distributions were measured by using tensiometers of mercury-water[11),12)] or pressure transducers.[6),7),8),9),10),13)] In these techniques reported in the literature, Hillel's method[8)] was made to give the most detailed description of a simplified procedure for determining the intrinsic hydraulic properties of a complete soil profile in situ. These methods have proven the feasibility of determining the unsaturated hydraulic conductivity function of soils in the field. However, these methods have complexity in treating the experimental apparatus.

In the latter, there has been considerable interest in the possibility of calculating the conductivity from other properties of the medium that may be easier to measure. There are many publications that deal with the relationship of conductivity to various aspects of pore space geometry or water retention data.[2)] These methods were also summarized and evaluated in the literature and further works were recently proposed.[14),15),16),17)] Though these methods give the merit to calculate hydraulic conductivity from water retention data, water retention data must be obtained on soil cores taken to the laboratory. It should be understood that no field sampling technique yet available provides truely undisturbed samples. Therefore this method suffers from above limitation.

By the way, all of the methods that are reviewed above have been applied for only the hydraulic characteristics of surface layered soils above the depth of three or four meters. This reason is that these methods have been established on the sense of agricultural engineering to solve the problems involving irrigation, drainage, water conservation, nutrient transport and runoff pollution, as well as infiltration. These methods can be also applied to determine the hydraulic properties of center core of rock-fill dam or to check the quality of a constitutive soil of a bank. To solve problems of groundwater recharge and discharge due to pumping or excavation, it is necessary to determine the unsaturated hydraulic properties of the soil texture which is layered above and below the water table as shown in Fig.7.1 with hatching. Unfortunately, there is no technique to obtain the properties so far as author knows. It may be believed that the case of accomplishing determination of hydraulic properties

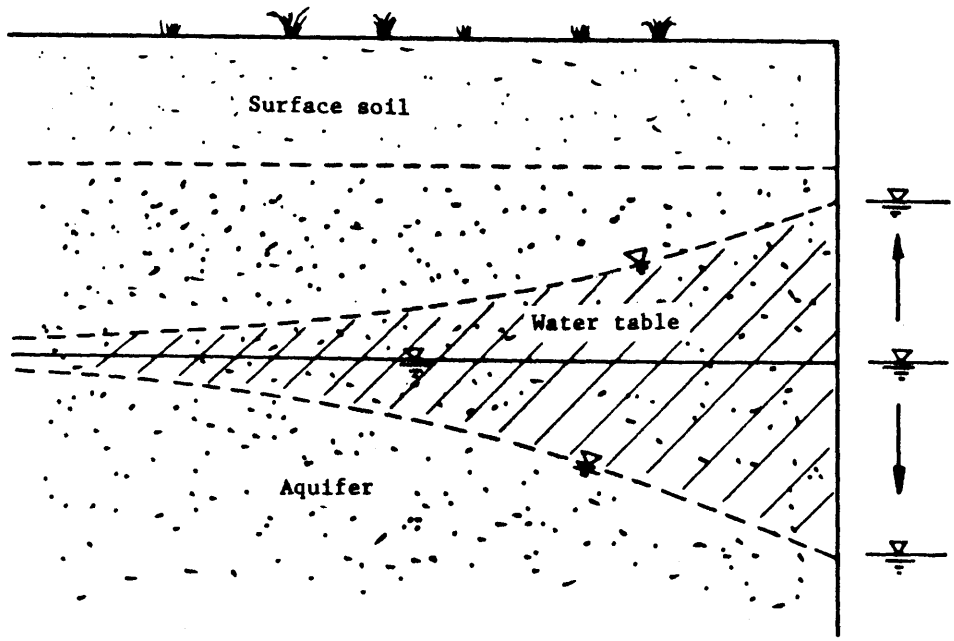

Fig.7.1 Schematic figure of underground

of soils in situ will improve with additional field experience and improvements in equipment and instrumentation in the near future.

The values of hydraulic conductivity (K_s) and storage coefficient (S) in the saturated region can be determined by using the techniques described in Chapter 6. The value of specific yield (S_y) can be considered the equivalent value of effective porosity (n_e).

7.3 Flow through Sand Bank at Flood Water Level

7.3.1 Introduction

In July 1972 and September 1976 the basin of the River Ohota in Hiroshima Prefecture suffered damage from leakage or piping water when the water level of the river was raised due to localized torrential downpour. Acting on information received the damaged district in landside was mainly shown in Fig.7.2 with the shaded region and the leakage and piping were happened after two or three hours from the peak of river water level. These phenomena can be considered symptoms of a disaster of embankment failure due to flood, then it is necessary to work out a countermeasure for leak prevention. The purposes of this section are to simulate the flow pattern in the embankment when the river water level is raised to the height of July 1972, September 1976 and high water level (HWL), and to evaluate the effectiveness of bank protection. To ascertain geologic and ground water conditions six test drillings were driven until 20m depth. Four test holes of this six holes also were used as observation wells for measuring water levels and for conducting drawdown tests. The position of test holes are shown in Fig.7.2. Fig.7.3 shows the geologic condition estimated from well logs constructed from drilling samples.

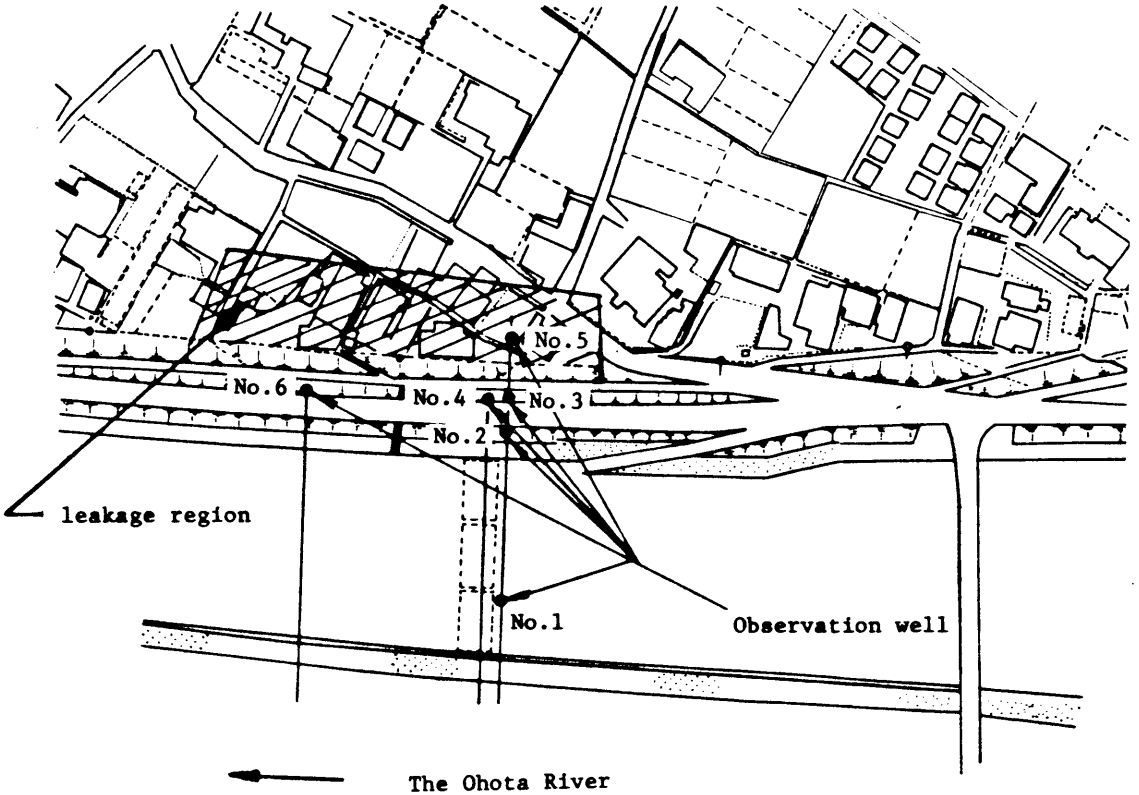

Fig.7.2 Plane view of damaged district

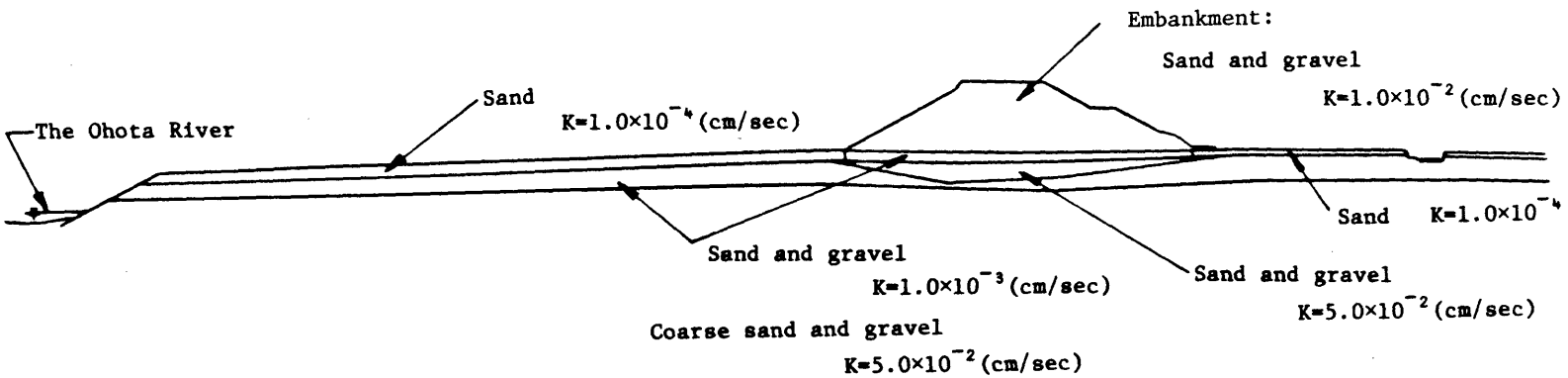

Fig.7.3 Hydrogeological cross-section

Saturated hydraulic conductivities of the various soil layers were measured in the field by the auger hole method (USBR Method E-18)[20]. The mean hydraulic conductivities of each layer are also shown in Fig.7.3. As mensioned earlier the complex multilayer systems that one can encounter in the field can not be certainly handled analytically. On the other hand, the numerical procedures embodied in the finite element method provide a practical means of analyzing complex systems. Therefore the change of flow pattern in the embankment due to flood water level and the other environmental effects were investigated by the saturated-unsaturated finite element method.

7.3.2 Selection of boundary condition

In many practical situations, one may encounter geometries and boundary conditions that cannot be defined. For instance, in the case of flow in or out of riverbanks, tidal beaches, and extensive aquifers, one has to deal with infinite extents of the media. It is then necessary to include only significant finite zones in an analysis, and one has to make proper assumptions concerning potential and flow conditions on the discretized boundaries. Proper choice of these conditions will depend upon the geological properties and conditions of groundwater flow and will require engineering judgement. Some criteria were proposed to determine extents of discretized zones for free surface flow through earth banks[18]. It was found that if the end boundary is placed beyond a distance of about 8H to 12H, measured from the final point of drawdown (Fig.7.4), the behavior of the free surface near the sloping face of the bank will not be influenced significantly. The assumption of an "impervious" base in an infinite medium will be approximately valid if the bottom boundary is placed beyond a distance of about 3H to 6H (Fig.7.4).

Three possible boundary conditions were assumed to occur at the discretized end boundary, namely impervious, constant level, and equipotential as

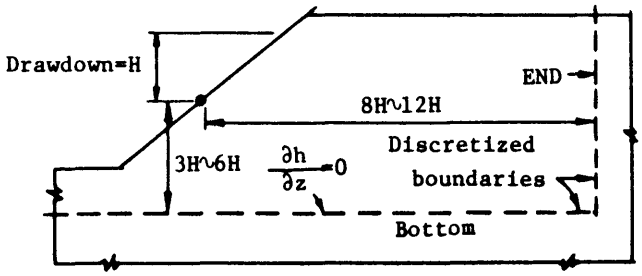

Fig.7.4 Discretized end and bottom boundaries(after Desai)[18)]

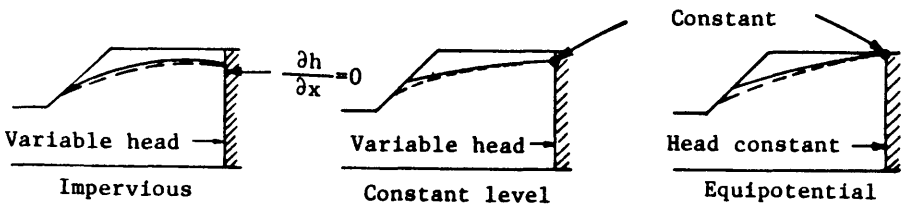

Fig.7.5 Different boundary conditions(after Desai)[18)]

in Fig.7.5. Both the impervious and constant-level conditions yielded about the same results, which compared well with observations, whereas the equipotential condition gave results that differed from the other two and from the observations. Hence, it was concluded that for long homogeneous banks, the boundary condition at large distances can be assumed to be impervious or constant level. In this work, the boundary as shown in Fig.7.6 was applied to simulate this boundary problem. Fig.7.6 also shows the finite element mesh. The aquifer has been divided into 211 elements with a total of 240 nodes, the grid being denser in embankment than at the outskirt.

[18]

7.3.3 Determination of hydraulic properties in unsaturated region.

The water level in the coarse sand and gravel layer is about G.L. -3.5m. and the aquifer of coarse sand and gravel layer is revealed an unconfined aquifer. There is a need to determine unsaturated hydraulic properties of these region to simulate the flow through these region. Unfortunately these properies were not reported, so some other method must be taken to obtain these properties. A numerical method was used to investigate in detail certain physical aspects. Using this numerical method, it can be shown that if the saturated conductivity were accurately determined, slight changes in the shape of the rest of the conductivity-water content relationship will cause small changes in the calculated discharge-time curves. Thus a computer method of using an accurately determined value of several shapes for the rest of conductivity-water content relationships to calculate several discharge-time is proposed. These calculated curves could then be compared with the experimentally observed discharge-time curve to select the appropriate conductivity-water content relationship. In this problem, discharge-time curve could not be obtained, so the groundwater table - time curve which was the results of measuring the groundwater fluctuations at the observation well No.1, No.2, No.3 and No.5 (as shown in Fig.7.6)

[19]

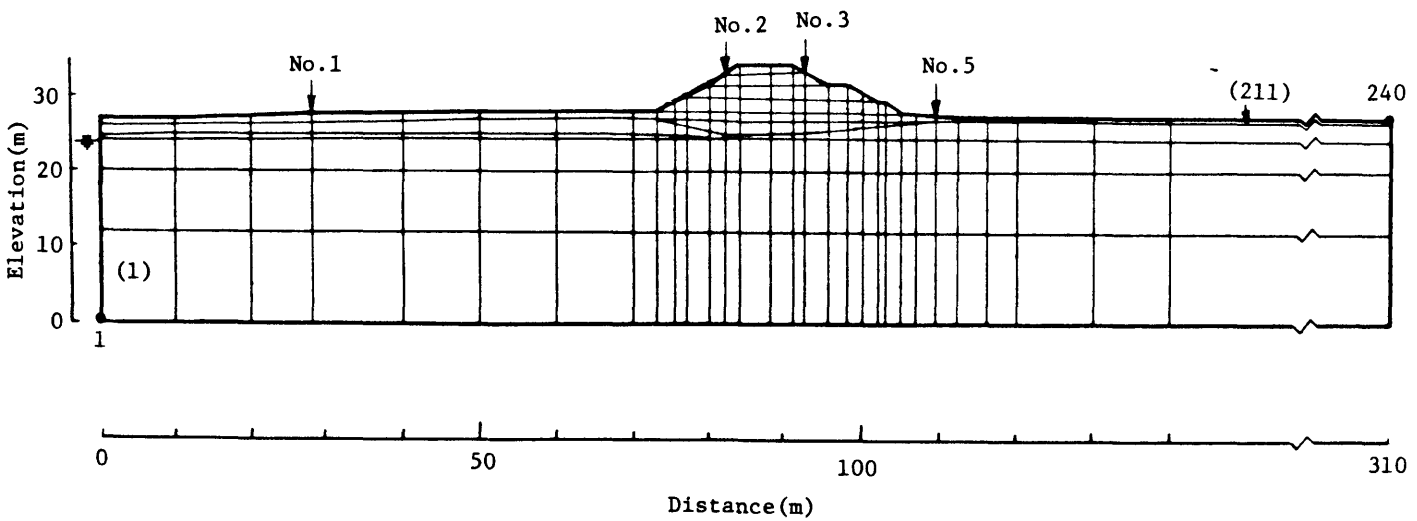

Fig.7.6 Finite element network of field problem

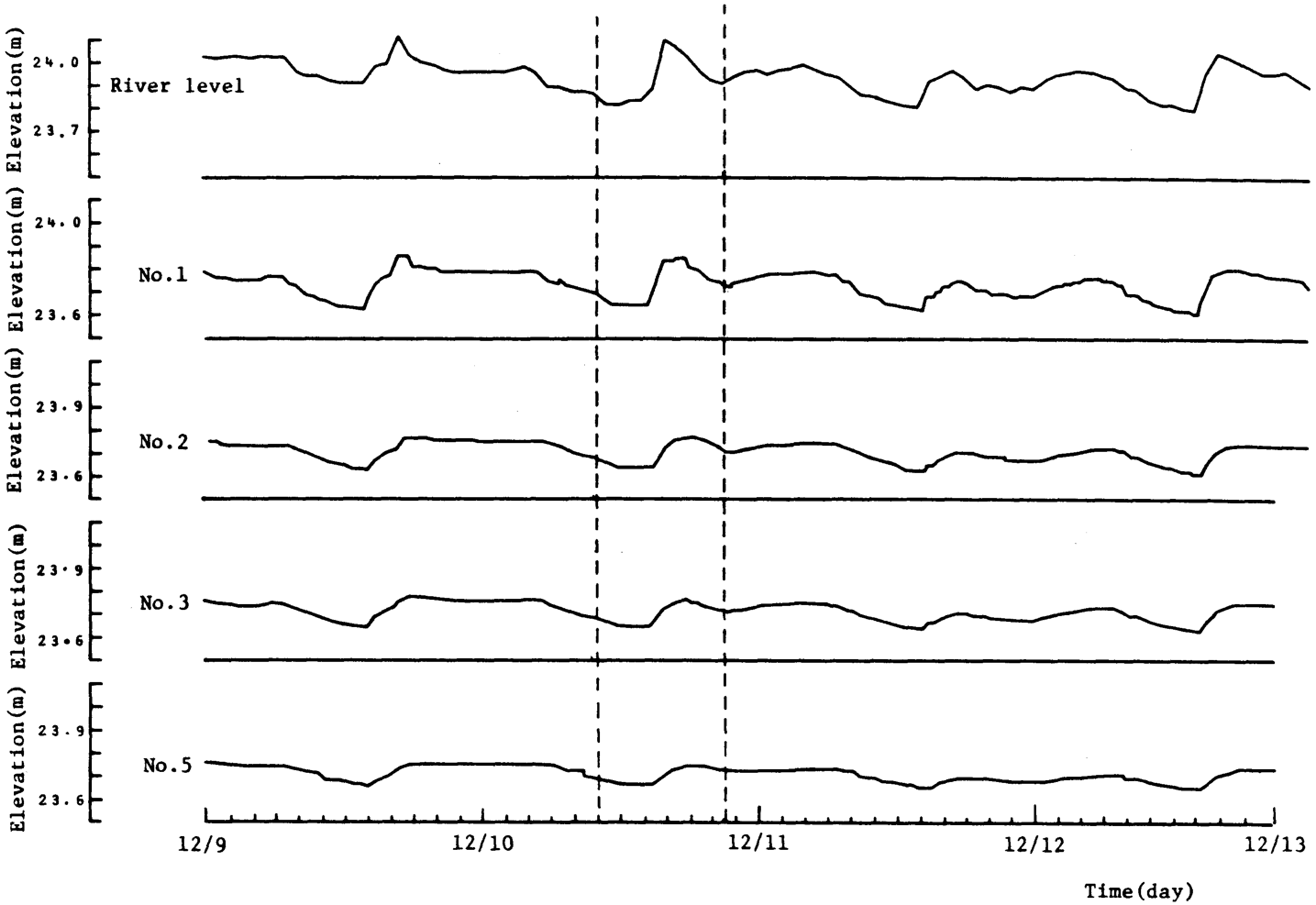

Fig.7.7 Observation results of water level of river and water table for each observation well with time

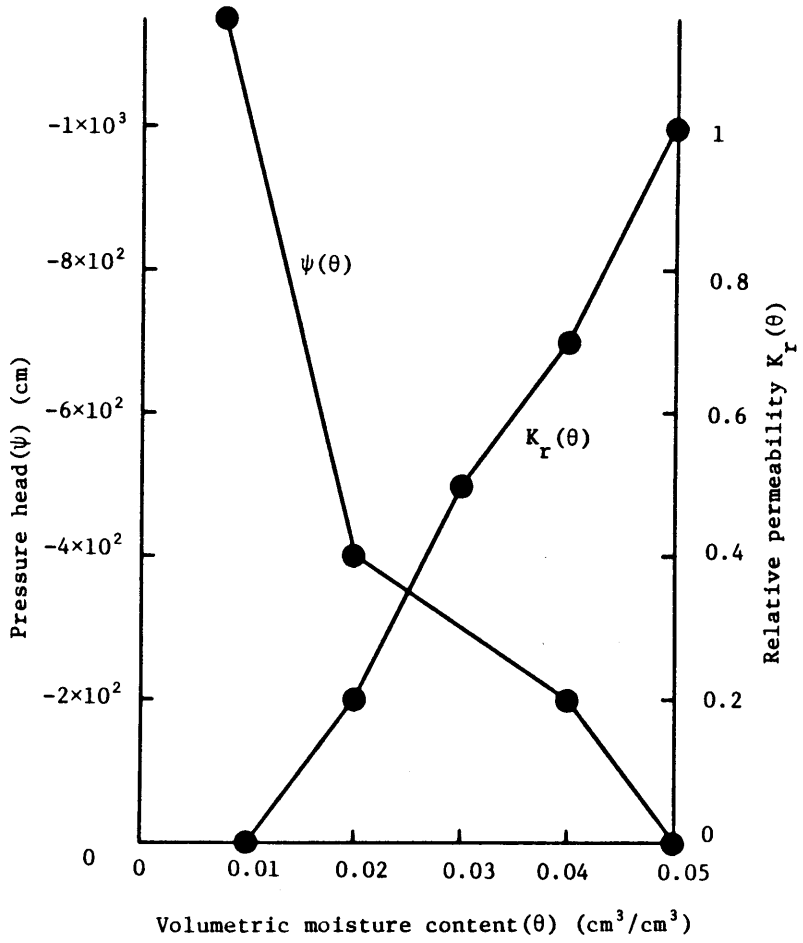

Fig.7.8 Unsaturated property of soil

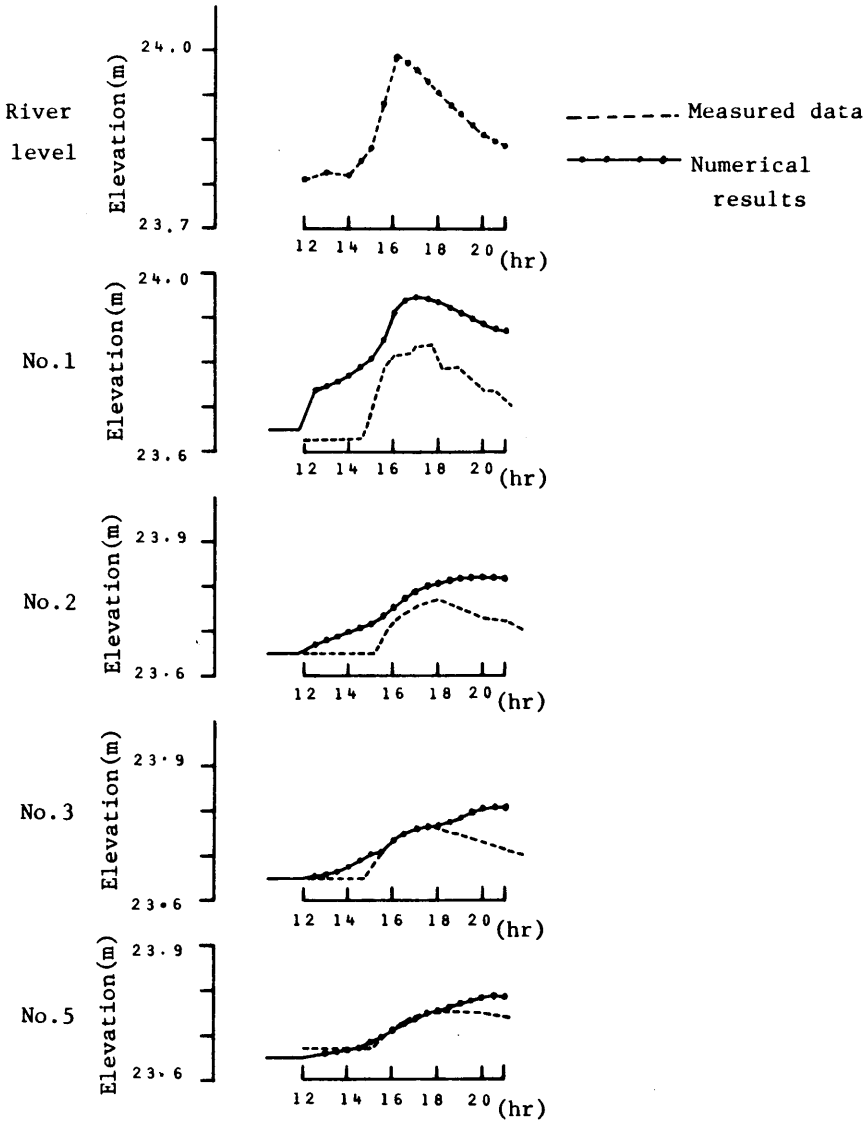

Fig.7.9 Comparison of measured and computed water table

were used to compare with the calculated curves. Fig.7.7 shows the observation results of water level charges of river and water table changes for each observation well with time for the period from December 9 to December 13, 1977. In Fig.7.7 the change of the river level in a day might be due to the variation of flood from the dam for water power plant.

The hydraulic property of unsaturated flow domain which was determined with trial and error method by the numerical approach is shown in Fig.7.8 and Fig.7.9 compares the computes water table variation with the measured data for each observation well. A period, 12 O,clock to 21 O,clock on December 10, was selected as the comparison period. In computation the river level change during this period was used as boundary condition at the river. There is a reasonably good agreement between the computed and the measured data during the first 6 hours. During the last 3 hours the agreement is somewhat less satisfactory. Here the measured data are lower than those indicated by the computed results. At least past of this discrepancy may be due to the adoption of a single soil moisture retention curve and a single hydraulic conductivity curve for the entire soil profile and the effect of hysteresis. This general agreement is certainly good enough to simulate the river level raises suddenly to the flood water level and water begins to flow through the embankment by using the relationships as shown in Fig.7.8.

7.3.4 Simulation of earth embankment subject to sudden raise in a river level

As simulated, the following four cases were calculated with the saturated-unsaturated finite element analysis. The solution advances in time by means of a fully implicit finite difference scheme, Hysteresis was not taken into account.

Case 1. At time t equal to zero the water level of the river is suddenly

raised to the height of 29.630m from the bottom of flow domain as shown in Fig.7.6. This value of the river level is adopted the highest value of the flood it occurred in July 1972 as shown in Fig.7.10.

Case 2. The river level is 29.067m from the bottom of flow domain (Simulation of September 1976 flood).

Case 3. Simulation of the flow through the embankment when the river level reaches the higt water level of 33.451 m.

Case 4. To evaluate the efficiency of bank protection the hydraulic conductivity of this protection is choosen $K=1.0\times10^{-6}$cm/sec. The river level is in H.W.L.

In Figs.7.11 through 7.14, a series of numerical solutions for unsteady state seepage are presented for various river water levels, accounting the effect of bank protection. It is worth noting in the simulation of 1972 flood that after three hours, seepage face appears at the toe of embankment. This result well agrees with the information received. In the simulation of 1976 flood level seepage face also appears after about 4 hours. These simulation can be considered the most dangerous situations for the practical flow problems. The comparison of Fig.7.13 and Fig.7.14 is the most interesting result of the numerical analysis. Due to the effect of bank protection the water table profile in Fig.7.14 is extremely different from that in Fig.7.13. The computed results is shown for the water flow out of the embankment (Fig.7.15). It is evident with comparing case 4 and case 3 that if bank protection is worked out as a countermeasure for leak prevention outflow rate from seepage face is reduced to about one-third of that of case 3, and the time lag of seepage face appearing is three times longer than that in the case without bank protection.

To summarize the results of this section, it would appear that this finite element analysis can be adapted to solve complicated practical problems involving soil stratification and variations in soil hydraulic conductivity and this

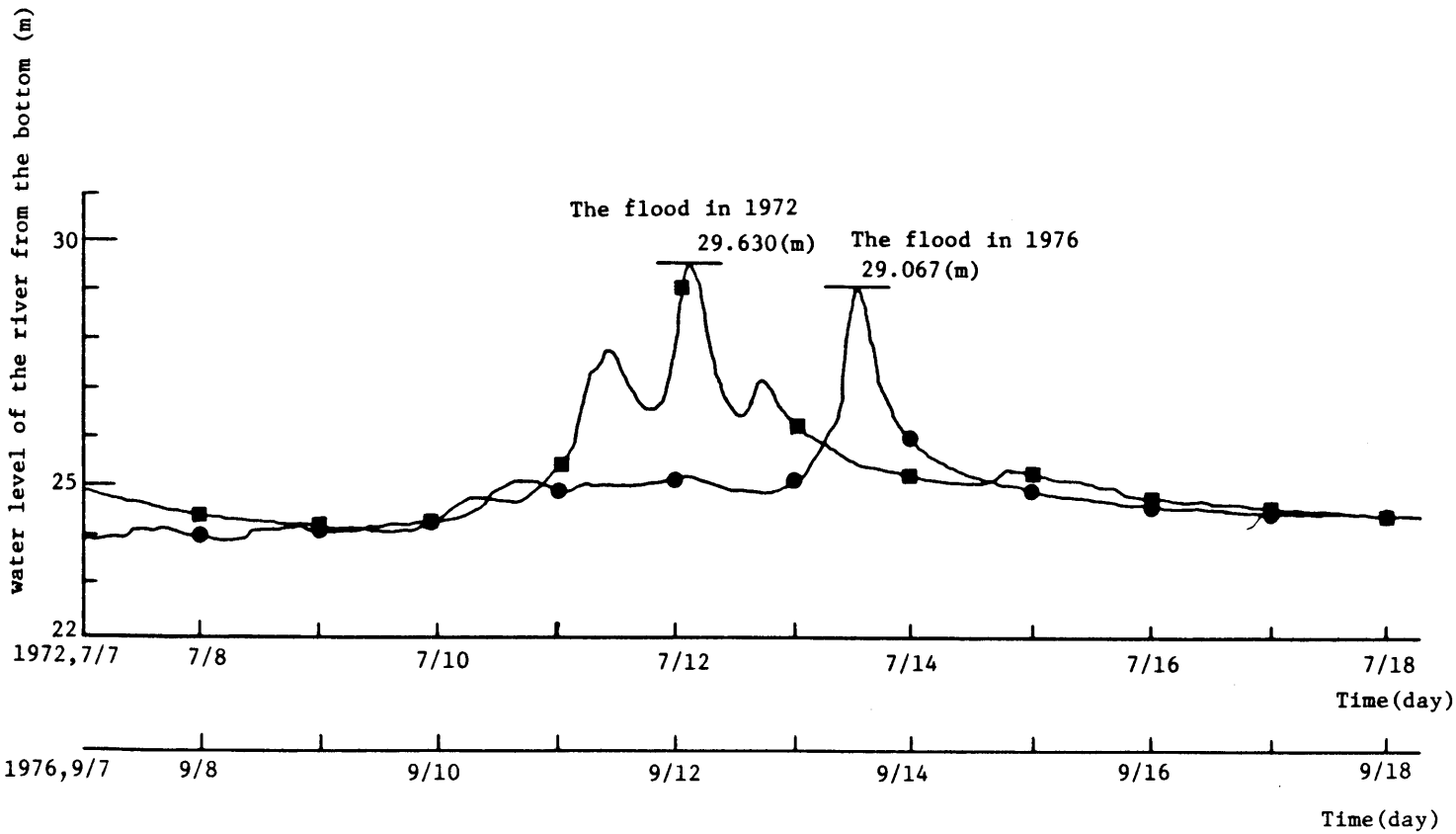

Fig.7.10 The change of the river level during the flood in July 1972 and September 1976.

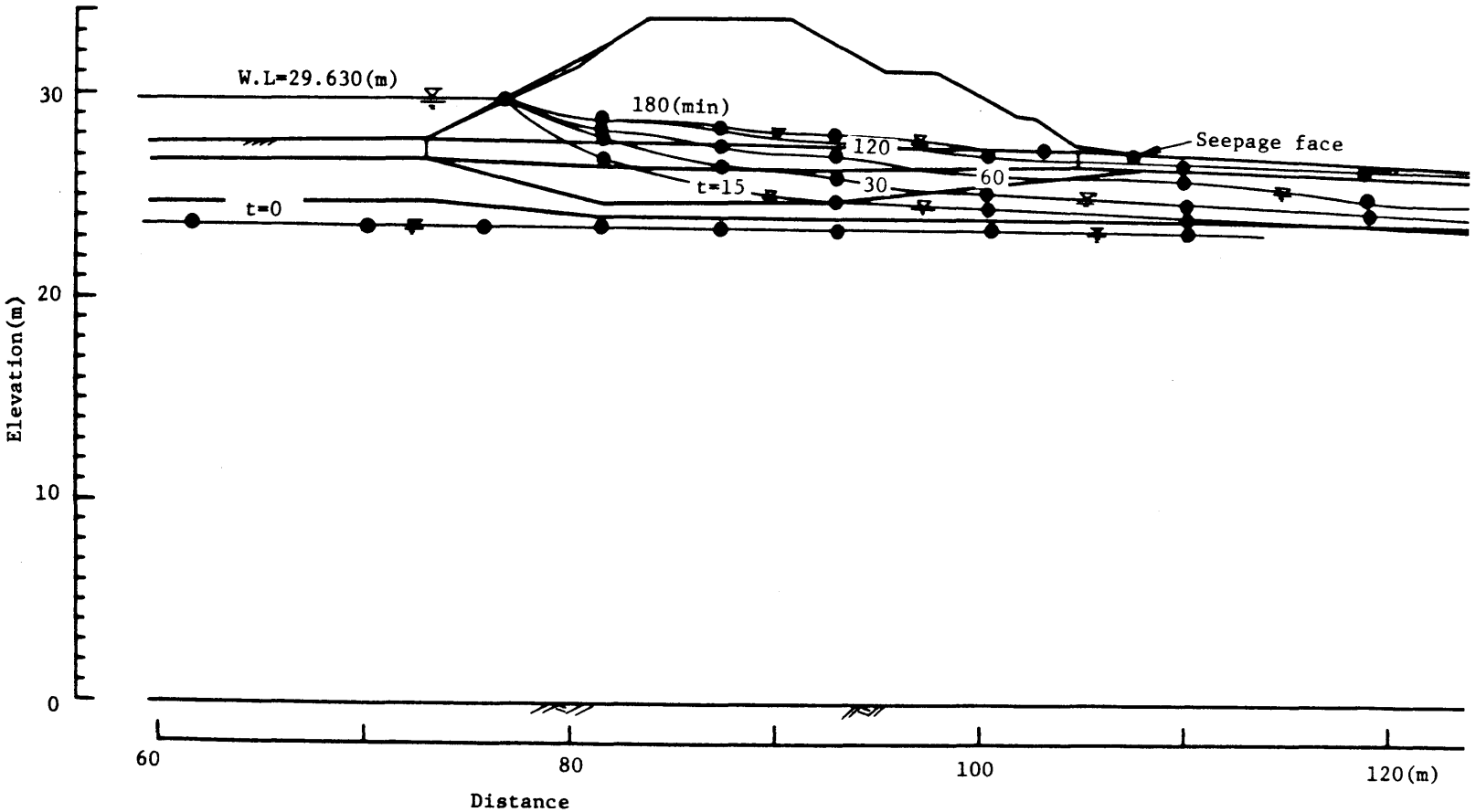

Fig.7.11 The numerical results of flow problem at the July 1972 flood level water

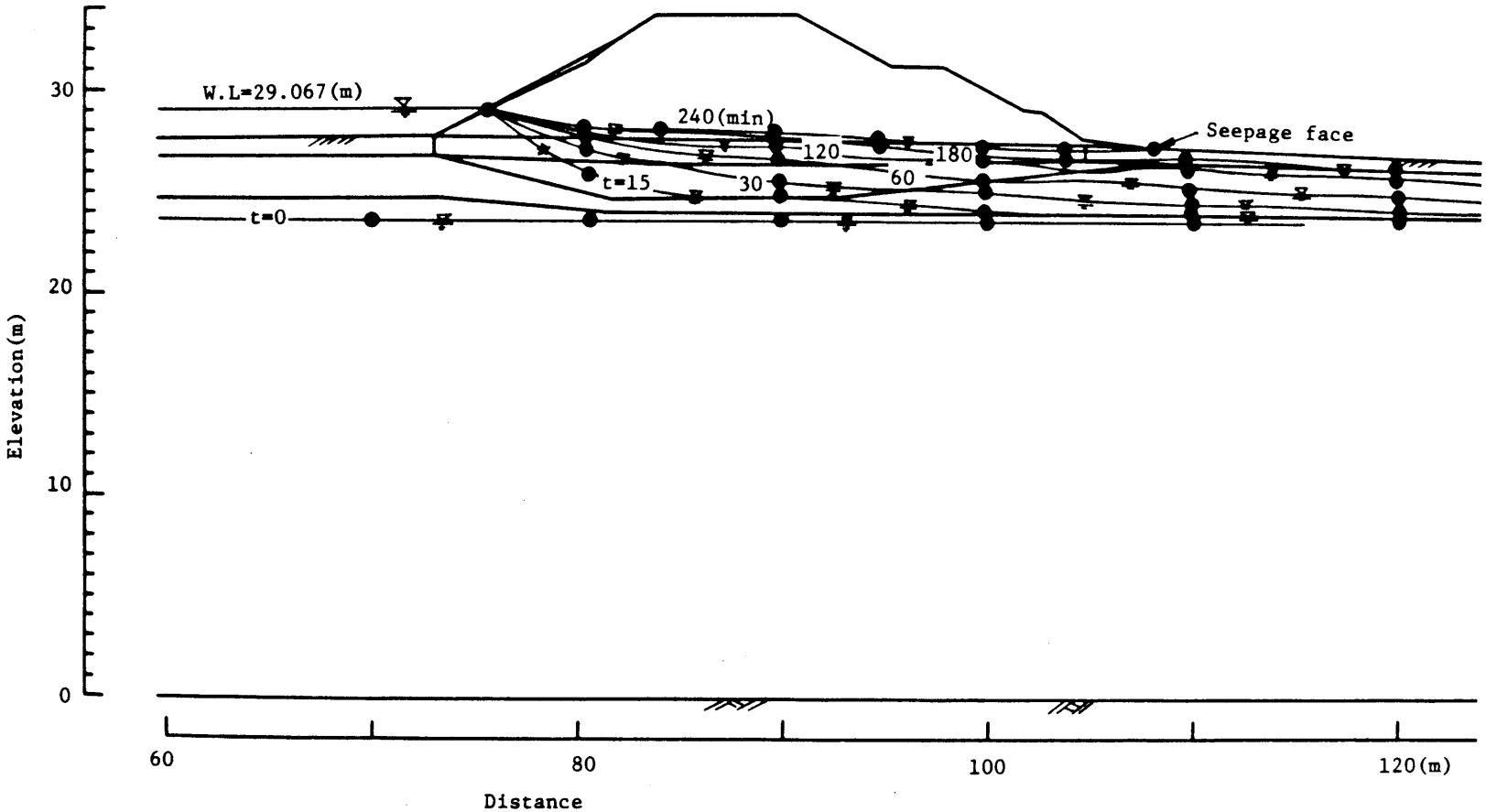

Fig.7.12 The numerical results of flow problem at the September 1976 flood water level

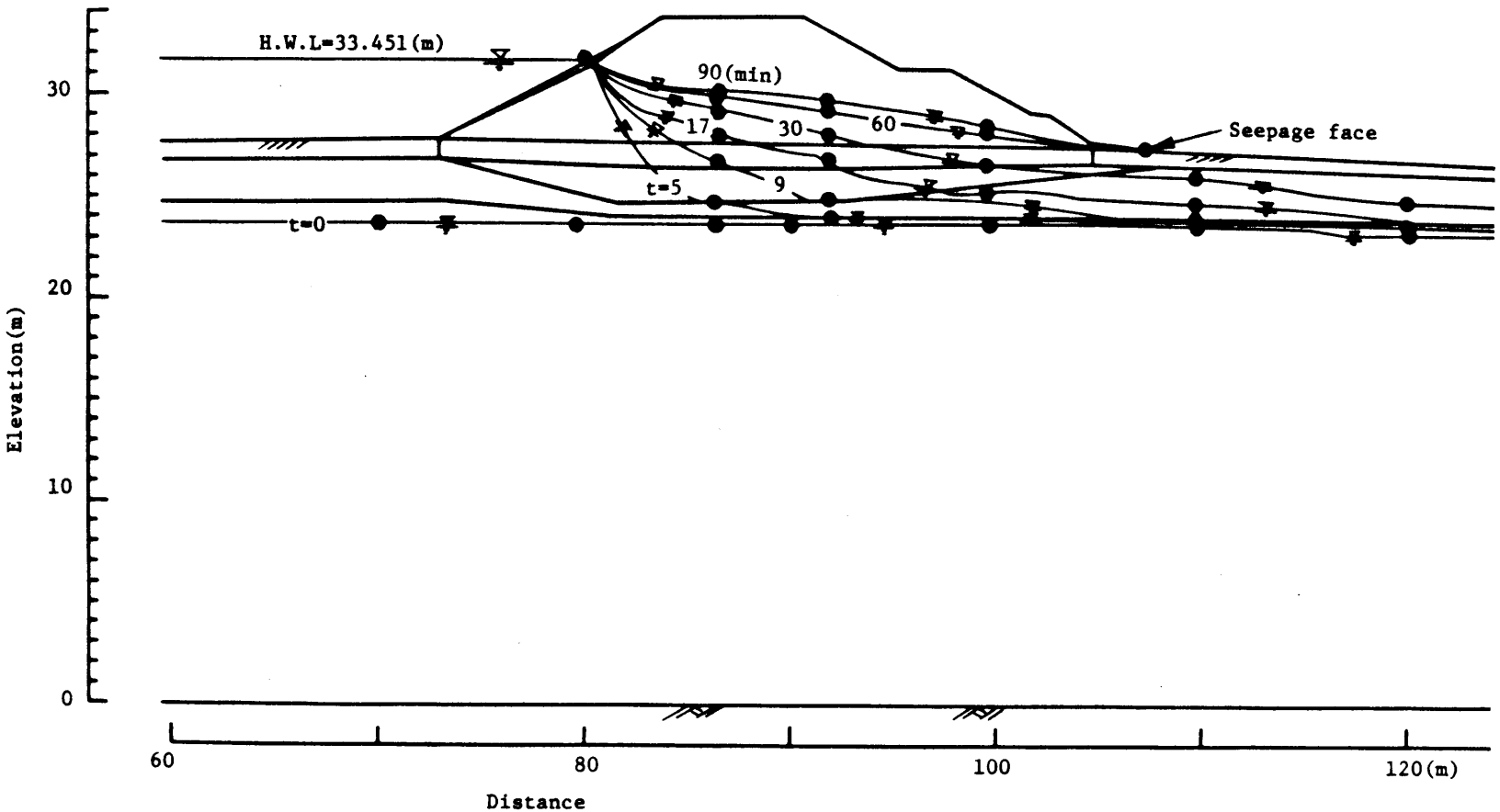

Fig.7.13 The numerical results of flow problem at H.W.L.

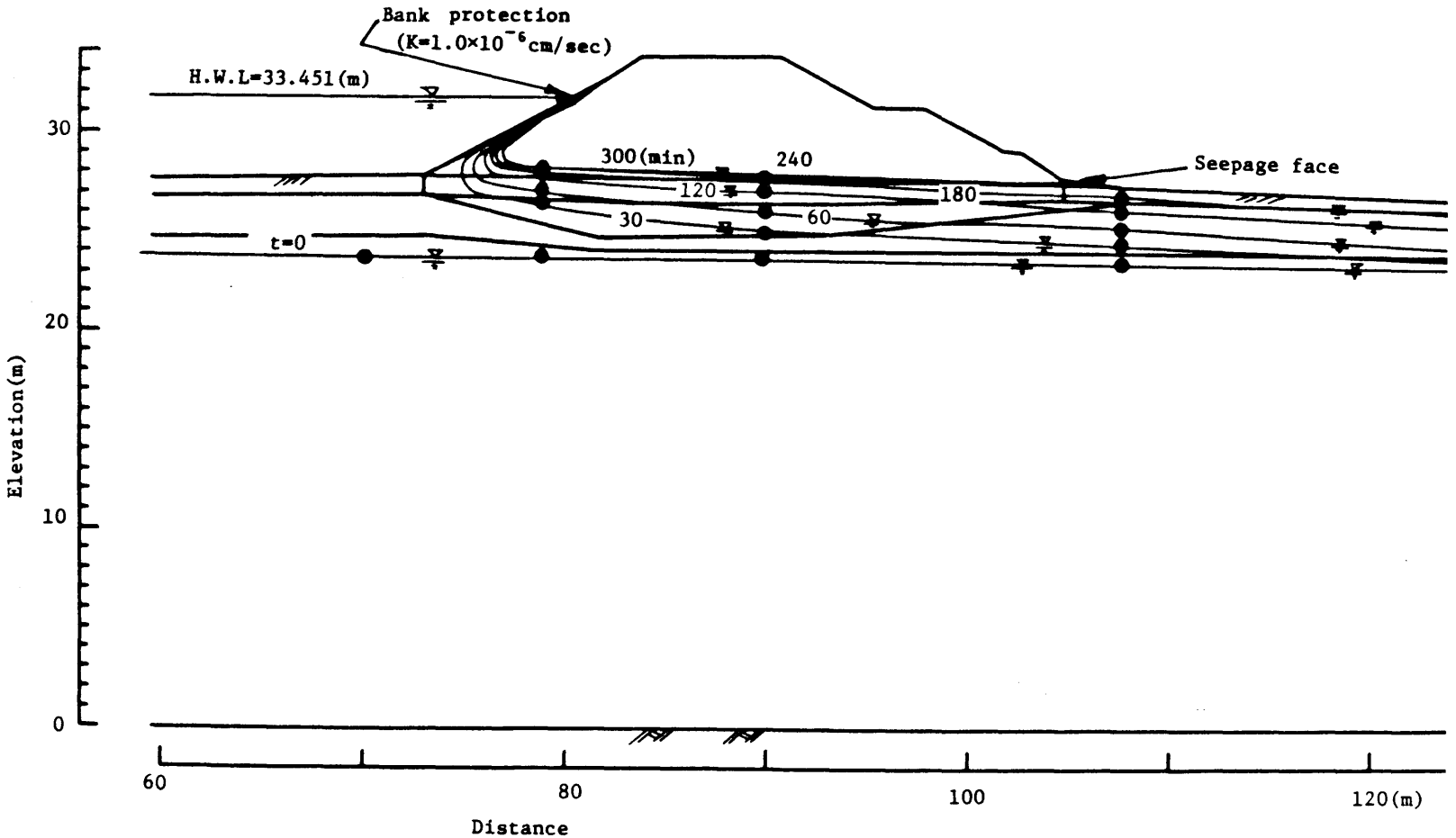

Fig.7.14 The numerical results of flow problem at H.W.L. taking account of the effect of bank protection.

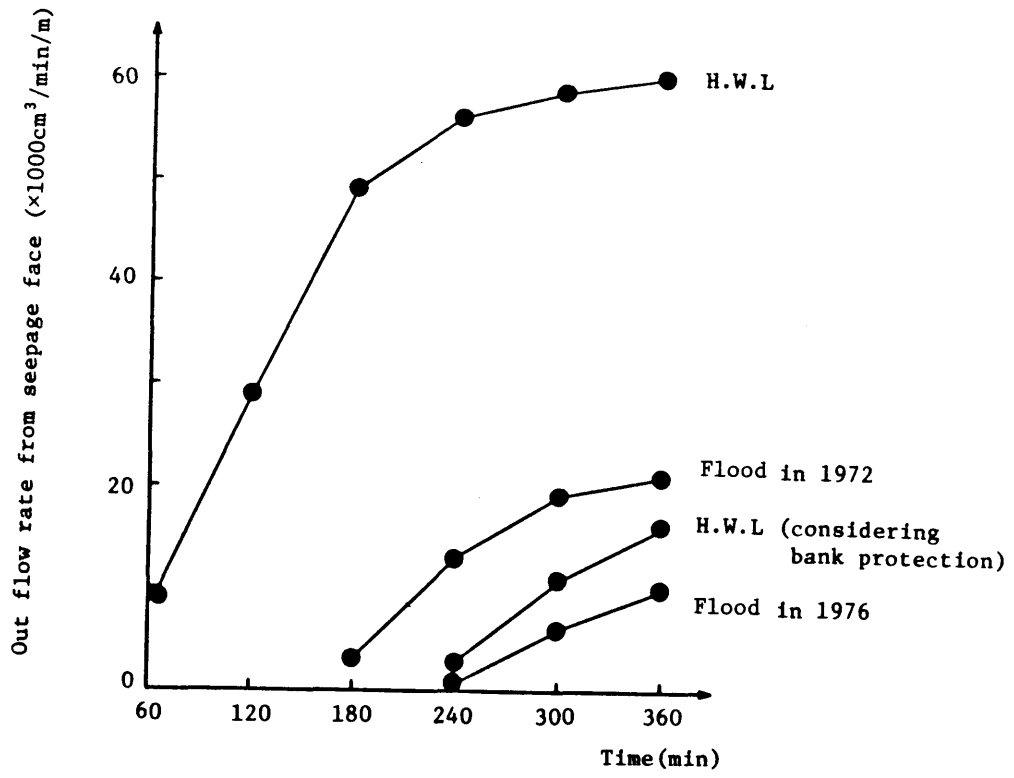

Fig.7.15 Out flow rate from seepage face with time

method is very effective to detect the realistic change of the flow pattern.

7.4 Open Cut Excavation Model

7.4.1 Introduction

In section 5.4.2 the comparisons between the three-dimensional numerical analysis and laboratory experimental results have been shown on the problem of flow through three-dimensional sand model. In this section the problem of groundwater controlling for foundation excavations will be considered as more practical problem which is some interest to the foundation engineer. Many types of engineering construction require the excavation of soil and rock below the natural groundwater table. If the formations are well cemented, water control

may be simply a matter of allowing the water to seep down the excavation slopes into shallow ditches or sumps from which it is removed by pumping. On the other hand, if the water bearing materials have low strengths, extensive dewatering systems may be required.

Either of the two fundamental methods of controlling seepage can be used for the control of groundwater during construction: (1) Those that keep the water out or (2) those that depend on its control by drainage processes. Chemical grout, cement grout, sheet pile walls, and caissons are means that serve to keep out most of the water. Usually when these methods are used, pumps are required to maintain dry conditions in excavations. Most excavations in water bearing formations such as gravels, sands, silts, and stratified clays are stabilized by wellpoints, deep pumped wells, or other groundwater control systems.

Groundwater control for fundation excavations may be accomplished in a number of differnt ways. The most appropriate method for a given job should be determined by adequate soil surveys and test borings to delineate important soil strata and locate sources of water. On important projects the permeability of the formations should be determined by field drawdown tests or other adequate methods. For any dewatering project in which failures could lead to extensive structural damage or serious flooding the design and installation of water-control systems should be carried out with deep considerations.

Most dewatering systems are flexible with respect to discharge capacity and can be enlarged in capacity to take care of unexpectedly large rates of flow. Nevertheless, the approximate rate of discharge shoud be known in advance so that approximate power requirements will be known. The design of dewatering systems involves two important steps

1. Evaluation of the magnitude of the dewatering project, including an estimate of the probable rate of inflow and power consumption.

2. Design of a system capable of providing the required ground water lowering for the length of time needed for the construction that is to be carried out below the natural groundwater level.

To estimate the probable inflow rates to dewatered excavations and to provide the ground water lowering seepage systems must be analyzed. All fluid systems must necessarily extend in three dimensions, but in former methods seepage systems analyzed are predominately two-dimensional flow with assumption of the infinite lenghth of excavation as shown in Fig.7.16.

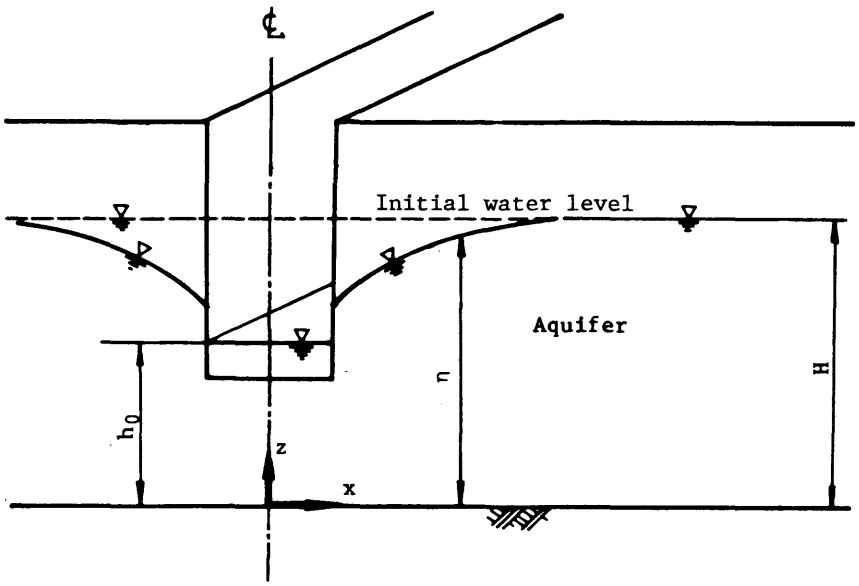

Fig.7.16 Two-dimensional ditch drainage

In practical excavations the length of excavation is finite as shown in Fig. 7.17. This system has the effect of sheet pile walls so that there is no known nonsteady analytical solution. In this section the nonsteady state flow analysis will be performed in this hypothetical case of an open cut excavation.

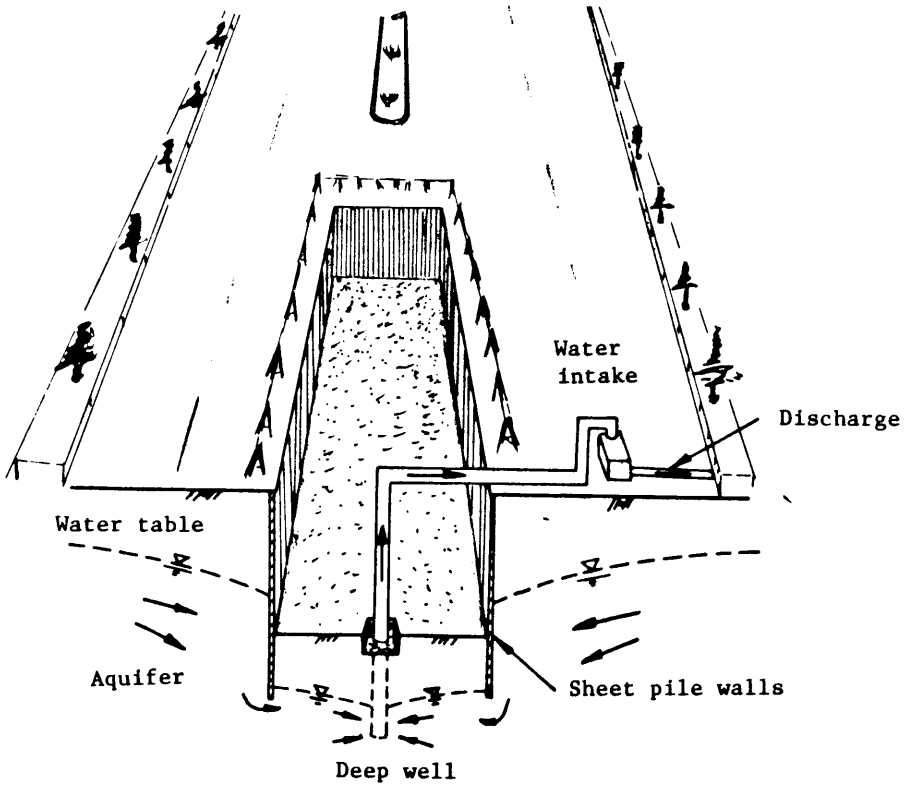

Fig.7.17 Excavation stabilized with deep well system (Artist's view of a deep well system including cutaway sketch of an deep well.)

7.4.2 Simulation of seepage through three-dimensional aquifer

The problem is as follows: A 20 m sandy aquifer is under hydrostatic equilibrium with fluid potential h everywhere equal to 15 m. In this aquifer an excavation (10 m wide, 10 m deep and 60 m long) is made. The problem is to study the drainage pattern imposed within the sandy aquifer due to the excavation, that is, due to a rapid 5 m drawdown of groundwater table in the excavation. A quarter of the flow domain was indentified by a system of finite elements as shown in Fig.7.18. The model is composed of 288 nodal points, and 168 eight node elements.

The boundary conditions are illustrated in Fig.7.19. The floor of the excavation is assumed to be constantly covered with a thin film of water so as

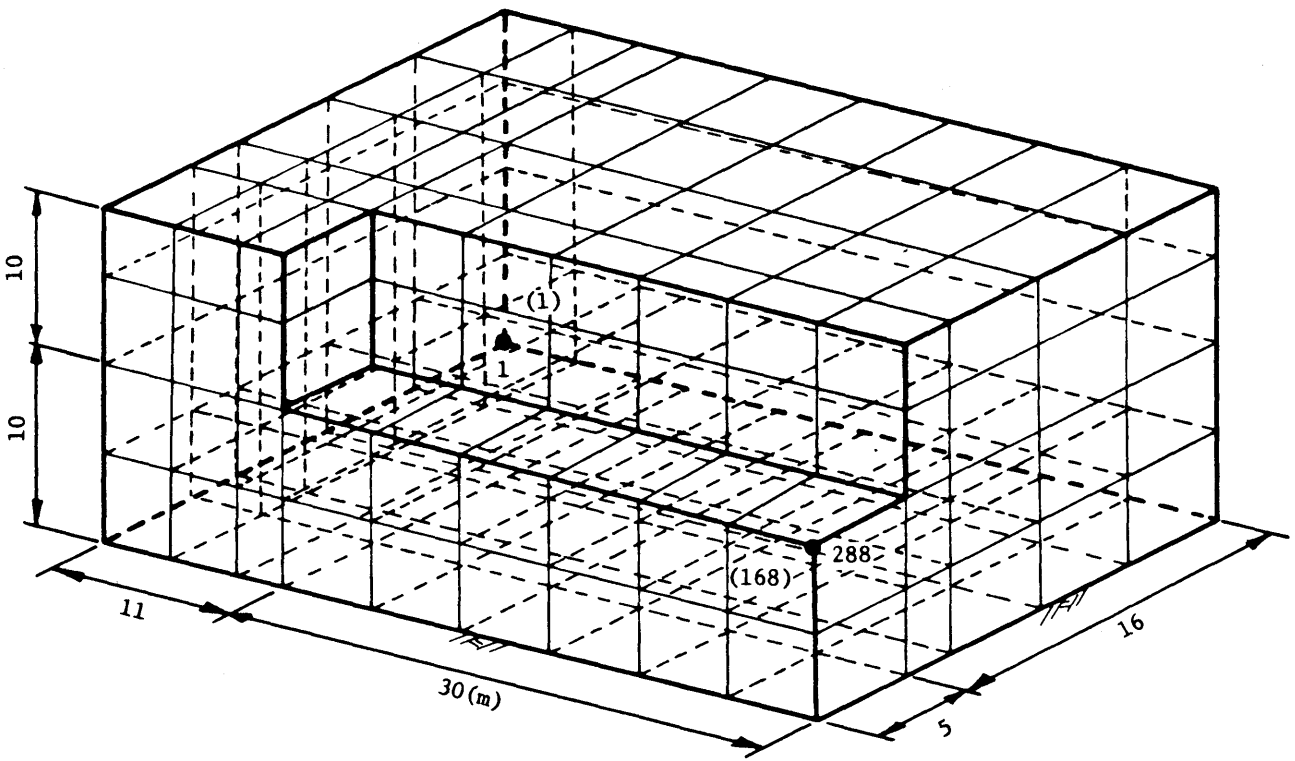

Fig.7.18 Three-dimensional finite element grid for the sandy aquifer

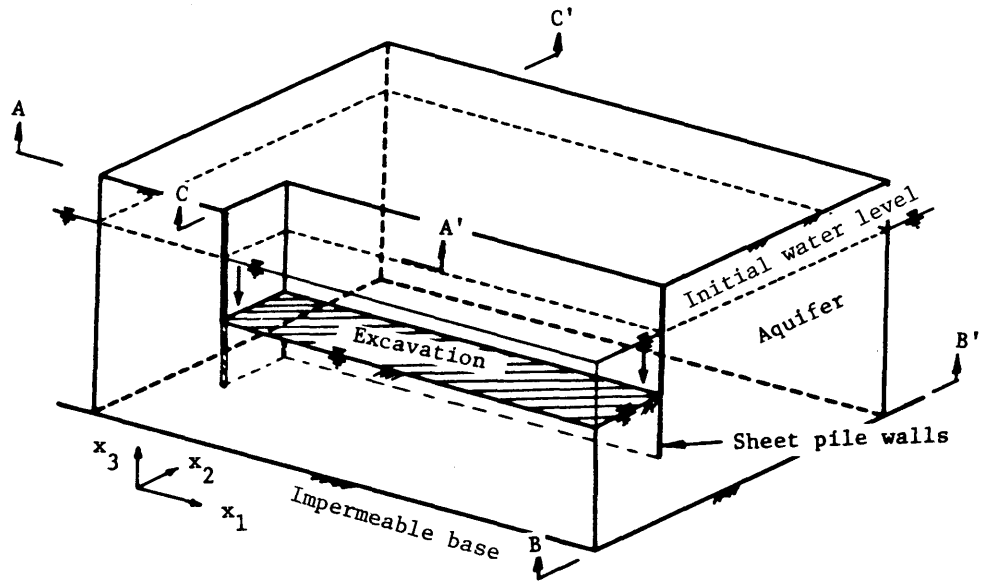

Fig.7.19 Transient flow toward an excavation face following rapid drawdown

to form a fixed potential boundary, while the wall of the excavation is an impermeable boundary (due to sheet pile walls). The bed rock is also an impermeable boundary. All the other boundaries of the flow region are assumed constant head.

For this hypothetical problem Fig.7.20 was used as a set of curves for unsaturated properties of the soil in the sandy aquifer. When ψ is equal to zero, $K_s=1.0\times10^{-2}$cm/sec and $\theta_o=0.46$. The solution advances in time by means of a fully implicit finite difference scheme. Hysteresis was not taken into account.

The drainage computations were carried out for a period of 4 days from the start of the drainage process and the results of the computations are summarized in Figs.7.21 through 7.24. The time-dependent changes in the evolution

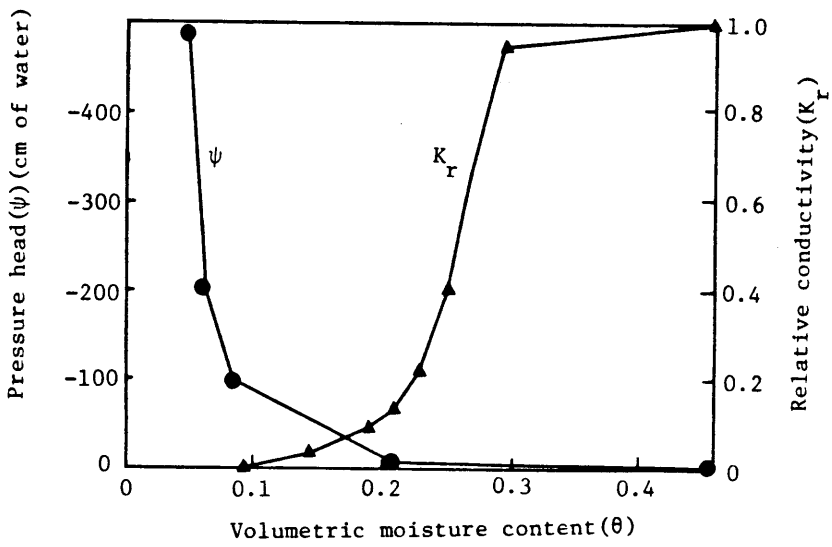

Fig.7.20 Unsaturated property of soil

of the surface ψ=0 (water table) are presented in Figs.7.21, 7.22 and 7.23 along three cross sections, A-A', B-B' and C-C'. The topographic contours for approximately steady state (after 4 days) are also shown in Fig.7.24. The comparisons of three dimensional and two dimensional analytical results are shown for steady state water table in Figs.7.25 a. through 7.25 c.. Along sections A-A' and B-B' there are good agreements with two-dimensional results. Along section C-C', however, three-dimensinal result differs significantly from the two-dimensional result. This discrepancy may be due to the effect of the three-dimensional flow.

The rates of seepage into dewatered excavations was Q_{3-D}=1.72m^3/min by using three-dimensional analysis, while the rates of seepage was Q_{2-D}=1.56m^3/min which was estimated by using the two-dimensional analysis and the next equation.

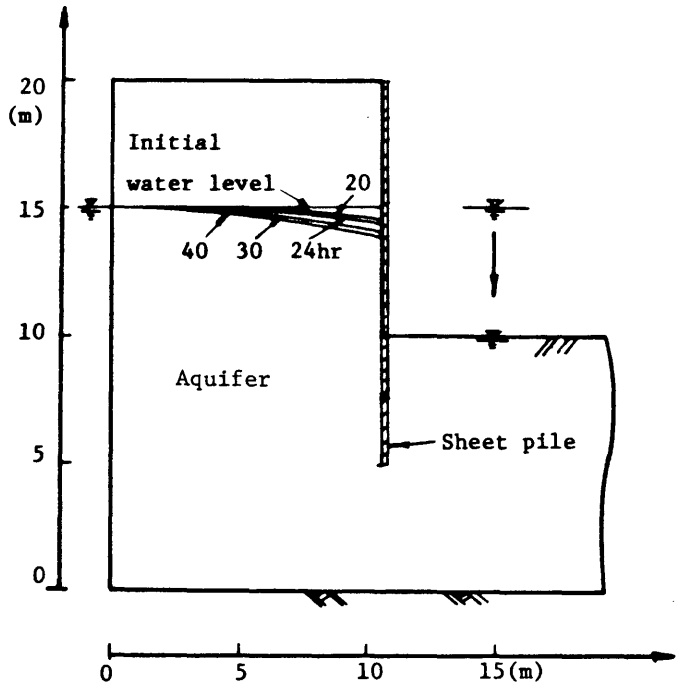

Fig.7.21 Numerical results (cross section A-A')

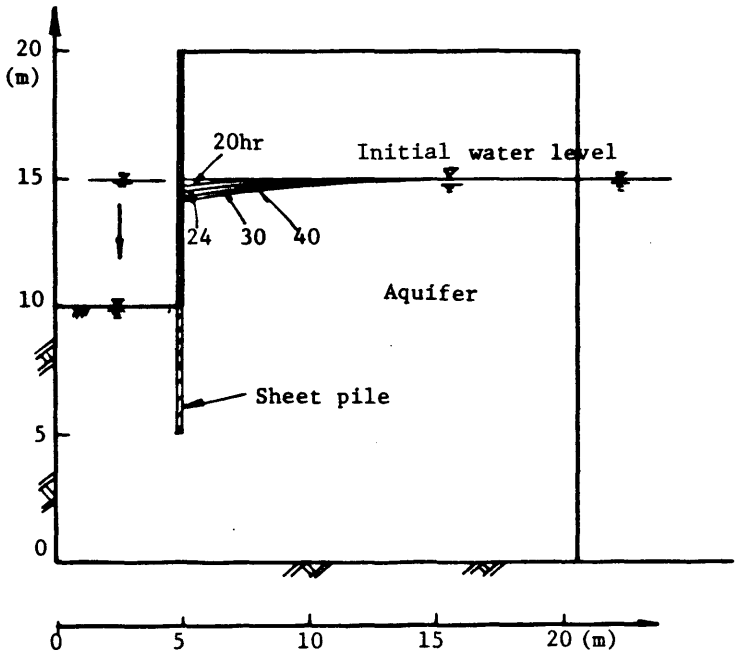

Fig.7.22 Numerical results (cross section B-B')

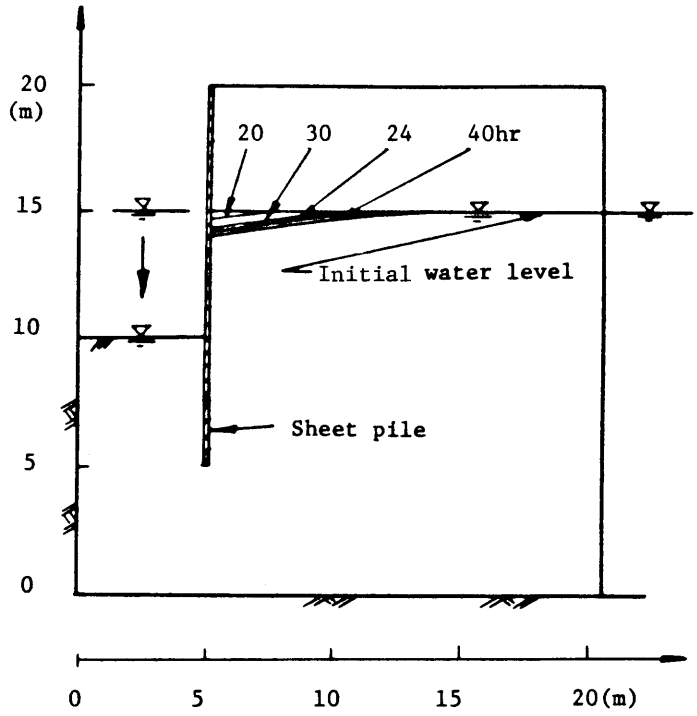

Fig.7.23 Numerical results (cross section C-C')

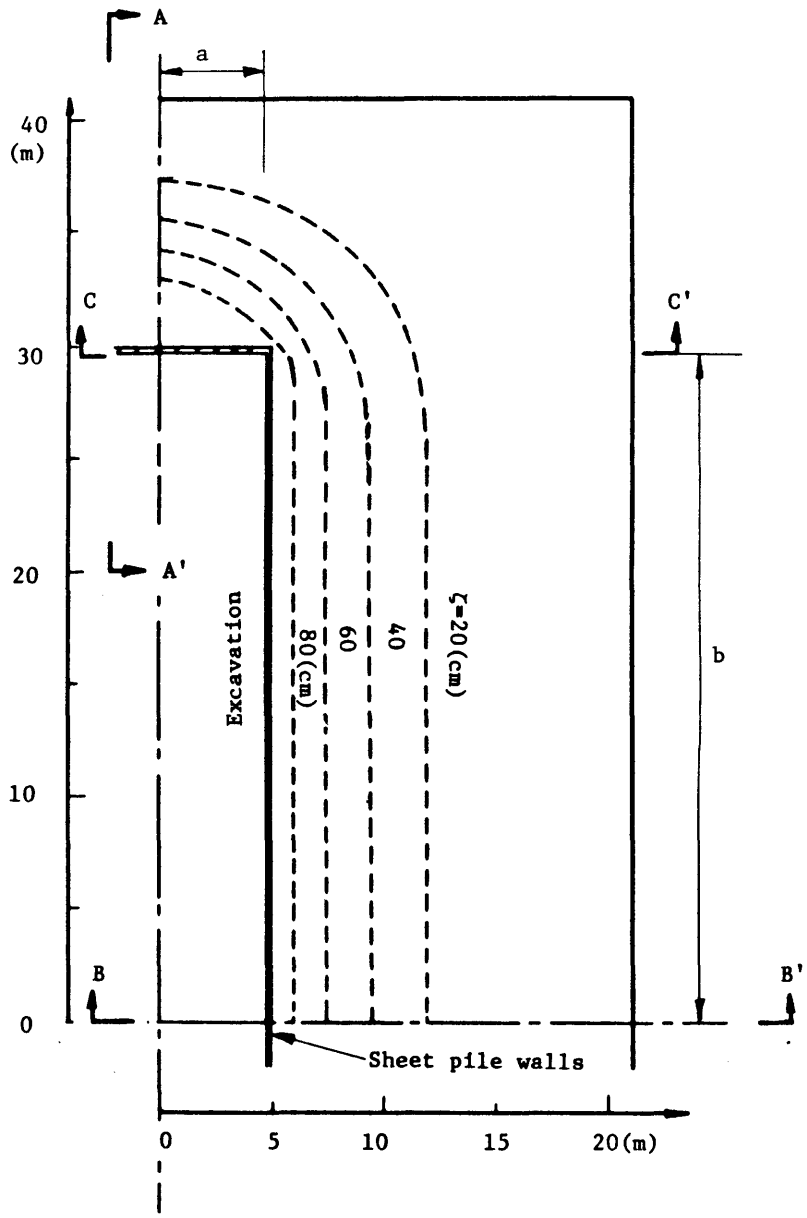

Fig.7.24 Topographic contours(in cm below original water level(ζ))
(afer 4 days)

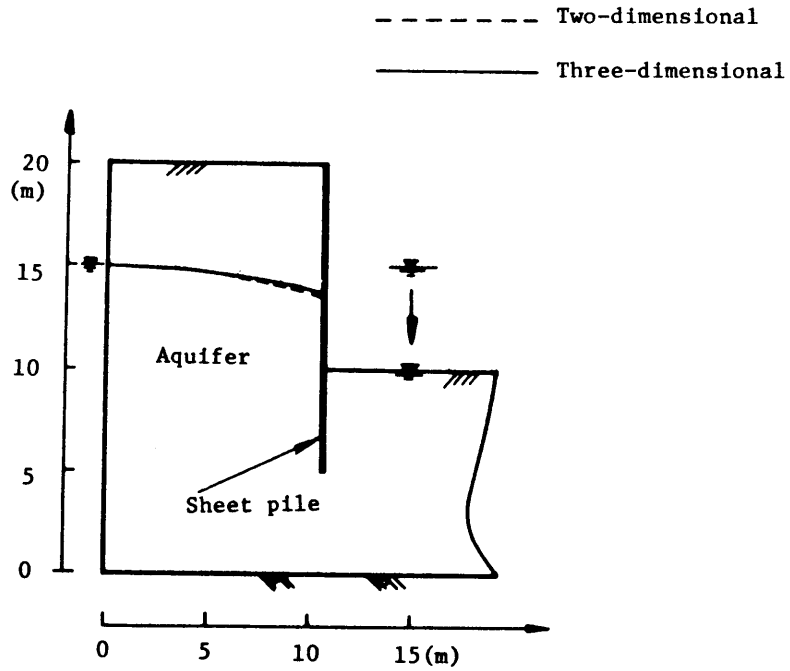

Fig.7.25a(cross section A-A')

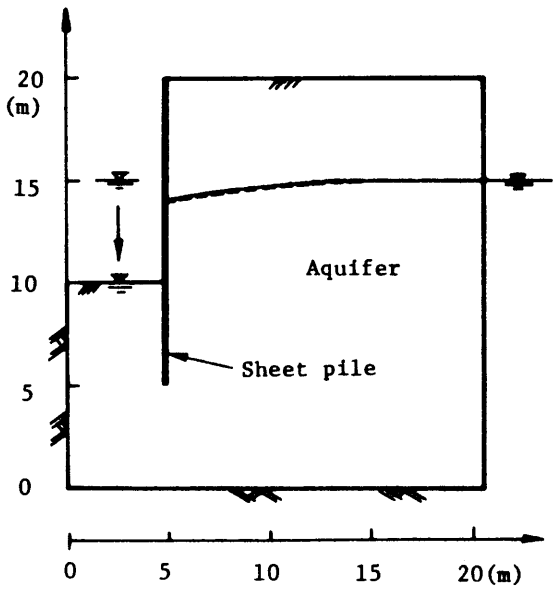

Fig.7.25b(cross section B-B')

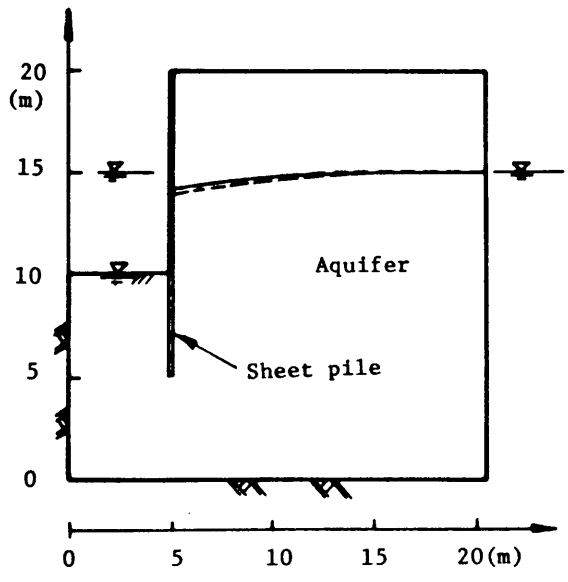

Fig.7.25c(cross section C-C')

Fig.7.25 Comparisons of three-dimensional and two-dimensional numerical analysis results

$$Q_{2-D} = 4 \times (a \cdot q_{A-A'} + b \cdot q_{B-B'}) \qquad (7.1)$$

where a and b are the length shown in Fig.7.24,and $q_{A-A'}$ and $q_{B-B'}$ are the rate of inflow along cross section A-A' and B-B', respectively. From this result the estimated value of Q_{2-D} is smaller than that of Q_{3-D}. This discrepancy may be due to the difference in the profile of water table along cross section C-C'.

As it was said earlier, three-dimensinal analyses are used only in those cases for which two-dimensional models are grossly inappropriate. It is therefore of interest to know the corresponding additional cost. The two-dimensional equivalent of this model along cross section A-A' has 28 nodes. The simulation in 34 time steps of 4 days of drainage required 10.2 sec of computer time on the ACOS-700 and 10K of core storage. As a comparison, the similar three-dimensional analyses performed with this model required 60.5min of computer time and 45K of core storage. To summarize the results of this section, it would appear that the use of three-dimensional finite element analysis is a step forward from the two-dimensional analysis used so frequently for analyzing excavation seepage problem because it allows the variation of flow in the third dimension. It is evident that the three-dimensional analysis is accurate enough to evaluate the behavior of the groundwater in the complex soil media qualitatively and quantitatively. However, the computer program, limited to the core storage of the available computer facility, is intended only to solve the simple illustrative problems. With increased capacity, it would be possible to handle problems of complex geometry and arbitrary boundary conditions. It is concluded that three-dimensional analysis is an expensive but valid alternative.

7.5 Conclusions

In this chapter some attempts have been made to apply the two-and three-dimensional finite element analysis of seepage to the field problem. These examples clearly demonstrate the flexiblility of this finite element approach and its capability in treating complex situations which are often encountered in the field. Consideration of anisotropy is clearly warranted in seepage analysis. Since the effects of saturated anisotropy have been widely studied in the seepage field[21], any anisotropic examples have not been included in this chapter. Throughout of this chapter, the following conclusiona are obtained.

(1) The results of simulating the flow pattern in an inhomogeneous embankment when a river water level is raised to the flood heights and high water level have been shown.

(2) There are good qualitative agreements between the numerical results and the informations received.

(3) For three-dimensional flow example model, the seepage into dewatered excavations has been shown.

(4) The three-dimensional analysis is accurate enough to evaluate the behavior of groundwater and it is a step forward from the two-dimensional analysis. However, by using the three-dimensional analysis it accentuates computer limitations by reducing the maximum size of problem that can be simulated on any given computer installation and increasing the computer time required to solve it.

(5) The two-and three-dimensional saturated-unsaturated finite element method was found to be very effective to detect the realistic change of the flow pattern.

(6) Finally main problems to use the saturated-unsaturated finite element procedure are to obtain the material properties of soils, especially the water retention curve in the unsaturated zone. And so there is a need to determine on a systematic basis the spectrum of problems for which consideration of the unsaturated flow domain retains engineering importance.

References

1) Mitchell,J.K., D.R.Hooper and R.G.Campanella: Permeability of compacted clays, ASCE, 91(SM4), 1965, pp.41-66.

2) Klute,A.: The determination of the hydraulic conductivity and diffusivity of unsaturated soils, Soil Sce. Vol.113(4), 1972, pp.264-276.

3) Youngs,E.G.: An infiltration method of measuring the hydraulic conductivity of unsaturated porous materials, Soil Sci. 107, 1964, pp.307-311.

4) Hillel,D. and W.R.Gardner: Measurement of unsaturated conductivity and diffusivity by infiltration through an impeding layer, Soil. Sce. 109, 1970, pp.149-153.

5) Bouma,J., D.I.Hillel, F.D.Hole. and C.R.Amerman: Field measurement of unsaturated hydraulic conductivity by infiltration through artificial crusts, Soil Sci. Soc. Amer. Proc., 32, 1971, pp.362-364.

6) van Bavel, C.H.M., Stirk, G.B., and Brust,K.J.: Hydraulic properties of a clay loam soil and the field measurement of water uptaken by roots. I. Interpretation of water content and pressure profiles. Soil Sci. Soc. Amer. Proc. 32, 1968, pp.310-317.

7) Davidson,J.M., L.R.Stone, D.R.Nielsen and M.E.LaRue: Field measurement and use of soil-water properties, Water Res. Res. 5, 1969, pp.1312-1321.

8) Hillel,D.,V.D.Krentons and Y.Stylianou: Procedure and test of an internal drainage method for measuring soil hydraulic characteristics in situ. Soil Sci. vol.114, No.5, 1972, pp.395-400.

9) Robins,J.S., L.L.Kelly, and W.R.Hamon, Reynolds Creek in south west Idaho: An outdoor hydrologic laboratory, Water Res. Res. 1(3), 1965, pp.407-413.

10) Jeppson,R.W., W.J.Rawls, W.R.Hamon and D.L.Schreider: Use of axisymmetric infiltration model and field data to determine hydraulic properties of soils. Water Res. Res. 11(1), 1975, pp.127-138.

11) Richards,L.A., Gardner,W.R., and Ogata,G.: Physical processes determining water loss from soil, Soil Sci.Soc. Amer. Proc. 20, 1956, pp.310-314.

12) Ogata,G.and Richards,L.A.: Water content changes following irrigation of bare field soil that is protected from evaporation, Soil Sci. Soc. Amer. Proc. 21, 1956, pp.355-356.

13) Gardner,W.R.: Field measurement of soil water diffusivity. Soil Sci. Soc. Amer. Proc. 34, 1970, pp.832-833.

14) Jackson,R.D.: On the calculation of hydraulic conductivity, Soil Sci. Soc. Amer. Proc. 36, 1972, pp.380-382.

15) Gardner,W.R.: The permeability problem, Soil Sci. 117, 1974, pp.243-249.

16) Cassel,D.K. and A.Baver: Spatial variability in soils below depth of tillage: Bulk density and fifteen atmosphere percentage, Soil Sci. Soc. Amer. Proc. 39, 1975, pp.247-250.

17) Carvallo,H.O., D.K.Cassel, J.Hammon, and A.Baver: Spatial variability of in situ unsaturated hydraulic conductivity of Maddock sandy loam, Soil Sci., 121, 1976, pp.1-8.

18) Desai,C.S.: Seepage analysis of earth banks under drawdown, ASCE, Vol.98, (SM11), 1972, pp.1143-1162.

19) Whisler,F.C. and K.K.Watson: One-dimensional gravity drainage of uniform columns of porous materials, J. Hydrology, 6, 1968,pp.277-296.

20) Cedergen,H.R.: Seepage, Drainage and Flow Nets, John Wiley, New York, 1967, pp.74-78.

21) Selim,H.M.: Water flow through a multilayer stratified hill side, Water Res. Res. 11(6), 1975, pp.949-957.

CHAPTER 8

CONCLUSIONS

The purposes of this thesis were primarily to research on behavior of groundwater flow in the saturated-unsaturated zone, to present the fundamentals of the theory of groundwater flow, and to develop the most effective methods for solving groundwater flow problems occuring in civil engineering practice. Namely, the main objectives of this thesis were as follows.

(1) To evaluate and discuss the governing equation of flow in the saturated-unsaturated porous media.

(2) To develop the mathematical model which provides a finite element solution to two- or three-dimensional problems involving transient flow in the saturated and unsaturated domains of nonhomogeneous, anisotropic porous media.

(3) To propose better methods for determining or estimating hydraulic properties of porous media in the laboratory and in the field.

(4) To show the applications of the developed model and methods to practical groundwater flow problems.

In this chapter, the main conclusions which are based on the information presented in the previous chapters are summarized and the need for future research in various areas is pointed out.

8.1 Conclusions

In Chapter 1, the objective and general scope of this investigation were noted, and the histories of previous studies on drawdown test and on numerical analyses were reviewed.

In Chapter 2, the physics of the saturated-unsaturated groundwater motion was discussed. The governing equation of saturated-unsaturated flow in porous media was derived from the law of mass conservation and the Darcy's law. The governing equation was compared with the Klute's diffusion equation which has been widely used in the analysis of flow in unsaturated region. As a result, it is concluded that the governing equation has the advantage that can be applied for the whole flow region, including saturated and unsaturated flow. Typical boundary and initial conditions were enumerated.

In Chapter 3, the governing equation derived in Chapter 2 was formulated into the finite element discretizations which are evolved into the study of either two-dimensional or three-dimensional or radially symmetric models. These models can take into account the effects of hysteresis in the volumetric moisture content-pressure head in unsaturated region. In conjunction with the finite element discretization weighted residual procedures, particularly the Galerkin method was used. Based on this theory, two finite element groundwater flow programs have been developed. The first program is capable of solving nonlinear groundwater flow problems in both two-dimensioned and axisymmetric region by using triangle element. The second program is capable of solving nonlinear groundwater flow problems in three-dimensional region with isoparametric element. For time integration, the time-centered scheme and the fully implicit backward difference scheme have been incorporated into programs. Both schemes can be used with equilibrium interation within each time step. Without loss of solution accuracy, depending on the nonlinearities, the equilibrium iteration may allow to dispense with the calculation of a new effective conductivity matrix in each time step and in this way improve solution efficiency.

In Chapter 4, the need for determining the hydraulic properties of soil profiles was pointed out and available methods are reviewed. An apparatus was constructed and test procedures were developed to measure the pressure head and

volumetric moisture content by using pressure transducer and law-energy gamma ray attenuation respectively. Experimental tests have been performed to determine the relationships between volumetric moisture content (θ) and hydraulic conductivity(K), and between pressure head (ψ) and volumetric moisture content (θ). The distribution of pressure head and moisture content above the free surface was obtained at the equilibrium condition in order to applied this distribution to the numerical analysis of drainage and infiltration in soil as an initial condition.

In Chapter 5, the validity and the accuracy of the two-or three-dimensional finite element approach which has been described in Chapter 3 have been investigated with comparing the numerical results with the experimental data. The relationships K-θ and ψ-θ which were obtained in Chapter 4 were used as input data. The results were that the good agreements between computed and measured pressure head profiles have been obrained. It should be remarked the saturated-unsaturated finite element analysis to two-or three-dimensional model is very powerful for the analysis of transient flow through porous media.

In order to apply the numerical method to practical groundwater flow problem in the field, the hydraulic properties must be estimated. In Chapter 6, new methods of analyzing drawdown tests were developed and illustrated with some examples to determine hydraulic properties of aquifer. Firstly, analysis of drawdown test data for partially penetrating well in a confined or an unconfined aquifer have been shown to determine anisotropic hydraulic conductibities and storage coefficient. Secondly, to analyze drawdown test data obtained in the much groundwater supplied aquifer, a conception of "Island Model" has been applied in unsteady state flow and theoretical solutions in a confined or an unconfined aquifer were developed. By using these solutions, new methods of analyzing drawdown test were given.

In Chapter 7, having looked into the reasonableness and validity of this

finite element model in Chapter 5, the possible applications of this model was finally described. The applications of models to field situation were the flows through sand bank at flood water levels and the flow through aquifer due to an excavation. These example analysis clearly demonstrated the flexibility of this finite element approach and its capability in treating complex situations which are often encountered in the field.

8.2 Recommendations for Future Research

The considerable effort, test procedures and numerical analysis developed during this investigation have been quite successful in evaluating the behavior of groundwater flow quantitatively. A considerable amount of additional research will be necessary as follows:

(1) The theoretical concepts of fluid flow in porous media have been established and basic theory for generating approximate solutions to nonlinear problems developed. However, the computer program, limited to the core storage of the available computer facility, was intended only to solve the simple illustrative problems especially in three-dimensional flow. With increased capacity, it would be possible to handle problems of complex geometry and arbitary boundary conditions. However it is necessary to research how to reduce the core.

(2) A great deal more research is required for determining or estimating hydrogeologic properties of the aquifers and aquitards from geologic, geophysical, and hydraulic evidence, namely, in determining storage capacity, including improvement of direct field methods for measuring moisture content, porosity, and negative pressure head, and also relating laboratory results to field data and applying them to field conditions.

(3) With regard to future research, important development is needed in analyzing multiphase flow. The mathematical development in this investigation is based on the usual assumption that the air phase is continuous and always in connection

with constant external atmospheric pressure. This assumption is not restrictive, but there are some critical ones that limit the sphere of application. In particular, on rewetting a drained or draining profile, the pore air entrapped between the descending wetting frint and the lower saturated zone will increase in pressure, there by causing further drainage. The next step in the program is therefore the study of vertical drainage under the combined effect of both gravity and increased pore-air pressure. And also it is necessary to extend this numerical method to principles of multiphase flow and diffusion, including contiguous salt water and fresh water or oil and fresh water under natural conditions.

(4) Finally, it must be emphasized for future research to consider an interaction between the disciplines of soil mechanics, soil physics and hydrogeology.